INVESTIGATIONS OF THE RENORMALIZATION GROUP APPROACH TO THE NUCLEON-NUCLEON INTERACTION

DISSERTATION

Presented in Partial Fulfillment of the Requirements for

the Degree Doctor of Philosophy in the

Graduate School of The Ohio State University

By

Sunethra Ramanan, B.S., M.S.

* * * * *

The Ohio State University

2007

Dissertation Committee:

Prof. R. J. Furnstahl, Adviser

Prof. S. Jeschonnek

Prof. T. Humanic

Prof. D. Stroud

Approved by

Adviser

Graduate Program in Physics

ABSTRACT

This thesis work has investigated the Renormalization Group theory for the nucleon-nucleon interaction. Conventional nuclear many-body calculations have the following sources of non-perturbative physics: 1. a strongly repulsive short-range interaction, 2. a tensor force, e.g. from pion exchange, which is highly singular at short-distances, 3. the presence of low-energy bound states or nearly bound states (in the S waves).

The RG approach exploits the insensitivity of low-energy processes to the details of the high-energy physics. Using any of the high-precision potentials as input, the high-momentum intermediate states in the Lippmann-Schwinger equation for the T matrix in a particular partial-wave are cut-off at Λ. The details of the physics beyond this limit of resolution are integrated out and included in the potential by requiring that the half-off shell T matrix elements be independent of the cut-off Λ. This requirement leads to a low-momentum potential "$V_{\mathrm{low}\,k}$", which is energy independent.

The choice of the regulator which cuts off the high momentum intermediate states is investigated. Sharp cut-offs, though straight forward, lead to convergence issues in few-body calculations that are eliminated using smooth regulators. The construction of low-momentum potentials using a smooth regulator is explored in detail. In the course of this study, a three-step process to calculate $V_{\mathrm{low}\,k}$ requiring the cut-off independence of the fully-off shell T matrix elements has been established and this yields better numerical stability than the energy-independent RG.

The complex eigenvalues (Weinberg eigenvalues) of the operator $G_0(z)V$, which appears in the Lippmann-Schwinger equation, are a useful tool for investigating the convergence of the Born series. Weinberg eigenvalues for $V_{\mathrm{low}\,k}$ potentials, including chiral effective theory potentials, have been investigated as a function of cut-off. The studies reveal the density and/or scale dependence of the sources of non-perturbative physics. The in-medium eigenvalues near the Fermi surface give a good estimate of the pairing gaps. Using two-particle Nambu-Gorkov propagators, the eigenvalue equation at $E = 2\varepsilon_{\mathrm{F}}$ is the gap equation and the eigenvectors corresponding to the largest eigenvalue gives the first approximation to the gap function $\Delta(k)$, which can be further iterated using the BCS gap equation to give self-consistent gaps.

This work is dedicated to my parents

ACKNOWLEDGMENTS

I would like to express deep gratitude to my advisor, Prof. Richard J. Furnstahl. I really appreciate his constant support and guidance throughout my graduate career. He has been an exemplary advisor and his immense patience while dealing with graduate students is worth mentioning. His curiosity and enthusiasm for physics has heightened my own interests in the field. I have learnt a great deal from him and definitely consider it an honour to have worked with him.

I would like to thank all the faculty of the Nuclear Theory Group, specially Prof. Robert Perry and Prof. Sabine Jeschonnek. I have had the opportunity of working with Prof. Jeschonnek during my second year and I currently have her on my committee. I sincerely appreciate her guidance through these years. I would like to acknowledge the postdoctoral researchers in the group Dr. Achim Schwenk and Dr. Scott K. Bogner for useful discussions. I really enjoyed collaborating with them.

I would like to thank my fellow graduate students Anirban Bhattacharyya, Amy Hummel, Anthony J. Kuhlman (AJ) and Evan Frodermann. It has been really pleasant sharing my office space with them. I would specially like to acknowledge Anirban and AJ for useful discussions from time to time.

I would like to thank Prof. David Stroud and Prof. Thomas Humanic for serving on my committee.

My deep gratitude to my friend Rajdeep Sen Sarma from the condensed matter theory group, who spent endless hours discussing physics with me.

My parents have been the greatest source of support for me. Though far away, their constant encouragement saw me through these years away from home. I would like to thank my brother for his sweet emails. I sincerely appreciate my husband's emotional support and constant encouragement during the entire course of my graduate career. I deeply acknowledge the support my in-laws have extended towards my career.

I would also like to thank my thesis advisor during my master's program at IIT(M), Prof. V. Balakrishnan, for motivating me towards physics research in the first place.

My friends here in Columbus have made these years really fun and life outside school would have been boring but for them. I would like to acknowledge my best friend, Sharmistha Pal, who has been like family to me. She has made these years very special and stood by me through rough times.

VITA

August 28 1976	Born - Chennai, India
May 1997	B.Sc Physics, Stella Maris College, Chennai, India
May 1999	M.Sc Physics, Indian Institute of Technology, Chennai, India
July 1999 - May 2000	Graduate School in Physics, Tata Insititute of Fundamental Research, Mumbai, India
June 2000 - present	Department of Physics, The Ohio State University, Columbus, Ohio, U.S.A.

PUBLICATIONS

Research Publications

"Convergence of the Born series with low-momentum interaction", S. K. Bogner, R. J. Furnstahl, S. Ramanan, and A. Schwenk, Nucl.Phys.A **773**,203-220,2006, arXiv:nucl-th/0602060.

"Low-momentum potentials with smooth cut-offs", S. K. Bogner, R. J. Furnstahl, S. Ramanan, and A. Schwenk, Nucl.Phys.A **784**, 79-103,2006, arXiv:nucl-th/0609003

FIELDS OF STUDY

Major Field: Physics

Studies in Investigations of the Renormalization Group Approach to the Nucleon-Nucleon Interaction: Prof. Richard J. Furnstahl

TABLE OF CONTENTS

LIST OF TABLES

Table **Page**

LIST OF FIGURES

Figure **Page**

CHAPTER 1

INTRODUCTION

1.1 Nuclear Physics and QCD - the connection

One of the main challenges of nuclear physics is to build up a microscopic theory for finite nuclei and nuclear matter. Based on Yukawa's first field theoretic attempt to derive nucleon-nucleon interaction through pion-exchange, followed by subsequent heavy meson exchange theories of the 60's, different parts of the nuclear force can be divided into the following three regions: strong repulsion at short distances, often called "hard-core repulsion", intermediate range attraction, described by two-pion or sigma meson exchange, and an exponential tail at long distances described by one-pion exchange.

Since nucleons interact through the strong interaction, it should be possible to start from Quantum Chromodynamics (QCD), which is the underlying theory. But at the energy scale of nuclear physics, QCD is non-perturbative and as a result direct solutions are impossible (at present). This connection with QCD inspired many QCD-based models, but because these were just models, they did not result in significant progress in understanding the connection between nuclear physics and QCD. Instead, this connection is established through effective field theories (EFT) [1, 2, 3].

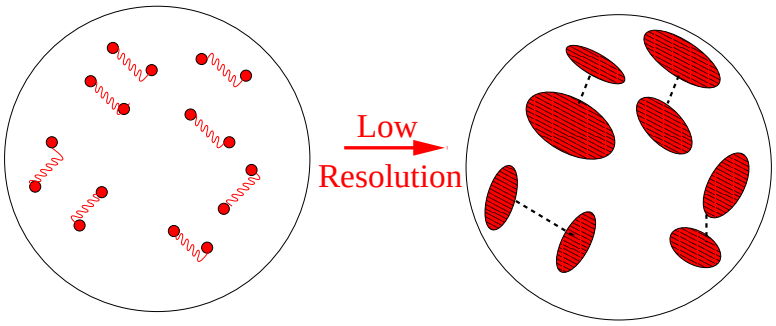

Figure 1.1: Schematic of Renormalization Group Principle. The resolution scale determines the relevant details of an interaction. At low resolution, all the details of the interaction shown in the left panel can be replaced by simpler ones that are valid in the low-energy domain

An EFT is a field theory which is valid in a limited domain, but reproduces the underlying theory in a systematic and model-independent way [4, 5, 6, 7, 8, 9]. The basic philosophy of an effective field theory is that the dynamics at low energies is independent of the *details* of the dynamics at high energies. Therefore the low-energy theory can be described by an effective lagrangian with low-energy degrees of freedom. The high-energy theory manifests as low-energy constants and in the symmetries of the effective lagrangian.

The first step towards building an EFT is to look at the momentum scales of the problem at hand. QCD has the following scales: 1. At momenta of order of few GeV, i.e., $\Lambda \geq \Lambda_{\rm pQCD} \approx$ few GeV, where Λ denotes the momentum scale, QCD is asymptotically free and the interactions between quarks and gluons become perturbative. 2. At $\Lambda \approx 500\,{\rm MeV} - 1\,{\rm GeV}$, the physics is that of strongly interacting hadrons (mesons and baryons) and their resonances as QCD is non-perturbative at this scale. 3. At lower momenta i.e, $\Lambda \leq \Lambda_{\rm nucl} \approx 300\,{\rm MeV} \ll \Lambda_\chi = 1\,{\rm GeV}$ we have

traditional nuclear physics which involves interactions between nucleons mediated by the lightest hadrons.

Working at this lowest scale, the details of the physics at higher scales cannot be resolved, as the resolution is limited by $\frac{1}{\Lambda}$. This is where the idea of an EFT comes in. The physics at distances smaller than the limit of resolution can be replaced by something simpler, e.g., regulated local interactions (multiplied by low-energy constants or LECs). Using this key idea we can approximate the full theory by an effective theory (see figure (1.1)). As a result, problems at lower scales decouple from the details of the physics at higher energy scales and we are left with a simpler theory valid at that scale.

Any effective theory of nuclear interaction should have the chiral symmetry breaking of QCD. This is manifested in the presence of pions, which are the corresponding Goldstone bosons. Through this symmetry constraint on the low-energy lagrangian, nuclear EFT connects to the underlying theory of strong interaction (QCD). When the underlying theory is known, the LEC's in the low-energy lagrangian are determined by matching to the high-energy theory at the breakdown scale of the low-energy theory. When the underlying high-energy theory is not known, the LEC's are obtained by matching to experiments. In a nuclear EFT, though the underlying theory is known (QCD), it is not yet possible to obtain the low-energy constants from QCD as it is strongly coupled at the scales relevant to nuclear physics. Attempts to obtain the low-energy constants directly from QCD are being made through lattice calculations, and recent progress make this a plausible future [10, 11, 12, 13]. So at present, any nuclear EFT has to be fit to experimental observables (scattering data, binding energies etc.).

1.2 Nuclear interactions and EFT

This section briefly reviews the advances in understanding nuclear interactions through effective field theories (EFT) and the Renormalization Group (RG) principles. An EFT program can be established in the following steps [8, 14]:

1. Define the most general lagrangian with the relevant degrees of freedom (d.o.f.) i.e., d.o.f. relevant at the given momentum scale Λ such that the lagrangian is consistent with the global and local symmetries of the underlying theory.

2. Declare a regularization and renormalization scheme.

3. Establish a well defined power-counting.

In Nuclear EFTs (Chiral Effective Field theory [16]- [25]), the typical momentum scale is of the order of the pion mass m_π. The break-down scale is around $\Lambda_\chi \approx 700\,\mathrm{MeV} - 1\,\mathrm{GeV}$, where the lower limit corresponds to the scale at which heavier hadrons begin to get resolved. Therefore, working at low momenta, the suitable degrees of freedom are pions and nucleons. QCD imposes chiral symmetry breaking on the low-energy lagrangian. The Chiral lagrangian can be expressed as follows:

$$\mathcal{L}_{\text{eff}} = \mathcal{L}^2_{\pi\pi} + L^1_{\pi\mathrm{N}} + L^2_{\pi\mathrm{N}} + L^3_{\pi\mathrm{N}} + \cdots \tag{1.1}$$

where the superscripts refer to the number of derivatives or pion mass insertions.

As an example, let us look at the $\mathcal{L}^2_{\pi\pi}$ term:

$$\mathcal{L}^2_{\pi\pi} = \frac{f_\pi}{4}\mathrm{tr}\left[\partial^\mu U \partial_\mu U^\dagger + m_\pi^2 (U + U^\dagger)\right] \tag{1.2}$$

$$U = \exp \frac{2i\mathbf{T}\cdot\pi}{f_\pi} \tag{1.3}$$

where T are the Pauli matrices and f_π, the pion decay constant. $\mathcal{L}^2_{\pi\pi}$ can be expanded in terms of the pion fields, as the pions interact weakly at low-energies. Further the small mass term ($m_\pi \approx 140\,\mathrm{MeV}$) is indicative of the chiral symmetry breaking of the low-energy theory. Notice that such a series has an infinite number of terms, which can be truncated so that the truncation error can be estimated *a priori*.

Once we include the two-nucleons in the interaction, then a new scale enters the problem, namely the deuteron binding energy. The low value of binding energy ($-2.224\,\mathrm{MeV}$) precludes a perturbative expansion and the above power counting scheme breaks down. Weinberg proposed a power counting scheme in the potential and then solving the Schroedinger equation, which provides a non-perturbative resummation. The NN potential can be expanded as follows:

$$V_{\mathrm{NN}} = \sum_{\nu=\nu_{\mathrm{min}}}^{\infty} c_\nu Q^\nu \tag{1.4}$$

where Q is the generic momentum or the pion mass and ν is determined from the topology of the corresponding Feynman diagram.

Using the above scheme, EFT-based nuclear interactions (chiral EFT potentials) have now been developed to N^{3}LO, i.e. to $(\frac{Q}{\Lambda_\chi})^4$ [26, 27]. The low-energy constants at each order are fitted to neutron-proton, neutron-neutron and proton-proton scattering data. There are twenty four LEC's at N^{3}LO. These chiral potentials reproduce two-body observables to $\frac{\chi^2}{d.o.f} \approx 1$ up to energies of $E_{\mathrm{lab}} \approx 300\,\mathrm{MeV}$. The key connection with QCD is the broken chiral symmetry, which allows a description in terms of the psuedo-goldstone bosons (pions).

In an EFT framework, many-body forces are naturally introduced. Figure (1.2) shows that even a two-body interaction generates three- and higher-body interactions when the resolution scale limits the momenta of the intermediate states. There are

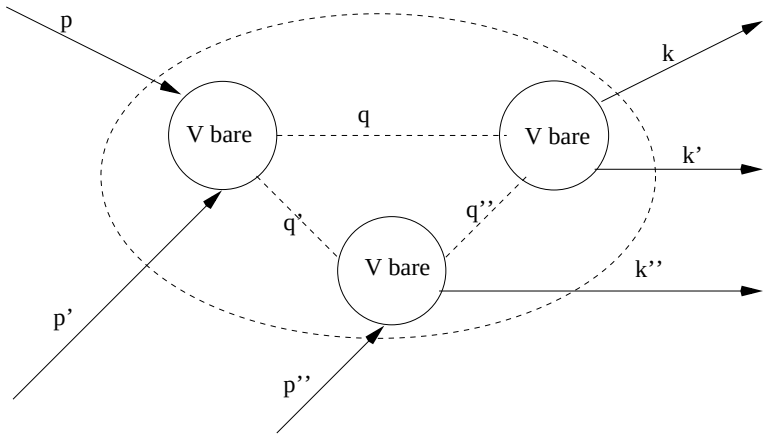

Figure 1.2: Schematic of the origin of Three-body forces. The solid lines represent interacting nucleons, and the arrows represent their direction. The dashed lines are the intermediate states. Here we have two-nucleons interacting through a two body force, and a third nucleon interacts with the intermediate state, again through a two body force, producing the respective out-going states as seen. The ellipse represents the resolution of the intermediate states. If Λ is the cut-off on the momentum of these intermediate states (i.e. $q \leq \Lambda$), then for an incoming-momenta $p, p', p'' \ll \Lambda$ intermediate states with momenta close to Λ cannot be resolved. So we just have three nucleons interacting through a three-body potential.

also other sources, such as the excited intermediate states (example Δ s) that are not degrees of freedom in the EFT. The chiral potentials [26, 27] order the many-body forces in powers of $(\frac{Q}{\Lambda_\chi})$. At leading order (LO) and next-to-leading order (NLO) only two-body forces enter the interaction. A three-body force first appears at N^2LO, as a result their effects are suppressed by a factor of $(\frac{Q}{\Lambda_\chi})^3$ compared to the two-body force at NLO. Four-body and higher many-body forces are further suppressed by higher powers of the expansion parameter. Nuclear EFT therefore gives an hierarchy of many-body forces in the nuclear lagrangian and also gives an error estimate if these are not included in calculations.

Renormalization group ideas add further insight into nuclear interactions. As discussed earlier, phenomenological potentials that describe nucleon-nucleon interactions include one-pion exchange for the long-distance part, while the intermediate and the short-distance regions have different inputs in various potential models. These potentials reproduce the two-body observables (phase shifts and deuteron binding energy) with a $\frac{\chi^2}{d.o.f} \approx 1$ in the low-momentum region ($E_{\rm lab} \leq 350\,{\rm MeV}$). This indicates that in order to reproduce low-momentum observables, only the coarse details of the high-energy physics matter. While including short-distance details explicitly, although inaccurately, does not affect low-energy observables, they result in non-zero momentum space matrix elements for large values of momentum k. When these potentials are used as input in a many-body calculation, these high-momentum states have to be taken into account and as a result make such calculations hard and often intractable.

The Renormalization Group (RG) can be applied to greatly improve this situation. As an example, consider the case of two-body scattering. The Lippmann-Schwinger equation for the l^{th} partial wave is

$$T^l_{\rm NN}(k', k; E_{\rm k}) = V^l_{\rm NN}(k', k) + \frac{2}{\pi}\int_0^\infty p^2 dp\, V^l_{\rm NN}(k', p)\, G^{(2)}(p, E_{\rm k})\, T^l_{\rm NN}(p, k; E_{\rm k}), \quad (1.5)$$

where we have chosen the center of momentum frame, k and k' are the incoming and outgoing momenta, p denotes the intermediate state momenta, $G^{(2)}(p, E_{\rm k})$ is the two-particle propagator and $E_{\rm k} = k^2$ is the scattering energy. We use units with $\hbar^2/m_{\rm N} = 1$, where $m_{\rm N}$ is the nucleon mass. Figure (1.3) is a schematic of the T matrix equation.

The intermediate states include all momenta ranging from 0 to ∞. For conventional potentials, a wide range of high-momentum states is required to obtain

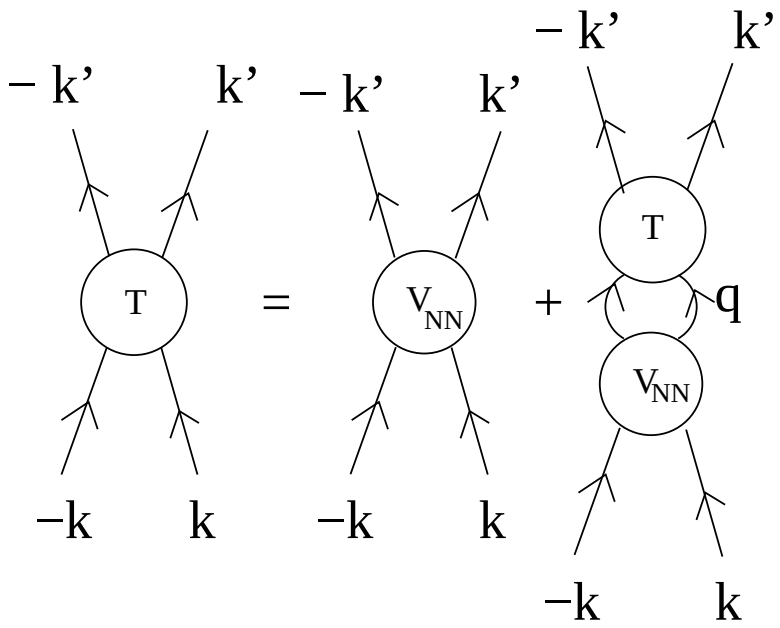

Figure 1.3: Schematic of two-body scattering with $V_{\rm NN}$: The intermediate states include both low and high-momentum modes as q ranges between 0 and ∞.

convergence of the sum over these intermediate states. Such fine-tuning also enters many-body problems, when these conventional potentials are used as inputs. The Renormalization Group idea is to restrict the intermediate state momenta to be less than a cut-off Λ, which is successively lowered through the RG evolution equation by integrating out the states lying above this cut-off; at each step the potential has to be changed to $V_{\rm eff}^{\Lambda}$ in order to maintain the cut-off independence of two-body observables. This is schematically shown in figure (1.4) and the Lippmann-Schwinger equation now reads,

$$T^{l}_{{\rm low}\,k}(k',k;E_{\rm k}) = V^{l}_{{\rm low}\,k}(k',k) + \frac{2}{\pi}\int_0^{\Lambda} p^2 dp\, V^{l}_{{\rm low}\,k}(k',p)\, G^{(2)}(p,E_{\rm k})\, T^{l}_{{\rm low}\,k}(p,k;E_{\rm k}). \tag{1.6}$$

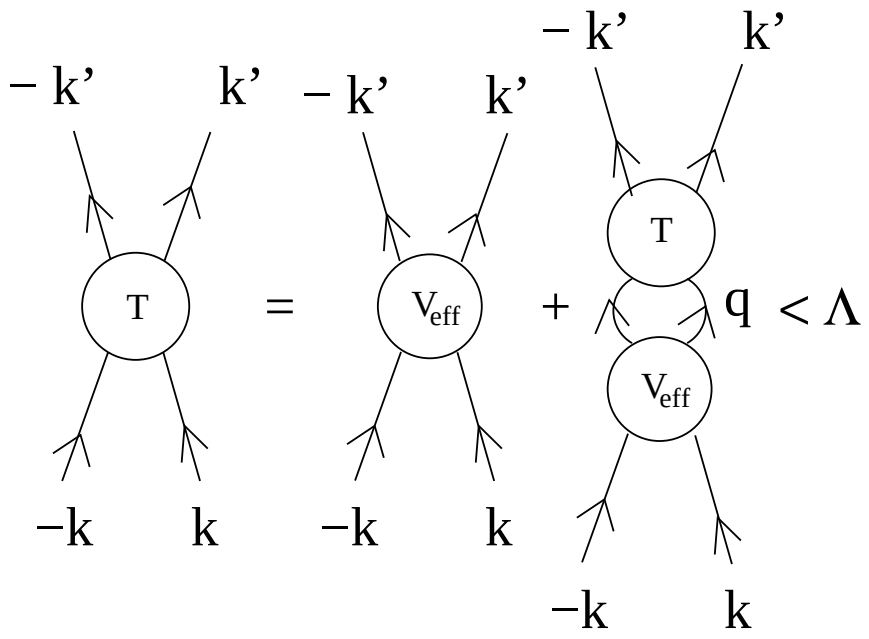

Figure 1.4: Schematic of two-body scattering with $V_{\mathrm{low}\,k}$: The intermediate states include only low-momentum modes as the high-momentum modes have been integrated out. The potential changes to a effective potential V_{eff} also known as "$V_{\mathrm{low}\,k}$"

This idea of integrating out high-momentum states is equivalent to replacing the short-distance physics by an infinite series of renormalized contact interactions in an EFT framework (see figure 1.5).

The RG principle [28] requires the invariance of the on-shell T matrix as the cut-off Λ is varied (i.e., $T_{\mathrm{low}\,k}(k', k; k^2) = T_{\mathrm{NN}}(k, k'; k^2)$ up to factors of the regulator). This results in phase shifts being independent of the resolution scale Λ. One way of executing the above idea is to require the invariance of the half-off shell T matrix elements instead. This choice results in an energy-independent low-mometum potential, $V_{\mathrm{low}\,k}$. The low-momentum interactions satisfy equation (1.6). Once we have discretized the momentum, the cut-off independence of the half-off shell T matrix elements imply

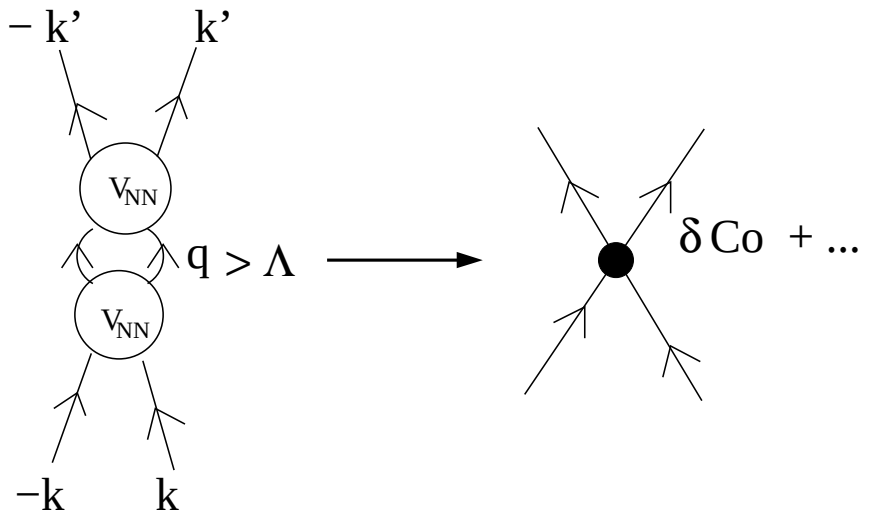

Figure 1.5: Schematic shows the equivalence between running the cut-off down followed by integrating out high-momentum modes and the EFT formalism

$\frac{dT^l(k',k;E_\mathrm{k})}{d\Lambda} = 0$, which leads to a set of first-order coupled differential equations determining $V_{\mathrm{low}\,k}(k',k)$ using any of the conventional high-precision potentials as the starting point. As the cut-off is lowered successively, the high-momentum intermediate states which lie above the cut-off are integrated out. $V_{\mathrm{low}\,k}(k',k)$ thus evolved from any of the high-precision potential models has non-zero matrix elements only in the low-momentum region (i.e., up to the cut-off Λ) as shown in figure (1.6)(figure taken from [32]).

The typical momentum scale one encounters in a nuclear many-body problem is of the order of the Fermi momentum $k_\mathrm{F} \approx 1.35\,\mathrm{fm}^{-1}$ (rms value relative to k_F is 0.55 MeV and is much lower). This is a low-momentum scale and as a result using effective interactions valid at these scales should prove beneficial. Recent work by Bogner *et al.* [37] shows that nuclear matter calculations become perturbative, at least

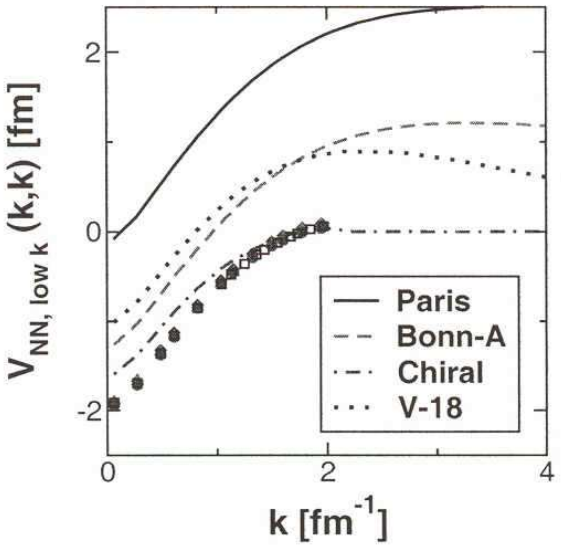

Figure 1.6: The diagonal matrix elements of V_{NN} and $V_{\mathrm{low}\,k}$ for the various model potentials in the ${}^1S_0$ channel. The dark dots represent the low-momentum potential $V_{\mathrm{low}\,k}$ for $\Lambda = 2.0\,\mathrm{fm}^{-1}$. We see that all the potential models nearly collapse on to the same $V_{\mathrm{low}\,k}$ [32, 34, 35].

in the particle-particle channel, when renormalization-group-based low-momentum potentials are used as inputs. Saturation at low momenta is driven by the three-body force, contrary to conventional wisdom that insists on an iterated tensor force.

Recent studies have shown that three-nucleon (3N) interactions become perturbative at lower cut-offs [36], although their contributions become important. Bogner *et al.* use $V_{\mathrm{low}\,k}$ for the two-body part and the three-body force is approximated by fitting to the leading-order $3N$ force from chiral EFT. Using nuclear interactions with high-momentum modes imply large values of the cut-off. This requires expensive cancellations of loop contributions from high-momentum states, thereby necessitating stronger $3N$ forces. Lowering the cut-off shifts the contributions between different terms in the lagrangian. The result that the three-body force becomes perturbative

at lower cut-offs and that it drives saturation in the particle-particle channel in a nuclear matter calculation indicates that many-body calculations could be much more tractable. Recent calculations using these RG based low-momentum potentials show that simple variational calculation of deuteron and triton yield good convergence for lower model spaces [38, 39]. All these results are encouraging, but still a lot of work needs to be done.

Effective field theories and renormalization group principles pave the way to better understand nuclear interactions. EFT formalism provides a basis for incorporating many-body forces *systematically*, which is a major draw-back with the phenomenological approaches. Nuclear systems share a lot of similarities with other physics sub-field such as atomic and condensed matter systems. Deeper understanding of nuclear systems could result in better understanding of many-body systems as a whole.

1.3 Thesis Organization

The following ideas are original contribution to this thesis:

1. The study of regulator dependence of renormalization group based low-momentum potentials, including smoothly regulated potentials.

2. Quantification of "perturbativeness" seen in many-body calculations using $V_{\mathrm{low}\,k}$ through the eigenvalues of the operator $G_0(E)V$ - Weinberg eigenvalue ananlysis. A spin-off being a separable approximation for the two-body interaction.

3. Analysis of pairing using Weinberg eigenvalue analysis.

The T matrix equation as seen in equation (1.6) uses a simple cut-off Λ on the intermediate states. As a result, states up to Λ are included explicitly in the interaction and states lying beyond Λ are integrated out and used to change the interaction as the cut-off is lowered. This is an example of a sharp regulator (theta function). Invariance of the half-off shell T matrix elements leads to the following set of coupled first-order differential equation for the potential:

$$\frac{dV^l_{\text{low}\,k}(k',k)}{d\Lambda} = \frac{2}{\pi}\frac{V^l_{\text{low}\,k}(k',\Lambda)T_{\text{low}\,k}(\Lambda,k;\Lambda^2)}{1-\dfrac{\Lambda^2}{k^2}} \tag{1.7}$$

The equation for the left on-shell T matrix in equation (1.7) is

$$T_{\text{low}\,k}(\Lambda,k;\Lambda^2) = V^l_{\text{low}\,k}(\Lambda,k) + \frac{2}{\pi}\mathcal{P}\int_0^\Lambda q^2 dq \frac{T_{\text{low}\,k}(\Lambda,q;\Lambda^2)V^l_{\text{low}\,k}(q,k)}{\Lambda^2-q^2} \tag{1.8}$$

where $T_{\text{low}\,k}(\Lambda,k;\Lambda^2)$ is the left-on shell T matrix element, Λ being the on-shell energy (units of $\dfrac{\hbar^2}{m}=1$). The RG condition requires that $T_{\text{low}\,k}(k',k;k^2) = T_{\text{NN}}(k',k;k^2)$ up to factors of the regulator, where T_{NN} are the half-off shell T matrix elements calculated using the bare interactions (starting point for $V_{\text{low}\,k}$ evolution).

The form of the above sets of equations (1.7) and (1.8) depend on the regulator function used to cut-off intermediate state momenta in the half-off shell T matrix equation. Also notice that the left-on shell T matrix equation (1.8) has a principal value integral with a pole at the end point and therefore is ill-defined. So we need to regulate this equation. Using a simple trick of defining the pole at Λ as $\Lambda \to \lim_{\epsilon\to 0}\Lambda(1\pm\epsilon)$ or equivalently $\Lambda \to \lim_{\epsilon\to 0}\Lambda\pm\epsilon$, where $0\le\epsilon\le 1$, we see that the pole at the end point is pushed out or pulled in to the integration region respectively, so that the equation is well-defined. The first part of this thesis explores the ϵ dependence of the observables calculated using the corresponding $V_{\text{low}\,k}$ potentials. The motivation for this investigation comes from the need to understand the errors in using $V_{\text{low}\,k}$

potentials for few and many-body calculations. These investigations show that the dependence of phase shifts on ϵ is linear for most values but become logarithmic at smaller values of this parameter.

Using sharp cut-offs lead to convergence issues [38] in variational calculations of deuteron and triton binding energies. Using smooth regulator functions on the other hand results in a complicated form for the first-order coupled differential equations, but leads to better convergence in few-body calculations [39, 40] (NOTE: The smooth cut-off potentials ultimately used in these calculations are not obtained by directly solving an energy independent RG equation. This involves a three-step RG which we shall see subsequently.) This thesis explores different smooth regulators, in particular the exponential regulator and the Fermi-Dirac regulator, for various values of the regulator parameters.

While half-off shell T matrix invariance leads to an energy-independent low-momentum potential, it was observed that when using smooth cut-offs, the complexity of the differential equations resulted in numerical instability. As a result, a three-step procedure is explored, where the first step is the invariance of the off-shell the T matrix elements, i.e., $\dfrac{dT(k,k';k_0^2)}{d\Lambda} = 0$ where k_0^2 is on-shell energy. This leads to an energy-dependent low-momentum potential $V_{\text{eff}}(k,k';k_0^2)$. This energy dependence is transformed away, followed by hermitization. to obtain an energy-independent hermitian low-momentum potential. Though the steps seem involved, this three-step process results in better numerical stability [40]. These investigations result in a better understanding of $V_{\text{low}\,k}$ potentials for the two-body interaction.

Another direction in this thesis work is to quantify the perturbativeness seen in the particle-particle channel when $V_{\text{low}\,k}$ is used in nuclear matter calculations. This

is done using the idea put forth by Weinberg [41], which is to look at the eigenvalue spectrum of the operator $G_0(E)V$ where $G_0(E)$ is the two-body Green's function. This operator appears in the Born series expansion of the T matrix, that is,

$$T(E) = V + VG_0(E)V + VG_0(E)VG_0(E)V + \cdots. \tag{1.9}$$

We introduce Weinberg eigenvalues $\eta_\nu(E)$ such that,

$$G_0(E)V|\Gamma_\nu(E)\rangle = \eta_\nu(E)|\Gamma_\nu(E)\rangle \tag{1.10}$$

where $|\Gamma_\nu(E)\rangle$ are the eigenvectors. Then the T matrix equation reads,

$$T|\Gamma_\nu(E)\rangle = V(1 + \eta_\nu(E) + \eta_\nu(E)^2 + \cdots)|\Gamma_\nu(E)\rangle. \tag{1.11}$$

From equation (1.11) it is clear that the T matrix expansion converges at energy E if $|\eta_\nu(E)| \leq 1$. In this thesis, we calculate and analyze these eigenvalues for the low-momentum potential for various cut-offs [42].

Using Weinberg eigenvalue analysis both in free space and in medium it is seen that reducing the cut-off decreases the magnitude of these eigenvalues in various partial wave channels (see figure (1.7)). This can be tied to the elimination of the sources of non-perturbative physics for the two-body interaction. As a result the interactions in these channels are soft. This decreases the correlations in few and many-body calculations, as can be seen by looking at the deuteron wave function as a function of cut-off in position and momentum space [40].

Using the same analysis in-medium, it is seen that at finite densities the eigenvalues are small compared to free space values in the S channel, which dominates. This can be tied to the fact that shallow bound states present in the S channel are no longer present in-medium due to Pauli blocking. But close to the Fermi surface

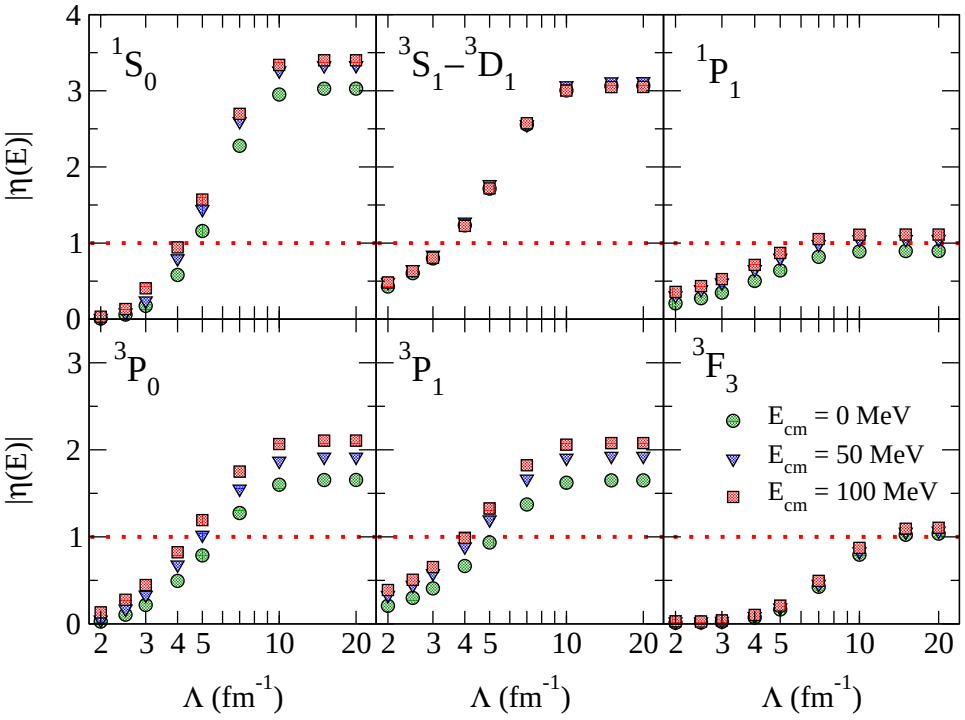

Figure 1.7: Repulsive Weinberg eigenvalues in various partial wave channels as a function of the cut-off Λ for different center of mass energies $E_{\rm cm}$. Note that decreasing the cut-off decreases the magnitude of the Weinberg eigenvalues.

an important non-perturvative phenomenon is the pairing instability. This should be reflected in the eigenvalues. In fact the eigenvalues around the Fermi surface drastically increase in magnitude and calculating the energy difference between $2\varepsilon_{\rm F}$ and the energy at which the largest eigenvalue crosses 1 gives a good estimate of the pairing gap, as seen is figure (1.8).

In his original paper, Weinberg puts forth the idea of introducing quasi-particles, which in turn change the interaction to a reduced interaction. The choice for the quasi-particle interaction is a function of the eigenvectors corresponding to the large

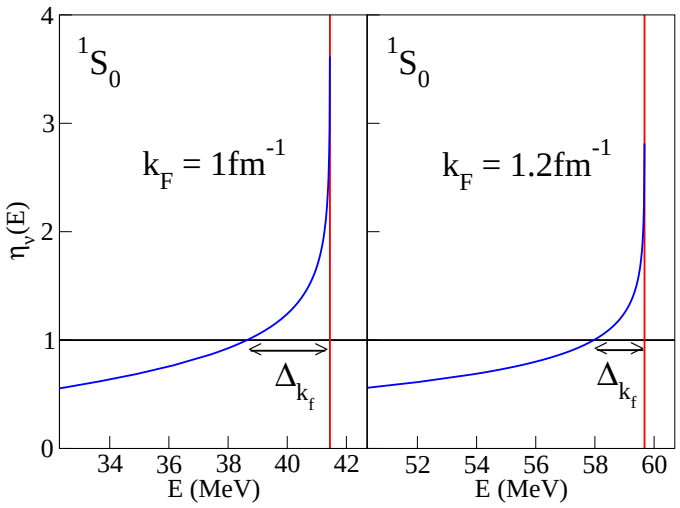

Figure 1.8: Eigenvalues as a function of energy around $2\varepsilon_{\mathrm{F}}$ for two different densities for $^1S_0$ channel. Note that the eigenvalues increase magnitude around $k = k_{\mathrm{F}}$ and we can get an estimate of the pairing gap.

eigenvalues of the operator $G_0(E)V$. Once the pieces corresponding to large eigenvalues are subtracted out, the reduced potential has only small eigenvalues (i.e. eigenvalues less than 1), so a Born-series expansion for the T matrix converges. This work attempts to understand the connection between Weinberg formalism (quasi-particle picture) and the pairing instability.

The general layout of this thesis is as follows: chapter two discusses the general formalism of two-body scattering and introduces $V_{\mathrm{low}\,k}$ in detail. The connection of this approach to EFT is explored in chapter three. These set up all the essential formalism. Chapter four deals with the regulator dependence, where smooth and sharp regulators are discussed. This chapter also discusses the three-step procedure to obtain $V_{\mathrm{low}\,k}$ involving an energy-dependent potential, followed by transformation to an energy independent potential and then hermitization. As mentioned earlier, this

procedure has greater numerical stability when smooth regulators are used compared to the energy-independent formulation.

Chapter five discusses the Weinberg eigenvalue formalism. Here we also derive and test a separable approximation for the nucleon-nucleon interaction using the Weinberg eigenstates, as a spin-off of the eigenvalue analysis. The extention of the Weinberg eigenvalue approach to pairing is explored in chapter six.

We conclude in chapter seven and discuss possible future directions. The various appendices serve to fill out the details skipped in the various sections.

CHAPTER 2

TWO-BODY SCATTERING

This section sets up the formalism for constructing $V_{\mathrm{low}\,k}$ potentials. As mentioned in the introduction, $V_{\mathrm{low}\,k}$ is obtained from the Renormalization Group condition that requires the $T^l(k', k; k^2)$ does not change with the cut-off Λ. In order for this thesis to be self contained, we will begin by reviewing two body scattering and set up T matrix equation. Then we will review the partial-wave basis, before we set up the RG equation which can be solved to obtain $V_{\mathrm{low}\,k}$.

2.1 Scattering in free space

This section reviews scattering theory in free space and sets up the Lippmann-Schwinger equation for the T matrix in the partial-wave basis. Consider two-body scattering as seen in figure (2.1). Here we have two nucleons scattering off each other. In the equivalent one body approach, we have a particle of mass μ, which is the reduced mass $\dfrac{m_1 m_2}{m_1 + m_2}$ of the two incoming nucleons. The result of this scattering could be varied. Within elastic limits ($E_{\mathrm{lab}} \leq 350\,\mathrm{MeV}$), the effect of scattering is to change the asymptotic direction of the outgoing particles. If the scattering is not elastic, then we have particle production, excited nucleons, etc. We are going to work within elastic limit. The reason to choose low energy goes back to our motivation to study

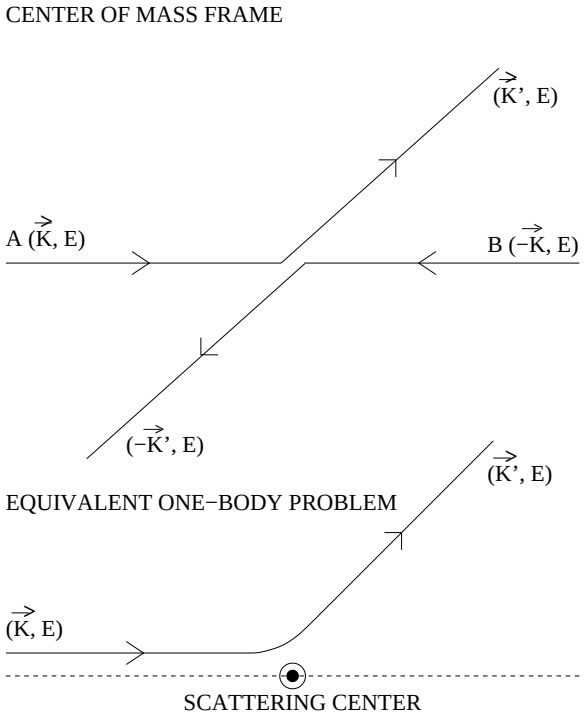

Figure 2.1: Nucleon-Nucleon scattering in the center-of-mass frame and the equivalent one-body representation. In the center of mass frame we have two nucleons approaching each other each with energy and momenta as indicated. In the equivalent one-body approach, we have reduced the two-body problem to an equivalent one-body problem and the in-coming and the out-going states have the energy and momenta as shown. This is an elastic scattering process as the energies of the outgoing nucleons remain the same and the effect of scattering is changing the direction of $\mathbf{k}$, $\mathbf{k}'$, the momentum of the nucleons.

the R.G. approach for nucleon-nucleon scattering and its application to many-body systems. The scale for nuclear momenta is around 250 MeV ($k_{\mathrm{F}} \approx 1.3\,\mathrm{fm}^{-1}$ in the interior of a nucleus). By restricting to low momenta we will integrate out the high-momentum modes and include those effects by changing the potential to an effective potential. The low-momentum potential reproduces two-body low-momentum data by construction. This procedure yields a smaller basis for the many-body problem.

In a scattering experiment [43], only the asymptotes are observed, i.e.,

$$|\psi_{in}\rangle \rightarrow |\Psi\rangle \rightarrow |\psi_{out}\rangle \tag{2.1}$$

where $|\Psi\rangle$ is the actual orbit, $|\psi_{in}\rangle$ and $|\psi_{out}\rangle$ are the in- and out-asymptotes. The asymptotic condition is given by:

$$\lim_{t\rightarrow-\infty} \widehat{U}(t)|\Psi\rangle = \widehat{U}_0(t)|\psi_{in}\rangle \tag{2.2}$$

$$\lim_{t\rightarrow+\infty} \widehat{U}(t)|\Psi\rangle = \widehat{U}_0(t)|\psi_{out}\rangle \tag{2.3}$$

where $\widehat{U}(t)$ and $\widehat{U}_0(t)$ are the full and free evolution operators respectively. We can relate the in- and out-asymptotes directly to each other using an isometric operator $\widehat{\Omega}_{\pm}$ (Moller Operators). From equations (2.2) and (2.3) we can write the wave function $|\Psi\rangle$ as

$$|\Psi\rangle = \lim_{t\rightarrow-\infty} \widehat{U}(t)^{\dagger}\widehat{U}_0(t)|\psi_{in}\rangle \equiv \Omega_+|\psi_{in}\rangle, \tag{2.4}$$

or equivalently

$$|\Psi\rangle = \lim_{t\rightarrow+\infty} \widehat{U}(t)^{\dagger}\widehat{U}_0(t)|\psi_{out}\rangle \equiv \Omega_-|\psi_{out}\rangle. \tag{2.5}$$

Therefore,

$$|\psi_{out}\rangle = \widehat{\Omega}_-^{\dagger}\,\widehat{\Omega}_+|\psi_{in}\rangle. \tag{2.6}$$

Setting $\widehat{\Omega}_-^{\dagger}\,\widehat{\Omega}_+ = \widehat{S}$, we get:

$$|\psi_{out}\rangle = \widehat{S}|\psi_{in}\rangle. \tag{2.7}$$

In the absence of the interaction (no scatterer), $\widehat{S} = 1$, so we can define a difference operator $\widehat{T} = \widehat{S} - 1$. It turns out that evaluating the $\widehat{T}$ operator in a suitable basis enables calculation of observables, as these are related to the diagonal on-shell matrix elements. In momentum space basis:

$$\langle \mathbf{k}'|S|\mathbf{k}\rangle = \delta^3(\mathbf{k}', \mathbf{k}) + \langle \mathbf{k}'|T|\mathbf{k}\rangle \tag{2.8}$$

where $\langle \mathbf{k}'|T|\mathbf{k}\rangle = -2\pi i\delta(E_{k'} - E_k)t(|\mathbf{k}'| = |\mathbf{k}|)$, which is the on-shell T matrix. The on-shell T matrix is directly related to the scattering amplitude and hence to the cross section.

Now we will attempt to get the scattered state $|\Psi\rangle$ in terms of the $\widehat{T}$ operator and the Green's operator $\widehat{G}(E \pm i\epsilon)$. The Moller operators connect the asymptotic state $|\psi_{in}\rangle$ (or $|\psi_{out}\rangle$). Let us denote the asymptotes as $|\Phi\rangle$. The Moller operators can be expressed in terms of $\widehat{G}$, the full Green's operator [43]. We can define the Moller operators in terms of the evolution operators using equations (2.4) and (2.5) as

$$\Omega\pm = \lim_{t\to\mp\infty} \widehat{U}(t)^\dagger \widehat{U}_0(t) \tag{2.9}$$

Next we write $\widehat{U}^\dagger(t)\widehat{U}_0(t)$ as an integral of a derivative:

$$\begin{aligned} \frac{d}{dt}\widehat{U}(t)^\dagger \widehat{U}_0(t) &= ie^{iHt}(H - H_0)e^{-iH_0t} \\ &= i\widehat{U}(t)^\dagger\, V\, \widehat{U}_0(t). \end{aligned} \tag{2.10}$$

which gives:

$$\begin{aligned} \Omega_\pm|\psi_{in}\rangle &= \lim_{t\to\pm\infty} \widehat{U}(t)^\dagger \widehat{U}_0(t)|\psi_{in}\rangle \\ &= \lim_{t\to\pm\infty} \left[|\psi_{in}\rangle + i\int_0^t d\tau \widehat{U}(\tau)^\dagger\, V\, U_0(\tau)|\psi_{in}\rangle\right]. \end{aligned} \tag{2.11}$$

Inserting a complete set of states $\int_0^\infty d^3p|\mathbf{p}\rangle\langle\mathbf{p}| = 1$ and integrating over τ we get

$$\widehat{\Omega}_\pm = 1 + \widehat{G}(E \pm i\epsilon)\widehat{V} \tag{2.12}$$

where $\pm i\epsilon$ is the convergence factor introduced into the the τ integration. From equations (2.4) and (2.5), the state $|\Psi\rangle$ is related to $|\Phi\rangle$ as,

$$|\Psi\rangle = \widehat{\Omega}_\pm|\Phi\rangle \tag{2.13}$$

Using equation (2.12), we can write the above as follows:

$$|\Psi\rangle = |\Phi\rangle + \widehat{G}(E \pm i\epsilon)\widehat{V}|\Phi\rangle \tag{2.14}$$

The $\widehat{T}(E)$ operator introduced earlier is defined as,

$$\widehat{T} = \widehat{V} + \widehat{V}G(E \pm i\epsilon)\widehat{V}. \tag{2.15}$$

As a result,

$$\widehat{T}|\Phi\rangle = \widehat{V} + \widehat{V}G(E \pm i\epsilon)\widehat{V}|\Phi\rangle, \tag{2.16}$$

Using the definition of $\Omega_{\pm}$ (equation (2.12)) and the asymptotic condition,

$$\widehat{T}|\Phi\rangle = \widehat{V}\Omega_{\pm}|\Phi\rangle, \tag{2.17}$$

$$\widehat{T}|\Phi\rangle = \widehat{V}|\Psi\rangle, \tag{2.18}$$

where E refers to the energy eigenvalue of the state $|\Psi\rangle$. Now,

$$\widehat{G}(E \pm i\epsilon)\widehat{V} = \widehat{G}_0(E \pm i\epsilon)\widehat{T}. \tag{2.19}$$

This can be understood intuitively as a resummation of the full Green's operator by the T operator, resulting in the free Green's operator. Using this result, equation (2.14) can be written as,

$$|\Psi\rangle = |\Phi\rangle + \widehat{G}_0(E \pm i\epsilon)\widehat{T}|\Phi\rangle \tag{2.20}$$

The free Green's operator can be written as:

$$\widehat{G}_0(E \pm i\epsilon) = \frac{1}{E - H_0 \pm i\epsilon} \tag{2.21}$$

Finally the Lippman-Schwinger equation [43, 44] for elastic scattering is given by:

$$|\Psi\rangle = |\Phi\rangle + \frac{1}{E - \widehat{H}_0 \pm i\epsilon}\widehat{V}|\Psi\rangle. \tag{2.22}$$

where we have used equation (2.18). Here $|\Psi\rangle$ represents the scattered state and $|\Phi\rangle$ represents the incident state (asymptotic state). The $\pm i\epsilon$ is introduced as the operator $\frac{1}{E-\widehat{H}_0}$ is singular at the eigenvalues of $\widehat{H}_0$. The physical meaning of making E complex becomes evident when we look at the scattered wave in the position basis at large distances. Then it turns out that choosing $+i\epsilon$ or $-i\epsilon$ corresponds to out-going or in-coming spherical waves. Equation (2.22) is an operator equation independent of a particular representation. Let us left-multiply by the operator $\widehat{V}$, so that:

$$\widehat{V}|\Psi\rangle = \widehat{V}|\Phi\rangle + \widehat{V}\frac{1}{E-\widehat{H}_0 \pm i\epsilon}\widehat{V}|\Psi\rangle. \tag{2.23}$$

Once again using equation (2.18) we get,

$$\widehat{T}|\Phi\rangle = \widehat{V}|\Phi\rangle + \widehat{V}\frac{1}{E-\widehat{H}_0 \pm i\epsilon}\widehat{T}|\Phi\rangle. \tag{2.24}$$

In momentum space the asymptotic states are the plane-wave states represented by $|\mathbf{k}\rangle$. Therefore the Lippman-Schwinger equation in momentum space is

$$\langle \mathbf{k}'|T^{\pm}(E)|\mathbf{k}\rangle = \langle \mathbf{k}'|V|\mathbf{k}\rangle + \int d^3q \langle \mathbf{k}'|V\frac{1}{E-\widehat{H}_0 \pm i\epsilon}|\mathbf{q}\rangle\langle \mathbf{q}|T^{\pm}(E)|\mathbf{k}\rangle. \tag{2.25}$$

Here we have introduced a complete set of ($|\mathbf{q}\rangle$) states. Physically, it means that we have allowed intermediate states with all possible momenta values. We will see later that this feature turns out to be the nemesis. Working in units where $\frac{\hbar^2}{2\mu} = \frac{\hbar^2}{m} = 1$, (where we have assumed that the incoming nucleons have the same mass m, so that $\mu = m/2$) we have:

$$\langle \mathbf{k}'|T^{\pm}(k^2)|\mathbf{k}\rangle = \langle \mathbf{k}'|V|\mathbf{k}\rangle + \int d^3q \frac{\langle \mathbf{k}'|V|\mathbf{q}\rangle\langle \mathbf{q}|T^{\pm}(k^2)|\mathbf{k}\rangle}{k^2 - q^2 \pm i\epsilon}. \tag{2.26}$$

As a next simplification, we will expand the above equation in the partial wave basis, so that it amounts to picking up a particular l value and we can do the angular

integration; this reduces the three dimensional integral to a one dimensional integral. We only sketch the details below [44, 47]:

$$|\mathbf{k}\rangle \equiv |klm\rangle = 4\pi\, i^l\, Y_{lm}(\widehat{\mathbf{k}})\, |k\rangle. \tag{2.27}$$

Therefore any matrix element for example $\langle \mathbf{k}'|V|\mathbf{k}\rangle$ can be written as

$$\langle \mathbf{k}'|V|\mathbf{k}\rangle = (4\pi)^2 \sum_{l,l'} \sum_{m} i^{l-l'} \langle k'l'm|V|klm\rangle Y_{lm}(\widehat{\mathbf{k}}) Y^*_{l'm}(\widehat{\mathbf{k}'}). \tag{2.28}$$

For uncoupled channels, the sum $\langle k'l'm|V|klm\rangle = \langle k'l'm|V|klm\rangle \delta_{l,l'}$, otherwise we will have the summation over l and l'. For uncoupled channels, equation (2.28) can be simplified as follows

$$\langle \mathbf{k}'|V|\mathbf{k}\rangle = (4\pi) \sum_{l} (2l+1) P_l(\widehat{\mathbf{k}} \cdot \widehat{\mathbf{k}'}) \langle k'|V_l|k\rangle. \tag{2.29}$$

where

$$\langle k'|V_l|k\rangle = \int r^2 dr j_l(k'r) V(r) j_l(kr) \tag{2.30}$$

and the $j_l(kr)$'s are the spherical Bessel functions. The partial waves states are normalized as [47]

$$\langle k'|k\rangle = \frac{\pi}{2} \frac{\delta(k-k')}{k^2}. \tag{2.31}$$

Decomposing all the matrix elements in the T matrix equation into the partial wave basis and picking out the l^{th} partial wave, the Lippman-Schwinger equation reads:

$$\langle k'|T_l(k^2)|k\rangle = \langle k'|V_l|k\rangle + \frac{2}{\pi} \mathcal{P} \int_0^\infty q^2 dq \frac{\langle k'|V_l|q\rangle \langle q|T_l(k^2)|k\rangle}{k^2 - q^2}. \tag{2.32}$$

Note that for coupled channels, equation (2.32) would be a matrix equation given by

$$\langle k'|T_{ll'}(k^2)|k\rangle = \langle k'|V_{ll'}|k\rangle + \sum_{l''} \frac{2}{\pi} \mathcal{P} \int_0^\infty q^2 dq \frac{\langle k'|V_{ll''}|q\rangle \langle q|T_{l''l'}(k^2)|k\rangle}{k^2 - q^2}. \tag{2.33}$$

Here we have averaged over the in-coming and the out-going waves, so as to get standing waves. Matrix elements satisfying standing wave boundary conditions are usually referred to as the K matrix elements. However, we shall continue calling it the T matrix. This sets up all the formalism required for two-body scattering in free-space. In the next section we will derive first order coupled differential equation for $V_{\mathrm{low}\,k}$ using R.G. approach, starting with the T matrix equation.

2.2 Renormalization Group based low-momentum potentials

In the previous section, we reviewed two-particle scattering in free space and set up all the essential ingredients to derive $V_{\mathrm{low}\,k}$. The T matrix equation in momentum space for the l^{th} partial wave is given as follows:

$$\langle k'|T_l(k^2)|k\rangle = \langle k'|V_l|k\rangle + \frac{2}{\pi}\mathcal{P}\int_0^\infty q^2 dq \frac{\langle k'|V_l|q\rangle\langle q|T_l(k^2)|k\rangle}{k^2-q^2}. \tag{2.34}$$

Let us focus on the intermediate states in equation (2.34). We see that the intermediate state momenta can take all possible values. Therefore the low and high momentum states are coupled even for a low-energy process. Using the R.G idea, let us cut-off the intermediate state at Λ. This cut-off represents the scale up to which the details of the interaction can be resolved. This idea was schematically shown in figure (1.4). The piece integrated out is included in the potential, so as to keep the T matrix elements constant. With the cut-off on the intermediate states the T matrix equation reads as follows:

$$\langle k'|T_l(k^2)|k\rangle = \langle k'|V_{\mathrm{low}\,k}|k\rangle + \frac{2}{\pi}\mathcal{P}\int_0^\Lambda q^2 dq \frac{\langle k'|V_{\mathrm{low}\,k}|q\rangle\langle q|T_l(k^2)|k\rangle}{k^2-q^2}. \tag{2.35}$$

Since $T_l(k,k;k^2)$ is a physical obervable, we require

$$\frac{dT_l(k,k;k^2)}{d\Lambda} = 0, \tag{2.36}$$

or in general,

$$\frac{dT_l(k',k;k^2)}{d\Lambda} = 0. \tag{2.37}$$

In the second condition we have put a restriction on the Half-On Shell (HOS) T matrix, in spite of it not being a physical observable. This is just a choice which results in an energy-independent low-momentum potential. This choice in addition preserves the long-range wave function of the scattered states. If the HOS T matrix is preserved then the fully on-shell T matrix is automatically preserved.

We shall outline a brief derivation leading to the renormalization group equation. We start with the equation to the T matrix:

$$T(k',k;k^2) = V_{\text{low}\,k}(k',k) + \frac{2}{\pi}\mathcal{P}\int_0^\Lambda q^2 dq \frac{V_{\text{low}\,k}(k',q)T(q,k;k^2)}{k^2-q^2}. \tag{2.38}$$

Now we will use the condition given in equation (2.37) to get the following equation,

$$\begin{aligned}\frac{dV_{\text{low}\,k}(k',k)}{d\Lambda} + \frac{2}{\pi}\mathcal{P}\int_0^\Lambda q^2 dq \frac{dV_{\text{low}\,k}(k',q)}{d\Lambda}\frac{T(q,k;k^2)}{k^2-q^2} \\ + \frac{2}{\pi}\frac{\Lambda^2 V_{\text{low}\,k}(k,\Lambda)T(\Lambda,k;k^2)}{k^2-\Lambda^2} = 0.\end{aligned} \tag{2.39}$$

The standing wave scattering states of the effective theory are given by (equation (2.20)):

$$|\chi_k\rangle = |k\rangle + \frac{2}{\pi}\mathcal{P}\int_0^\Lambda q^2 dq \frac{1}{k^2-q^2}T(q,k;k^2)|q\rangle, \tag{2.40}$$

Here we have used $|\chi_k\rangle$ for the scattered states $|\Psi\rangle$. The normalization condition for the $|k\rangle$ states is: $\langle k'|k\rangle = \frac{\pi}{2}\frac{\delta(k'-k)}{k^2}$; left-multiply equation (2.40) by $\langle p|$ to get

$$\chi_k(p) = \frac{\pi}{2}\frac{\delta(k-p)}{p^2} + \frac{1}{k^2-p^2}T(p,k;k^2). \tag{2.41}$$

Substituting the above result into equation (2.39), we get

$$\frac{2}{\pi}\mathcal{P}\int_0^\Lambda \frac{dV_{\text{low}\,k}(k',q)}{d\Lambda}\chi_k(q)q^2 dq = \frac{2}{\pi}\frac{V_{\text{low}\,k}(k',\Lambda)T(\Lambda,k;k^2)}{1-(\frac{k}{\Lambda})^2}. \tag{2.42}$$

Next we write $T(\Lambda, k; k^2) = \langle \Lambda | V_{\text{low}\,k} | \chi_k \rangle$. We know *a priori* that the effective potential is non-hermitian. We can argue as follows. Consider the Hamiltonian matrix, which has all the low and high-momentum modes. We can always construct a similarity transformation so that the low and high-momentum modes decouple and we have an upper-triangular block diagonal hamiltonian, which is H_{eff}, the effective hamiltonian. By doing this transformation we have preserved the eigenvalues. Since physical observables are related to diagonal matrix elements, the upper-triangular block diagonal form is sufficient. But this form is not hermitian.

As we shall see in later chapters, we can always hermitize the potential. So the simple completeness relation is replaced by the biorthogonal complement,

$$\frac{2}{\pi} \int p^2 dp |\chi_p\rangle \langle \tilde{\chi_p}| = 1. \tag{2.43}$$

This is a generalization of the completeness relation. When a hermitian operator acts on a linear vector space, the vector space and its dual space has the property that they are complex conjugates of each other. But this does not hold for non-hermitian operators; the completeness relation is then generalized to the biorthogonal component. Using this result, equation (2.42) becomes:

$$\frac{dV_{\text{low}\,k}(k', q')}{d\Lambda} = \frac{2}{\pi} V_{\text{low}\,k}(k', \Lambda) \mathcal{P} \int_0^\Lambda \frac{\langle \Lambda | V_{\text{low}\,k} | \chi_k \rangle \langle \tilde{\chi}_k | q' \rangle}{1 - (\frac{k}{\Lambda})^2} k^2 dk, \tag{2.44}$$

Inserting a complete set of q states: $\frac{2}{\pi} \int q^2 dq |q\rangle\langle q| = 1$ we get,

$$\frac{dV_{\text{low}\,k}(k', q')}{d\Lambda} = \frac{2}{\pi} \Lambda^2 V_{\text{low}\,k}(k', \Lambda; \Lambda) \mathcal{P} \int_0^\Lambda q^2 dq V_{\text{low}\,k}(\Lambda, q) \mathcal{G}(q, q'; \Lambda^2), \tag{2.45}$$

where $\mathcal{G}(q, q'; \Lambda^2) = \frac{2}{\pi} \int k^2 dk \langle q | \chi_k \rangle \langle \tilde{\chi}_k | q' \rangle \frac{1}{k^2 - \Lambda^2}$ is the interacting Green's function in the truncated Hilbert space. We can show by expanding this Green's function in

the low-momentum region, that this is in fact the T matrix equation. Therefore we find the following Renormalization Group equation

$$\frac{dV_{\text{low}\,k}(k',k)}{d\Lambda} = \frac{2}{\pi}\frac{V_{\text{low}\,k}(k',\Lambda)T(\Lambda,k;\Lambda^2)}{1-(\frac{k}{\Lambda})^2}. \tag{2.46}$$

This simple form for the coupled first-order differential equations for the potential is regulator dependent. Here we have used a sharp regulator (cut-off at the scale Λ). It turns out that the sharp cut-offs cause convergence problems in few and many-body calculations [38]. We will discuss the regulator dependence in subsequent chapters.

2.3 Separable Model Potential

The previous section sets up the formalism for $V_{\text{low}\,k}$. As mentioned in the conclusion of the previous section, the final form of the differential equations is regulator dependent. Though we defer discussion of regulator dependence to later chapters, we will explore the RG based potentials before we proceed. A good check for the renormalization group evolution of the potential is that the two-body observables should be independent of the cut-off Λ. This will be demonstrated in this section using a simple separable model originally introduced in [32].

Separable potentials are defined as follows in position and momentum space:

$$V(r,r') = \lambda v(r)u(r'), \tag{2.47}$$

$$V(k,k') = \lambda v(k)u(k'), \tag{2.48}$$

where Λ is a constant. Note that realistic nuclear potentials are not separable; but they can be written as a sum of separable potentials, which we will see in chapter (5). The advantage of studying separable potentials is that they simplify the problem and,

as we shall show, the T matrix equation is also separable. Separable potentials can have all the features of a nucleon-nucleon potential, as we can write the attractive and the repulsive parts as separable pieces. Using the separable approximation in equation (2.48), the T matrix equation (2.38) becomes

$$T(k', k; k^2) = \lambda u(k') \left[v(k) + \frac{2}{\pi} \int_0^\Lambda q^2 dq \frac{v(q) T(q, k; k^2)}{k^2 - q^2} \right]. \tag{2.49}$$

Therefore,

$$T(k', k; k^2) = \lambda u(k') \tau(k; k^2) \tag{2.50}$$

where

$$\begin{aligned} \tau(k; k^2) &= v(k) + \frac{2}{\pi} \int_0^\Lambda q^2 dq \frac{\lambda u(q) v(q)}{k^2 - q^2} \tau(k; k^2), \\ &= \frac{v(k)}{1 + \dfrac{2}{\pi} \displaystyle\int_0^\Lambda q^2 dq \, \dfrac{V(q, q)}{q^2 - k^2}}. \end{aligned} \tag{2.51}$$

where we have used equation (2.50). Therefore T matrix equation has the following separable form

$$\langle k' | T_{\text{low}\, k} | k \rangle = \frac{V_{\text{low}\, k}(k', k)}{1 + \dfrac{2}{\pi} \mathcal{P} \displaystyle\int_0^\Lambda q^2 dq \frac{V_{\text{low}\, k}(q, q)}{q^2 - k^2}}. \tag{2.52}$$

This can be obtained straightforwardly from the T matrix equation (2.38), by using separable potentials. Physical observables (phase shifts) depend only on the diagonal matrix elements $\langle k | T_{\text{low}\, k} | k \rangle$, so taking the diagonal matrix elements for the above equation we get:

$$\langle k | T_{\text{low}\, k} | k \rangle = \frac{V_{\text{low}\, k}(k, k)}{1 + \dfrac{2}{\pi} \mathcal{P} \displaystyle\int_0^\Lambda q^2 dq \frac{V_{\text{low}\, k}(q, q)}{q^2 - k^2}}. \tag{2.53}$$

Using the separable form of T matrix in equation (2.52) the differential equations for $V_{\mathrm{low}\,k}(k',k)$ (equation (2.36)) simplifies as follows:

$$\frac{dV_{\mathrm{low}\,k}(k,k)}{d\Lambda} = \frac{2}{\pi}\frac{V_{\mathrm{low}\,k}(k,\Lambda)}{1-\left(\frac{k}{\Lambda}\right)^2}\frac{V_{\mathrm{low}\,k}(\Lambda,k)}{1+\frac{2}{\pi}\mathcal{P}\int_0^\Lambda q^2dq\frac{V_{\mathrm{low}\,k}(q,q)}{q^2-\Lambda^2}}. \tag{2.54}$$

Since $V_{\mathrm{low}\,k}$ is separable, we can do the following:

$$\frac{dV_{\mathrm{low}\,k}(k,k)}{d\Lambda} = \frac{2}{\pi}\frac{V_{\mathrm{low}\,k}(\Lambda,\Lambda)}{1-\left(\frac{k}{\Lambda}\right)^2}\frac{V_{\mathrm{low}\,k}(k,k)}{1+\frac{2}{\pi}\mathcal{P}\int_0^\Lambda q^2dq\frac{V_{\mathrm{low}\,k}(q,q;)}{q^2-\Lambda^2}}. \tag{2.55}$$

Here we have used: $V_{\mathrm{low}\,k}(k,\Lambda)V_{\mathrm{low}\,k}(\Lambda,k) = \lambda^2u(k)v(\Lambda)u(\Lambda)v(k)$, which can be written as:

$$\lambda^2u(k)v(k)u(\Lambda)v(\Lambda) = V_{\mathrm{low}\,k}(k,k)V_{\mathrm{low}\,k}(\Lambda,\Lambda). \tag{2.56}$$

We can solve the above equation numerically. But first we note that the integral in the denominator is a principal value integral with a pole at the end point. We first need to 'regulate' this integral, as it is mathematically ill-defined. Let us look at the following principal value integral,

$$\mathcal{P}\int_0^\Lambda \frac{f(k)dk}{k^2-k_0^2} \tag{2.57}$$

We can add and subtract the piece $\dfrac{f(k_0)}{k^2-k_0^2}$ so that we get,

$$\int_0^\Lambda \frac{[f(k)-f(k_0)]dk}{k^2-k_0^2}+f(k_0)\mathcal{P}\int_0^\Lambda \frac{dk}{k^2-k_0^2} = \int_0^\Lambda \frac{[f(k)-f(k_0)]dk}{k^2-k_0^2}+f(k_0)\log|\frac{\Lambda-k_0}{\Lambda+k_0}|. \tag{2.58}$$

We do the same in our case, but with a little caution. Since we are doing a numerical evaluation, we have k on a grid, so the basis is discrete. We make Λ, which is the cut-off, to lie in between the levels and not directly on top of it, so this means that k is less than Λ, by a small quantity ϵ'. Also we note that the intermediate states

Parameter	model 1	model 2	model 3
n	1/2	1	1
α	1.8199	4.5354	0
g	3.1429	3.3542	1.7166
m	1.0962	1.3892	1.1647

Table 2.1: Parameters for models 1,2 and 3, fitted to $^1S_0$ phase shifts close to the origin and where the phase shifts change sign [32].

have a pole at the end point of the principal value integral. So we slightly shift the pole at the end point so that $\Lambda \to \Lambda(1-\epsilon)$. This is our choice for regulating the integral [32, 45, 34, 29]. As a result, the term $(1-(\frac{k}{\Lambda})^2)$ becomes $(1-(\frac{k}{\Lambda(1+\epsilon')})^2)$ as we have Λ to lie slightly above the allowed k value. By allowed, we mean the maximum value of k less than Λ. The pole piece inside the integral becomes $(q^2-(\Lambda(1-\epsilon))^2)$. As a result this equation can now be solved numerically. This is only one type of regularization. We can always come up with different regularization procedures. We will see more about regularization in later chapters.

In order to obtain an effective potential valid at low momentum, we shall look at the following form for the separable model potential, which reproduces the attractive and the repulsive features of a real nucleon-nucleon potential

$$V_{\rm bare}(k',k) = \frac{g}{(k'^2+m^2)^n}\left(-\frac{g}{(k^2+m^2)^n}+\frac{\alpha g(k^2+m^2)^n}{(k^2+\eta^2m^2)^{2n}}\right). \tag{2.59}$$

For the diagonal matrix elements,

$$V_{\rm bare}(k,k) = -\frac{g^2}{(k^2+m^2)^{2n}}+\frac{\alpha g^2}{(k^2+\eta^2m^2)^{2n}}, \tag{2.60}$$

where we can clearly see the attractive and repulsive piece. The parameters appearing in the model are fitted to reproduce the essential features of the phase shift ($^1S_0$) such

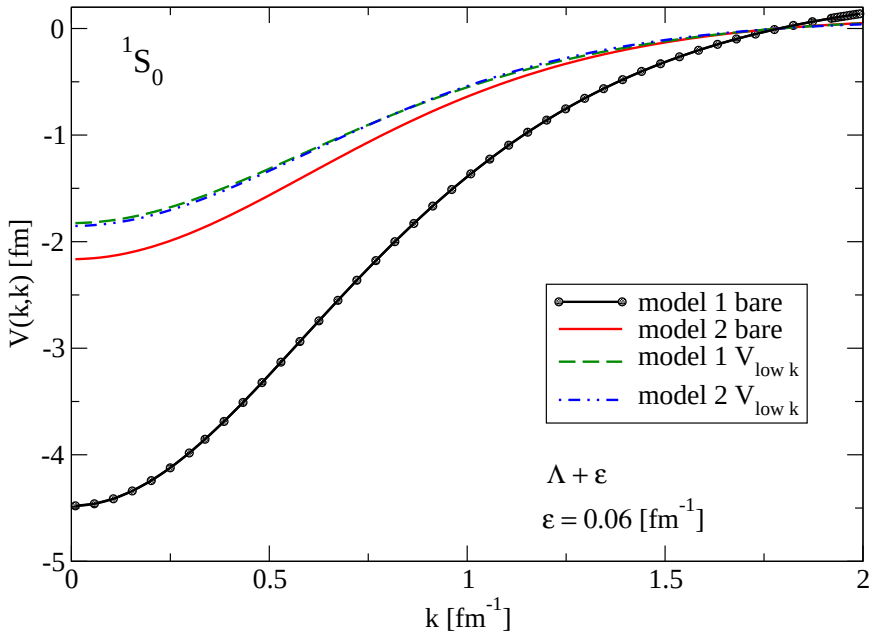

Figure 2.2: The diagonal matrix elements of model 1 and 2 and corresponding $V_{\text{low}\,k}$ in the $^1S_0$ channel $\Lambda = 2.0\,\text{fm}^{-1}$. We see that both potential models collapse on to *nearly* the same $V_{\text{low}\,k}$ [32, 34, 35].

as the low momentum behavior, and the point where the phase shift changes sign, corresponding to the potential becoming repulsive. This fitting is done up to lab engeries $E_{lab} \leq 350\,\text{MeV}$. The parameter values for the three separable models are given in Table (2.3).

The figure (2.2) shows the diagonal matrix elements of models 1 and 2. The initial cut-off is fixed at a sufficiently large value Λ_0, such that,

$$V_{\text{bare}}(\Lambda_0, \Lambda_0) \approx 0. \tag{2.61}$$

The initial condition of the R.G. equation is given by,

$$V_{\text{low}\,k}(k, k; \Lambda_0) = V_{\text{bare}}(k, k). \tag{2.62}$$

We integrate out momenta lying in the region between the cut-off Λ and $\Lambda - d\Lambda$, to obtain new $V_{\mathrm{low}\,k}(k,k)$. Using this as the set of initial conditions we repeat the same procedure until we reach a cut-off of $\Lambda_{min} = 2.0\,\mathrm{fm}^{-1}$, corresponding to lab energies of $E_{\mathrm{lab}} \leq 350\,\mathrm{MeV}$.

The phase shifts for the l^{th} partial wave are related to the on-shell T matrix in the uncoupled channel as follows:

$$\delta_l(k^2) = -\frac{1}{k} T_l(k', k; k^2). \tag{2.63}$$

The figure (2.3) shows that the phase shifts are reproduced for the simple model potentials, which is expected by construction.

Next we look at the diagonal matrix elements for the model potentials given in figure (2.2). We see that they collapse onto the same *unique* $V_{\mathrm{low}\,k}$ curve for $\Lambda \leq 2.0\,\mathrm{fm}^{-1}$, which implies that the low-momentum effective potential is model independent for *a* particular regularization procedure. This collapse is not unexpected as now the low-momentum potential contains only the long-distance physics, as all the short-distance model dependent details have been integrated out.

In this section we have derived the R.G. equation and demonstrated how it can be implemented practically. This way of directly solving the R.G. equation is only one of the ways to get the effective potentials. There exist the KLR folded diagram techniques and the Lee Suzuki transformations, which also give the effective potential [35]. This will be derived briefly in the appendices. The figure (2.4) shows the collapse for the various high-precision potentials (figure taken from [32]). Notice that $V_{\mathrm{low}\,k}$ has only low-momentum matrix elements. This results in smaller model spaces in many-body calculations, which actually make them more tractable.

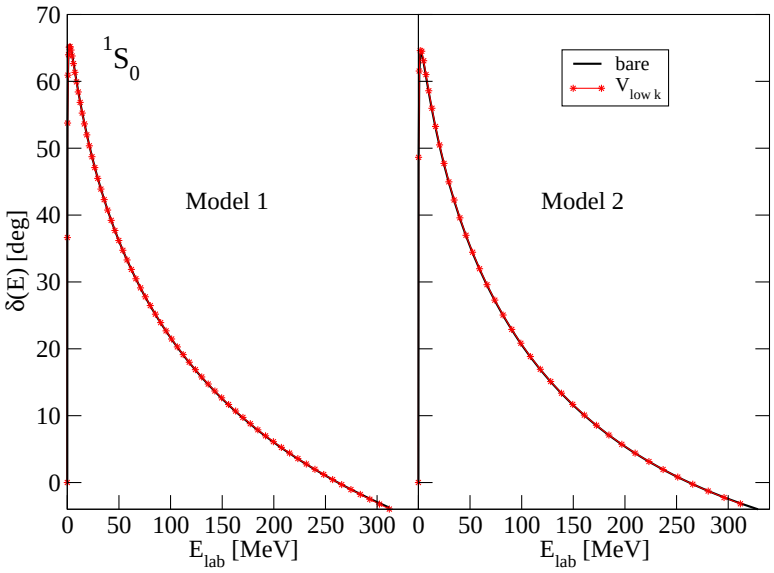

Figure 2.3: Phase shifts for models 1 and 2 as a function of lab energies. Note that the phase shifts are preserved in the RG evolution.

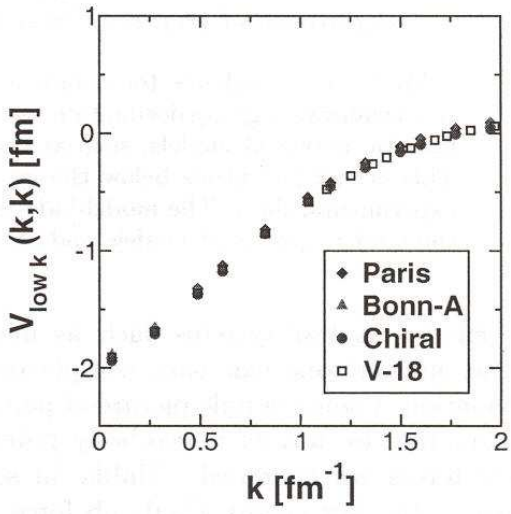

Figure 2.4: This is a plot of diagonal matrix elements of $V_{\mathrm{low}\,k}$ versus k for the various nucleon-nucleon potentials in the $^1S_0$ channel for $\Lambda = 2.0\,\mathrm{fm}^{-1}$. We clearly see a *nearly* unique $V_{\mathrm{low}\,k}$ [35]

CHAPTER 3

EFT AND $V_{\text{low } k}$

In this chapter, we review the idea of an effective field theory (EFT) following references [7, 4, 6, 5], and explore the connection between the renormalization group approach and traditional EFTs.

3.1 Effective Field Theory

We begin our discussion of effective field theories by looking at the following high-school problem [6]. Consider a body of mass m, at a height h above the surface of the earth. The mass and radius of the earth are M and R respectively. Then the gravitational potential energy difference at a height h above the earth's surface is given by:

$$\Delta U = mgh, \tag{3.1}$$

where g is the acceleration due to gravity. But from Newton's Theory of Gravitation, we know that the potential energy difference is given by:

$$\Delta U = -\frac{GMm}{r_f} + \frac{GMm}{r_i}, \tag{3.2}$$

where $r_{\text{i}} = R$ and $r_{\text{f}} = R + h$, so that equation (3.2) becomes:

$$\Delta U = -\frac{GMm}{R+h} + \frac{GMm}{R} \tag{3.3}$$

$$\Delta U = \frac{GMm}{R^2}\frac{Rh}{R+h}. \tag{3.4}$$

If $h \ll R$ then we can expand equation (3.4) as a series in $\frac{h}{R}$ as follows:

$$\Delta U = \frac{GMm}{R^2}h\left(1 - \frac{h}{R} + \frac{h^2}{R^2} + \cdots\right) \tag{3.5}$$

where $\frac{GMm}{R^2} = g$, so that equation (3.5) reads,

$$\Delta U = mgh\left(1 - \frac{h}{R} + \frac{h^2}{R^2} + \cdots\right). \tag{3.6}$$

We clearly see that the usual expression for the potential energy difference for a body of mass m, at a height h above the surface of the earth given by equation (3.1), is just the first term of the series given in equation (3.6). This series rapidly converges if $h \ll R$ and is the effective theory expansion for the gravitational potential energy difference.

The above is an example of a simple Effective Theory. Yet it illustrates the following key features of an Effective Field Theory (EFT). An EFT is a systematic expansion, which is valid in a limited domain. The rate of convergence, working in momentum space, depends on the smallness of the expansion parameter, which is usually a ratio of scales (small momentum scale p over a large scale Λ - also known as the breakdown scale). The expansion breaks down as the scale p of the problem approaches the breakdown scale Λ, as the series is no longer convergent. This problem also shows that the series usually contains an infinite number of terms. In an Effective Field theory, one would expect this feature of having an infinite number of terms for the lagrangian as pathological, as the theory becomes non-renormalizable. We will talk more about this issue in the following discussion.

An Effective Field Theory can be formally defined as a *low-energy approximation to a corresponding high energy theory* [6]. The construction of an EFT is based on the

following principle, that low-energy processes do not depend on the fine details of the high-energy physics. An EFT is set up by defining the lagrangian or the hamiltonian of the system of interest as a sum of long-range and short-range interaction terms. The long-range terms contain the long-distance physics explicitly. The short-distance terms are local interactions that mimic the effects of the short-distance physics from the high-energy theory. The exact form of these local terms does not affect the low-energy properties of the system.

In order to clarify this point, consider a probe of wavelength λ. Interactions which takes place on length scales less than λ can be replaced by localized interactions as the resolution is limited by the wavelength of the probe, or in momentum space the limit of resolution goes as $\frac{1}{p}$, where p is the momentum of the probe. Therefore a low-momentum probe cannot "see" the details of interactions on distance scales less than $\frac{1}{p}$. Using this idea, we replace the short-distance interactions by a series of local terms resulting in an expansion in powers of $\frac{p}{\Lambda}$, where p represents the momentum scale of the low-momentum interaction, and Λ is the scale beyond which the details of the short-distance interaction are resolved. Any term allowed by the symmetry of the underlying high-energy theory is present in the effective lagrangian. As mentioned earlier, the low-energy constants (which depend on the scale Λ) contain the essential high-energy physics. Further since the short-distance physics is encoded as an expansion in $\frac{p}{\Lambda}$, it is clear that this expansion and hence this representation of short-distance physics breaks down when the $\frac{p}{\Lambda} \approx \mathcal{O}(1)$.

Consider the following example where the effective hamiltonian H_{eff} (valid at low-energies) is given by [7]:

$$H_{\text{eff}} = T_{\text{kinetic}} + V_{\text{eff}}, \tag{3.7}$$

where

$$V_{\text{eff}} = V_L + V_S. \tag{3.8}$$

V_{eff} is the effective potential, which has the long-distance interaction grouped in the term V_L and purely short-distance physics is contained in the term V_S. Let us assume that the model potential is isotropic. Then all the short-distance physics contained in the term V_S looks like,

$$V_S(\mathbf{r}) = c\delta^3(\mathbf{r}) + d\nabla^2\delta^3(\mathbf{r}) + \cdots . \tag{3.9}$$

Note that this is consistent with the symmetry specified (isotropic potential), as only even powers of the derivatives appear. But this results in a potential that is too singular to be of any use. In momentum space, a delta function interaction of the type in equation (3.9) is a constant, and therefore high-momentum states enter a low-momentum calculation and in order for the above expansion to be meaningful, it has to be regulated. Let us focus for now on a simple cut-off, so that only states with momentum $k \leq \Lambda$ are explicitly included. This results in smeared-out delta-function interactions. The physics which lies beyond the scale Λ is included by changing the coupling constants.

Following Lepage's lectures [7], we smear out the delta function interaction over the scale $a = \dfrac{1}{\Lambda}$ so that,

$$\delta_a^3(\mathbf{r}) = \frac{e^{-r^2/2a^2}}{(2\pi)^{3/2}a^3}. \tag{3.10}$$

This leads to an effective potential:

$$V_{eff}(\mathbf{r}) = ca^2\delta_a^3(\mathbf{r}) + da^4\nabla^2\delta_a^3(\mathbf{r}) + \cdots . + ga^{n+2}\nabla^n\delta_a^3(\mathbf{r}) + \cdots \tag{3.11}$$

In momentum space equation (3.11) leads to an expansion in $\dfrac{p}{\Lambda}$ where Λ is the cut-off in momentum space corresponding to the position space cut-off a and p is the

momentum scale of the interaction process. Making the coefficients explicitly Λ or equivalently a dependent we get,

$$v_s(q^2) = c(\Lambda)v_s(0) + d_1(\Lambda)\frac{q^2}{\Lambda^2}v_s'(0) + \cdots \tag{3.12}$$

where $v_s(q^2)$ is the fourier transform of the position space potential. The exact value of the coupling is obtained either by fitting to experimental data (as in the case of strongly coupled theories) or by matching the EFT to the full theory at the scale Λ (valid for weakly-coupled theories). Recent advances suggest that it would be possible to match the coupling to lattice calculations in the future.

We note that the EFT lagrangian has an infinite number of local terms representing short-distance physics. So in the conventional sense it is not even renormalizable. The reason we can renormalize an effective field theory is because we can always truncate the expansion at a particular order $(\frac{q}{\Lambda})^n$, and this leads to an error of the order $(\frac{q}{\Lambda})^{n+1}$. Since we retain only order n terms (finite), the lagrangian can be renormalized. The concept of EFT has revolutionized these ideas of renormalizability [5].

We learn the following from an EFT approach:

1. The Lagrangian includes explicit long-distance terms.

2. Short-distance physics is described by local, renormalized terms, which are usually an expansion in powers of $\frac{p}{\Lambda}$, where p is the low-momentum or mass scale and Λ is the breakdown scale of the effective field theory.

3. The effect of high-momentum states is encoded in the low-energy constants.

As mentioned in the chapter (1), nuclear EFTs (Chiral Effective Field theory [16]-[25]), the typical momentum scale is of the order of the pion mass m_π. The breakdown scale is around $\Lambda_\chi \approx 700\,\mathrm{MeV} - 1\,\mathrm{GeV}$, where the lower limit corresponds to

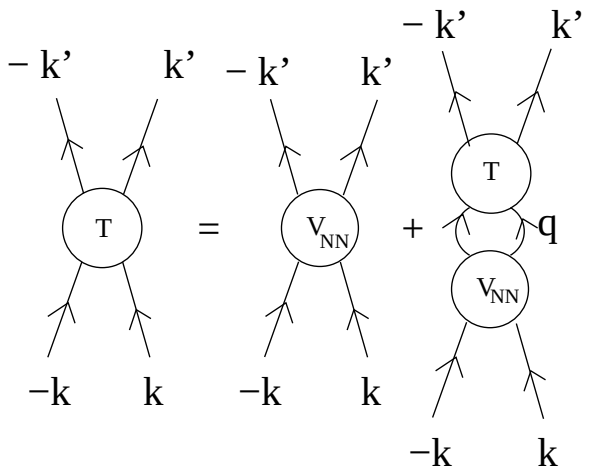

Figure 3.1: The full two-nucleon amplitude T_{NN} as an iteration of the two-nucleon scattering potential V_{NN}. We see that the intermediate states can take all values. So these states include both high and low energy processes.

the scale at which heavier hadrons begin to get resolved. Therefore, working at low-momenta, the suitable degrees of freedom are pions and nucleons. Chiral Effective Theory has been very successful in treating low-energy nuclear systems as discussed in these references [7, 8], [18] - [24].

3.2 RG approach

The Renormalization Group approach to the nucleon-nucleon interaction used here starts with the Lippmann-Schwinger equation for the T matrix. Using any of the standard two-nucleon potentials (bare potential) as input, the intermediate states are cut-off at some high value Λ_0 (bare cut-off). Requiring the invariance of the half off-shell (HOS) T matrix elements leads to a set of coupled first-order differential equation for the potential with respect to the cut-off Λ. The bare potential

is the initial condition when $\Lambda = \Lambda_0$. The RG approach in schematically shown in figures (3.1) and (3.2).

The renormalization group procedure results in a new potential which is the low-momentum effective potential. Successively solving the RG equation, where the cut-off is lowered at each step, amounts to integrating out more and more of the short-distance interactions, until finally we are left with mostly long-distance physics ($\Lambda \approx 2.1\,\mathrm{fm}^{-1}$). At this scale Λ, all theories with the same low-momentum behaviour are equivalent, irrespective of the details of the high-energy interaction. Since the low and high momentum spaces no longer couple, a low-momentum process involves only long-distance physics. This decoupling results in smaller model spaces in many-body calculations. At this point it is appropriate to comment that the decoupling in this RG approach occurs through setting high-momentum matrix elements to zero by construction while modifying low-momentum matrix elements to keep the low-energy

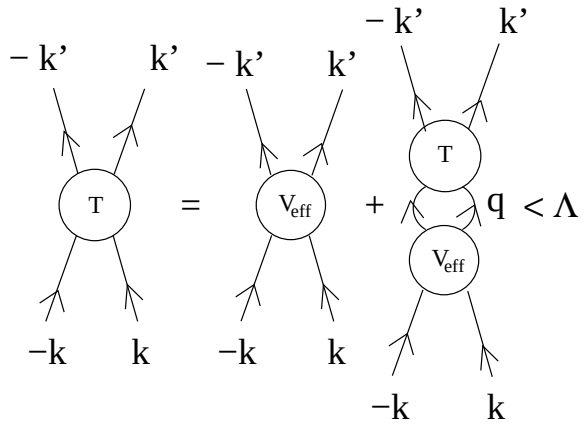

Figure 3.2: The effective two-nucleon amplitude T as an iteration of the effective two-nucleon scattering potential $V_{\mathrm{low}\,k}$. Note the restriction on intermediate states, as a result these intermediate states now include only low-energy processes.

physics invariant. This is just one way of decoupling low and high momentum modes. Other methods do exist [46] and we will discuss this briefly in Appendix.

3.3 The connection

Though the philosophies of the RG approach and EFT are the same, we see that their implementation is rather different. In RG we start with the high-momentum theory (or model interaction) and obtain the low-momentum theory by successively decimating down to the low-momentum scale. This is a non-perturbative approach, that is, this procedure results in summing all terms in an EFT expansion at each step, the expansion parameter being p and m_π over Λ. On the other hand in nuclear EFTs, we start with a theory valid at low-energies, consistent with the symmetries of the problem, and match the low-energy constants with the high-energy theory (or data). Going to higher orders in the expansion includes many-body effects automatically (part of the power-counting), while in an RG approach, we need to start with the $2N$ and $3N$ potential and simulataneously run to lower $\Lambda \approx 2.1\,\mathrm{fm}^{-1}$ in order to get Λ independent results in a many-body calculation. Both the techniques lead to a theory valid at low-energies which are in fact more useful than the corresponding full theory at that range of energies.

We may wonder if there exists a common point between these two different approaches [54]. There exists one for sure! Let us look at diagonal elements of $V_{\mathrm{low}\,k}$ compared to the other potential models (Bonn, Nijmegen, Paris..) in figure (3.3) (figure taken from [32]). Here we see that below a certain k value ($k \leq 2fm^{-1}$), where only long-distance intermediate states exist as all the short-distance physics has been integrated out, we can observe a constant shift in the potential, close to the origin.

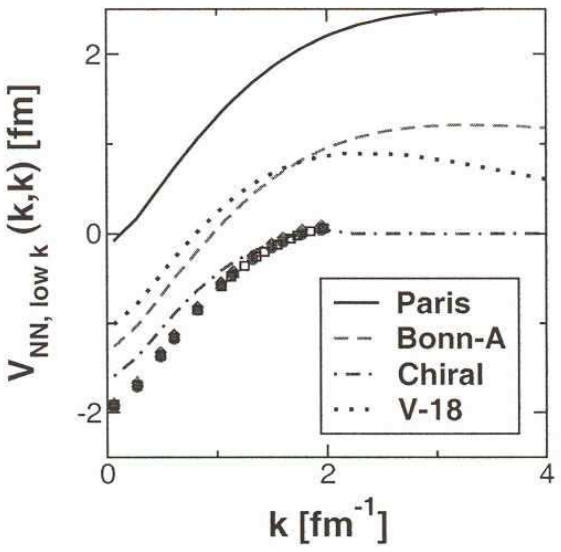

Figure 3.3: The diagonal matrix elements of V_{NN} and $V_{\mathrm{low}\,k}$ for the various model potentials in the ${}^1S_0$ channel. The dark dots represent the low-momentum potential $V_{\mathrm{low}\,k}$ for $\Lambda = 2.0\,\mathrm{fm}^{-1}$. We see that all the potential models nearly collapse on to the same $V_{\mathrm{low}\,k}$. [32, 34, 35]

This constant shift in k space corresponds to a smeared delta-function-type term in position space. That is exactly what an EFT does for us! It obtains an expression for the low-energy interaction, taking into account the short-distance physics in the form of a perturbative expansion of the contact interactions. So the RG evolution results in an infinite series of counter terms consistent with the input interactions. In fact we can write the following algebraic expression for $V_{\mathrm{low}\,k}$:

$$V_{\mathrm{low}\,k}(k', k) = PV_{\mathrm{NN}}(k', k)P + V_{\mathrm{counter}}(k', k) \tag{3.13}$$

where we have supressed the l^{th} partial wave label and $P = \sum_{k<\Lambda} |k\rangle\langle k|$ is the projection operator to project on to the low-momentum states. We can expand

$V_{\rm counter}(k',k)$ as follows [54] in the partial wave basis:

$$V^{ll'}_{\rm counter}(k',k) = q^l q^{l'} \left[C_0 + C_2(q^2+q'^2) + C_4(q^2+q'^2)^2 + C_6(q^6+q'^6) + C'_4 q^2 q'^2 + \cdots \right]. \tag{3.14}$$

The counter terms in the above equation can be determined such that the difference between $V_{\rm low\,k}$ and $PV_{\rm NN}P + V_{\rm counter}$ is minimized. This expression clearly demonstrates that the long-distance part of the interaction is the bare interaction ($V_{\rm NN}$) projected on to the low-momentum states. The short-distance physics is included via the counter terms which are the determined by matching to the two-body data (elastic phase shifts and binding energy). Both these steps are automatically included in the $V_{\rm low\,k}$ running using T matrix invariance.

In an EFT approach, the accuracy of the low-momentum calculation can be improved systematically by including more terms in the lagrangian. In an RG approach, the low-momentum interaction contains all the terms required to preserve the corresponding low-momentum observables as discussed above. Any additional cut-off dependence can be linked to "missing" physics. For instance using just the two-body low-momentum potential, which reproduces two-body scattering data in free-space, for calculating bulk properties in-medium leads to Λ dependent results. This is due to the fact that in-medium there are many-body forces which have to be taken into account. So far we do not have a framework for running two and three-body interactions simultaneously. So currently the three-body force is approximated by fitting to the leading-order $3N$ force from chiral EFT [37]. In an EFT framework, many-body forces are introduced naturally. For example if we consider interaction between three bodies, at low-energies we cannot resolve the details of the high-energy interaction,

so the three-body potential looks like a contact interaction of the type

$$V_{3\mathrm{N}}(x_1, x_2, x_3) = \delta(x_1 - x_2)\delta(x_2 - x_3)\delta(x_1 - x_3). \tag{3.15}$$

Conventional Potentials have high-momentum states built-in through "explicit" modeling of the short-distance physics. From an EFT point of view, these details do not improve our understanding of short-distance physics, but only complicate low-momentum calculation by including high-momentum states (as these potentials model the "hard-core" explicitly). The difference between conventional potential models and EFT based interactions is that the latter systematically decouples the low and high-momentum modes, thereby eliminating the dependence on the details of the short-distance interactions. This decoupling is achieved by expanding the short-distance interaction as a series in $\frac{p}{\Lambda}$ times a renormalized local term. In an RG approach, where we use these potentials as a starting point, the short-distance details are traded for a low-monentum potential, which is not singular. Renormalization group based potentials are a class of low-momentum potentials where the freedom in defining short-distance terms in a conventional EFT, now translates into defining hermitization procedures and regularizations, as will be seen in subsequent chapters.

CHAPTER 4

REGULATOR DEPENDENCE OF $V_{\mathrm{low}\,k}$ POTENTIALS

The motivation to investigate the regulator dependence of $V_{\mathrm{low}\,k}$ potentials arises from the necessity to understand the numerical artifacts while solving for $V_{\mathrm{low}\,k}$ in free-space. Once the free-space running is in control, the potential can be used in-medium, that is for finite nuclei and nuclear many-body calculations. This chapter explores the regulator dependence of the renormalization-group-based low-momentum potentials. We first study the sharp regulator encountered in chapter 2, section (2.2). Then we generalize the renormalization group equations to accomodate smooth regulators [40], both in an energy-independent and energy-dependent scheme. The latter requires an additional step of transforming the energy dependence for momentum dependence. It turns out that smooth regulators are more advantageous than sharp regulators, as can be seen in simple variational calculation of few-body systems [38, 39], where the former choice improves convergence. We shall discuss these results in detail.

4.1 Sharp regulator and $V_{\mathrm{low}\,k}$

The renormalization group equation as seen in chapter 2 is by equation (2.46) as:

$$\frac{dV_{\mathrm{low}\,k}(k',k)}{d\Lambda} = \frac{2}{\pi}\frac{V_{\mathrm{low}\,k}(k',\Lambda)T(\Lambda,k;\Lambda^2)}{1-(\frac{k}{\Lambda})^2}, \tag{4.1}$$

where $T(\Lambda, k, ; \Lambda^2)$ is the left-on shell T matrix element, which is given by the following equation:

$$T(\Lambda, k; \Lambda^2) = V_{\text{low}\,k}(\Lambda, k) + \mathcal{P}\frac{2}{\pi}\int_0^\Lambda q^2 dq \frac{T(\Lambda, q; \Lambda^2) V_{\text{low}\,k}(q, k)}{\Lambda^2 - q^2}. \tag{4.2}$$

The above equation (4.2) can be easily obtained by taking the transpose of the T matrix integral equation and making it on-shell at $k = \Lambda$. As discussed in sections (2.2) and (2.3), we solve for $V_{\text{low}\,k}(k', k)$ on a momentum grid. We start with the bare potential V_{bare} (initial condition) at some initial cut-off Λ_0, so that,

$$V_{\text{low}\,k}(k', k)|_{\Lambda_0} = V_{\text{bare}}(k', k)|_{\Lambda_0}, \tag{4.3}$$

where the initial cut-off Λ_0 is determined such that,

$$V_{\text{bare}}(\Lambda_0, \Lambda_0) \approx 0. \tag{4.4}$$

The differential equation (4.1) is solved for a small change in Λ, so that we get $V_{\text{low}\,k}(k', k)$ at a new Λ', where

$$\Lambda' = \Lambda - d\Lambda. \tag{4.5}$$

This process is continued so that at each step we get $V_{\text{low}\,k}(k', k)$ at a lower value of the cut-off Λ. This process results in integrating out the model-dependent high-momentum states in stages, until we are left with long-distance physics, when we reach the final cut-off $\Lambda \approx 2.0 - 2.1\,\text{fm}^{-1}$. Note that in this process we need to solve for the left on-shell T matrix element given by equation (4.2) at each step.

We had noted that using a separable form for the bare potential $V_{\text{bare}}(k', k)$ given by equations (2.48), (2.59) and (2.60), simplifies the T matrix equation (4.2) and is given by:

$$T(\Lambda, k; \Lambda^2) = \frac{2}{\pi}\frac{V_{\text{low}\,k}(\Lambda, k)}{1 + \mathcal{P}\frac{2}{\pi}\int_0^\Lambda q^2 dq \frac{V_{\text{low}\,k}(q, q)}{q^2 - \Lambda^2}}. \tag{4.6}$$

The separable potential we introduced in section (2.2) reproduce all the essential features of NN interaction, that is, phase shifts and deuteron binding energy. But NN potentials in general are not separable. As a result, we no longer get a nice closed form for the T matrix equation as seen in equation (4.6). In general, we would have to solve an integral equation for the T matrix (equation (4.2)) and use this to calculate $V_{\mathrm{low}\,k}(k', k)$.

Note that equations (4.2) and (4.6) have an ill-defined principal value integral, namely a pole at the end point of the principal value integration. As a result we need to regulate this principal value integral. This is done by either pushing the pole into or out of the range of integration, i.e.,

$$\Lambda_{\mathrm{reg}} = \Lambda(1 \pm \epsilon), \tag{4.7}$$

$$\Lambda_{\mathrm{reg}} = \Lambda \pm \epsilon. \tag{4.8}$$

where Λ_{reg} is the regulated value of the cut-off and ϵ is a small number ($0 \leq \epsilon \leq 1$). Equation (4.7) refers to a multiplicative regulator while equation (4.8) is an additive regulator. We also ensure that Λ does not coincide with any of the grid points k_{i}. This means that k_{max}, which is the maximum value of the k grid, is less than Λ by a small quantity ϵ'. As a result, the term $1 - \left(\frac{k}{\Lambda}\right)^2$ becomes $1 - \left(\frac{k}{\Lambda(1+\epsilon')}\right)^2$. The pole piece inside the integral becomes $(q^2 - \Lambda_{\mathrm{reg}}^2)$. Using the regulated value of Λ, we get the following RG equation,

$$\frac{dV_{\mathrm{low}\,k}(k', k)}{d\Lambda} = \frac{2}{\pi} \frac{V_{\mathrm{low}\,k}(k', \Lambda) T(\Lambda, k; \Lambda^2)}{1 - \dfrac{k^2}{(\Lambda_{\mathrm{reg}})^2}}, \tag{4.9}$$

and the left-on shell T matrix equation (4.2) now becomes:

$$T(\Lambda, k; \Lambda^2) = V_{\mathrm{low}\,k}(\Lambda, k) + \frac{2}{\pi} \mathcal{P} \int_0^{\Lambda} q^2 dq \frac{T(\Lambda, q; \Lambda^2) V_{\mathrm{low}\,k}(q, k)}{\Lambda_{\mathrm{reg}}^2 - q^2}. \tag{4.10}$$

where for practical purposes we do not distinguish for between ϵ and ϵ', so that $\Lambda_{\rm reg}$ represents the regulated value of Λ and also ensures that the cut-off Λ does not lie directly on top of any grid points $k_{\rm i}$.

We will now analyze the error introduced in the left-on shell T matrix elements for the sharp regulation schemes given in equations (4.7) and (4.8). Since the left-on shell T matrix elements appears in the RG differential equation, this error propagates to $V_{{\rm low}\,k}$ and finally the phase shifts. We first look at regulators which shift the pole outside the range of integration i.e.

$$\Lambda_{\rm reg} = \Lambda(1+\epsilon), \tag{4.11}$$

$$\Lambda_{\rm reg} = \Lambda+\epsilon. \tag{4.12}$$

as a result we no longer have a principal value integral in the T matrix equation. Let us define the following change of variable: $\Lambda' = \Lambda+\epsilon$, then the T matrix equation (4.10) reads:

$$T(\Lambda,k;\Lambda^2) = V_{{\rm low}\,k}(\Lambda,k) + \frac{2}{\pi}\int_0^{\Lambda'-\epsilon} q^2dq\frac{T(\Lambda,q;\Lambda^2)V_{{\rm low}\,k}(q,k)}{\Lambda'^2-q^2} + \mathcal{O}(\epsilon). \tag{4.13}$$

Differentiating the above equation with respect to ϵ we get,

$$\frac{dT(\Lambda,k;\Lambda^2)}{d\epsilon} = -\frac{2}{\pi}\frac{(\Lambda'-\epsilon)^2T(\Lambda,\Lambda'-\epsilon;\Lambda^2)V_{{\rm low}\,k}(\Lambda'-\epsilon,k')}{\Lambda'^2-(\Lambda'-\epsilon)^2} + C'. \tag{4.14}$$

$$\frac{dT(\Lambda,k;\Lambda^2)}{d\epsilon} = \frac{2}{\pi}\frac{\Lambda^2}{2\epsilon\Lambda}T(\Lambda,\Lambda;\Lambda^2)V_{{\rm low}\,k}(\Lambda,k') + C'. \tag{4.15}$$

where C' is a constant. As $\epsilon\to 0$, the $1/\epsilon$ term dominates. Therefore

$$\frac{dT(\Lambda,k;\Lambda^2)}{d\epsilon} = \frac{2}{\pi}\frac{\Lambda}{2\epsilon}T(\Lambda,\Lambda;\Lambda^2)V_{{\rm low}\,k}(\Lambda,k') \tag{4.16}$$

$$\Rightarrow \lim_{\epsilon\to 0} T(\Lambda,k;\Lambda^2) \sim C\log(\epsilon). \tag{4.17}$$

where C is a constant.

Let us check the ϵ dependence for the other type of regulator: $\Lambda_{\rm reg} = \Lambda \to \Lambda(1+\epsilon)$. Note that in this regularization ϵ is a dimensionless quantity, while in the previous type of regularization: $\Lambda \to \Lambda + \epsilon$, ϵ has the same dimension as Λ, which has dimensions of momentum. The equation for the T matrix reads:

$$T(\Lambda, k; \Lambda^2) = V_{\text{low}\,k}(\Lambda, k) + \frac{2}{\pi}\int_0^{\Lambda} q^2 dq \frac{T(\Lambda, q; \Lambda^2) V_{\text{low}\,k}(q, k)}{(\Lambda(1+\epsilon))^2 - q^2}. \tag{4.18}$$

We introduce the following change of variables:

$$\Lambda' = \Lambda(1+\epsilon). \tag{4.19}$$

So the T matrix equation (4.18) with the above change of variables now becomes

$$T(\Lambda, k; \Lambda^2) = V_{\text{low}\,k}(\Lambda, k) + \frac{2}{\pi}\int_0^{\frac{\Lambda'}{(1+\epsilon)}} q^2 dq \frac{T(\Lambda, q; \Lambda^2) V_{\text{low}\,k}(q, k)}{(\Lambda')^2 - q^2} + \mathcal{O}(\epsilon). \tag{4.20}$$

Now differentiating the above equation (4.20) with respect to ϵ we get,

$$\frac{dT(\Lambda, k; \Lambda^2)}{d\epsilon} = \frac{2}{\pi}\left(\frac{\Lambda'}{1+\epsilon}\right)^2 \frac{T(\Lambda, \Lambda'/(1+\epsilon); \Lambda^2) V_{\text{low}\,k}(\Lambda'/(1+\epsilon), k)}{\Lambda'^2 - (\frac{\Lambda'^2}{1+\epsilon})^2}\left(-\frac{\Lambda'}{(1+\epsilon)^2}\right) + C'. \tag{4.21}$$

$$\frac{dT(\Lambda, k; \Lambda^2)}{d\epsilon} = -\frac{\Lambda'}{\pi}\frac{1}{\epsilon} T(\Lambda, \Lambda; \Lambda^2) V_{\text{low}\,k}(\Lambda, k) + C'. \tag{4.22}$$

As $\epsilon \to 0$ the $1/\epsilon$ dominates, so that

$$\frac{dT(\Lambda, k; \Lambda^2)}{d\epsilon} = -\frac{\Lambda(1+\epsilon)}{\pi}\frac{1}{\epsilon} T(\Lambda, \Lambda; \Lambda^2) V_{\text{low}\,k}(\Lambda, k). \tag{4.23}$$

$$\Rightarrow \lim_{\epsilon \to 0} T(\Lambda, k; \Lambda^2) \sim C \log(\epsilon). \tag{4.24}$$

where C is a constant independent of ϵ. Again we note the the relative error has a logarithmic dependence on ϵ analogous to equation (4.17).

Next we want to look at an entirely different regularization. Consider the following regularization scheme:

$$\Lambda \to \Lambda - \epsilon. \tag{4.25}$$

In this scheme we note the following: (1) the pole has now been shifted inside the range of integration which goes from 0 to Λ and (2) ϵ has the same dimensions as Λ. Consider the left on-shell T matrix equation with Λ_{reg} given by the above regulator.

$$T(\Lambda, k; \Lambda^2) = V_{\text{low}\,k}(\Lambda, k) + \mathcal{P}\frac{2}{\pi}\int_0^\Lambda q^2 dq \frac{T(\Lambda, q; \Lambda^2) V_{\text{low}\,k}(q, k)}{(\Lambda - \epsilon)^2 - q^2}. \tag{4.26}$$

Note that the integral in equation (4.26) is a principal value integral. Following the standard trick in evaluating a principal value integral, we add and subtract a piece:

$$\int_0^\Lambda dq (\Lambda - \epsilon)^2 \frac{T(\Lambda, \Lambda - \epsilon; \Lambda^2) V_{\text{low}\,k}(\Lambda - \epsilon, k)}{(\Lambda - \epsilon)^2 - q^2} \tag{4.27}$$

to the above integral equation. As a result we get,

$$\begin{aligned} T(\Lambda, k; \Lambda^2) &= V_{\text{low}\,k}(\Lambda, k) \\ &+ \frac{2}{\pi}\int_0^\Lambda dq \left[\frac{q^2 T(\Lambda, q; \Lambda^2) V_{\text{low}\,k}(q, k) - (\Lambda - \epsilon)^2 T(\Lambda, \Lambda - \epsilon; \Lambda^2) V_{\text{low}\,k}(\Lambda - \epsilon, k)}{(\Lambda - \epsilon)^2 - q^2}\right] \\ &+ \frac{2}{\pi} T(\Lambda, \Lambda - \epsilon; \Lambda^2) V_{\text{low}\,k}(\Lambda - \epsilon, k)(\Lambda - \epsilon)^2 \mathcal{P}\int_0^\Lambda dq \frac{1}{(\Lambda - \epsilon)^2 - q^2}. \end{aligned} \tag{4.28}$$

After evaluating the principal value integral appearing in the second term of the equation (4.28), we get the following equation for the left on-shell T matrix,

$$\begin{aligned} T(\Lambda, k; \Lambda^2) &= V_{\text{low}\,k}(\Lambda, k) \\ &+ \frac{2}{\pi}\int_0^\Lambda dq \left[\frac{q^2 T(\Lambda, q; \Lambda^2) V_{\text{low}\,k}(q, k) - (\Lambda - \epsilon)^2 T(\Lambda, \Lambda - \epsilon; \Lambda^2) V_{\text{low}\,k}(\Lambda - \epsilon, k)}{(\Lambda - \epsilon)^2 - q^2}\right] \\ &+ \frac{2}{\pi}\frac{T(\Lambda, \Lambda - \epsilon; \Lambda^2) V_{\text{low}\,k}(\Lambda - \epsilon, k)(\Lambda)}{2} \log\left|\frac{2\Lambda}{\epsilon} - 1\right|. \end{aligned} \tag{4.29}$$

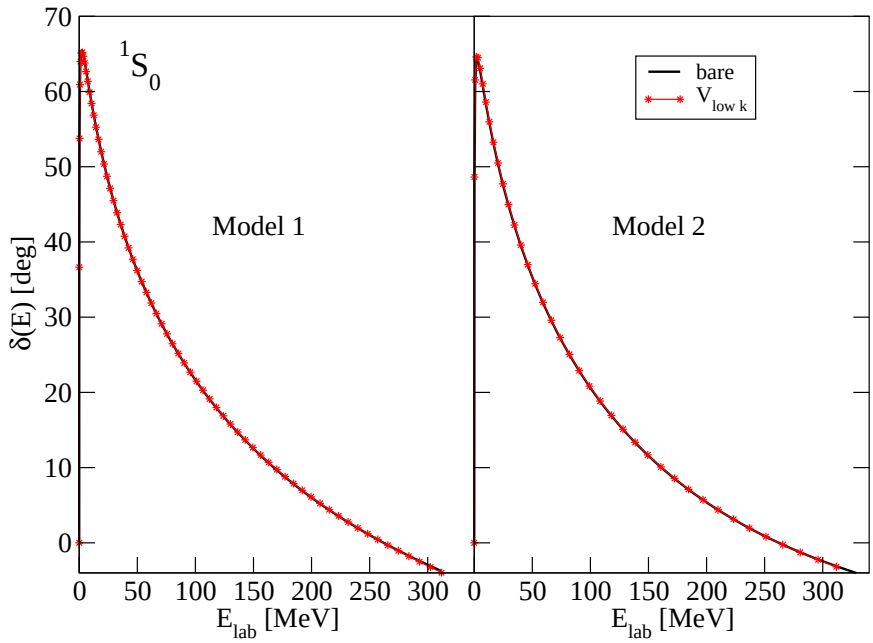

Figure 4.1: $^1S_0$ phase shifts for model 1 and model 2 for parameterizations given in chapter 2, table (2.3).

Next we define the following change of variable: $\Lambda' = \Lambda - \epsilon$, so that the T matrix equation (4.29) now becomes

$$\begin{aligned} T(\Lambda, k; \Lambda^2) &= V_{\text{low}\,k}(\Lambda, k) \\ &+ \frac{2}{\pi} \int_0^{\Lambda'+\epsilon} dq \left[\frac{q^2 T(\Lambda, q; \Lambda^2) V_{\text{low}\,k}(q, k) - (\Lambda')^2 T(\Lambda, \Lambda; \Lambda^2) V_{\text{low}\,k}(\Lambda, k)}{(\Lambda')^2 - q^2} \right] \\ &+ \frac{2}{\pi} \frac{T(\Lambda, \Lambda; \Lambda^2) V_{\text{low}\,k}(\Lambda, k)(\Lambda)}{2} \log \left| \frac{2\Lambda}{\epsilon} - 1 \right| + \mathcal{O}(\epsilon). \end{aligned} \tag{4.30}$$

Now differentiating the above equation with respect to ϵ, the terms in the integral vanish to zeroth order in ϵ, so that

$$\frac{dT(\Lambda, k; \Lambda^2)}{d\epsilon} = -\frac{1}{\epsilon} \frac{1}{\pi} T(\Lambda, \Lambda; \Lambda^2) V_{\text{low}\,k}(\Lambda, k) + C'. \tag{4.31}$$

$$\Rightarrow \lim_{\epsilon \to 0} T(\Lambda, k; \Lambda^2) = C \log \epsilon. \tag{4.32}$$

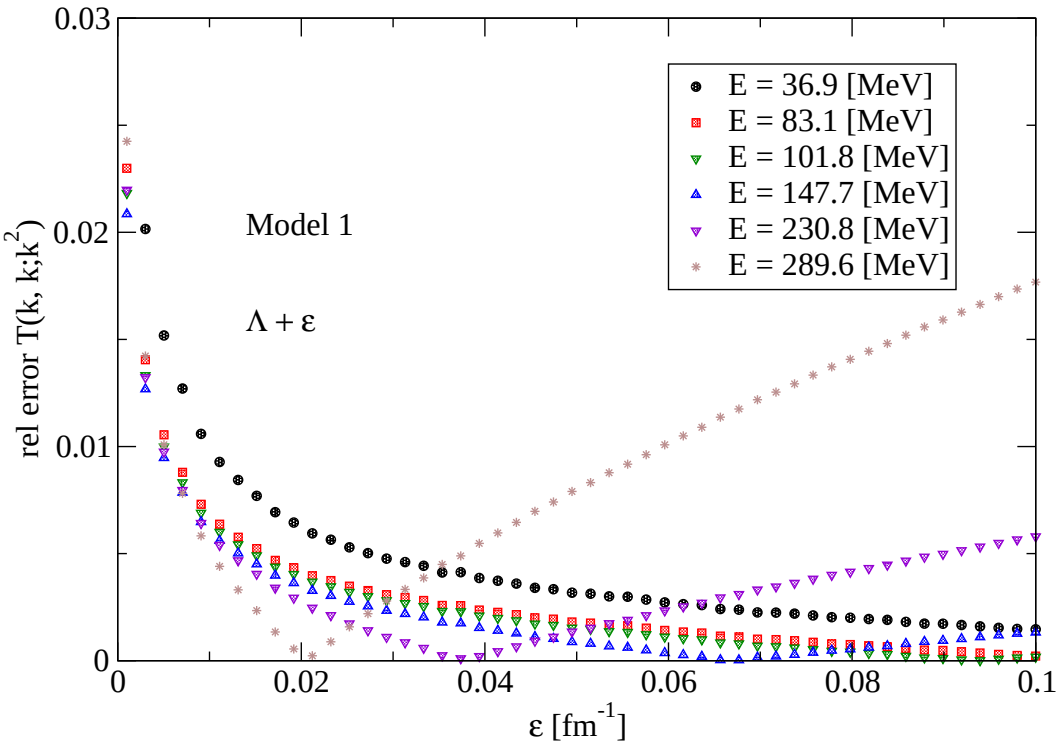

Figure 4.2: Relative Error in T matrix as a function of ϵ for model 1 parametrized in chapter 2, table (2.3). Notice that for small values of ϵ, the log term domintes and the error increases, while it is linear for larger values of ϵ.

Once again we note that the left-on shell T matrix elements have a logarithmic dependence on ϵ. Next we solve for $V_{\text{low}\,k}$ for the separable potentials defined in section (2.2) by equations (2.48), (2.59) and (2.60) using the sharp regulator and one of the choices for Λ_{reg} given in equations (4.7) and (4.8) and will study how the ϵ dependence of the left-on shell T matrix elements propagate to the physical observables, namely the phase shifts.

Figure (4.1) shows the $^1S_0$ phase shift as a function of lab energy E_{lab} for model potentials 1 and 2. The phase shifts calculated using V_{bare} and $V_{\text{low}\,k}$ potentials are

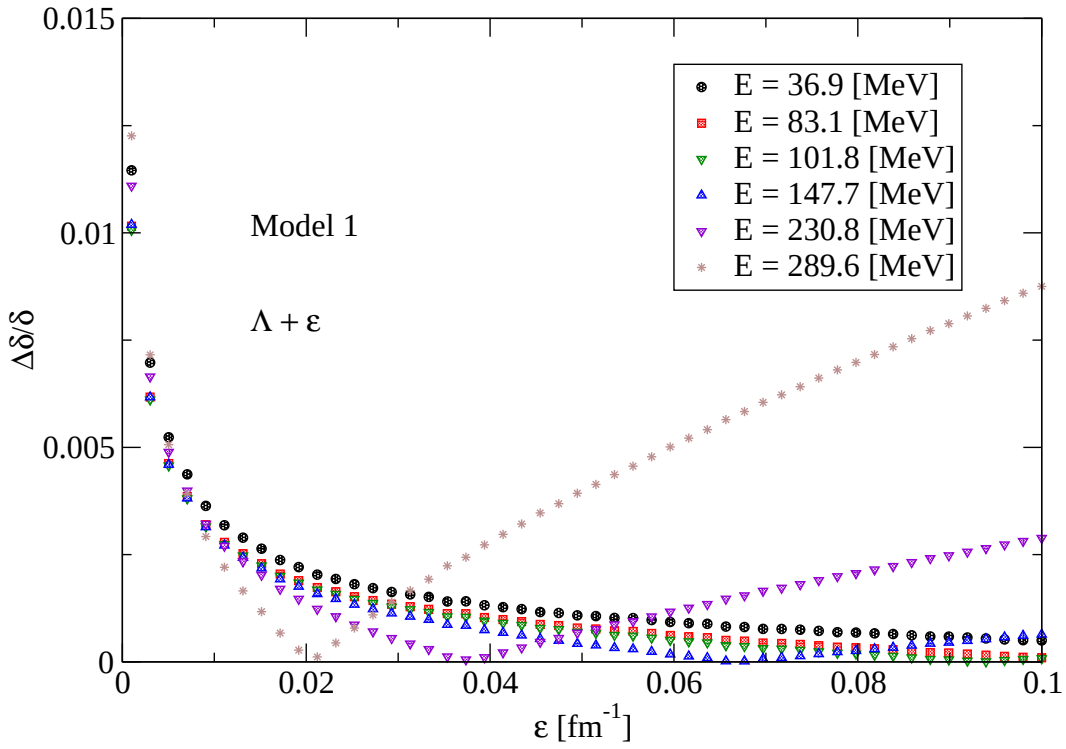

Figure 4.3: Relative Error in the phase shifts as a function of ϵ for model 1. The ϵ dependence of the phase shifts is similar to that of the diagonal T matrix elements.

in close agreement. The "closeness" of this agreement is explored in figure (4.2), where we look at the diagonal on-shell T matrix elements at fixed values of energy ($E_{\rm lab} = k^2$) as a function of ϵ. We define the relative error in preserving the on-shell T matrix elements during the RG evolution as

$$\Delta T_{\rm rel}(k,k;k^2) = \frac{T_{\rm NN}(k,k;k^2) - T_{{\rm low}\,k}(k,k;k^2)}{T_{\rm NN}(k,k;k^2)}. \tag{4.33}$$

At any energy, there is always a range of ϵ where the relative error in the diagonal T elements is a linear function of ϵ. At lower values of ϵ, the relative error increases due to the logarithmic dependence of the left on-shell T matrix elements on ϵ. The value of ϵ, at which the logarithmic term dominates is dependent on energy. For low

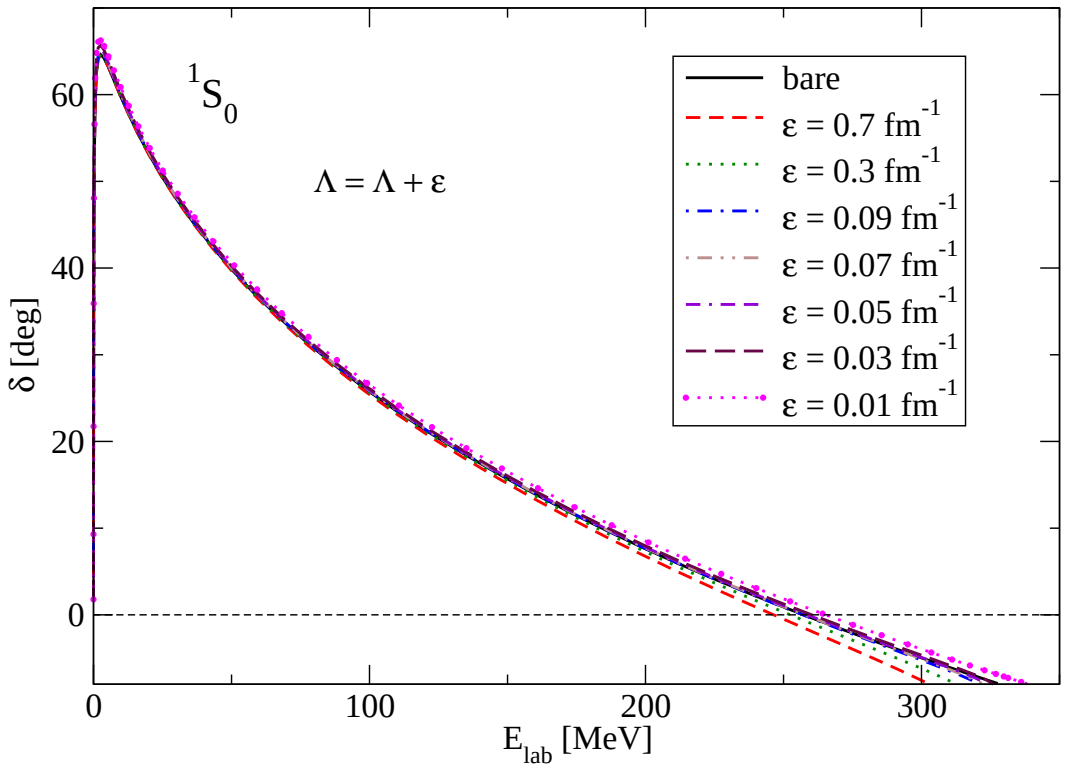

Figure 4.4: Bare and $V_{\mathrm{low}\,k}$ phase shifts for the $^1S_0$ channel of the Argonne v_{18} potential [31] as a function of lab energies E_{lab} for a particular choice of the sharp regulator, parametrized by the value of ϵ. $\epsilon \leq 0.01\,\mathrm{fm}^{-1}$ results in increased errors in reproducing the phase shifts.

energies, which are far below the cut-off Λ, the only sharp cut-off artifact is the ϵ dependence of the left-on shell T matrix elements and therefore we see an increase in the relative error for the diagonal T matrix elements for low values of ϵ. At higher energies, there are additional errors introduced due the energies being close to the cut-off Λ. Therefore initially decreasing ϵ seems beneficial but the errors increase once the $\log(\epsilon)$ term kicks in. Similar trends are observed in the phase shifts as seen in figure (4.3).

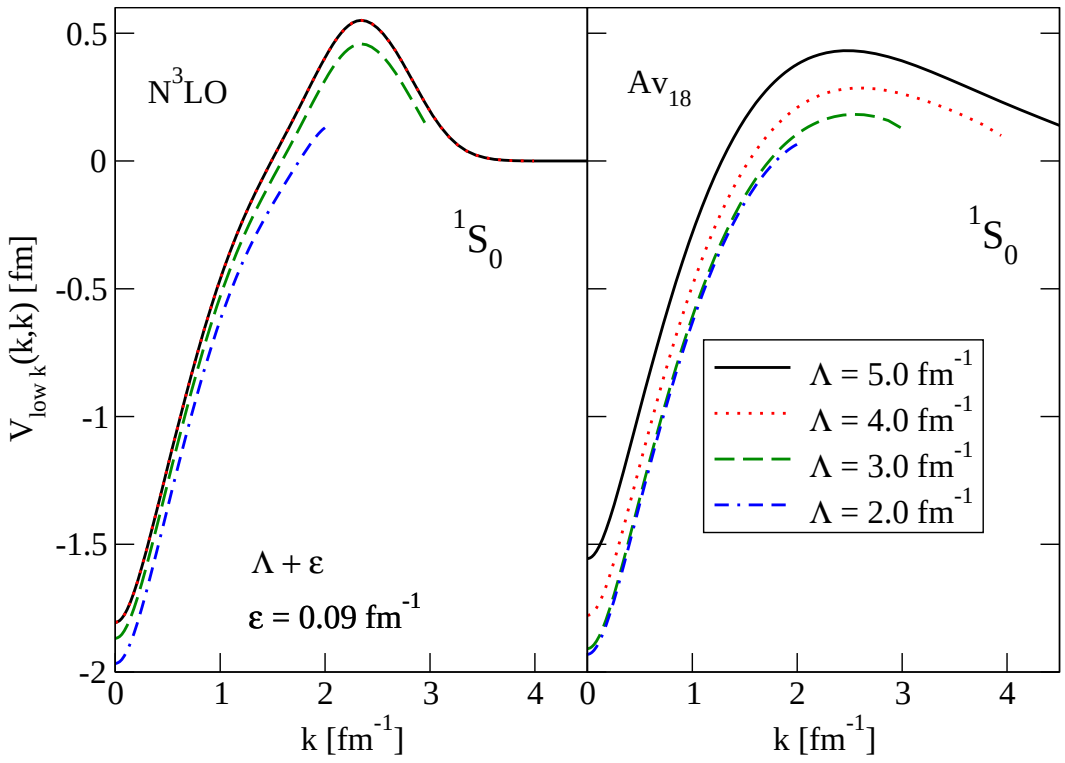

Figure 4.5: $V_{\mathrm{low}\,k}$ running for N^{3}LO (left) [26] and Av_{18} (right) [31] potential. Here we show only the diagonal matrix elements of the potential for different cut-offs. Notice that the N^{3}LO potential does not start running before $\Lambda \approx 3.0\,\mathrm{fm}^{-1}$ in contrast to the Av_{18} potential. The different $V_{\mathrm{low}\,k}(k,k)$ at $\Lambda = 2.0\,\mathrm{fm}^{-1}$ are close but *not identical*.

Though we just saw results for a model potential, these trends with sharp regulator carry over to the case of real potentials as seen in figure (4.4) for the Argonne v_{18} potential [31] in the $^1S_0$ channel. Decreasing the value of ϵ leads to an improvement in the result, but once ϵ becomes small enough for the logarithmic term to dominate, the results start to deteriorate. These artifacts carry over to few-body calculations as well when $V_{\mathrm{low}\,k}$ using a sharp regulator is used as input. It has been shown that a sharp regulator, leads to convergence issues when used in variational calculations [38, 40].

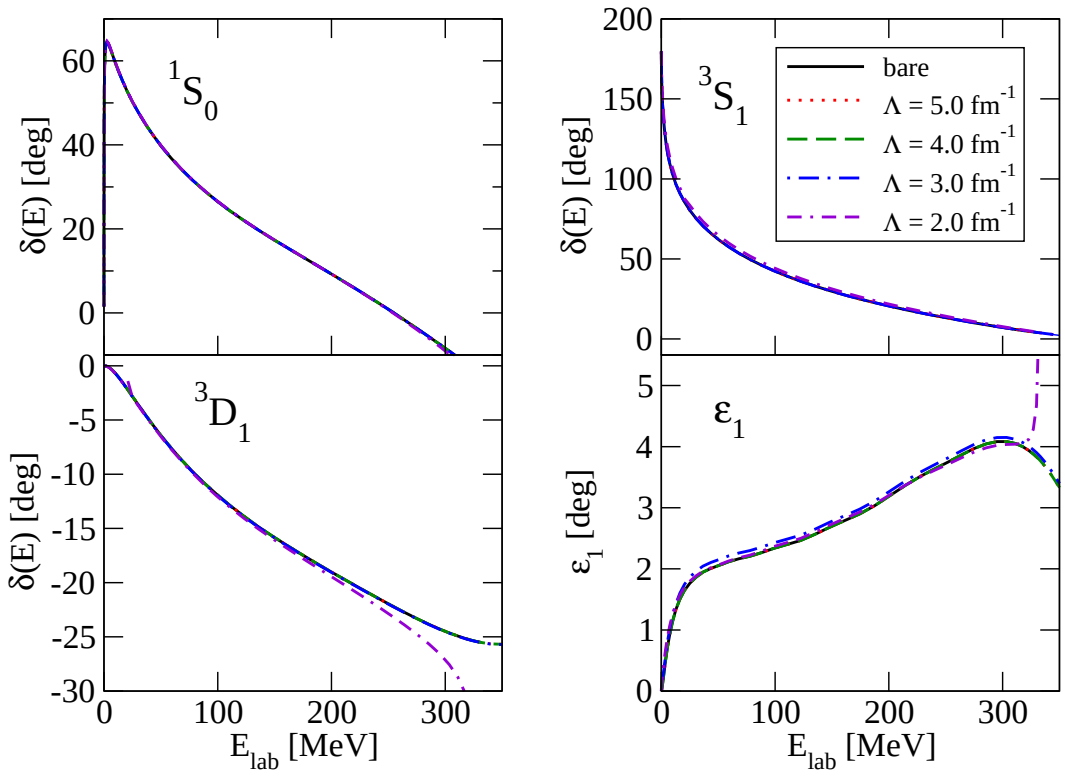

Figure 4.6: Bare and $V_{\mathrm{low}\,k}$ S wave phase shifts for the chiral N^{3}LO potential [26] as a function of lab energies E_{lab} for the sharp regulator, $\Lambda + \epsilon$, parametrized by the value of $\epsilon = 0.09\,\mathrm{fm}^{-1}$. We can see the numerical errors accumulating as the cut-off is lowered.

The running of the low-momentum potential for realistic NN interactions using a sharp regulator $\Lambda + \epsilon$, where $\epsilon = 0.09\,\mathrm{fm}^{-1}$ is documented in figure (4.5). We can see the differences in the running of the chiral EFT and Argonne potentials. Also we notice that the low-momentum potentials at $\Lambda = 2.0\,\mathrm{fm}^{-1}$ are close but not identical. These differences can be paralleled by differences in the corresponding short-range three-body interactions. The differences in the running of Argonne and chiral EFT potentials are important when we determine the corresponding low-momentum potential by directly solving the differential equation (4.1). For the chiral N^{3}LO potentials

it is possible to start with smaller values of the bare cut-off Λ_0, as they do not start running until $\Lambda \approx 4.0$ or $5.0\,\mathrm{fm}^{-1}$. This introduces smaller numerical errors while decimating down to $\Lambda \approx 2.0\,\mathrm{fm}^{-1}$, in contrast to A$v_{18}$ which necessitates a starting cut-off of $\Lambda_0 \approx 30\,\mathrm{fm}^{-1}$ due to the presence of high-momentum components. The propagation of these numerical errors is already evident in figure (4.6), which is a plot of the bare and $V_{\mathrm{low}\,k}$ phase shifts for the S waves for the chiral N^{3}LO potential for a particular choice of the sharp regulator. These errors can be eliminated by using an equivalent method to obtain $V_{\mathrm{low}\,k}$, namely the Lee-Suzuki transformation, which decouples the low- and high-momentum states by a unitary transformation, thereby eliminating the need for an expensive numerical solution of the RG differential equation (4.1) for sharp regulators [28, 29]. For this reasons, for practical calculations, Lee-Suzuki technique is used instead of the one presented in this section. But there is no generalization of the Lee-Suzuki transformation for smooth cut-offs.

Figure (4.7) shows the triton binding energy calculated from a direct diagonalization in a harmonic oscillator basis, using $V_{\mathrm{low}\,k}$ matrix elements derived from the Argonne v_{18} potential with a cut-off of $\Lambda = 2.0\,\mathrm{fm}^{-1}$, as a function of the size of the oscillator space N_{max}. The figure shows slow convergence at the 100 KeV level. Using a smooth regulator solves solves the convergence problem, thereby demonstrating the regulator dependence of the low momentum potentials. The type of smooth regulator used and the form of RG equation is the topic of following section.

4.2 Smooth Regulators and $V_{\mathrm{low}\,k}$ potentials

In order to arrive at the RG equation, we start with the half-off shell (HOS) T matrix equation (2.38) and require that the corresponding matrix elements are

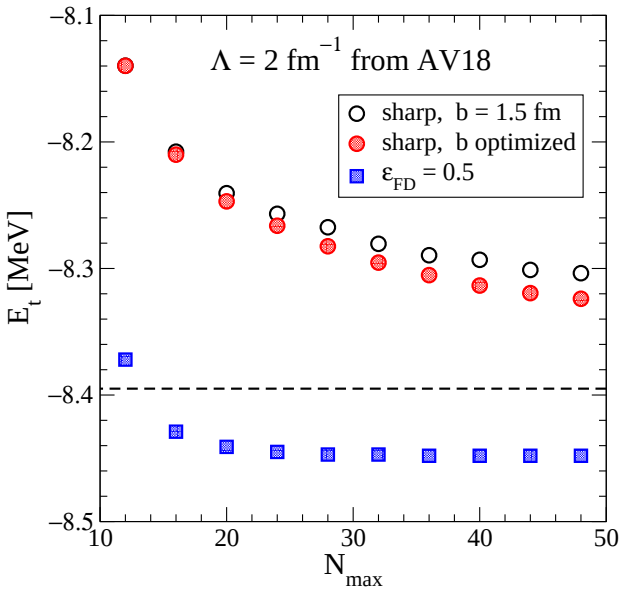

Figure 4.7: The triton binding energy E_t calculated from a direct diagonalization in a harmonic oscillator basis of the low-momentum Hamiltonian derived from the Argonne v_{18} potential [31] with cutoff $\Lambda = 2\,\mathrm{fm}^{-1}$, as a function of the size of the oscillator space ($N_{\max}\,\hbar\omega$ excitations). The open circles are calculated with a sharp cutoff for a fixed oscillator parameter b while the filled ones correspond to optimizing b at each $N_{\max}$. The dashed line indicates the exact Faddeev result using the sharp-cutoff interaction [30], and shows the slow convergence of the diagonalization at the 100 kev level. The squares are for a smooth Fermi-Dirac regulator that solves the convergence problem.

independent of the cut-off Λ, which cuts off the intermediate states, thereby defining a resolution limit on them. The HOS T matrix equation is,

$$T(k',k;k^2) = V_{\mathrm{low}\,k}(k',k) + \frac{2}{\pi}\mathcal{P}\int_0^\Lambda q^2 dq \frac{V_{\mathrm{low}\,k}(k',q)T(q,k;k^2)}{k^2-q^2}, \tag{4.34}$$

where we have used a sharp cut-off Λ to limit the intermediate states. Let us define a function $f(k,\Lambda)$ such that:

$$f(k,\Lambda) = \left\{ \begin{array}{ll} 1 & \text{if } k \leq \Lambda - \dfrac{\epsilon}{2} \\ > 0 \text{ and } < 1 & \text{if } \Lambda - \dfrac{\epsilon}{2} > k \leq \Lambda + \dfrac{\epsilon}{2} \\ 0 & \text{otherwise} \end{array} \right\} \tag{4.35}$$

where ϵ represents the width over which the function falls to 0. Using this function $f(k,\Lambda)$, we can re-write equation (4.34) as,

$$t(k',k;k^2) = v(k',k) + \frac{2}{\pi}\mathcal{P}\int_0^\infty q^2 dq \frac{v(k',q)f^2(q,\Lambda)t(q,k;k^2)}{k^2-q^2}. \tag{4.36}$$

where

$$T(k',k;E) = f(k',\Lambda)t(k',k;E)f(k,\Lambda) \tag{4.37}$$

$$V_{\text{low}\,k}(k',k) = f(k',\Lambda)v(k',k;E)f(k,\Lambda) \tag{4.38}$$

The function $f(k,\Lambda)$ so defined in equation (4.35) is the smooth regulator function and the limit when $\epsilon \to 0$ gives the sharp regulator, which cuts off the intermediate states sharply at Λ (see equation (4.34)).

We further relax the conditions given in equation (4.35) by modifying the regulating function as follows:

$$f(k,\Lambda) \overset{k\ll\Lambda}{\to} 1 \tag{4.39}$$

$$f(k,\Lambda) \overset{k\gg\Lambda}{\to} 0 \tag{4.40}$$

where $f(k,\Lambda)$ now just approaches 1 for $k \leq \Lambda - \dfrac{\epsilon}{2}$ in contrast to the conditions in equation (4.35) where $f(k,\Lambda) = 1$ for $k \leq \Lambda - \dfrac{\epsilon}{2}$. We immediately see that an infinite number of functions satisfy the above conditions. This reflects the freedom in defining low-energy EFTs. We present results for two choices for $f(k)$, each with a range of parameters. These are the exponential form used in current chiral EFT potentials [26, 27] with integer $n = n_{\text{exp}}$ determining the smoothness,

$$f(k) = e^{-(k^2/\Lambda^2)^n}\,, \tag{4.41}$$

and a Fermi-Dirac form with a sharper cutoff achieved with smaller $\epsilon = \epsilon_{\text{FD}}$,

$$f(k) = \frac{1}{1+e^{(k^2-\Lambda^2)/\epsilon^2}}\,. \tag{4.42}$$

It may be interesting in the future to explore other choices for the regulator function, but the general features and advantages are covered by the above choices. Other possible regulators (used in different applications, e.g., see reference [86]) include a power law form with integer n,

$$f(k) = \frac{1}{1 + (k^2/\Lambda^2)^n}\,, \tag{4.43}$$

a hyperbolic tangent form with an ϵ parameter that plays a similar role as in the Fermi-Dirac function,

$$f(k) = \frac{1}{2}\left[1 + \tanh\left(\frac{\Lambda^2 - k^2}{\Lambda k \epsilon}\right)\right]\,, \tag{4.44}$$

a complementary error function with ϵ parameter,

$$f(k) = \frac{1}{2}\,\mathrm{erfc}\left(\frac{k - \Lambda}{\epsilon}\right)\,, \tag{4.45}$$

and a Strutinsky averaging with ϵ parameter,

$$f(k) = \frac{1}{2}\left[\mathrm{erf}\left(\frac{\Lambda^2 + k^2}{\epsilon^2}\right) + \mathrm{erf}\left(\frac{\Lambda^2 - k^2}{\epsilon^2}\right)\right]\,. \tag{4.46}$$

In each case, the function and its derivatives are continuous, and the parameter n or ϵ controls the smoothness.

The figure (4.8) plots the function $[f(k,\Lambda)]^2$ as a function of k for a cut-off of $\Lambda = 2.0\,\mathrm{fm}^{-1}$. While a sharp cut-off preserves phase shifts up to the cut-off Λ, a smooth regulator distorts the phase shifts for momenta close to the cut-off, though it eliminates sharp cut-off artifacts. The exponential regulator with $n = 3$ is what is used in chiral N^{3}LO potentials. It is evident that such a choice distorts the phase shifts to a large extent. As n is increased the exponential regulator gets sharp and the phase shift distortion is reduced. We found out in our investigations that $n = 10$ presents a

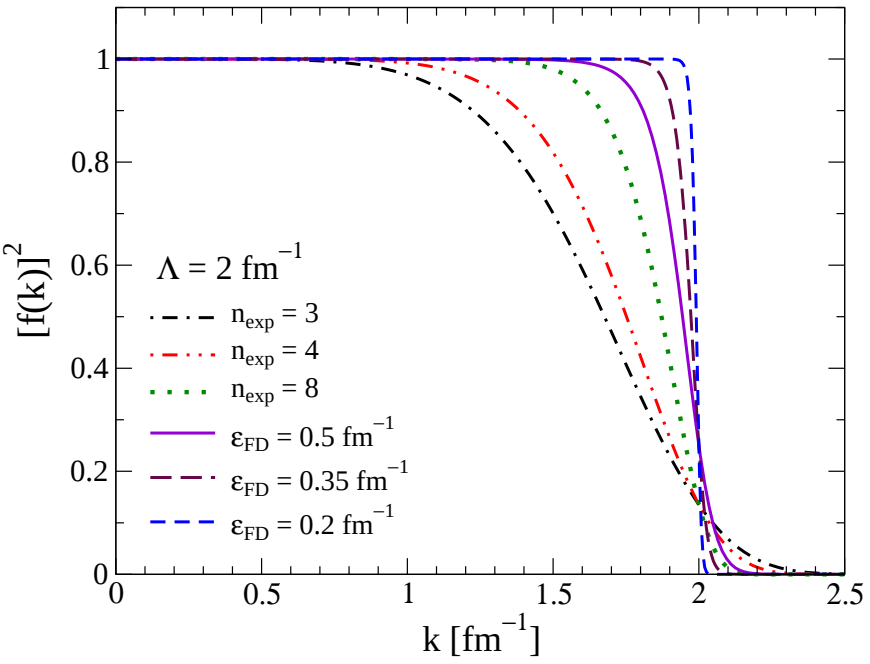

Figure 4.8: Plots of the exponential and Fermi-Dirac regulators squared as a function of momentum k for $\Lambda = 2\,\mathrm{fm}^{-1}$ and a range of parameters n and ϵ.

practical upper limit. The Fermi-Dirac regulator interpolates smoothly between the sharp and the exponential regulator and distorts much less at low-momenta.

The distortion in the bare phase shifts and the mixing angle is shown for the S waves in figure (4.9). Here we have shown the bar phase shifts. In each case the diagonal T matrix elements which are used to calculate the phase shifts are distorted by the function $[f(k,\Lambda)]^2$, which then distorts the phase shifts. We see that Fermi-Dirac regulator distorts much less compared to the exponential regulator. This figure can also be understood as the distortion that would be present if the numerical errors in solving for $V_{\mathrm{low}\,k}$ were negligible. Therefore we can expect the

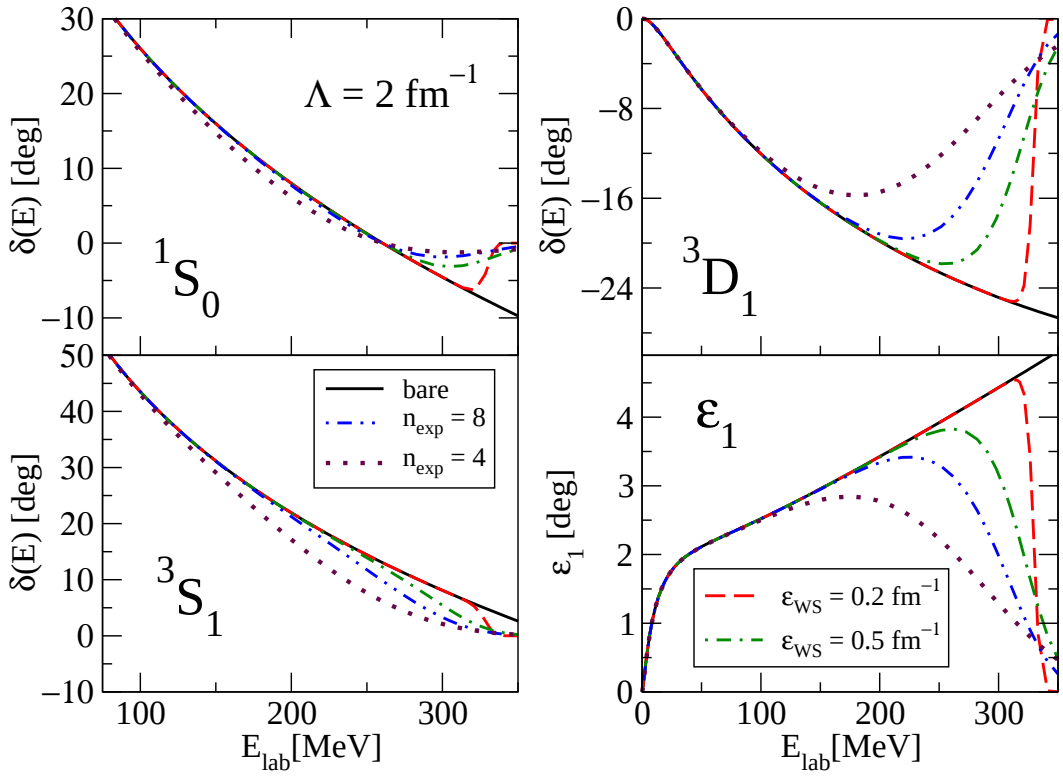

Figure 4.9: Bare phase shifts distorted by the regulator function. The phase shifts are calculated using the N^{3}LO chiral potential from reference [26].The distortion occurs in the T elements, which then carries over to the phase shifts.

phase shifts calculated from $V_{\text{low}\,k}$ matrix elements to cause additional distortions. We will examine this in the next section.

We have no universal rule for deciding whether a distortion is acceptable; it depends on how it propagates to the observable in question. For example, for the low-energy bound-state of the deuteron, none of the distortions in figure (4.9) is important. The distortion is analogous to the error band from a chiral EFT truncation (but we have not formulated a corresponding power counting rule). Therefore, we

expect that there is no concern if the distortion is comparable to the EFT truncation error. In addition, for low-energy properties, the error incurred here can be absorbed by the short-range part of the corresponding three-body interactions. Consequently, the propagation of phase-shift errors to many-body observables can only be studied after including three-nucleon forces. It is evident, however, that $n_{\exp} = 8$ and $\epsilon_{\mathrm{FD}} = 0.5$ only distort minimally. We will show below that these are also good choices for convergence. In future applications, the regulator effects can be tested by varying the parameters determining the smoothness.

We had previously derived the RG equation requiring cut-off independence of the HOS T elements as seen in section (2.2). But this requirement is a choice. Cut-off independence of the HOS T elements leads to an energy independent low-momentum potential. We can alternatively formulate RG evolution, where we require cut-off independence of the fully off-shell T elements, i.e., $T(k', k; E)$ where $(k')^2 \neq (k)^2 \neq E$. This condition leads to an energy independent low-potential denoted as V_{eff}. But this undesirable energy independence is traded for momentum independence as a next step and finally the potential is hermitized to yield an energy-independent, hermitian low-momentum potential $V_{\mathrm{low}\,k}$. There will be differences in the matrix elements of $V_{\mathrm{low}\,k}$. But these differences just reflect the freedom in defining low-energy effective field theories.

4.2.1 Energy Independent Smooth $V_{\mathrm{low}\,k}$

We first look at constructing energy independent smooth low-momentum potentials. which are a direct generalization of the RG equations derived for sharp regulators. Analogous to the derivation for a sharp cutoff [29], we impose that the reduced

half-on-shell t matrix is independent of the cutoff, $dt(k',k;k^2)/d\Lambda = 0$. This choice preserves the on-shell t matrix while also maintaining energy independence. The result is

$$0 = \frac{2}{\pi}\int_0^\infty p^2 dp\,\frac{dv(k',p)}{d\Lambda}\left[\frac{\pi\,\delta(p-k)}{2k^2} + \frac{f^2(p)\,t(p,k;k^2)}{k^2-p^2}\right] - \frac{2}{\pi}\int_0^\infty p^2 dp\,\frac{v(k',p)\,\frac{d}{d\Lambda}[f^2(p)]\,t(p,k;k^2)}{p^2-k^2}\,. \quad (4.47)$$

Next, we express the term in the square brackets in equation (4.47) by the exact scattering state $|\chi_k\rangle$ of $V_{\mathrm{low}\,k}$. From $V_{\mathrm{low}\,k}|\chi_k\rangle = V_{\mathrm{low}\,k}|k\rangle + V_{\mathrm{low}\,k}\,G_0(k^2)\,T_{\mathrm{low}\,k}|k\rangle$, it follows that $\langle p\,|\,\chi_k\rangle = \langle p\,|\,k\rangle + [f(p)\,t(p,k;k^2)\,f(k)]/(k^2-p^2)$. We can therefore write equation (4.47) as

$$\frac{2}{\pi}\int_0^\infty p^2 dp\,\frac{dv(k',p)}{d\Lambda}\frac{f(p)}{f(k)}\,\chi_k(p) = \frac{2}{\pi}\int_0^\infty p^2 dp\,2\,\frac{df(p)}{d\Lambda}\,\frac{v(k',p)\,f(p)\,t(p,k;k^2)}{p^2-k^2}\,, \quad (4.48)$$

or equivalently

$$\frac{2}{\pi}\int_0^\infty p^2 dp\,\frac{dv(k',p)}{d\Lambda}\,f(p)\,\chi_k(p) = \frac{2}{\pi}\int_0^\infty p^2 dp\,2\frac{df(p)}{d\Lambda}\,\frac{v(k',p)}{p^2-k^2}\,\Lambda p\,|\,V_{\mathrm{low}\,k}\,|\,\chi_k\rangle = \frac{2}{\pi}\int_0^\infty p^2 dp\,2\frac{df(p)}{d\Lambda}\,v(k',p)\,\Lambda p\,|\,V_{\mathrm{low}\,k}\,G(p^2)\,|\,\chi_k\rangle, \quad (4.49)$$

where $G(E) = (E - H_{\mathrm{low}\,k})^{-1}$ is the interacting two-nucleon Green's function. Using the completeness relation, $\int k^2 dk\,\widetilde{\chi}_k^*(p')\,\chi_k(p) = \frac{\pi}{2}\delta(p-p')/p^2$ and $V_{\mathrm{low}\,k}\,G(E) = T_{\mathrm{low}\,k}(E)\,G_0(E)$, we have

$$\frac{d}{d\Lambda}\,v(k',k) = \frac{2}{\pi}\int_0^\infty p^2 dp\,\frac{v(k',p)\,\frac{d}{d\Lambda}[f^2(p)]\,t(p,k;p^2)}{p^2-k^2}\,, \quad (4.50)$$

which describes the evolution of the reduced low-momentum interaction with the cutoff.

If we take an energy-independent NN potential as the large-cutoff initial condition and numerically integrate the RG equation, then the resulting v preserves the half-on-shell $T_{\rm NN}$ matrix for *all* external momenta, $t(k',k;k^2) = T_{\rm NN}(k',k;k^2)$. Therefore, $V_{\text{low}\,k}(k',k) = f(k')\,v(k',k)\,f(k)$ preserves the low-momentum half-on-shell $T_{\rm NN}$ matrix up to factors of the smooth cutoff function. In the limit $f(p) \to \theta(\Lambda - p)$ and thus $d[f(p)^2]/d\Lambda \to \delta(\Lambda - p)$, we recover the RG equation for a sharp cutoff [29]

$$\frac{d}{d\Lambda} V_{\text{low}\,k}(k',k) = \frac{2}{\pi} \frac{V_{\text{low}\,k}(k',\Lambda)\, T_{\text{low}\,k}(\Lambda,k;\Lambda^2)}{1-(k/\Lambda)^2}\,. \tag{4.51}$$

Finally, we can use the Okubo transformation to hermitize $V_{\text{low}\,k}$. In order to generalize the hermitization to smooth cutoffs, we consider the sharp-cutoff Okubo transformation under an infinitesimal change of the cutoff. In this case, one can show that the RG equation for the hermitian $\overline{V}_{\text{low}\,k}$ is given by a symmetrized version of equation (4.51),

$$\frac{d}{d\Lambda} \overline{V}_{\text{low}\,k}(k',k) = \frac{1}{\pi} \left[\frac{\overline{V}_{\text{low}\,k}(k',\Lambda)\, \overline{T}_{\text{low}\,k}(\Lambda,k;\Lambda^2)}{1-(k/\Lambda)^2} + \frac{\overline{T}_{\text{low}\,k}(k',\Lambda;\Lambda^2)\, \overline{V}_{\text{low}\,k}(\Lambda,k)}{1-(k'/\Lambda)^2} \right]. \tag{4.52}$$

A simple generalization of the Okubo transformation to smooth cutoffs is therefore obtained by symmetrizing the smooth-cutoff RG equation, equation (4.50), to obtain

$$\frac{d}{d\Lambda}\, \overline{v}(k',k) = \frac{1}{\pi} \int_0^\infty p^2 dp \left[\frac{\overline{v}(k',p) \frac{d}{d\Lambda}[f^2(p)]\, \overline{t}(p,k;p^2)}{p^2-k^2} + \frac{\overline{t}(k',p;p^2)\, \frac{d}{d\Lambda}[f^2(p)]\, \overline{v}(p,k)}{p^2-k'^2} \right]. \tag{4.53}$$

The hermitian low-momentum interaction $\overline{V}_{\text{low}\,k}$ preserves the low-momentum fully-on-shell $T_{\rm NN}$ matrix, up to factors of the regulator function and the deuteron binding

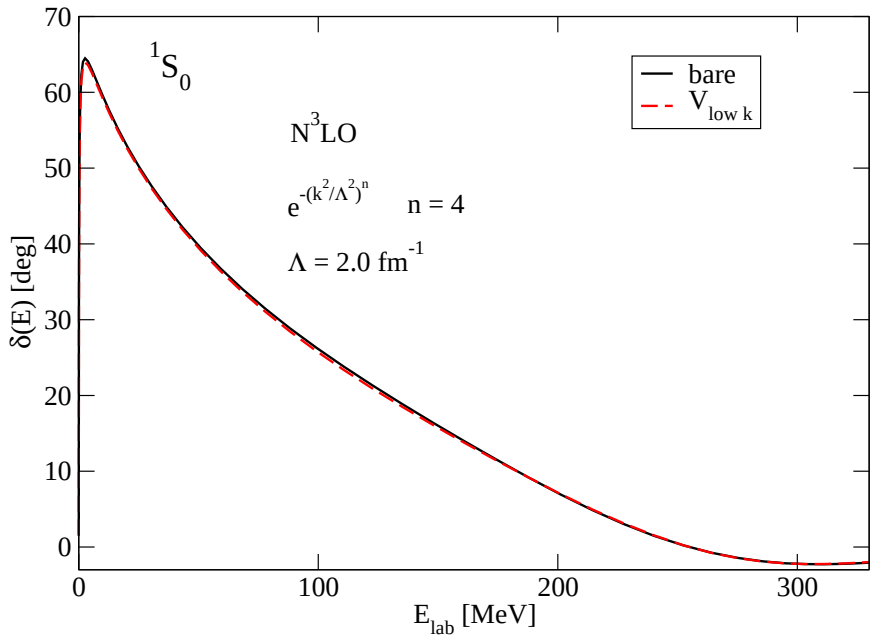

Figure 4.10: Bare and $V_{\mathrm{low}\,k}$ phase shifts for the chiral N^{3}LO potential [26] in the $^1S_0$ partial wave at a cut-off of $\Lambda = 2.0\,\mathrm{fm}^{-1}$. The phase shifts are reproduced to $\mathcal{O}(10^{-2})$ for a gaussian mesh with 100 points between 0 and Λ. This region of integration had be sub-divided into 4 regions of 25 points each.

energy. The freedom in the hermitization method can be expressed as an auxiliary condition $dt(k', k; k^2)/d\Lambda = (k^2 - k'^2)\,\Phi(k', k)$, where $\Phi(k', k)$ is a function with $\lim_{k\to k'}(k^2 - k'^2)\,\Phi(k', k) = 0$. The above RG equation derived from the Okubo transformation makes a particular choice for $\Phi(k', k)$.

Figure (4.10) shows that the phase shifts are reproduced. The results are for an exponential regulator with $n_{\mathrm{exp}} = 4$. Here we compare the distorted phase shifts obtained using the bare and $V_{\mathrm{low}\,k}$ potentials, in order to isolate the errors introduced by the RG evolution. In fact the error in reproducing the distorted phase shifts is of $\mathcal{O}(10^{-2})$ for a gaussian mesh with 100 points between 0 and Λ. We have shown

results only for the $^1S_0$ channel for the chiral potentials, as these potentials do not start running before $\Lambda \approx 4.0$ or $5.0\,\mathrm{fm}^{-1}$. For the sake of numerical accuracy we use a bare cut-off of $\Lambda_0 = 6.0\,\mathrm{fm}^{-1}$, compared to $\Lambda_0 = 30\,\mathrm{fm}^{-1}$ for the Argonne potential. As a result the chiral potentials facilitate shorter run times and less accumulation of errors due to numerical implementation of the RG evolution. For the Argonne potential (not shown here), the run times were so long that it was not practical to present the results here.

The numerical solution of the energy-independent RG equation is complicated by the t matrix calculation involved in each step. The computational overhead slows down the ODE solver significantly. In addition, the RG equation involves two-dimensional interpolations and principal-value integrals over narrowly peaked functions. Therefore, it is easy to introduce small errors at each step that can accumulate as the cutoff is lowered. Finally, some potential models exhibit spurious resonances (at order GeV energies and momenta) and these need to be subtracted before solving the energy-independent RG equation for these potentials.

4.2.2 Energy Dependent three-step RG

In the previous section (4.2.2) the energy-independent smooth counterpart to the sharp RG equation is obtained starting from the cut-off independence of the HOS T matrix elements. As mentioned earlier, this is just one of the choices, as we require the diagonal T matrix elements to be cut-off independent as these are related to phase shifts (physical observables). Requiring HOS T matrix elements to be cut-off independent automatically ensures the same for the diagonal T matrix elements. Similarly requiring cut-off independence of *all* the T matrix elements, $T(k', k; E)$ again

results in cut-off independent diagonal on-shell T matrix elements, $T(k,k;E=k^2)$. Using this as the starting point, we will now derive the energy-dependent formulation. This will be the first of the three steps involved to obtain an energy-independent hermitian low-momentum potential $V_{\text{low}\,k}$. The fully off-shell T matrix equation can be written using equation (4.36) as:

$$t(k',k;E) = v(k',k) + \frac{2}{\pi}\mathcal{P}\int_0^\infty q^2 dq \frac{v(k',q)f^2(q,\Lambda)t(q,k;k^2)}{E-q^2}. \tag{4.54}$$

where $T(k',k;E) = f(k',\Lambda)t(k',k;E)f(k,\Lambda)$, $V(k',k) = f(k',\Lambda)v(k',k)f(k,\Lambda)$, and $V(k',k)$ could be $V_{\text{low}\,k}(k',k)$ or $V_{\text{eff}}(k',k;E)$. Now the RG condition is $\dfrac{dt(k',k;E)}{d\Lambda} = 0$. Equation (4.54) can be written as

$$t = v + vG_0(\Lambda)t. \tag{4.55}$$

where $G_0(\Lambda) = f(\Lambda)G_0$. Using the RG condition:

$$\frac{dt}{d\Lambda} = 0 = \frac{dv}{d\Lambda}G_0 t + v\frac{dG_0(\Lambda)}{d\Lambda}t. \tag{4.56}$$

$$\Rightarrow \frac{dv}{d\Lambda} = -v\frac{dG_0(\Lambda)}{d\Lambda}t\left[1+G_0(\Lambda)t\right]^{-1}. \tag{4.57}$$

But from equation (4.55), we can write,

$$v = t\left[1+G_0(\Lambda)t\right]^{-1}. \tag{4.58}$$

Therefore equation (4.57) becomes:

$$\frac{dv}{d\Lambda} = -v\frac{dG_0(\Lambda)}{d\Lambda}v. \tag{4.59}$$

Now inserting complete set of states $\dfrac{2}{\pi}\displaystyle\int_0^\infty q^2 dq|q\rangle\langle q| = \mathbb{1}$, we get the following first order coupled differential equation for the energy-dependent low-momentum potential

denoted as $V_{\text{eff}}(k', k; E)$:

$$\frac{dv(k', k; E)}{d\Lambda} = -\frac{2}{\pi}\int_0^\infty q^2 dq\, v(k', q; E)\frac{[\frac{df(q,\Lambda)}{d\Lambda}]^2}{E - q^2}v(q, k; E), \tag{4.60}$$

$$V_{\text{eff}}(k', k; E) = f(k', \Lambda)v(k', k; E)f(k, \Lambda). \tag{4.61}$$

Solving the energy-dependent first-order coupled differential equations (4.60) for $v(k', k; E)$ is much simpler than the corresponding energy-independent case (equation (4.50)), as the LHS does not require the numerically expensive T matrix evaluation. But the reduced potential obtained by solving equation (4.60) is energy dependent. This energy dependence has to be transformed away for momentum dependence. Before we go into the details of this transformation, let us look at the two different ways available for solving equations (4.60). One way is to solve the differential equation directly using a numerical differential equation solver routine. This procedure entails the calculation of $v(k', k; E)$ as Λ is reduced by a small amount $d\Lambda$, until the minimum cut-off of $\Lambda \approx 2.1\,\text{fm}^{-1}$ is reached. This procedure is very stable numerically compared to T matrix evaluation at each step.

The stability and speed of computations for the reduced low-momentum potential can be improved drastically by formally integrating equation (4.60). Equation (4.56) can be written as:

$$\frac{dt}{d\Lambda} = 0 = \frac{dv}{d\Lambda} + \frac{d}{d\Lambda}(vG_0(\Lambda)t). \tag{4.62}$$

But we know that:

$$t = v + v\,G_0(\Lambda)\,t \tag{4.63}$$

$$= v + t\,G_0(\Lambda)\,v \tag{4.64}$$

$$\Rightarrow v\,G_0(\Lambda)\,t = t\,G_0(\Lambda)\,v, \tag{4.65}$$

which is true for any v. Also,

$$t = V_{\rm NN} + V_{\rm NN}\, G_0(\Lambda_0)\, t, \tag{4.66}$$

$$= v + v\, G_0(\Lambda)\, t \tag{4.67}$$

where equations (4.66) and (4.67) are the statement of the RG condition, that is, T matrix elements are independent of the cut-off Λ. Using equation (4.65), we can write equation (4.62) as:

$$-\frac{dv}{d\Lambda} = \frac{d}{d\Lambda}(t\, G_0(\Lambda)\, v). \tag{4.68}$$

Substitute for t in the second term of equation (4.68) so that,

$$-\frac{dv}{d\Lambda} = \frac{d}{d\Lambda}(V_{\rm NN}\, G_0(\Lambda)\, v + V_{\rm NN}\, G_0(\Lambda_0)\, t\, G_0(\Lambda)\, v). \tag{4.69}$$

From equation (4.67), $(t - v) = tG_0(\Lambda)v$, so that equation (4.69) is now given by:

$$-\frac{dv}{d\Lambda} = \frac{d}{d\Lambda}(V_{\rm NN}\, G_0(\Lambda)\, v + V_{\rm NN}\, G_0(\Lambda_0)\, (t - v)) \tag{4.70}$$

$$= \frac{d}{d\Lambda}(V_{\rm NN}\, (G_0(\Lambda) - G_0(\Lambda_0))\, v) + \frac{d}{d\Lambda}(V_{\rm NN}\, G_0(\Lambda_0)\, t). \tag{4.71}$$

where the second term in equation (4.71) is identically 0. Now we are ready to formally integrate the following equation:

$$\frac{dv}{d\Lambda} = -\frac{d}{d\Lambda}(V_{\rm NN}\, (G_0(\Lambda) - G_0(\Lambda_0))\, v), \tag{4.72}$$

$$\Rightarrow v = V_{\rm NN}\, (G_0(\Lambda_0) - G_0(\Lambda))\, v + V_{\rm NN}. \tag{4.73}$$

where we have used the initial condition $V_{\rm NN} = v$ for $\Lambda = \Lambda_0$. In momentum space equation (4.73) can be written as:

$$v(k', k; E) = V_{\rm NN}(k', k) + \frac{2}{\pi}\int_0^\infty q^2 dq V_{\rm NN}(k', q)\, \frac{(1 - f^2(q, \Lambda))}{E - q^2}\, v(q, k; E). \tag{4.74}$$

This is the smooth cut-off generalization of the Bloch-Horowitz equation. Finally, we note that the initial energy-dependent RG equation is not needed if one starts directly from the smooth-cutoff generalization of the Bloch-Horowitz equation. For this purpose, we separate the free two-nucleon propagator into a smooth cut-off low-momentum G_0^Λ and a high-momentum part $\overline{G_0^\Lambda}$. The Lippmann-Schwinger equation then reads $T_{\rm NN}(E) = V_{\rm NN} + V_{\rm NN}\,(G_0^\Lambda(E) + \overline{G_0^\Lambda}(E))\,T_{\rm NN}(E)$, and a rearrangement gives the fully-off-shell $T_{\rm NN}(E)$ matrix with only low-momentum propagators,

$$T_{\rm NN}(E) = v(E) + v(E)\,G_0^\Lambda(E)\,T_{\rm NN}(E)\,, \tag{4.75}$$

where $v(E)$ is the solution to the smooth-cutoff Bloch-Horowitz equation, equation (4.74).

Next we address issue of energy dependence. This is done using a method similar to field redefinitions. For this purpose, let us introduce the energy-independent non-hermitian $V_{{\rm low}\,k}(k',k)$ which reproduce the HOS $T_{\rm eff}(k',k;k^2)$ as $V_{\rm eff}(k',k;k^2)$. That is,

$$\langle k'|T_{\rm eff}(p^2)|\chi_p\rangle = \langle k'|V_{\rm eff}(p^2)|\chi_k\rangle \equiv \langle k'|V_{{\rm low}\,k}|\chi_p\rangle. \tag{4.76}$$

where $|\chi_p\rangle$ are the eigenstates of the energy-dependent Hamiltonian $H_{\rm eff}(p^2) = T_0 + V_{\rm eff}(p^2)$ with relative kinetic energy T_0. Using the completeness of the interacting eigenstates, this leads to

$$V_{{\rm low}\,k}(k',k) = \int_0^\infty p^2 dp\,\frac{2}{\pi}\int_0^\infty p'^2 dp'\,V_{\rm eff}(k',p';p^2)\,\chi_p(p')\,\widetilde{\chi}_p^*(k)\,. \tag{4.77}$$

The energy dependence of $H_{\rm eff}(p^2)$ necessitates the use of bi-orthogonal complement vectors $\langle\widetilde{\chi}_p|$ in the completeness relation, $\int p^2 dp\,|\chi_p\rangle\langle\widetilde{\chi}_p| = \mathbb{1}$. If bound states are present, the integral over the continuous scattering states includes a summation over bound states as well.

For the numerical solution of equation. (4.76), we first obtain the eigenstates of the energy-dependent $H_{\rm eff}$ by self-consistently diagonalizing the discretized eigenvalue equation

$$\sum_k \big(\delta_{k'k}\, k^2 + V^{\rm eff}_{k',k;E_p}\big)\chi_{k,p} = E_p\, \chi_{k',p}\,. \tag{4.78}$$

Next, the discretized bi-orthogonal complement vectors are obtained from the matrix equation $\sum_p \chi_{k,p}\, \widetilde{\chi}_{k',p} = \delta_{k,k'}$. Finally, equation (4.76) is evaluated by simple matrix multiplication

$$V_{{\rm low}\, k k',k} = \sum_{p,p'} V_{{\rm eff}\, k',p';E_p}\, \chi_{p',p}\, \widetilde{\chi}_{k,p}\,. \tag{4.79}$$

This procedure is straightforward in practice. The only subtlety arises when the discretization of the defining equations for the bi-orthogonal complement vectors is such that some of the $|\chi_p\rangle$ vectors appear to be linearly dependent. In this case, singular-value-decomposition methods are helpful to solve the singular system of equations by setting to zero the problematic small singular values when taking the inverse of the $\chi_{k,p}$ matrix [78]. The resulting energy-independent $V_{{\rm low}\, k}$ is non-hermitian, and is identical to the solution of the energy-independent RG equation derived from HOS t matrix equivalence in the previous section (4.2.1).

In the third step, we remove the non-hermiticity of $V_{{\rm low}\, k}$ by a similarity transformation that orthogonalizes the set of eigenvectors $\{|\chi_p\rangle\}$ of the non-hermitian Hamiltonian $H_{{\rm low}\, k} = T + V_{{\rm low}\, k}$. Following Holt *et al.* [79], we define a transformation Z by

$$Z\chi_p = |\xi_p\rangle \qquad \text{and} \qquad \langle\xi_p|\xi_{p'}\rangle = \delta_{pp'}\,, \tag{4.80}$$

where the Kronecker delta normalization implies the discretization procedure of the previous section has been carried out. The hermitian low-momentum interaction is

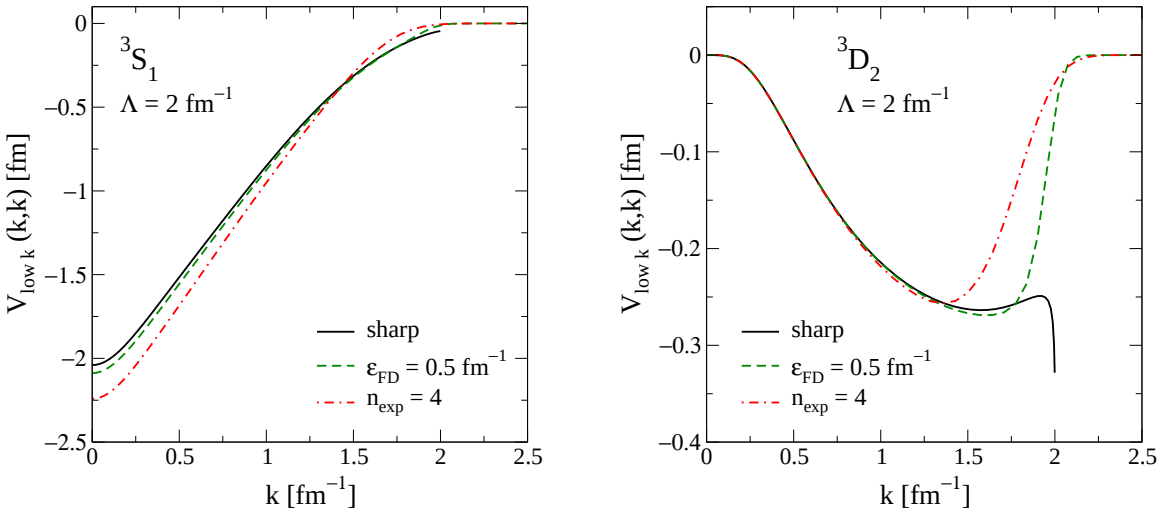

Figure 4.11: Diagonal matrix elements $V_{\mathrm{low}\,k}(k,k)$ for $\Lambda = 2\,\mathrm{fm}^{-1}$, derived from the N^{3}LO chiral potential of reference [26] with a sharp and two smooth regulators.

then given by

$$\overline{V}_{\mathrm{low}\,k} = Z\,H_{\mathrm{low}\,k}\,Z^{-1} - T\,. \tag{4.81}$$

There is not a unique choice for the transformation Z, which is a reflection of the general freedom in low-energy effective theories. In reference [79], it was shown how several common hermitization methods correspond to different choices for Z. For example, within the Lee-Suzuki framework [80, 81] for deriving effective interactions (which implies a sharp cutoff corresponding to orthogonal $PQ = 0$ projection operators), the eigenstates of the non-hermitian $V_{\mathrm{low}\,k}$ obey

$$\langle\chi_p|P + \omega^\dagger\omega|\chi_{p'}\rangle = \delta_{pp'}\,, \tag{4.82}$$

where $\omega = Q\omega P$ is the wave operator that parameterizes the Lee-Suzuki decoupling transformation. Identifying $Z^\dagger Z = P + \omega^\dagger\omega$ defines a class of valid transformations

for Z. For example, setting $Z = \sqrt{P + \omega^\dagger \omega}$ corresponds to the hermitization procedure of Okubo [82] and Okamoto and Suzuki [83]. Alternatively, one can perform a Cholesky factorization of the symmetric and positive-definite operator $LL^\dagger = P + \omega^\dagger \omega$, where L is the lower-triangular Cholesky matrix. Then, $Z = L^\dagger$ corresponds to the hermitization method of Andreozzi [84]. Another method discussed by Holt *et al.* is a Gram-Schmidt orthogonalization to construct the set of $\{|\xi_p\rangle\}$ directly from $\{|\chi_p\rangle\}$. This allows Z to be calculated directly from equation (4.80). Even within the Gram-Schmidt method, Z is not unique, due to the freedom in choosing the starting vector. All hermitization methods result in low-momentum interactions $\overline{V}_{\mathrm{low}\,k}$ that preserve the low-momentum fully-on-shell T_{NN} matrix, up to factors of the regulator function $T_{\mathrm{low}\,k}(k, k; k^2) = f^2(k)\, T_{\mathrm{NN}}(k, k; k^2)$, and the deuteron binding energy. The corresponding three-body interactions will differ, however, as discussed below.

The Gram-Schmidt method can be applied directly to the smooth-cutoff $V_{\mathrm{low}\,k}$. As in reference [79], the orthogonal basis $\{|\xi_p\rangle\}$ is constructed via

$$\begin{aligned} |\xi_1\rangle &= Z_{11}|\chi_1\rangle \\ |\xi_2\rangle &= Z_{21}|\chi_1\rangle + Z_{22}|\chi_2\rangle \\ |\xi_3\rangle &= Z_{31}|\chi_1\rangle + Z_{32}|\chi_2\rangle + Z_{33}|\chi_3\rangle \\ &\vdots \end{aligned} \tag{4.83}$$

where the $Z_{pp'}$ are determined sequentially so that $\langle \xi'_p | \xi_p \rangle = \delta_{pp'}$. We have chosen to take the eigenstate of $H_{\mathrm{low}\,k}$ with lowest energy as the starting vector, although any other linear combination could have been used. In practice, the modified Gram-Schmidt algorithm with re-orthogonalization of reference [85] is utilized to guard against round-off errors. The transformation Z corresponding to the Gram-Schmidt

hermitization is then given by

$$Z = \sum_p |\xi_p\rangle \langle\widetilde{\chi}_p| \qquad \text{and} \qquad Z^{-1} = \sum_p |\chi_p\rangle \langle\xi_p| \,. \tag{4.84}$$

In contrast to the Gram-Schmidt method, the other hermitization schemes are formulated in terms of the Lee-Suzuki wave-operator ω, which apparently relies on the use of orthogonal projection operators $PQ = 0$ corresponding to sharp cutoffs. In order to generalize the Okubo and Andreozzi hermitization schemes to smooth cutoffs, it is necessary to eliminate all references to ω. This is easily done by noting that the bi-orthogonal complement vectors are defined through $\langle\widetilde{\chi}_p \,|\, \chi_{p'}\rangle = \delta_{pp'}$. For a sharp cutoff, equation (4.79) implies $|\widetilde{\chi}_p\rangle = (P + \omega^\dagger\omega)|\chi_p\rangle$, and thus

$$P + \omega^\dagger\omega = \sum_p |\widetilde{\chi}_p\rangle \langle\widetilde{\chi}_p| \,. \tag{4.85}$$

For smooth cutoffs, the obvious generalization is to construct the operator $\sum_p |\widetilde{\chi}_p\rangle \langle\widetilde{\chi}_p|$ and decompose it as

$$Z^\dagger Z = \sum_p |\widetilde{\chi}_p\rangle \langle\widetilde{\chi}_p| \,. \tag{4.86}$$

As for sharp cutoffs, the generalized Okubo transformation corresponds to $Z = \sqrt{\sum_p |\widetilde{\chi}_p\rangle \langle\widetilde{\chi}_p|}$, where the square root is taken in the eigenbasis of the positive-definite operator $\sum_p |\widetilde{\chi}_p\rangle \langle\widetilde{\chi}_p|$. Similarly, the Andreozzi hermitization can be obtained from performing the appropriate Cholesky decomposition.

Before we conclude this section we will present some results for smooth $V_{\mathrm{low}\,k}$. The bare potential V_{NN} used here are the chiral N^{3}LO potentials [26, 27]. Using this as the starting point, we evolve to lower cut-offs and hence determine the corresponding low-momentum energy-independent hermitian potential, $V_{\mathrm{low}\,k}$. We will use the three step method for the results presented here as this yields better numerical stability

and have greater efficiency compared to the energy-independent procedure discussed in section (4.2.1).

Figure (4.11) shows the diagonal matrix elements $V_{\mathrm{low}\,k}(k,k)$ for a cut-off $\Lambda = 2.0\,\mathrm{fm}^{-1}$ for the chiral N^{3}LO potential of reference [26, 27]. We clearly see the effect of the sharp and smooth regulators. These differences are small in those partial wave channels where the potential is close to zero for momenta close to the cut-off. But in channels where the potential is non-zero for these momenta, the differences become significant as can be seen in the case of ${}^3D_2$ channel. We can particularly see cusp-like behavior with sharp regulator, which is the result of reproducing the phase shifts up to the cut-off Λ. The existence of sharp regulator artifacts is not a problem in principle, as the potential is not an observable, but in practice it can lead to convergence problems at the 10–100 keV level in the deuteron and triton.

As the momentum space cut-off Λ is lowered from its bare value, the intermediate states lying above the cut-off are integrated out. Therefore lowering the cut-off $\Lambda \sim 2.0\,\mathrm{fm}^{-1}$ leaves mostly the long-range pion exchange in the interaction potential. Therefore we expect the corresponding low-momentum potentials $V_{\mathrm{low}\,k}$ to be quite similar. This result in seen in figure (4.12) for the chiral N^{3}LO potentials [26, 27]. As the cut-off is lowered from a starting value of $\Lambda = 3.0\,\mathrm{fm}^{-1}$ down to $\Lambda = 1.5\,\mathrm{fm}^{-1}$, the low-momentum potentials corresponding to different chiral potentials are close but not *identical*. The differences are similar to the differences in the corresponding short-range three-body interactions.

Low-momentum potentials are phase-shift-equivalent potentials. In figure (4.9), we saw the distortion in the bare phase shifts. $V_{\mathrm{low}\,k}$ running causes further distortion (due to accumulation of numerical errors). The numerical errors can come from the

regulator used, the hermitization scheme, etc. This is documented in figure (4.13) for the ${}^1S_0$ channel, where we plot the absolute error in reproducing the distorted phase shifts of figure (4.9). Notice that the numerical errors associated with $V_{\mathrm{low}\,k}$ running is small. That is one of the key motivations to use the three-step method instead of the energy-indepedent RG (4.2.1). We can also conclude that Okubo hermitization yields stable results compared to Gram-Schmidt or Cholesky methods. Also a smooth cut-off works better than a sharp one at higher energies (close to the cut-off). We use the Okubo hermitization in the following unless otherwise specified. For fixed hermitization but different regulators, we have found that relatively smooth cutoffs (e.g., $\epsilon_{\mathrm{FD}} = 0.5\,\mathrm{fm}^{-1}$) achieve 10^{-4} degree accuracy with a moderate (of order 50) Gauss points, but sharper cutoffs (e.g., $\epsilon_{\mathrm{FD}} = 0.2\,\mathrm{fm}^{-1}$) have errors for energies above $E_{\mathrm{lab}} = 200\,\mathrm{MeV}$ that can grow as large as 10^{-1} degrees. Greater accuracy can be obtained with a more carefully prescribed distribution of points.[1]

4.3 Effect of Regulators on Few-body systems

Next we will switch gears and see how the choice of regulators affect properties of few body system. We will be considering the deuteron for the most part but also show some results for the triton (binding energy). The deuteron wave function in momentum space is obtained by directly diagonalizing the hamiltonian:

$$[T + V]|\Psi_d\rangle = E|\Psi_d\rangle. \tag{4.87}$$

[1]We note that the present scheme occasionally and unsystematically leads to numerical "glitches" in the low-momentum interaction, particularly for cutoffs close to the bare cutoff. These are manifested as discontinuities in the potential and are signaled by large discrepancies in calculated matrix elements. We have found that adjusting the momentum grid removes the glitches, but we do not yet have a preventive fix.

Working in the momentum space, in the partial wave basis equation (4.87) becomes:

$$T(k)\Psi_d(k) + \frac{2}{\pi}\int_0^\infty q^2 dq V(k,q)\,|\Psi_d(q) = E\Psi_d(k). \tag{4.88}$$

where $V(k,q)$ represents a generic $^3S_1$ potential. Notice that the integral is usually cut-off at some value Λ' where $\Lambda' = \Lambda_0$ for bare potential and $\Lambda' = \Lambda$ for $V_{\mathrm{low}\,k}$ potential. Since the deuteron in an admixture of $^3S_1 - ^3D_1$ states, the wave function has 2 components:

$$\Psi_d(k) = \begin{pmatrix} \widetilde{u}(k) \\ \widetilde{w}(k) \end{pmatrix} \tag{4.89}$$

and the wave function is normalized such that:

$$\int_0^\infty k^2 dk\,[|\widetilde{u}(k)|^2 + |\widetilde{w}(k)|^2] = 1. \tag{4.90}$$

The position space wave function [87] is given by:

$$\Psi_d(\mathbf{x}) = \frac{u(r)}{r}\mathcal{Y}^M_{101}(\theta,\phi) + \frac{w(r)}{r}\mathcal{Y}^M_{121}(\theta,\phi), \tag{4.91}$$

where

$$\mathcal{Y}^M_{JLS}(\theta,\phi) = \sum_{m_L,m_S}\langle J,M|L,m_L;S,m_S\rangle Y_{L,M}(\theta,\phi)|S,m_S\rangle \tag{4.92}$$

are the spin-spherical harmonics. The reduced wave functions correspond to the S and D waves respectively and are normalized as:

$$\int_0^\infty dr\,[|u(r)|^2 + |w(r)|^2] = 1. \tag{4.93}$$

The position and momentum space wave functions are related by the following fourier transforms:

$$\widetilde{u}(p) = \int_0^\infty u(r) j_0(r) r dr, \tag{4.94}$$

$$\widetilde{w}(p) = -\int_0^\infty w(r) j_2(r) r dr, \tag{4.95}$$

where $j_l(r)$ are the spherical bessel functions.

The figure (4.14) shows the deuteron wave function in momentum space for the chiral N^{3}LO [26] and the corresponding $V_{\mathrm{low}\,k}$ derived using sharp and smooth regulators for two different cut-offs of $\Lambda = 2.0\,\mathrm{fm}^{-1}, 1.5\,\mathrm{fm}^{-1}$. The corresponding r space wave functions are given in figure (4.15). In momentum space, we notice that sharp regulators lead to cusp-like structures in the wave function below a cut-off of $\Lambda = 2.0\,\mathrm{fm}^{-1}$, while this is eliminated by the smooth regulator. The influence of the regulator on the position space wave function is seen in the form of smaller amplitudes for large distance oscillations with increasing smoothing (for the S wave component this is visible only under further magnification). We also observe that the "wound" in the coordinate space wave function is removed by lowering the cut-off as seen in figure (4.16). This features implies smearing of the repulsive core and as a result the calculations in few- and many-body systems become more tractable [37, 38, 39].

Figure (4.17) shows the binding energy, D state probability and the asymptotic ratio as a function of the cut-off Λ for the Argonne v_{18} potential [31] on the left and the chiral N^{3}LO [26] on the right. We have used the exponential regulator with $n_{\mathrm{exp}} = 8$ for the Argonne potential and $n_{\mathrm{exp}} = 6$ for the chiral potential. The D-state probability P_D is defined as:

$$P_D \equiv \int_0^\infty dr[w(r)]^2 = \int_0^\infty dk k^2(\widetilde{w}(k))^2. \tag{4.96}$$

The cut-off dependence of the D-state probability implies that it is not an observable. It evolves with the short-range part of the tensor force. Therefore as the cut-off is lowered, the tensor force is softened, and as a result D-state probability decreases. This running is very important as it signals the decrease in the correlation of the many-body wave function. On the other hand the asymptotic D/S ratio η_d and

the deuteron binding energy E_d are observables and hence cut-off independent (up to numerical tolerance and are indicated on the right axis in figure (4.17)). The binding energy are the eigenvalues obtained by diagonalizing equation (4.88). For the asymptotic D/S ratio, we calculate the ratio $-\dfrac{\widetilde{w}(k)}{\widetilde{u}(k)}$ for positive energies (on a gaussian mesh) and then using a near-linear extrapolation to the deuteron pole $k^2 = -mE_d$. Therefore we see that $V_{\mathrm{low}\,k}$ preserves all *observable* properties of the deuteron.

Matrix elements of operators which are dominated by long-distance scales larger than the inverse of the cut-off will be predominately cut-off independent. We will examine the evolution of the quadrupole moment Q_d, rms radius r_d and the $\dfrac{1}{r}$ operator. The relevant formulas are [88]

$$\begin{aligned} Q_d &= \frac{1}{20}\int_0^\infty dr\, r^2\, w(r)\,(\sqrt{8}\,u(r) - w(r)) \\ &= -\frac{1}{20}\int_0^\infty dk \left[\sqrt{8}\left(k^2\,\frac{d\widetilde{u}(k)}{dk}\frac{d\widetilde{w}(k)}{dk} + 3k\,\widetilde{w}(k)\frac{d\widetilde{u}(k)}{dk}\right)\right. \\ &\qquad\qquad \left. + k^2\left(\frac{d\widetilde{w}(k)}{dk}\right)^2 + 6\,\widetilde{w}(k)^2\right], \end{aligned} \tag{4.97}$$

$$\begin{aligned} r_d &= \frac{1}{2}\left[\int_0^\infty dr\, r^2\,(u(r)^2 + w(r)^2)\right]^{1/2} \\ &= \frac{1}{2}\left[\int_0^\infty dk \left\{\left(k\,\frac{d\widetilde{u}(k)}{dk}\right)^2 + \left(k\,\frac{d\widetilde{w}(k)}{dk}\right)^2 + 6\,\widetilde{w}(k)^2\right\}\right]^{1/2}, \end{aligned} \tag{4.98}$$

and

$$\langle 1/r\rangle = \int_0^\infty dr\,\frac{1}{r}\,[u(r)^2 + w(r)^2]\,. \tag{4.99}$$

We note that the momentum-space expressions for Q_d and r_d show that these are only well-defined for a smooth cutoff [88].

Figure (4.18) shows the running of the expectation value of the quadrupole moment operator, for different regulators and hermitization schemes, while figures (4.19) and (4.20) show the running of the expectation value of the operators r_d and $\langle 1/r \rangle$. These operators are dominated by the long-distance scales and hence are mostly cut-off independent. We emphasize for instance in the case of the quadrupole moment, the experimentally measured value is obtained only if the bare operator is also evolved so as to get a corresponding low-momentum operator. Similar observations hold for the operators r_d and $\langle 1/r \rangle$.

The key motivation to explore the smooth regulator was the issue of slow convergence in few-body observables. Figure (4.21) shows the relative error in a variational calculation of the deuteron binding energy compared to the converged results as a function of the size of the oscillator space. We clearly see that going from a sharp to a smooth regulator which yields smaller relative error at the cost of considerably distorting the phase shifts for momenta close to the cut-off. Similar trends are seen in figure (4.22) where increasing the smoothness of the regulator improves convergence. In fact we see that the binding energy of the triton converges for small oscillator space $N_{max} = 20$ for the exponential regulator with $n_{\rm exp} = 4$ and the Fermi-Dirac regulator $\epsilon_{\rm FD} = 0.5\,{\rm fm}^{-1}$. The differences between the converged results for triton is a measure of the differences in the short-range three-body force with different regulators. Although it is possible to reproduce the experimental value of the triton binding energy using just the two-body force, the total three-body contribution does not vanish. We close this section emphasizing the need for simultaneous running of the two- and three-body interactions.

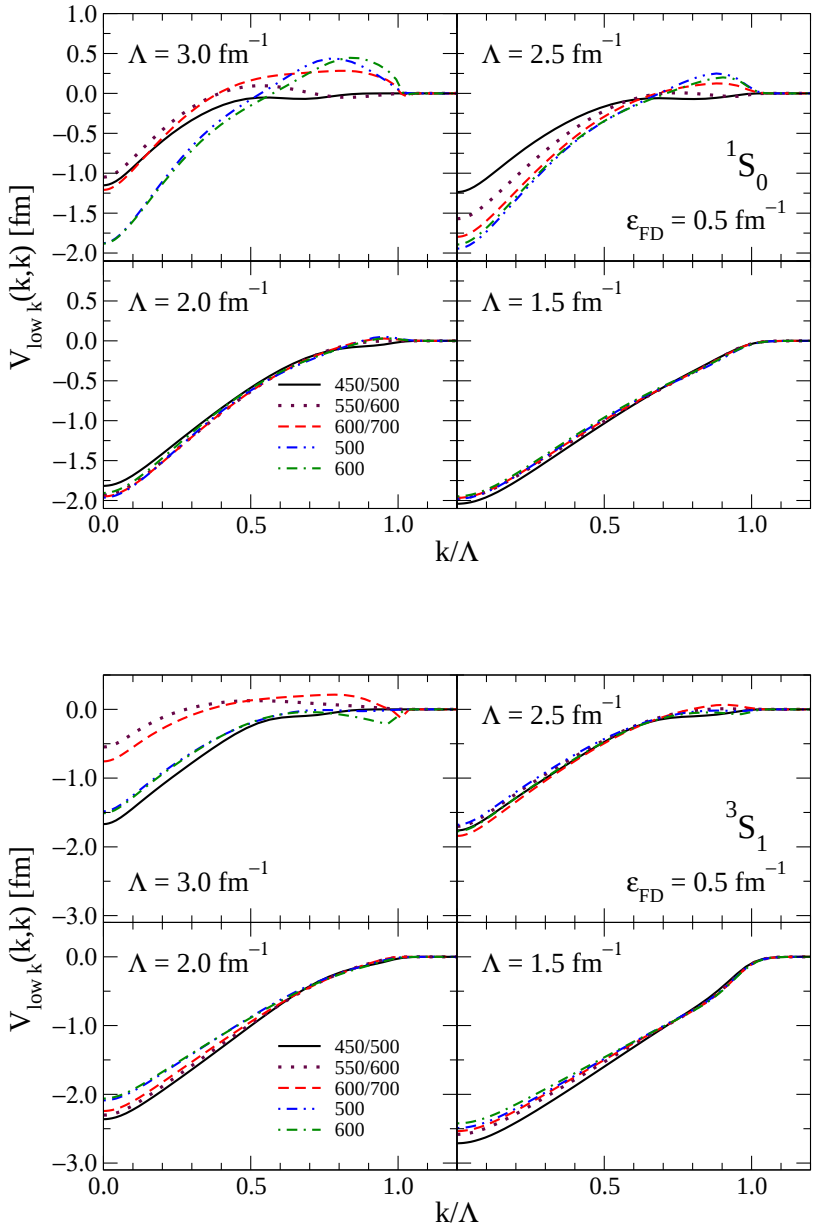

Figure 4.12: The "collapse" of $V_{\mathrm{low}\,k}$ interactions derived from N^{3}LO chiral potentials with a Fermi-Dirac regulator($\epsilon_{\mathrm{FD}} = 0.5\,\mathrm{fm}^{-1}$) as the cutoff is lowered in the ^{1}S$_0$ and ^{3}S$_1$ channels. The diagonal matrix elements $V_{\mathrm{low}\,k}(k,k)$ are shown, but we find similar results for the off-diagonal matrix elements. The different lines correspond to different starting potentials with the corresponding cutoffs, Λ [26] or $\Lambda/\widetilde{\Lambda}$ [27], in MeV given in the legends. $\widetilde{\Lambda}$ is the spectral function cutoff [27].

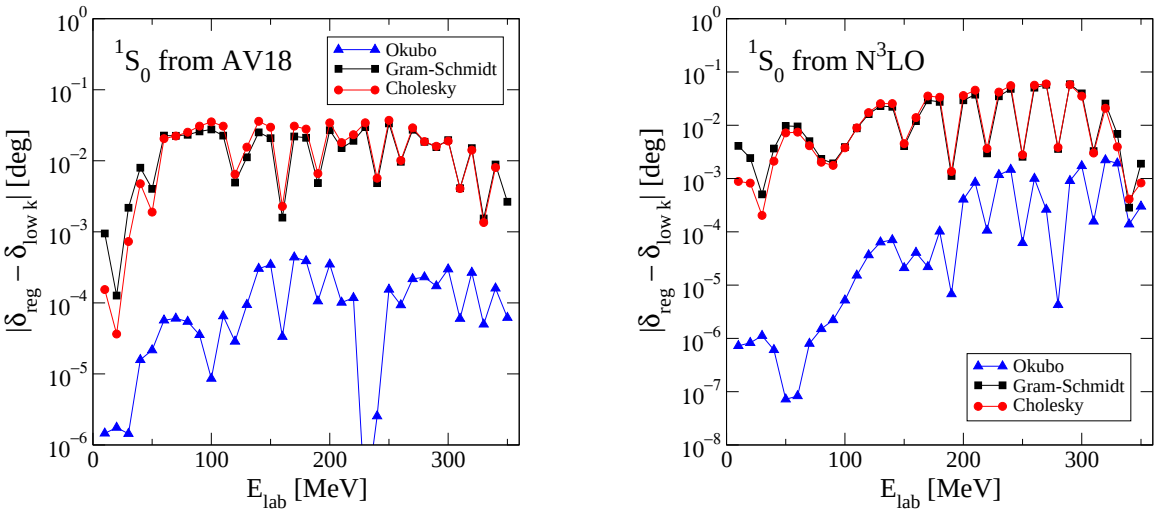

Figure 4.13: Errors in phase shifts relative to *regulated* bare phase shifts for three hermitization methods using the exponential regulator with $\Lambda = 2\,\mathrm{fm}^{-1}$. The potentials used on the left were derived from Argonne v_{18} [31] with $n_{\mathrm{exp}} = 4$ and those used on the right were derived from the N^{3}LO chiral potential from reference [26] with $n_{\mathrm{exp}} = 8$.

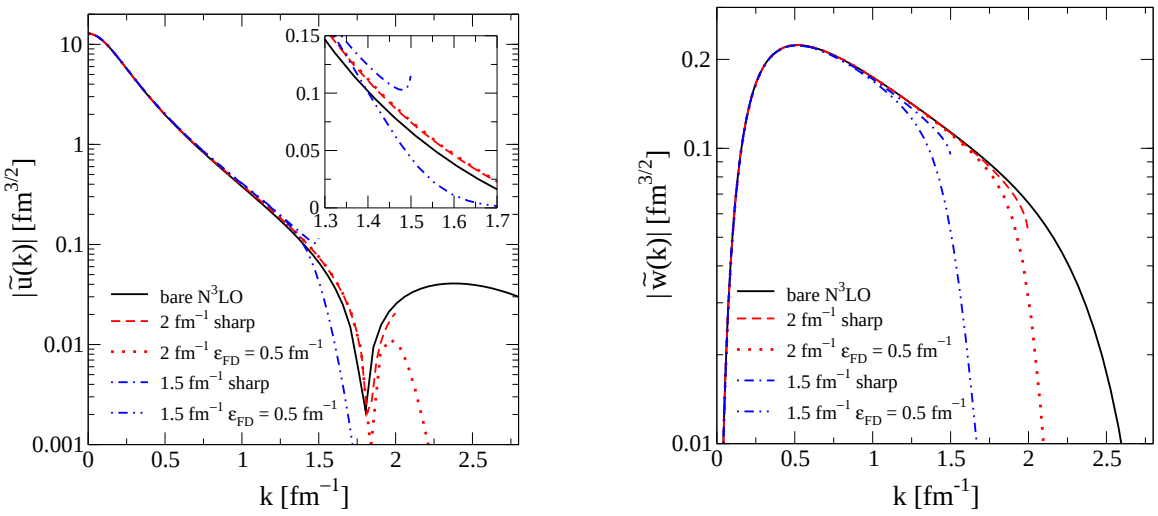

Figure 4.14: S–state and D–state components of the deuteron wave function in momentum space ($\widetilde{u}(k)$ and $\widetilde{w}(k)$ respectively) for the bare N^{3}LO chiral potential from reference [26] and those derived using smooth and sharp cutoffs at $\Lambda = 2.0\,\mathrm{fm}^{-1}$ and $1.5\,\mathrm{fm}^{-1}$.

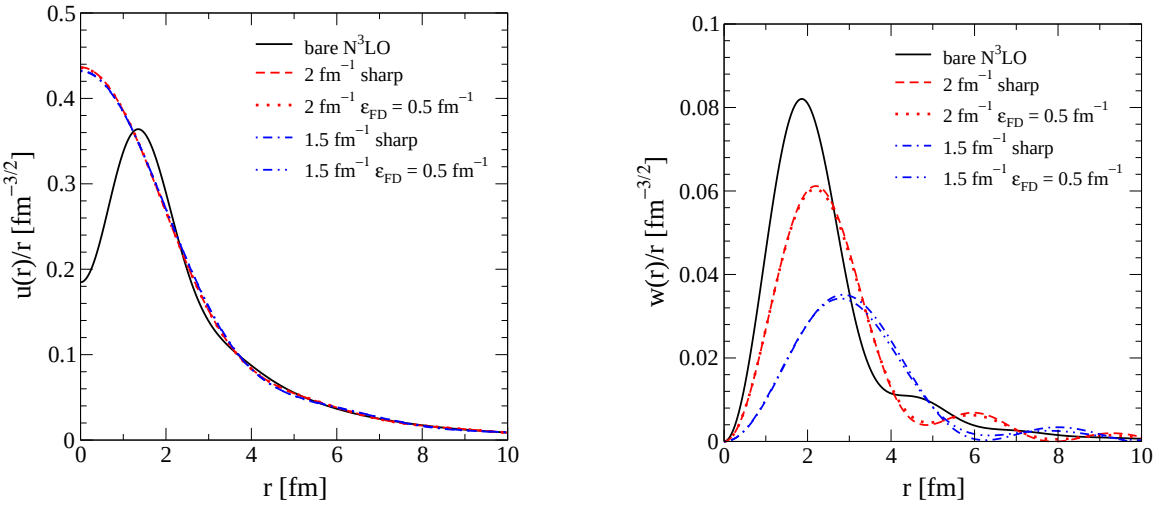

Figure 4.15: deuteron wave functions in coordinate space for smooth and sharp cutoffs as in Fig. 4.14.

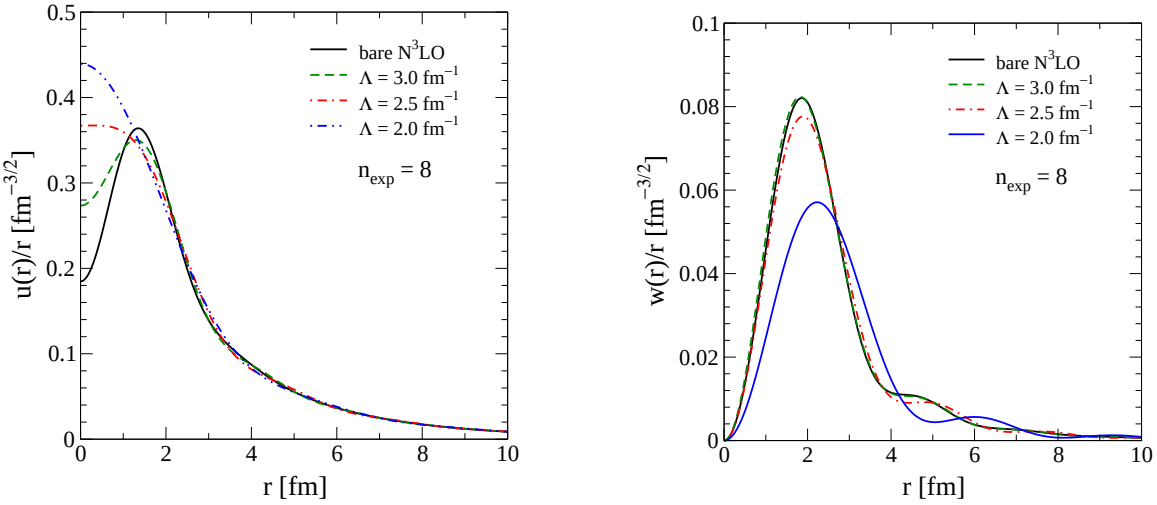

Figure 4.16: deuteron wave functions in coordinate space for low-momentum interactions at several different cutoffs using an exponential regulator with $n_{\rm exp} = 8$. The initial interaction is the N^{3}LO chiral potential from reference [26].

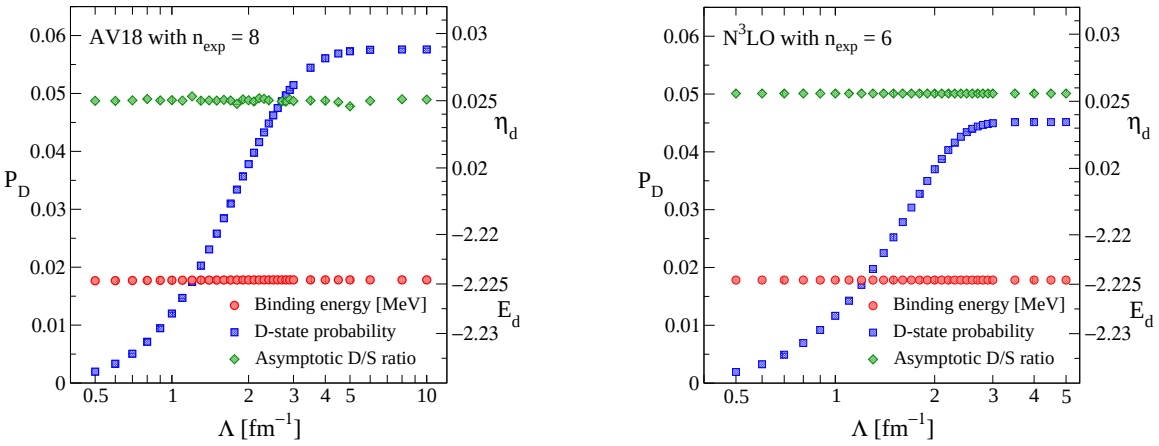

Figure 4.17: D–state probability $P_{\rm D}$ (left axis), binding energy E_d (lower right axis), and asymptotic D/S ratio η_d (upper right axis) of the deuteron as a function of the cutoff, starting from the Argonne v_{18} [31] (left) and the N^{3}LO chiral potential of reference [26] (right) with different smooth regulators.

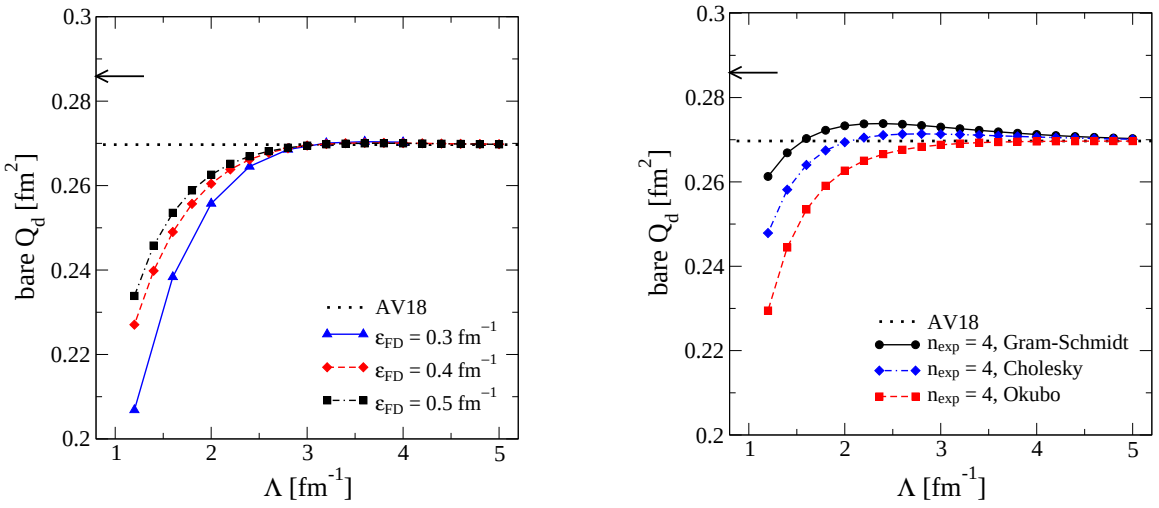

Figure 4.18: The quadrupole moment of the deuteron Q_d calculated with the bare operator as a function of the cutoff for different smoothness regulators (left) and for different hermitization schemes (right). The low-momentum interactions are derived from the Argonne v_{18} potential [31], and the experimental quadrupole moment is indicated with an arrow.

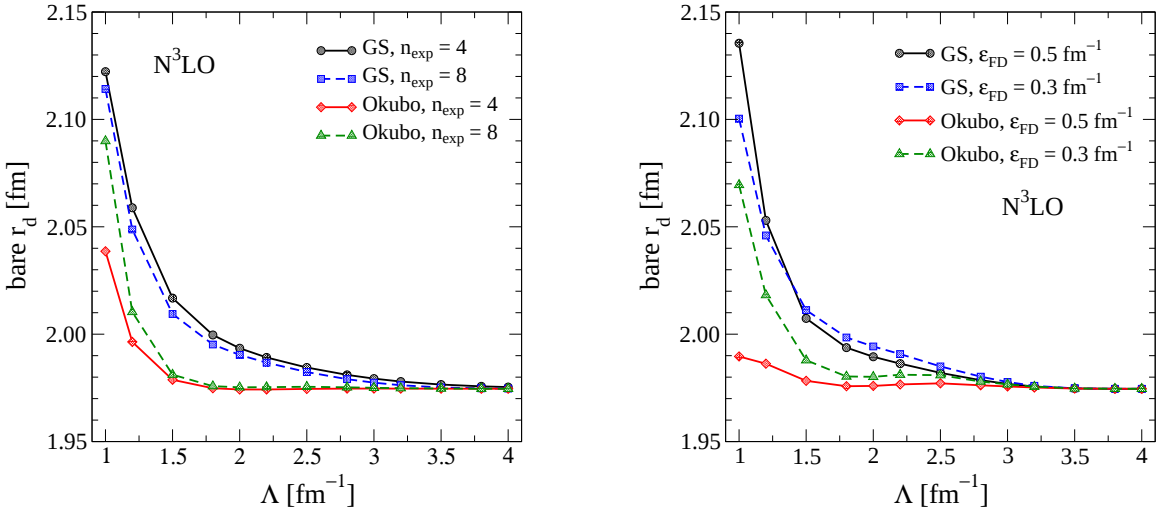

Figure 4.19: The rms radius r_d of the deuteron calculated with the bare operator as a function of the cutoff for different regulators and hermitization schemes. The low-momentum interactions are derived using the N^{3}LO chiral potential from reference [26].

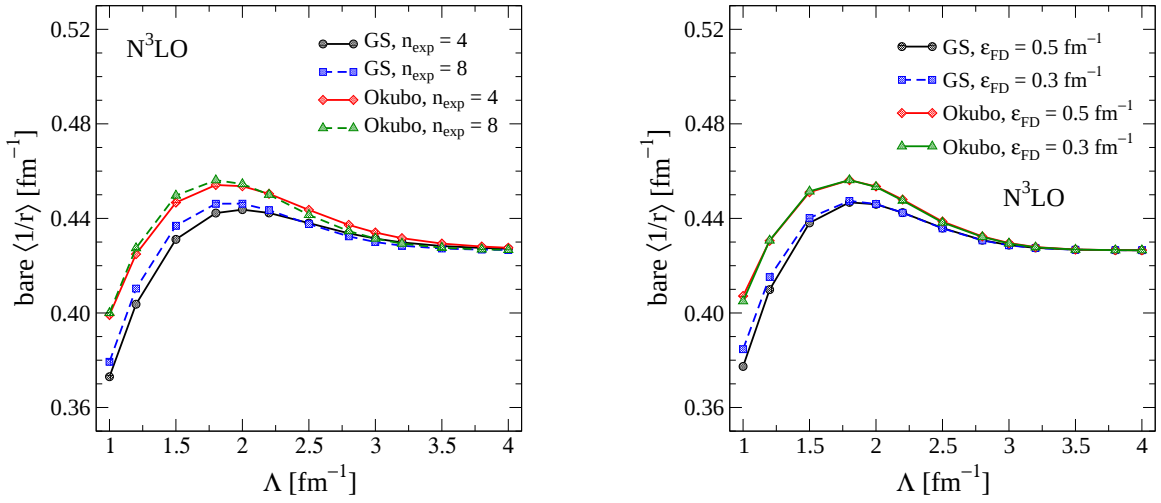

Figure 4.20: The matrix element of $1/r$ in the deuteron calculated with the bare operator as a function of the cutoff for different regulators and hermitization schemes. The low-momentum interactions are derived using the N^{3}LO chiral potential from reference [26].

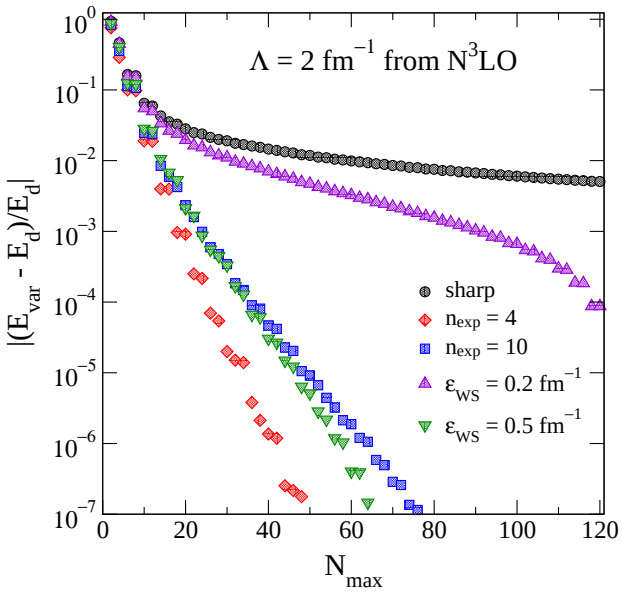

Figure 4.21: The relative error in the deuteron binding energy E_d as a function of the size of the oscillator space for sharp cutoff and various smooth regulators.

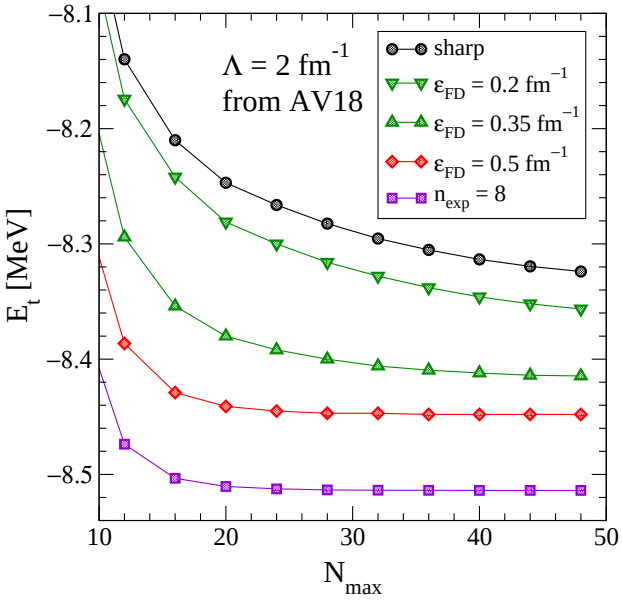

Figure 4.22: The triton binding energy E_t as a function of the size of the oscillator space,for different smoothness regulators starting from the Argonne v_{18} potential [31].

CHAPTER 5

CONVERGENCE OF LOW MOMENTUM BORN-SERIES

The first step towards building a microscopic theory for finite nuclei is to have a nucleon-nucleon interaction which is appropriate for nuclear physics at low and intermediate energies. In the previous chapters we had gone through in detail the construction of the renormalization group based low-momentum potentials $V_{\mathrm{low}\,k}$. Let us recall that these potentials are non-local, soft potentials. Our claim earlier was that the smearing of the short-distance physics by renormalization group running leads to convergence in smaller model spaces in many-body calculations. Therefore using $V_{\mathrm{low}\,k}$ as input makes many-body calculations more tractable. In this chapter we will investigate the simplifications introduced by these RG based potentials in the context of the convergence of the Born series in free space and in medium. Recent work [37] using $V_{\mathrm{low}\,k}$ shows that the ground-state energy of symmetric nuclear matter is perturbative in the particle-particle channel and that saturation is brought about by the three-body force, contrary to conventional wisdom, where saturation is due to the tensor force. We will quantify these ideas of perturbativeness using the eigenvalue approach due to Weinberg [41]. A spin-off of the Weinberg eigenvalue analysis is the separable approximation [41, 52] to the nucleon-nucleon interaction, which will be addressed towards the close of this chapter. We start our discussions with a quick

review of symmetric nuclear matter [56, 57, 58] as a simple starting point for many-body calculation.

5.1 Nuclear Matter

Nuclear matter is a hypothetical system of equal numbers of neutrons and protons which fill all space at a uniform density. This system offers several simplification compared to evaluating properties of finite nuclei. If we are interested in the bulk properties such as energy per particle $\frac{E}{A}$ for A nucleons (N neutrons and Z protons), then this is given by the semi-empirical Weizsäcker Mass formula:

$$\frac{E}{A} = -a_1 + a_2 A^{\frac{1}{2}} + a_3 Z^2 A^{-\frac{4}{3}} + a_4 (A - 2Z)^2 A^{-2} + \lambda a_5 A^{-\frac{7}{4}} \tag{5.1}$$

The first term is the volume term, the second term is the binding energy lost because of surface tension, the third term is the Coulomb energy, the fourth is the symmetry energy and the last term is the pairing energy where the parameter λ takes values $\{+1, 0, -1\}$ depending on odd-odd, even-odd and even-even nuclei. For symmetric nuclear matter, we let $A \to \infty$, so that the surface term drops out and the volume term dominates; the symmetry energy term has no contribution as we have equal number of neutrons and protons; we also neglect the coulomb effect, so that

$$\frac{E}{A} = -a_1 \approx -15.7\,\text{MeV} \tag{5.2}$$

The particle density in nuclear matter is $\rho_0 \approx 0.17\text{fm}^{-3}$. Since energy and particle density are both independent of the number of nucleons A, nuclear forces saturate at the equilibrium density ρ_0. This implies that a plot of $\frac{E}{A}$ versus density ρ has a minimum for $\rho = \rho_0$ and this corresponds to $\frac{E}{A} \approx -15.7\,\text{MeV}$. So a good check for

the nucleon-nucleon interaction potentials would be their ability to reproduce these empirical estimates.

A microscopic calculation of bulk properties of nuclear matter starts with the many-body hamiltonian,

$$H = \sum_{i=1}^{A} T_i + \sum_{i<j}^{A} v_{ij} + \cdots = H_0 + H_1. \tag{5.3}$$

Here A is the number of nucleons, T_i, the kinetic energy of the i^{th} particle and v_{ij} is the interaction energy between the i^{th} and j^{th} particles. Typically we will expect higher-body forces to contribute. But for the present discussion we will just consider two-body forces. Let $|\psi\rangle$ be the ground state of the interacting system, then we are seeking a solution to the following eigenvalue problem,

$$H|\psi\rangle = E|\psi\rangle. \tag{5.4}$$

Let $|\Phi_0\rangle$ be the non-interacting ground state, that is an eigenstate of $H_0 = T = \sum_i^{\infty} T_i$. This can be written as a direct product of single-particle eigenfunctions $|\phi_i\rangle$, which are antisymmetrized for this system of fermions as follows:

$$|\Phi_0\rangle = \frac{1}{A^{\frac{1}{2}}}\mathcal{A}(|\phi_1\rangle \cdots |\phi_A\rangle). \tag{5.5}$$

where $\mathcal{A}$ is the antisymetry operator. This non-interacting ground state corresponds to a filled fermi sea and the excited states are above the fermi sea.

Using the standard many-body machinery [56], the ground state energy E can be expanded as follows:

$$E = E_0 + \langle\Phi_0|H_1 \sum_{n=0}^{\infty} (\frac{1}{E - H_0} H_1)^n |\Phi_0\rangle_{connected} \tag{5.6}$$

so that the effect of the interaction, $H_1 = V = \sum_{ij}^{A} v_{ij}$, can be taken into account order by order in the perturbation theory. The above expansion can be diagrammatically

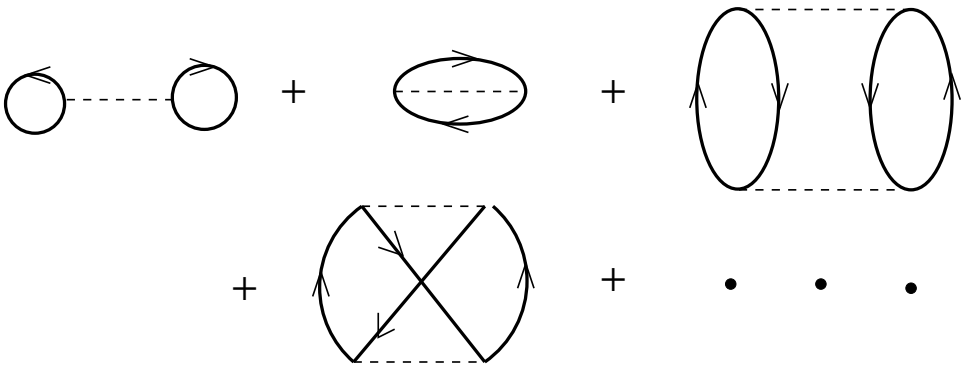

Figure 5.1: First and second-order Goldstone diagrams for $E - E_0$ for uniform fermi system

represented as shown in figure (5.1). Note that only connected diagrams contribute (Goldstone's Theorem). Each diagram can be interpreted as follows: starting with a filled fermi sea, the interaction creates two particle-hole pairs, which propagate. This is given by the corresponding two particle Green's function $\frac{1}{E - H_0}$. These paticle-hole pairs can either scatter back into the fermi sea or create more particle-hole pairs through the interaction V. These diagrams therefore give the change in the ground state energy due to the interaction order-by-order in the perturbation theory.

5.2 Convergence of Born series and the Reaction Matrix

The above expansion (equation (5.6)), cannot be used in its present form for nuclear calculations, as the nucleon-nucleon interaction potentials conventionally have the following sources of non-perturbative physics:

1. Strong short-range repulsion.

2. Iterated tensor force from the one-pion exchange.

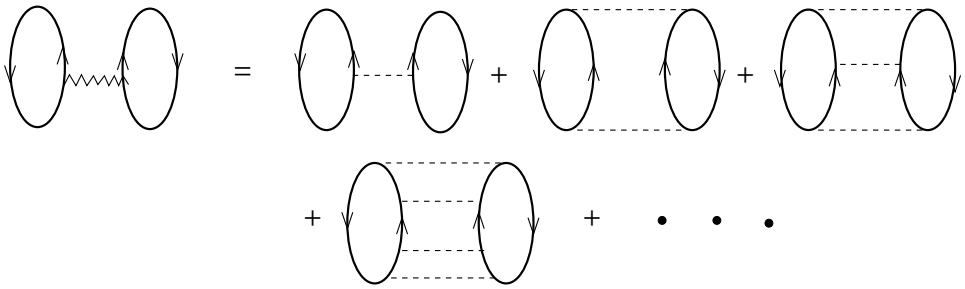

Figure 5.2: G resummation: Notice that all the ladder diagrams are summed to all orders to result in the G

3. Shallow bound states present in the S channel.

As a result the expansion in equation (5.6) does not converge.

The way around it is a partial resummation of several terms, which results in replacing the potential V by the Brueckner's reaction matrix, usually called the G matrix. The procedure followed for nuclei is analogous to resummations introduced for the nucleon-nucleon scattering in free space, the (T) matrix, which is equivalent to solving the two-particle Schrödinger equation. In-medium, the calculation of G matrix is equivalent to solving Schrödinger equation for two-body scattering in the presence of other particles.

Figure (5.2) serves to illustrate this method. The wiggly lines stand for the G summation:

$$G = V + V\frac{Q}{E - H_0}V + V\frac{Q}{E - H_0}V\frac{Q}{E - H_0}V + \cdots \tag{5.7}$$

$$G = V + V\frac{Q}{E - H_0}G \tag{5.8}$$

where Q is the Pauli-blocking operator, which restricts intermediate states to be above the Fermi sea. In the partial-wave basis, in momentum space, the G matrix equation

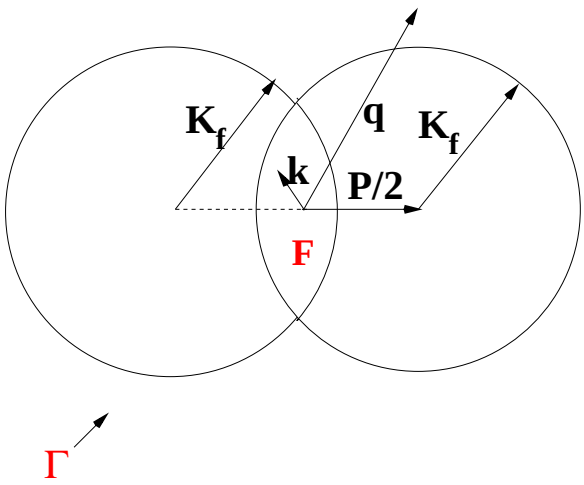

Figure 5.3: Schematic of integration region: Q operator present in the G equation restricts the intermediate states according Pauli exclusion principle.

is as follows:

$$G(k',k;E) = V(k',k) + \frac{2}{\pi}\int_{\Gamma}^{\infty} p^2 dp\, V(k',p)\,\frac{Q(p,k_{\rm F})}{E-p^2}\,G(p,k;E) \tag{5.9}$$

The integration region is shown in figure (5.3). Scattering from region F to the region Γ is allowed due to the Pauli exclusion principle. The equation (5.7) is an analogous expression for the Born series expansion of the T matrix in free-space. We will refer to this expansion as the "in-medium Born series". Writing equation (5.7) in the partial wave basis in momentum space, we get the following expression for the in-medium Born series:

$$\begin{aligned} G(k',k;E) &= V(k',k) + \frac{2}{\pi}\int_{\Gamma}^{\infty} p^2 dp V(k',p)\frac{Q(p,k_{\rm F})}{E-p^2}V(p,k) \\ &+ \frac{2}{\pi}\int_{\Gamma}^{\infty} p^2 dp \frac{2}{\pi}\int_{\Gamma}^{\infty} q^2 dq V(k',p)\frac{Q(p,k_{\rm F})}{E-p^2}V(p,q)\frac{Q(q,k_{\rm F})}{E-q^2}V(q,k) \\ &+ \cdots \end{aligned} \tag{5.10}$$

The corresponding equation in free-space is:

$$\begin{aligned} T(k',k;E) &= V(k',k) + \frac{2}{\pi}\int_0^\infty p^2 dp V(k',p)\frac{1}{E-p^2}V(p,k) \\ &+ \frac{2}{\pi}\int_0^\infty p^2 dp \frac{2}{\pi}\int_0^\infty q^2 dq V(k',p)\frac{1}{E-p^2}V(p,q)\frac{1}{E-q^2}V(q,k) \\ &+ \cdots \end{aligned} \tag{5.11}$$

Note that in free-space there is no Pauli-blocking so the intermediate states have all momenta available (compare equations (5.10) and (5.11)). We will re-examine the issue of the convergence of the Born series by comparing the first two terms in free-space and in-medium for Av_{18} (refered to as $V_{\rm NN}$ in the figure (5.4)) and $V_{{\rm low}\,k}$.

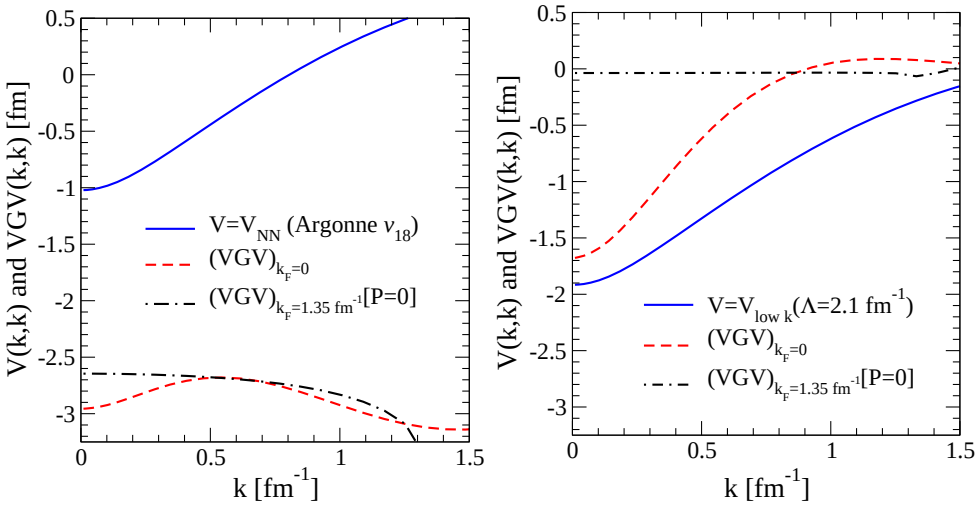

Figure 5.4: First and second term of $T(k,k';k^2)$ in momentum space for the $^1S_0$ channel. Notice for the Argonne Potential that the second term is bigger than the first in free space and this trend remains the same in-medium. On the other hand with corresponding $V_{{\rm low}\,k}$ the second term is smaller than the first for all k in free space and gets significantly smaller in-medium.

Figure (5.4) shows the momentum space matrix elements for the first two terms in the T matrix equation for the Av_{18} potential (left panel). We see that the second

term is bigger than the first for all k values and this trend does not change in-medium in spite of the Pauli-Blocking. On the other hand a similar plot using the corresponding $V_{\mathrm{low}\,k}(k',k)$ at Λ of 2.1 fm^{-1}, we see that the second term is smaller than the first for all k, this difference being the least for k close to the origin, which can be linked to the presence of shallow bound states (right panel). Therefore the non-perturbative physics which enters through the short-range repulsion and the iterated tensor force are scale dependent. Evolving the potential to lower cut-offs softens these contributions. But shallow bound states which are physical observables in free space are cut-off independent. The figure also shows the in-medium terms. We see that at finite density the third contribution of non-perturbative physics, namely the presence of shallow bound state is eliminated due to Pauli blocking.

We can understand the in-medium results by examining the integration region, which represents the available intermediate states. When $V_{\mathrm{low}\,k}(k',k)$ is used as input instead of the bare potential V_{NN}, the G matrix equation (5.10) gets modified as follows:

$$\begin{aligned} G(k',k;E) &= V_{\mathrm{low}\,k}(k',k) + \frac{2}{\pi}\int_{\Gamma}^{\Lambda} p^2 dp V_{\mathrm{low}\,k}(k',p)\frac{Q(p,k_{\mathrm{F}})}{E-p^2}V_{\mathrm{low}\,k}(p,k) \\ &+ \frac{2}{\pi}\int_{\Gamma}^{\Lambda} p^2 dp \frac{2}{\pi}\int_{\Gamma}^{\Lambda} q^2 dq V_{\mathrm{low}\,k}(k',p)\frac{Q(p,k_{\mathrm{F}})}{E-p^2}V_{\mathrm{low}\,k}(p,q)\frac{Q(q,k_{\mathrm{F}})}{E-q^2}V_{\mathrm{low}\,k}(q,k) \\ &+ \cdots \end{aligned} \tag{5.12}$$

The figure (5.5) shows a schematic of the available intermediate states. As before, scattering is allowed from the region F to the the region Γ. But notice that the region Γ now has an upper bound at the cut-off Λ (compare figure (5.3)). This sort of cut-off is true even for conventional potentials (usually some Λ_0), but those values are very high (for Av_{18}, $\Lambda_0 \approx 30$ fm^{-1}). The typical cut-off for $V_{\mathrm{low}\,k}$ is around $2.0 - 2.1$ fm^{-1}.

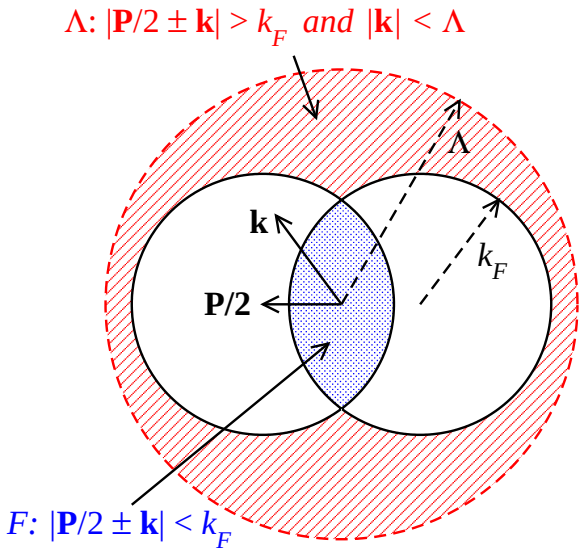

Figure 5.5: Schematic of integration region: Q operator present in the G equation restricts the intermediate states according Pauli exclusion principle. Note that using $V_{\mathrm{low}\,k}$ restricts allows intermediate state up to the cut-off Λ, apart from the lower bound due to Pauli blocking.

Therefore lowering the cut-off limits the intermediate states available for scattering. Therefore, from these phase space arguments and the fact that $V_{\mathrm{low}\,k}$ are soft potentials it is not surprising that the Born series expansion given by equation (5.12) is convergent when $V_{\mathrm{low}\,k}$ is used as input.

5.3 Weinberg Eigenvalue Analysis

We would like to quantify the above observation. This is done by examining the eigenvalue spectrum of the operator $G_0(z)V$ [41]. We will closely follow the analysis presented in reference [41, 52] and extend it to the RG based low-momentum potentials $V_{\mathrm{low}\,k}$. Independent of the choice of basis, T matrix equation at energy z:

$$T(z) = V + VG_0(z)T(z) \tag{5.13}$$

The above can be expanded to obtain a series in V (Born Series).

$$T(z) = V + VG_0(z)V + VG_0(z)VG_0(z)V + \cdots \tag{5.14}$$

Let us assume that V supports a bound state at $z = E_b < 0$. Therefore $T(z)$ has a pole at $z = E_b$, while the individual terms of the above series: $V\dfrac{1}{E_b - H_0}V\dfrac{1}{E_b - H_0}V\cdots$ are all finite. Therefore the only way $T(z)$ will have a pole at $z = E_b$ is if the series diverges as $z \to E_b$.

Let us now investigate how the above series behaves in the neighborhood of $z = E_b < 0$ and at positive energies. Look at the eigenvalue problem for the bound state:

$$(H_0 + V)|b\rangle = E_b|b\rangle \tag{5.15}$$

$$\Rightarrow |b\rangle = \frac{1}{E_b - H_0}V|b\rangle \tag{5.16}$$

$$\Rightarrow |b\rangle = G_0(E_b)V|b\rangle \tag{5.17}$$

Consider the following generalization:

$$\eta_\nu(z)|\Psi_\nu\rangle = G_0(z)V|\Psi_\nu\rangle \tag{5.18}$$

Here the index ν labels the Weinberg eigenvalues (which are always discrete [41, 52]) and eigenvectors.

Clearly if $|\Psi_\nu\rangle = |b\rangle$ then $\eta_\nu(z) = 1$. A rearrangement of equation (5.18) gives a simple interpretation of the eigenvalues $\eta_\nu(z)$ in terms of the Schrödinger equation,

$$\left(H_0 + \frac{1}{\eta_\nu(z)}\,V\right)|\Psi_\nu(z)\rangle = z\,|\Psi_\nu(z)\rangle. \tag{5.19}$$

The eigenvalue $\eta_\nu(z)$ can thus be viewed as an energy-dependent coupling that must divide V to produce a solution to the Schrödinger equation at energy z. We also

notice that if V is an attractive potential, then a value of $0 < \eta_\nu(z) < 1$ makes the $\dfrac{V}{\eta_\nu(z)}$ potential stronger, thereby resulting in a bound state at $z = -|E|$ for the potential $\dfrac{V}{\eta_\nu(z)}$. As a result, what matters for convergence at a given energy z is not simply the presence of nearby physical bound states, but rather the entire set of eigenstates that can be shifted to z when the interaction is divided by $\eta_\nu(z)$. For negative energies, a purely attractive V gives positive $\eta_\nu(z)$ values, while a purely repulsive V gives negative eigenvalues, as the sign of the interaction must be flipped to support a bound state. For this reason, we follow convention and refer to negative eigenvalues as repulsive and positive ones as attractive.

In the case of conventional nuclear interactions, the repulsive core generates at least one large and negative eigenvalue that causes the Born series to diverge in the low partial waves. When z is positive, the eigenvalues $\eta_\nu(z)$ are complex, but still discrete. In fact the eigenvalues are analytic functions cut along $0 \leqslant z < \infty$ [52]. Weinberg also showed that there are at most a finite number of eigenvalues with magnitudes greater than unity [41] for any energy z. This is used in Weinberg's "quasiparticle" method to systematically isolate the nonperturbative parts of the potential in separable form. For positive energies, the eigenvalues are defined as the limits on the upper or lower edges of the cut:

$$\lim_{\epsilon \to 0} G_0(E \pm i\epsilon) V |\Psi_\nu^{(\pm)}(E)\rangle = \eta_\nu^{(\pm)}(E)\, |\Psi_\nu^{(\pm)}(E)\rangle \,. \tag{5.20}$$

In the following, it is understood that for positive energy $\eta_\nu(E) = \eta_\nu^{(+)}(E)$. The eigenvalues vary continuously with energy, so they can be plotted as trajectories in the complex plane, as in figures (5.6) and (5.7). Let us see how the spectrum of this kernel is related to the convergence of the series expansion of T in terms of V.

Consider:

$$T(z)|\Psi_\nu(z)\rangle = (V + VG_0(z)V + \cdots)|\Psi_\nu(z)\rangle. \tag{5.21}$$

Using equation (5.18):

$$T(z)|\Psi_\nu(z)\rangle = (V + V\eta_\nu(z) + \cdots)|\Psi_\nu(z)\rangle \tag{5.22}$$

$$\Rightarrow T(z)|\Psi_\nu(z)\rangle = (V|\Psi_\nu(z)\rangle)(1 + \eta_\nu(z) + \eta_\nu^2(z) + \cdots). \tag{5.23}$$

The above sum diverges if $|\eta_\nu(z)| > 1$. Now any scattering state $|\Psi\rangle$ can be written as a linear combination of $|\Psi_\nu(z)\rangle$. So the expansion for T in terms of V will converge only if all the η_ν's lie within the unit circle. Therefore for each energy, the overall largest eigenvalue determines whether or not the Born series converges at that energy. But by considering attractive and repulsive eigenvalues separately we can isolate the contributions of different sources of nonperturbative behavior.

5.3.1 Weinberg eigenvalue and $V_{\text{low}\,k}$

We will now apply the above formalism to $V_{\text{low}\,k}$ [42] in order quantify the convergence of the Born series in free space and in-medium. First we will discuss the free space results. Here we calculate the Weinberg eigenvalues in different partial waves as a function of energy for $V_{\text{low}\,k}$ over a wide range of cutoffs. Working in the partial wave basis, in momentum space, the eigenvalue equation (5.18) is given by

$$\frac{2}{\pi}\int_0^\Lambda k^2 dk\, \frac{V_{\text{low}\,k}(k',k)}{p^2 - k'^2 + i\epsilon}\,\langle k|\Psi_\nu(p^2)\rangle = \eta_\nu(p^2)\,\langle k'|\Psi_\nu(p^2)\rangle\,. \tag{5.24}$$

We solve equation (5.24) by converting it to a left-eigenvalue problem, where we integrate over the singularity using $1/(x+i\epsilon) = \mathcal{P}/x - i\pi\delta(x)$. Alternatively, we can solve the complex right-eigenvalue problem for $VG_0(z)\,[V|\Psi_\nu(z)\rangle] = \eta_\nu(z)\,[V|\Psi_\nu(z)\rangle]$, which has the same spectrum as $G_0(z)V$ and integrates over the singularity directly.

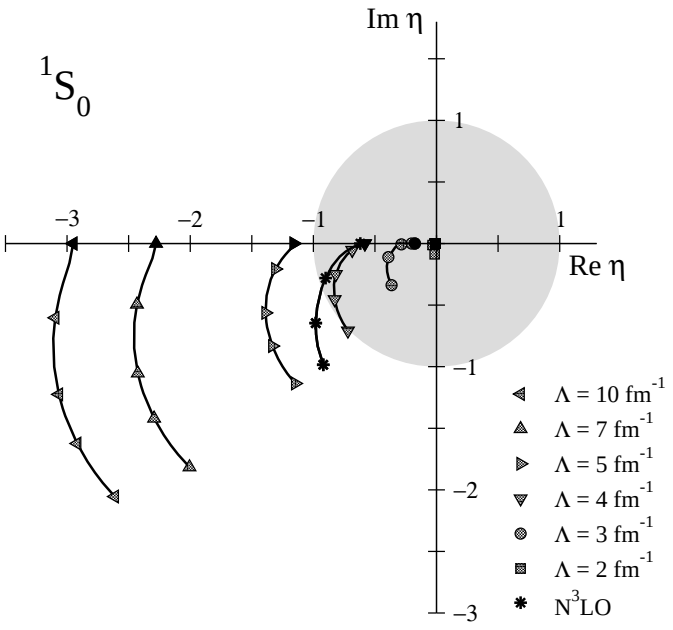

Figure 5.6: Largest repulsive eigenvalues in complex η plane for $^1S_0$ channel. The solid points on the $\Re\,\mathrm{e}\eta$ axis represents $E_{\mathrm{cm}} = 0\,\mathrm{MeV}$ for $\Lambda = 10\,\mathrm{fm}^{-1}$, $7\,\mathrm{fm}^{-1}$, $5\,\mathrm{fm}^{-1}$, $4\,\mathrm{fm}^{-1}$, $3\,\mathrm{fm}^{-1}$ and $2\,\mathrm{fm}^{-1}$ repectively starting from the left. Notice that decreasing the cut-off decreases the magnitude of the eigenvalues.

We see in figure (5.6) the largest repulsive eigenvalues for the $^1S_0$ channel in the complex η plane for the Av_{18} potential. The shaded area represents the unit circle. The solid points on the real axis are at $E_{\mathrm{cm}} = 0\,\mathrm{MeV}$. As the energy becomes positive the eigenvalues are complex. We see that the magnitude of the repulsive eigenvalues decrease as the cut-off is lowered from $10\,\mathrm{fm}^{-1}$ down to $2\,\mathrm{fm}^{-1}$. At large values of the cut-off the short distance repulsion dominates the eigenvalue spectrum which is indicated by large repulsive eigenvalues. As the cut-off is lowered, the short-distance repulsion is softened resulting in significant decreases in the magnitude of the repulsive eigenvalues. Smaller eigenvalues imply better convergence of the Born Series for the T matrix in free space.

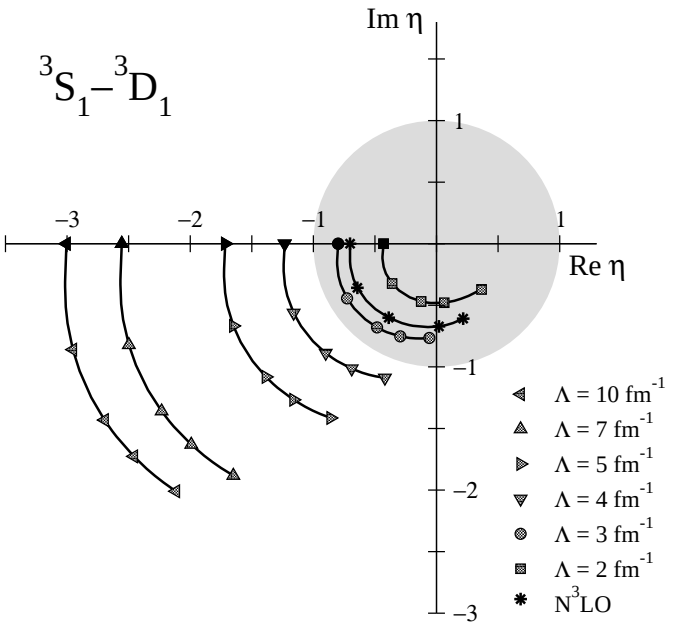

Figure 5.7: Largest repulsive eigenvalues in complex η plane for $^3S_1$ channel. The solid points on the $\Re\,\mathrm{e}\,\eta$ axis represents $E_{\mathrm{cm}} = 0\,\mathrm{MeV}$ for $\Lambda = 10\,\mathrm{fm}^{-1}$, $7\,\mathrm{fm}^{-1}$, $5\,\mathrm{fm}^{-1}$, $4\,\mathrm{fmi}$, $3\,\mathrm{fm}^{-1}$ and $2\,\mathrm{fm}^{-1}$ repectively starting from the left. Notice that decreasing the cut-off decreases the magnitude of the eigenvalues.

Next we study the largest repulsive eigenvalues for the $^3S_1 - ^3D_1$ coupled channel in figure (5.7). Again we note that lowering the cut-off decreases the magnitude of the eigenvalues. But we see that the rate of convergence in the $^3S_1 - ^3D_1$ channel is less compared to the $^1S_0$ channel (figure (5.6)). This difference can be attributed to the presence of the repulsive tensor force in the coupled channel in addition to the short-range repulsion at large values of Λ. Once again lowering the cut-off softens the tensor and the short-distance contribution and the eigenvalues are well within the unit circle.

The figure (5.8) shows the largest attractive eigenvalues for the S waves. Notice that the eigenvalues are all bunched around 1 and they do not change significantly

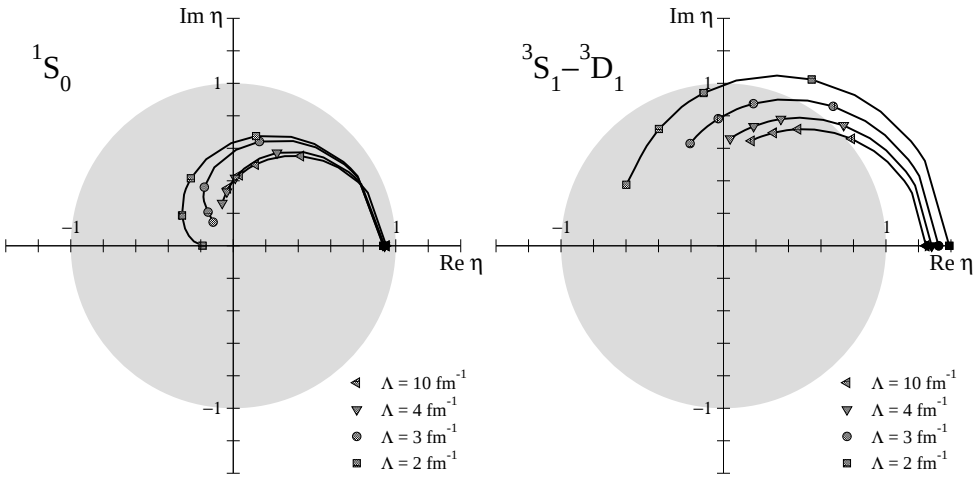

Figure 5.8: Largest attractive eigenvalues in complex η plane for $^1S_0$ and $^3S_1$ channel. Notice that the eigenvalues are all close to 1, indicating the presence of nearly bound state in the $^1S_0$ channel and shallow bound state in the $^3S_1$ channel, which is independent of the scale of resolution (cut-off).

with the cut-off. This clearly agrees with the fact that the shallow bound states are physical observables and should be independent of the resolution scale. However Pauli blocking in-medium does not allow the formation of bound states, and therefore the shallow bound states are density-dependent sources of non-perturbative physics. From these discussions we clearly see the advantages of lowering the cut-off for realistic nucleon-nucleon potentials and using the corresponding $V_{\mathrm{low}\,k}$ in calculations. It has been shown that these low-momentum renormalization group based potentials in many-body calculations are perturbative in the particle-particle channel perturbative [37]. Since the sources of non-perturbative physics are tamed, the wave functions (example: deuteron) are less correlated and as a result simple variational approaches to determine the binding energy of few-body systems, such as the deuteron and triton, yield good results [38, 39].

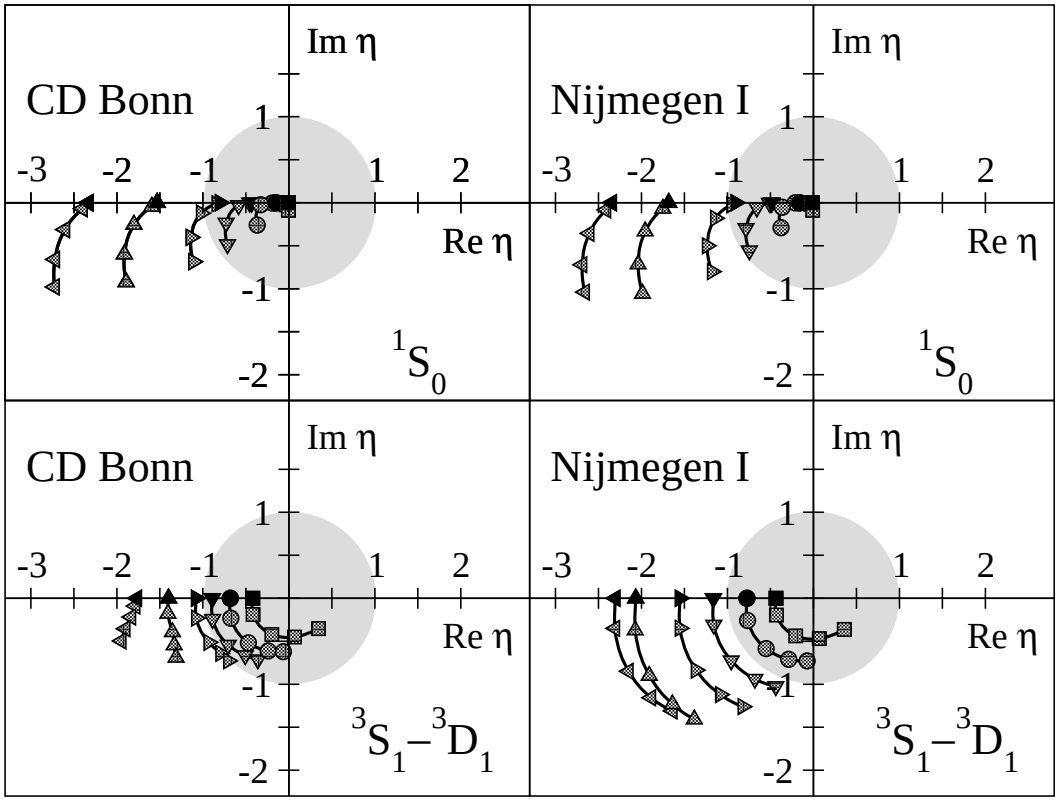

Figure 5.9: Largest repulsive eigenvalues in complex η plane for $^1S_0$ and $^3S_1$ channel for CD-Bonn and Nijmegen I potentials.

Weinberg eigenvalues for other high-precision potentials (results shown for CD-Bonn and Nijmegen I) also exhibit similar behavior as can be seen in figure (5.9).

Studying the variation of Weinberg eigenvalues as a function of the cut-off Λ serves as a diagnostic for understanding the scale dependence of the underlying physics. Figure (5.10) shows the largest repsulsive eigenvalues as a function of the cut-off Λ for different partial waves for center of mass energies $0\,\mathrm{MeV}, 50\,\mathrm{MeV}$ and $100\,\mathrm{MeV}$. One observes that lowering the cut-off decreases the magnitude of the repulsive eigenvalues. Different partial waves show different dependence on the cut-off. As noted before,

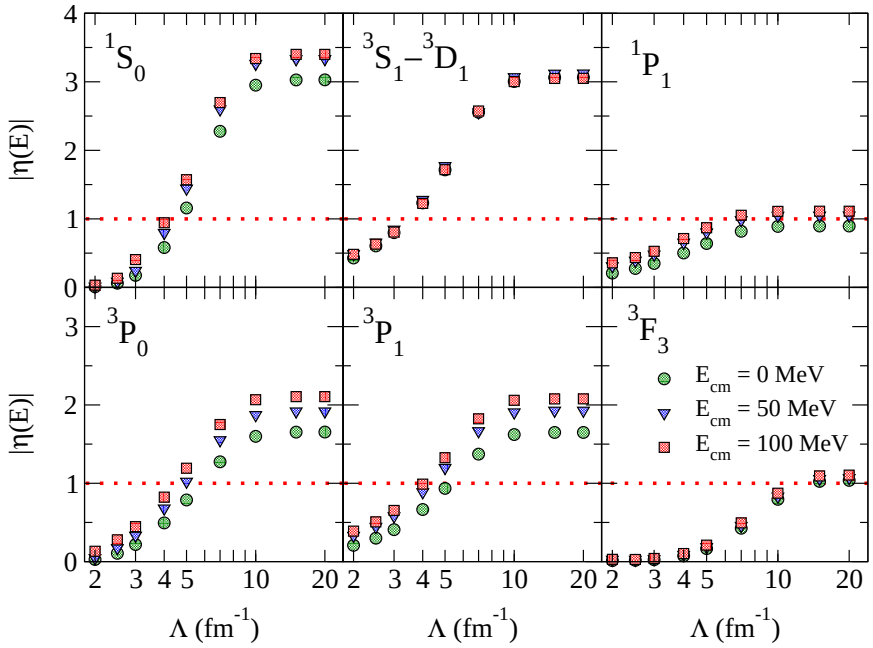

Figure 5.10: Largest repulsive eigenvalues as a function of the cut-off Λ for various partial waves for the Av_{18} potential.

the differences between the $^1S_0$ and the $^3S_1 -^3 D_1$ channel can be attributed to the presence of a repulsive tensor force in the latter in addition to the short-distance repulsion. Similarly we can explain the differences in the $^3P_0$ and $^3P_1$ channels. The tensor force is attractive in $^3P_0$ channel and repulsive in $^3P_1$ channel [53]. As a result the repulsive eigenvalues are significant at low values of the cut-off for the $^3P_1$ partial wave while the attractive eigenvalues are significant for the $^3P_0$ partial wave (figure (5.11)). In fact this holds in higher partial waves channels where the tensor force is active, but the centrifugal barrier decreases the manifestation of this effect as can be seen from figures (5.10) and (5.11). We also notice that the attractive eigenvalues vary much less compared to the repulsive eigenvalues as the cut-off is

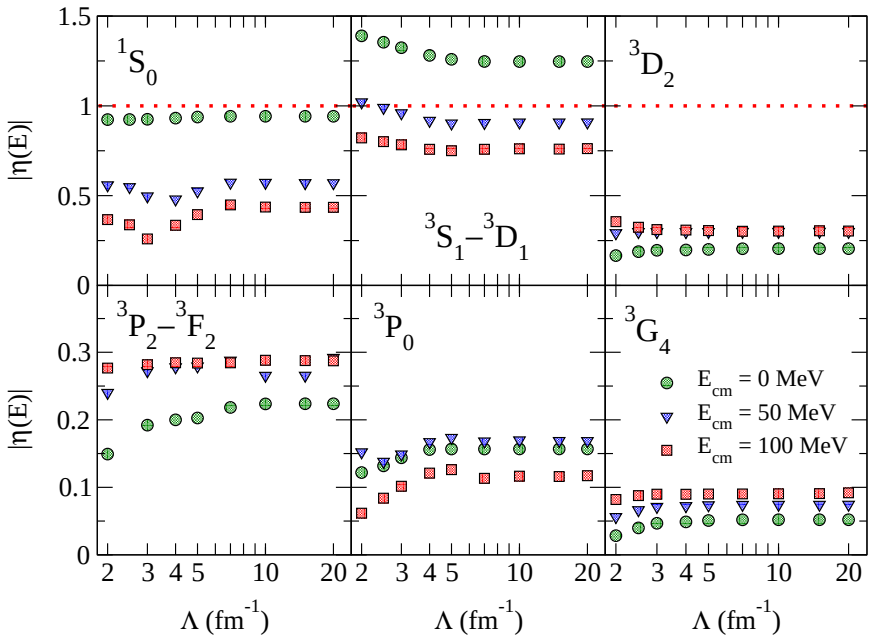

Figure 5.11: Largest attractive eigenvalues as a function of the cut-off Λ for various partial waves for the Av_{18} potential.

lowered. The repulsive parts of the potential probe the short-distance region, thereby coupling the low- and high-momentum modes; as a result, lowering the resolution scale changes these parts drastically, which is manifested as a stronger running of repulsive eigenvalues compared to the attractive eigenvalues.

Chiral EFT potentials typically have a cut-off $\approx 3.5\,\mathrm{fm}^{-1}$ imposed and are expected to be soft potentials. The figures (5.12), and (5.13) shows the repulsive eigenvalues for the chiral potentials at center of mass energy $E_{\mathrm{cm}} = 0\,\mathrm{MeV}$. The N^3LO potential of Machleidt *et al.*. [26] has large eigenvalues in both the S waves, which are comparable to the $V_{\mathrm{low}\,k}$ results of the Av_{18} potential at $\Lambda = 4.0\,\mathrm{fm}^{-1}$. Notice that the chiral potential of Epelbaum *et al.*. [27] also shows large eigenvalues in these channels. Apart from the tensor contributions, the potential [27] of Epelbaum *et al.*

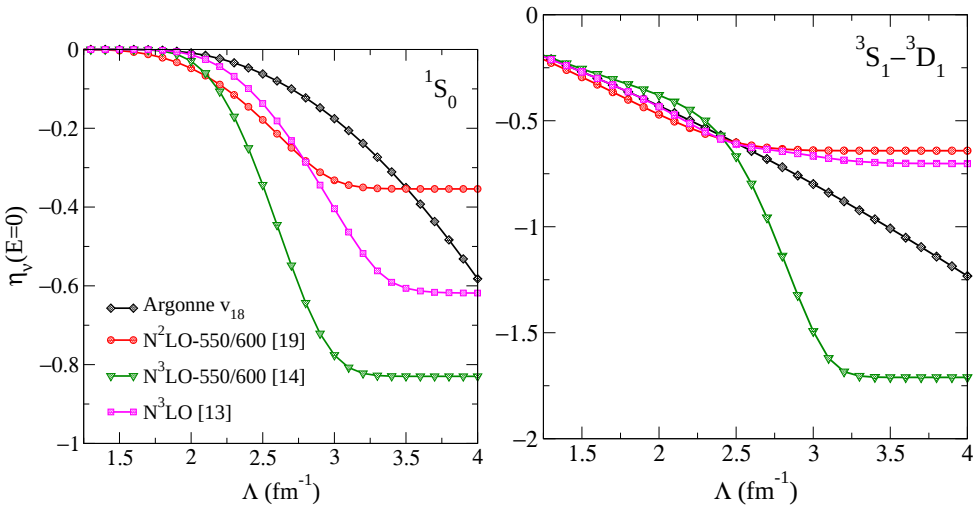

Figure 5.12: Largest repulsive eigenvalues as a function of the cut-off Λ for chiral Potentials (S waves) [26, 27, 55] at $E_{\rm cm} = 0\,$MeV. Notice around $\Lambda = 3.5\,{\rm fm}^{-1}$, the chiral potential at N^3LO [27] has large eigenvalues in both the S waves, indicative of a new source of non-perturbative physics at this order.

has a new source of non-perturbative physics which enters at this order, namely the singular part of the two-pion exchange [13]. It is important to note, however, that decreasing the cut-off from $3.0\,{\rm fm}^{-1}$ down to $2.0\,{\rm fm}^{-1}$ decreases the magnitude of the eigenvalues significantly even for these chiral potentials.

It is unclear why the repulsive eigenvalues of the N^{3}LO potential of Entem and Machleidt [26], which uses $\Lambda = 500\,$MeV, are smaller and close to $\Lambda = 450\,$MeV of the N^{3}LO potential of Epelbaum *et al.*. [27]. This could be due to adjustments in [26] or due to the spectral function regularization in [27]. Figures (5.12), and (5.13) clearly shows that it is advantageous to evolve chiral EFT interactions to lower cutoffs using the RG, since the singular central (at N^{3}LO) and the singular tensor parts are softened for lower cutoffs.

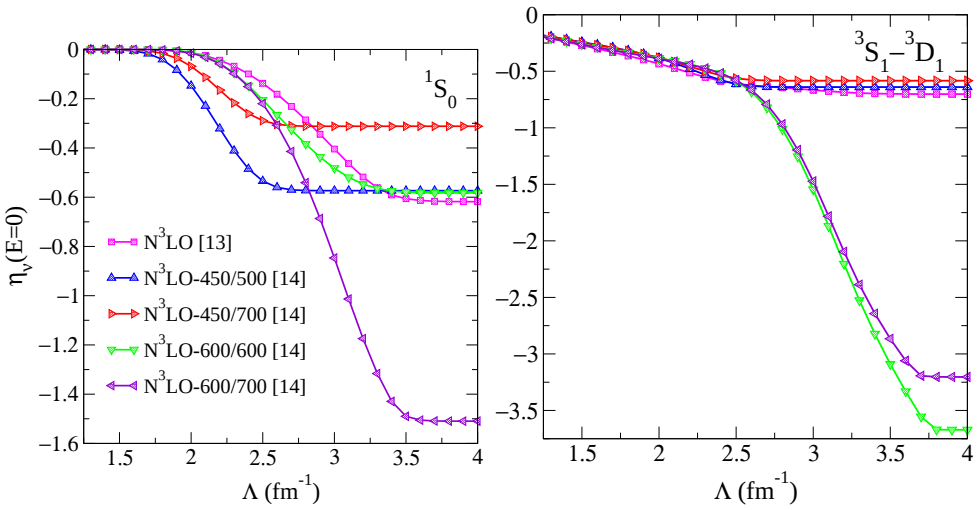

Figure 5.13: The largest repulsive Weinberg eigenvalues for $E = 0$ in the $^1S_0$ channel (left) and the $^3S_1$–$^3D_1$ coupled channel (right) as a function of cutoff for $V_{\mathrm{low}\,k}$ derived from chiral interactions. Results are shown for the N^{3}LO potential of Entem and Machleidt [26], for the N^{3}LO potential of Epelbaum *et al.*. [27] with different cutoffs $\Lambda/\tilde{\Lambda}$ (as indicated in MeV), and for the N^{2}LO potential [55]. For comparison, we have plotted the largest repulsive Weinberg eigenvalues for $V_{\mathrm{low}\,k}$ derived from the Argonne v_{18} potential.

In figure (5.14), we show the largest repulsive Weinberg eigenvalues as a function of the cutoff for selected channels for two different energy values, using the N^{3}LO chiral potential from reference [26], which is constructed with a cutoff of 500 MeV. Although this is already a fairly soft potential, we still observe the characteristic decrease with low-momentum cutoff starting as high as 3.5 fm^{-1} (rather than at 2.5 fm^{-1}, as one might naively expect). The rate of decrease is largely independent of the smoothness of the cutoff. The differences in the Weinberg eigenvalues correspond to the differences inherent with different regulating schemes.

So far we have addressed the issue of convergence of Born series for the T matrix in free space. In medium, there is Pauli blocking which prevents the formation of bound

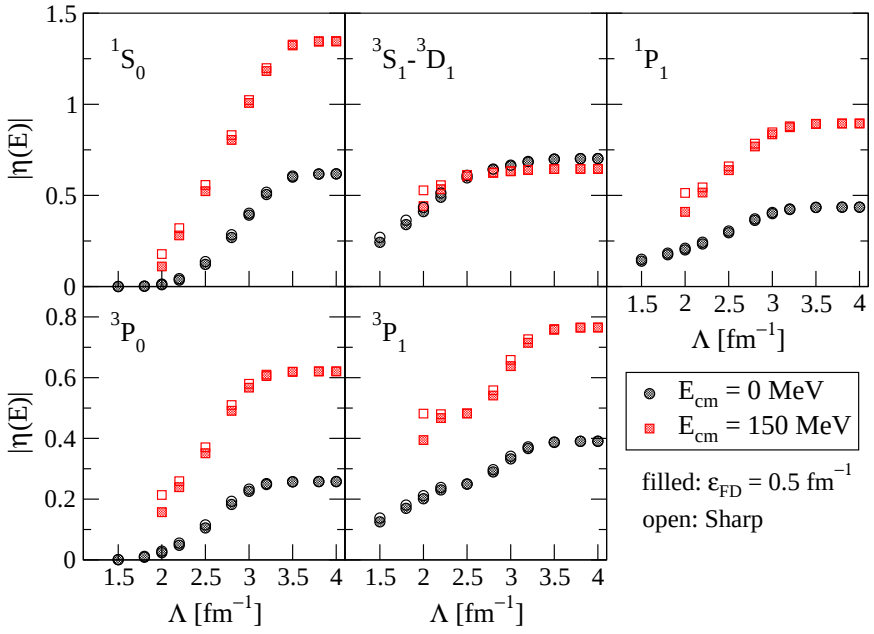

Figure 5.14: Repulsive Weinberg eigenvalues for the smooth regulator (Fermi-Dirac regulator) discussed in chapter 4 with $\epsilon_{\rm FD} = 0.5\,{\rm fm}^{-1}$. The filled symbols are the smooth regulator while the open symbols are the corresponding eigenvalues for the sharp cut-off regulator.

state in the S channel. In figure (5.15) the attractive and repulsive eigenvalues for various cut-off values at the deuteron pole is shown as a function of density ($k_{\rm F}$). In free space ($k_{\rm F} = 0\,{\rm fm}^{-1}$), the largest attractive eigenvalue is 1 for any Λ, indicating the deuteron pole. The repulsive eigenvalues show the expected cut-off dependence, that is lowering the cut-off results in smaller eigenvalues. At finite densities, both the attractive and the repulsive eigenvalues decrease in magnitude for all cut-offs. This running of the attractive eigenvalues is indicative of Pauli blocking which prevents the formation of bound state in medium. The behavior of the Weinberg eigenvalues as a function of the cut-off Λ supports the results shown by Bogner *et al.*. that nuclear matter calculations become perturbative in the particle-particle channel, when $V_{\text{low}\,k}$

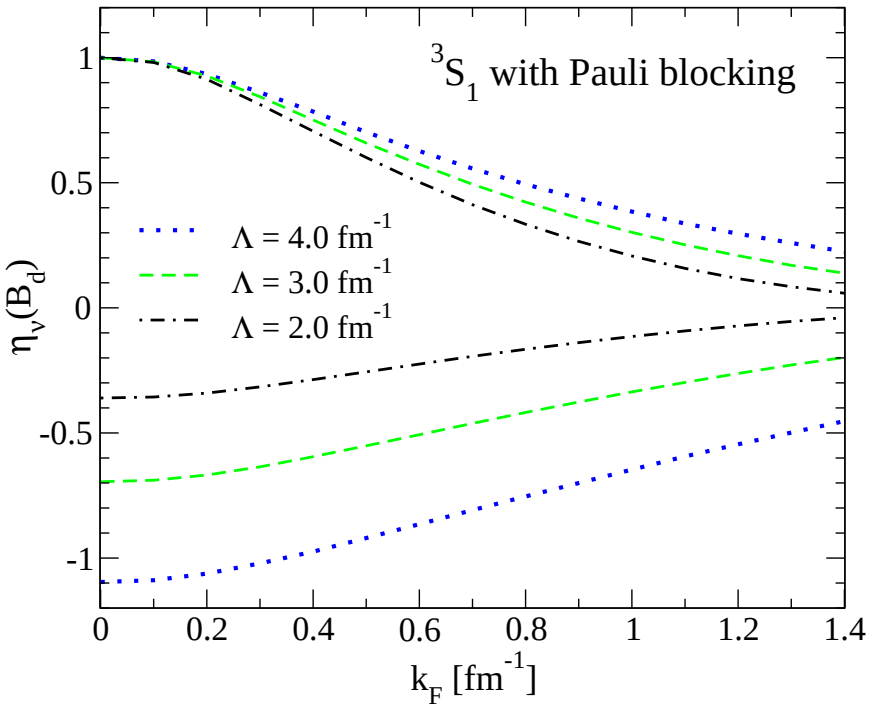

Figure 5.15: In-medium eigenvalues for the $^3S_1$ channel at $E_d = -2.224\,\mathrm{MeV}$. Notice that at finite densities both the attractive and repulsive eigenvalues decrease in magnitude for all values of the cut-off [37].

is used as the two-body input [37]. Further it was shown that saturation is brought about by the three-body forces at lower cut-offs. This is because running the cut-off down changes the contribution from the different terms present in the interaction.

We have so far seen that it is beneficial to lower the cut-off on high precision potentials and use the renormalization group based potentials $V_{\mathrm{low}\,k}$. The Weinberg eigenvalue analysis not only formalizes the notion of convergence of the Born series both in free space and in-medium but also provides useful insight into the physics which become important at different scales.

5.4 Separable Approximations to the Nucleon-Nucleon Interaction

The Weinberg eigenvalue analysis leads naturally to separable approximations for nucleon-nucleon potentials, which may be of practical interest for solving few-body problems such as four-body scattering [62, 63]. The Weinberg eigenstates $\{|\Psi_\nu\rangle\}$ can be used as a basis for a separable representation of the potential [41, 47, 64, 65], with various possible ways to construct such a representation. Here, we focus on the efficacy of a *given* separable expansion as a function of the cutoff, and choose for illustration the expansion in Weinberg eigenvectors at zero energy.

For $E \leqslant 0$, we use the following separable representation

$$V = \sum_{\nu=1}^{\infty} \frac{V|\Psi_\nu(E)\rangle\langle\Psi_\nu(E)|\,V}{\langle\Psi_\nu(E)|V|\Psi_\nu(E)\rangle}\,, \tag{5.25}$$

which is easily verified by substituting it into the eigenvalue problem, equation (5.18). Following reference [47] we introduce a metric for the difference ΔT between the exact T matrix at energy E and a rank-n approximation $T^{(n)}$

$$\big|\big|\Delta T(E)^2\big|\big| = \mathrm{Tr}\left[\big(G_0(E)\,T(E)\big)^\dagger G_0(E)T(E)\right]. \tag{5.26}$$

For the rank-n truncation of equation (5.25), this can be easily expressed in terms of the Weinberg eigenvalues *not* included in the representation

$$\big|\big|\big(T(E) - T^{(n)}(E)\big)^2\big|\big| = \sum_{\nu=n+1}^{\infty} \frac{1}{|1-1/\eta_\nu(E)|^2}\,. \tag{5.27}$$

Therefore, the minimal value and the optimal expansion follow from choosing the n eigenvalues in order of ascending $|1-1/\eta_\nu(E)|^2$. This illustrates a difference between the convergence of the separable expansion and that of the Born series (which depends on the eigenvalues of largest magnitude rather than those closest to unity).

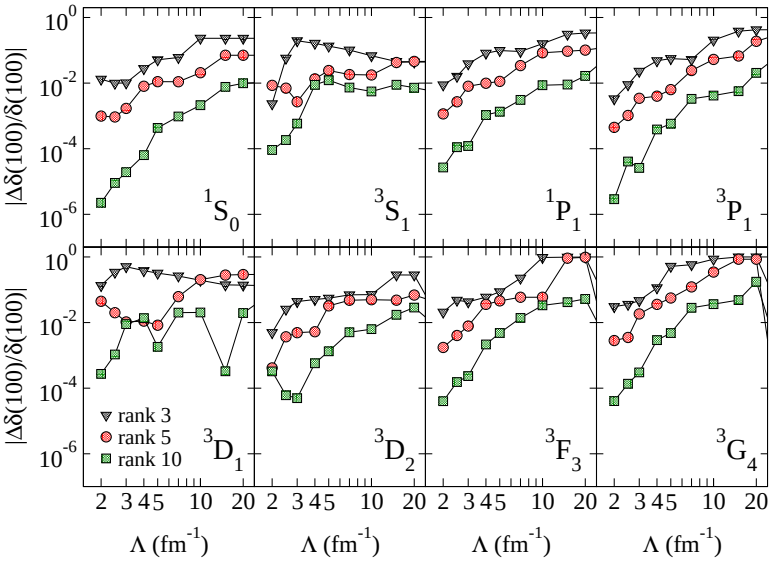

Figure 5.16: Relative error in the phase shifts for $E_{\rm lab} = 100\,\mathrm{MeV}$ as a function of Λ based on separable potentials generated from the Weinberg eigenvectors at $E = 0$ corresponding to the largest $n = 3, 5$ and 10 eigenvalues.

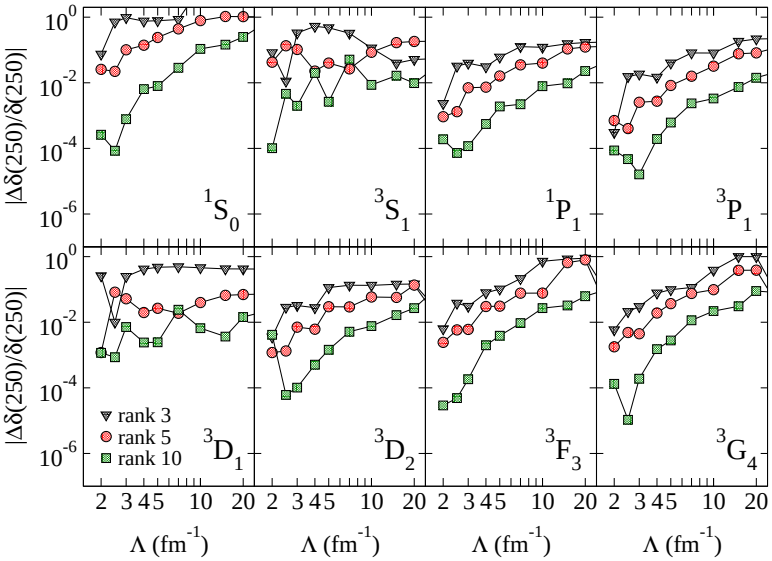

Figure 5.17: Relative error in the phase shifts for $E_{\rm lab} = 250\,\mathrm{MeV}$ as a function of Λ based on separable potentials generated from the Weinberg eigenvectors at $E = 0$ corresponding to the largest $n = 3, 5$ and 10 eigenvalues.

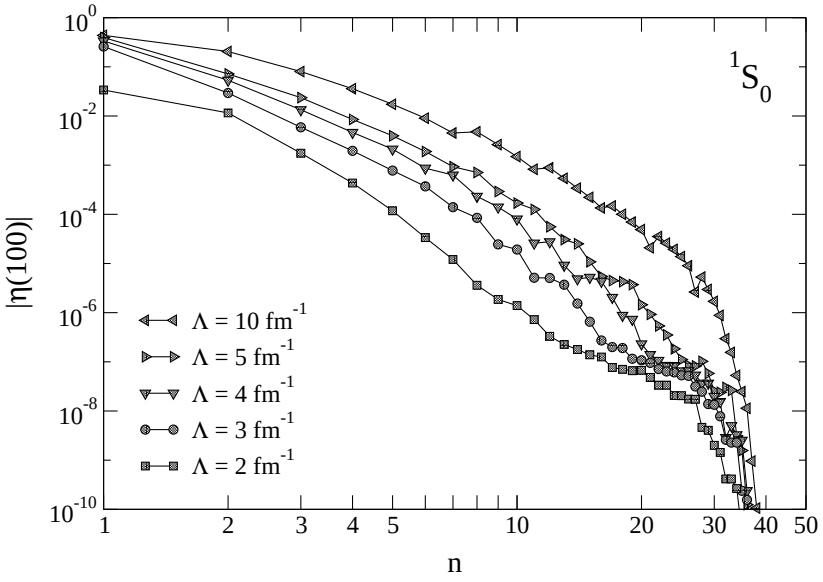

Figure 5.18: Magnitude of Weinberg eigenvalues in descending order for the $^1S_0$ channel at $E_{\rm lab} = 100\,\mathrm{MeV}$.

For practical calculations, we can apply the rank-n approximation at fixed energy E to calculate the T matrix at all energies E'. In this case, the analysis of convergence is no longer simply given by the eigenvalues, but we expect the general trends to carry over. Here we choose $E = 0$ and study the accuracy of observables calculated from the eigenvectors corresponding to the n largest eigenvalues, using the representation in equation (5.25). As the rank n increases, all eigenvalues that are not included decrease, and thus our expansion improves. In addition, we examine how the rank-n approximation performs as a function of the cutoff, where $V_{\mathrm{low}\,k}$ is evolved from the Argonne v_{18} potential for all results presented in this section.

In figures (5.16) and (5.17), the convergence of our truncation is shown by the relative error in the calculated phase shifts for $E_{\rm lab} = 100\,\mathrm{MeV}$ and $250\,\mathrm{MeV}$ (which

typify the full range of energies). Our results demonstrate that using a rank-n separable approximation at the particular energy $E = 0\,\mathrm{MeV}$ does reproduce phase shifts reasonably well for $E' \neq E$. Except in a few cases, the convergence improves monotonically as more terms are included in the separable approximation and, for a particular rank-n approximation, lower cutoffs yield better convergence. As expected, we observe that the convergence is slower in low partial waves where the tensor force is active ($^3\mathrm{S}_1$ and $^3\mathrm{D}_1$) in figure (5.16) and (5.17). Equation (5.27) implies that the fall-off of Weinberg eigenvalues should be tied to the rate of convergence. This is consistent with figure (5.18), which shows this fall-off in the $^1\mathrm{S}_0$ channel for $E_{\mathrm{lab}} = 100\,\mathrm{MeV}$.

In this chapter we have used Weinberg eigenvalues as a diagnostic to investigate the issue of convergence of the Born series. We see that the eigenvalues decrease in magnitude as the cut-off Λ is lowered. In medium there is an important source of non-perturbative physics which occurs close to the fermi surface, namely the pairing instability. We will investigate the behavior of the eigenvalues close to the fermi surface in the following chapter and as we shall see, this leads to a good estimation of the pairing gap.

CHAPTER 6

CONVERGENCE OF IN-MEDIUM BORN-SERIES AND PAIRING IN NEUTRON MATTER

In the previous chapter we saw that lowering the cut-off Λ brought about significant decreases in the magnitude of the Weinberg eigenvalues in free space and in-medium, which indicate improved convergence of the respective Born-series. But close to the Fermi surface, we expect the non-interacting ground state of a filled Fermi sea to be unstable to the formation of Cooper pairs when we turn on the interaction. This feature should be reflected in the in-medium Weinberg eigenvalues. In this chapter we will further investigate the in-medium eigenvalues for energies close to the Fermi surface. We explore the link between the convergence of in-medium Born-series and the pairing instability using the machinery of Weinberg eigenvalue analysis [41, 66]. As we shall see such an investigation gives a good estimate of the pairing gap.

6.1 Cooper Instability

In this section we will review a simple model due to Cooper, showing that an attractive interaction between two fermions in the Fermi sea leads to the formation of a bound pair [56]. The non-interacting ground state (filled Fermi sea) becomes

unstable and a finite gap opens up in the single-particle excitation spectrum. Consider two fermions in the Fermi sea interacting though a potential $\lambda V(x_1, x_2)$, where the magnitude of λ controls the strength of the potential. The sign of λ determines whether the potential is attractive or repulsive. Here we start our discussion in position space, though we will Fourier transform and work in momentum space. The Schrödinger equation is given by:

$$[T_1 + T_2 + \lambda V(1,2)]|\psi(1,2)\rangle = E|\psi(1,2)\rangle \tag{6.1}$$

where $V(1,2)$ is the short-hand notation for the two-particle potential $V(x_1, x_2)$ and $|\psi(1,2)\rangle$ is the two-particle wave function. Let $\{|\phi_n(1,2)\rangle\}$ be the basis of eigenstates of $H_0 = T_1 + T_2$ with eigenvalues E_n. Then $|\psi(1,2)\rangle$ can be expanded in this basis as follows:

$$\begin{aligned} |\psi(1,2)\rangle &= \sum_n c_n|\phi_n(1,2)\rangle, \\ &= c_0|\phi_0(1,2)\rangle + \sum_{n\neq 0} c_n|\phi_n(1,2)\rangle. \end{aligned} \tag{6.2}$$

For convenience, choose $c_0 = 1 \Rightarrow \langle\phi_0(1,2)|\psi(1,2)\rangle = 1$, which sets the normalization for $|\psi(1,2)\rangle$. Using equation (6.2), the Schrödinger equation (6.1) can be written as,

$$\langle\phi_n(1,2)|[H_0 + \lambda V(1,2)]|\psi(1,2)\rangle = E\langle\phi_n(1,2)|\psi(1,2)\rangle. \tag{6.3}$$

Equation (6.3) gives the following two-particle wave function,

$$|\psi(1,2)\rangle = |\phi_0(1,2)\rangle + \sum_{n\neq 0} |\phi_n(1,2)\rangle \frac{1}{E - E_n}\langle\phi_n(1,2)|\lambda V(1,2)|\psi(1,2)\rangle. \tag{6.4}$$

$$\langle\phi_0(1,2)|\psi(1,2)\rangle = \frac{\langle\phi_0(1,2)|\lambda V(1,2)|\psi(1,2)\rangle}{E - E_0} = 1 \tag{6.5}$$

From equation (6.5) we get:

$$E - E_0 = \langle\phi_0(1,2)|\lambda V(1,2)|\psi(1,2)\rangle. \tag{6.6}$$

If the system is confined to a large box of volume V, then the unperturbed wave functions are the plane waves with periodic boundary conditions:

$$\phi(1,2) = \frac{1}{\sqrt{V}} e^{i\mathbf{k_1}.\mathbf{x_1}} \frac{1}{\sqrt{V}} e^{i\mathbf{k_2}.\mathbf{x_2}}. \tag{6.7}$$

Next we incorporate the many-body aspect of the problem by restricting the sum over the intermediate states to lie above the filled Fermi sea. That is,

$$\sum_n \rightarrow \sum_{\mathbf{k_1},\mathbf{k_2}>k_\mathrm{F}}. \tag{6.8}$$

Working in the center of mass coordinates defined as

$$\mathbf{P} = \frac{\mathbf{k}_1 + \mathbf{k}_2}{2}, \tag{6.9}$$

$$\mathbf{k} = \mathbf{k}_1 - \mathbf{k}_2, \tag{6.10}$$

$$\Rightarrow \mathbf{k}_1 = \mathbf{P} + \frac{\mathbf{k}}{2}, \tag{6.11}$$

$$\Rightarrow \mathbf{k}_2 = \mathbf{P} - \frac{\mathbf{k}}{2}. \tag{6.12}$$

where $\mathbf{P}$ is the center of mass momentum, $\mathbf{k}$ is the relative momentum, the two-body wave function given by equation (6.2) can be written in the plane wave basis as

$$\psi(1,2) = \phi(1,2) + \sum_{\mathbf{q}>k_\mathrm{F}} \phi(1,2) \frac{1}{E - 2E_\mathbf{q}} \langle \phi(1,2)|\lambda V(1,2)|\psi(1,2)\rangle. \tag{6.13}$$

Here $E = \dfrac{\hbar^2\kappa^2}{m} + \dfrac{\hbar^2 P^2}{4m}$ is the energy of the pair and $E_\mathbf{q} = \dfrac{\hbar^2 q^2}{2m}$ is the single particle energy of the intermediate state. Converting the sum in equation (6.13) to an integral, the solution to the Schrödinger equation takes the form:

$$\psi(1,2) = \frac{1}{\sqrt{V}} e^{i\mathbf{P}.\mathbf{R}} \frac{1}{\sqrt{V}} \psi_{\mathbf{P},\mathbf{k}}(x), \tag{6.14}$$

$$\psi_{\mathbf{P},\mathbf{k}}(x) = e^{i\mathbf{k}.\mathbf{x}} + \lambda \int_\Gamma \frac{d^3t}{(2\pi)^3} e^{i\mathbf{t}.\mathbf{x}} \frac{1}{\kappa^2 - t^2} \langle t|\mathcal{V}|\psi_{\mathbf{P},\mathbf{k}}\rangle \tag{6.15}$$

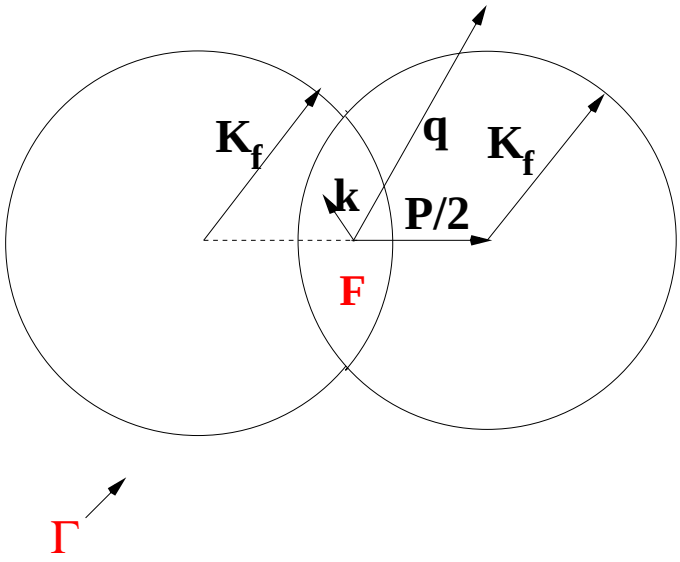

Figure 6.1: Schematic for the allowed integration region. Scattering from the region of intersection of the two-spheres to region Γ outside the filled Fermi sphere is allowed.

where $\mathcal{V} \equiv \frac{mV}{\hbar^2}$. In equation (6.14), the first factor describes the center of mass motion and the second factor is the internal wave function of the interacting pair. The center of mass momentum P can take values between 0 and $2k_{\rm F}$. In equation (6.15), $\Gamma = |\frac{\mathbf{P}}{2} \pm \mathbf{t}| > k_{\rm F}$ represents the region outside the filled Fermi sea. The relative momenta $\mathbf{k}$ and $\mathbf{P}$ are constrained by $|\frac{\mathbf{P}}{2} \pm \mathbf{k}| < k_{\rm F}$. The region of integration is as shown in figure (6.1).

The shift in the energy of the pair due to the interaction (equation (6.6)) in the plane wave basis takes the form:

$$\kappa^2 - k^2 = \frac{\lambda}{V}\langle \mathbf{k}|\mathcal{V}|\psi_{\mathbf{P},\mathbf{k}}\rangle. \tag{6.16}$$

Equation (6.15) is known as the *Bethe-Goldstone Equation* [67]. It is the Schrödinger equation for two fermions in a Fermi gas, where the Pauli exclusion principle prevents

the appearance of intermediate states that are already occupied by other fermions. Since the particles are initially inside the Fermi sea all the transitions to the region Γ outside the Fermi sea are virtual. We will now calculate the energy shift per pair due to the interaction $\mathcal{V}$ (equation (6.16)). We will use a separable form for the potential (rank 1 separable), as this yields analytical results. We assume the following separable form in position and momentum space respectively:

$$\mathcal{V}(\mathbf{x}, \mathbf{x}') = \lambda u(|\mathbf{x}|) u(|\mathbf{x}'|)^*. \tag{6.17}$$

$$\mathcal{V}(\mathbf{k}, \mathbf{k}') = \lambda u(|\mathbf{k}|) u(|\mathbf{k}'|)^*. \tag{6.18}$$

With the separable form for the potential as given in equations (6.17) and (6.18), the energy shift per pair, defined in equation (6.16) becomes,

$$\kappa^2 - k^2 = \frac{\lambda |u(k)|^2}{V} + \lambda \int_\Gamma \frac{d^3t}{(2\pi)^3} u(t)^* \frac{1}{\kappa^2 - t^2} u(t)(\kappa^2 - k^2). \tag{6.19}$$

Equation (6.19) can be rearranged as follows:

$$\frac{1}{\lambda} = \frac{1}{V} \frac{|u(k)|^2}{\kappa^2 - k^2} + \int_\Gamma \frac{d^3t}{(2\pi)^3} \frac{|u(k)|^2}{\kappa^2 - t^2} \equiv f(\kappa^2), \tag{6.20}$$

which determines the energy eigenvalue κ^2 and hence the energy shift per pair:

$$\Delta E = \frac{\hbar^2}{m}(\kappa^2 - k^2). \tag{6.21}$$

The function $f(\kappa^2)$ can be plotted as a function of κ^2 and the point of intersection with the horizontal line $\dfrac{1}{\lambda}$ determines the eigenvalue κ^2. We notice that the integral in $f(\kappa^2)$ is a monotonically decreasing function of κ^2. The first term contributes only in the vicinity of $\kappa^2 = k^2$. Therefore we can sketch the function $f(\kappa^2)$ as shown in figure (6.2), where the integral term is a smooth function, independent of k^2, with a

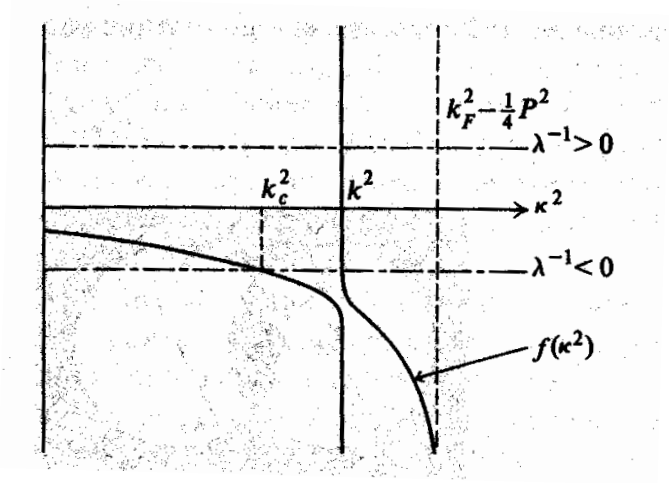

Figure 6.2: Sketch of the function $f(\kappa^2)$. The eigenvalue κ^2 is given by the intersection of the function $f(\kappa^2)$ with the horizontal line $\frac{1}{\lambda}$ [56].

logarithmic singularity which first appears at the Fermi surface i.e., $\kappa^2 = k_{\mathrm{F}}^2 - \frac{P^2}{4}$ and the first term is a singularity of narrow width at the variable point $\kappa^2 = k^2$.

For $\lambda > 0$ (repulsive potential), there is only one solution, occuring at

$$\kappa^2 - k^2 \approx \frac{\lambda}{V}|u(k)|^2 + \mathcal{O}(\lambda^2). \tag{6.22}$$

Here the integral term can be neglected as it is finite for $\kappa^2 \approx k^2$ and contributes only to higher order in λ. So the effect of a repulsive potential $\lambda > 0$ is to shift the energy of the pair by a small amount.

As seen in figure (6.2), for $\lambda < 0$, there are two solutions, as long as $|\lambda|$ does not become too large. Apart from the solution given by equation (6.22), there is another "anomalous" solution arising from the logarithmic singularity of $f(\kappa^2)$. Depending on the relative value of k^2 and $|\lambda|$, one of the two eigenvalues lies lower than the other. For a fixed value of $|\lambda|$ there is a corresponding critical value k_c such that the

anomalous solution is lower than the ordinary solution for all $k > k_c$. A value for k_c can be obtained from the equation:

$$\int_\Gamma \frac{d^3t}{(2\pi)^3} \frac{|u(t)|^2}{k_c^2 - t^2} = \frac{1}{\lambda}. \tag{6.23}$$

Here in equation (6.23), we have neglected the first term of equation (6.20) as it does not contribute far away from $\kappa \approx k$. Note that the anomalous solution is independent of the initial wave vector $\mathbf{k}$ as long as $k > k_c$. Let us examine this eigenvalue in detail. Setting $\lambda = -1$, we see that the eigenvalue equation (6.23) reduces to:

$$\int_\Gamma \frac{d^3t}{(2\pi)^3} \frac{|u(t)|^2}{k_c^2 - t^2} = -1. \tag{6.24}$$

so that k_c is defined as that eigenvalue which intersects 1. We simplify this problem further by setting $P = 0$, so that the eigenvalue equation (6.24) becomes:

$$1 = \int_{k_\mathrm{F}}^\infty \frac{t^2 dt}{2\pi^2} \frac{|u(t)|^2}{t^2 - \kappa^2} \tag{6.25}$$

$$= \frac{k_\mathrm{F}}{2\pi^2} \int_1^\infty x^2 dx \frac{|u(x)|^2}{x^2 - (\frac{\kappa}{k})^2} \tag{6.26}$$

Here we have used the fact that the eigenvalue κ is essentially k_c. We can isolate the logarithmic singularity by an integration by parts, so that,

$$1 \approx \frac{k_\mathrm{F}}{2\pi^2} |u(k_\mathrm{F})|^2 \log(\frac{k_\mathrm{F}^2}{k_\mathrm{F}^2 - \kappa^2}). \tag{6.27}$$

In order to arrive at equation (6.27) we have assumed the potential to be smooth (in addition to it being separable) and we have neglected the finite parts of the integral. Since κ^2 is less than k_F^2, we can write,

$$\kappa^2 = k_\mathrm{F}^2 - \frac{m}{\hbar^2}\Delta. \tag{6.28}$$

and equation (6.27) can be written as

$$\Delta = \frac{\hbar^2 k_\mathrm{F}^2}{m} \exp\left[-\frac{4\pi^2}{k_\mathrm{F}|u(k_\mathrm{F})|^2}\right]. \tag{6.29}$$

The energy shift per pair now becomes:

$$\begin{aligned} \Delta E &= \frac{\hbar^2}{m}(\kappa^2 - k^2) \\ &= 2(\varepsilon_{\mathrm{F}} - \varepsilon_{\mathrm{k}}) - \Delta. \end{aligned} \tag{6.30}$$

Close to the Fermi surface the energy shift per pair is negative and equal to Δ. So an attractive interaction between two fermions lowers the energy of the pair by an amount Δ. In other words a gap Δ opens up in the single-particle spectrum. The value of Δ is maximum for $P = 0$, as this maximizes the phase space where the denominator of the integral in equation (6.20) vanishes. Therefore close to the Fermi surface two fermions of equal and opposite spins will form a type of bound state (correlated state); note that this "bound state" has a positive energy but is lower than the non-interacting bound state and we will refer to this special kind of bound state as a paired state. This phenomenon is called *Pairing*. Since this new paired state has lower energy, the ground state of the filled Fermi sea becomes unstable. Equation (6.29) has an essential singularity in the interaction strength and perturbation theory is invalid in this case. So even an arbitrarily small attractive potential can create Cooper pairs and hence make the ground state of the filled Fermi sea unstable. In the next section, we look for a signature of this instability in the in-medium Weinberg eigenvalues.

6.2 In-medium Eigenvalues

The hole-hole contribution is quantitatively important for the pairing instability as close to the Fermi surface *both particles and holes* lying within a shell Δ about the Fermi surface form Cooper pairs. Therefore, the in-medium Weinberg eigenvalue equation is defined as follows:

$$G^0_{pphh}(E)V|\Psi_\nu(E)\rangle = \eta_\nu(E)|\Psi_\nu(E)\rangle \tag{6.31}$$

where $G^0_{pphh}(E)$ is the in-medium two-particle two-hole non-interacting propagator. In momentum space, this propagator is defined as [56]:

$$G^0_{pphh}(\mathbf{k}_1, \mathbf{k}_2; \omega) = \frac{\theta(|\mathbf{k}_1| - k_\mathrm{F})\theta(|\mathbf{k}_2| - k_\mathrm{F})}{\omega - \varepsilon(\mathbf{k}_1) - \varepsilon(\mathbf{k}_2) + i\epsilon} - \frac{\theta(k_\mathrm{F} - |\mathbf{k}_1|)\theta(k_\mathrm{F} - |\mathbf{k}_2|)}{\omega - \varepsilon(\mathbf{k}_1) - \varepsilon(\mathbf{k}_2) - i\epsilon} \tag{6.32}$$

where $\mathbf{k}_1$ and $\mathbf{k}_2$ are the momenta of the particles (holes), ω is the two-particle excitation energy measured from the Fermi surface. The above propagator represents propagation of two particles above the Fermi surface and two holes below the Fermi surface. Working in relative coordinates, the equation (6.32) becomes:

$$G^0_{pphh}(k, \omega) = \frac{\theta(k - k_\mathrm{F})}{\omega - 2\varepsilon(k) + i\epsilon} - \frac{\theta(k_\mathrm{F} - k)}{\omega - 2\varepsilon(k) - i\epsilon}, \tag{6.33}$$

where we have chosen the partial wave basis and have specialized to the case of center of mass momentum $P = 0$. This will hold true for the rest of this chapter. Notice that we have suppressed the partial wave label. In equation (6.33), $\omega = E - 2\mu$ and $\varepsilon(k) = k^2/2 - \mu$, where $\mu = k_\mathrm{F}^2/2$, the Fermi energy (at zero temperature). Using this definition, the in-medium propagator is defined as:

$$G^0_{pphh}(k, E = k_0^2) = \frac{\theta(k - k_\mathrm{F})}{k_0^2 - k^2 + i\epsilon} - \frac{\theta(k_\mathrm{F} - k)}{k_0^2 - k^2 - i\epsilon}, \tag{6.34}$$

where $E = k_0^2$. We now study the Weinberg eigenvalues for this kernel $G^0_{pphh}(E)V_{\mathrm{low}\,k}$. As in free space, we choose to solve for the eigenvalues of $V_{\mathrm{low}\,k}G^0_{pphh}(E)$ instead, which has the same eigenvalue spectrum but we can directly integrate over the singularity. In a given partial wave, the Weinberg eigenvalue equation is given by:

$$\frac{2}{\pi}\int_0^\Lambda q^2 dq V_{\mathrm{low}\,k}(k, q)\left(\frac{\theta(q - k_\mathrm{F})}{k_0^2 - q^2 + i\epsilon} - \frac{\theta(k_\mathrm{F} - q)}{k_0^2 - q^2 - i\epsilon}\right)\Psi_\nu(q) = \eta_\nu(k_0^2)\Psi_\nu(k) \tag{6.35}$$

Note that the eigenvectors are energy dependent, but for notational convenience we have suppressed the energy dependence in equation (6.35). Using the following identities,

$$\frac{1}{x - x_0 \pm i\epsilon} = \mathcal{P}\frac{1}{x - x_0} \mp i\pi\delta(x - x_0), \tag{6.36}$$

$$\delta(f(x)) = \sum_i \frac{\delta(x - x_i)}{|f'(x)|_{x=x_i}}, \tag{6.37}$$

equation (6.35) becomes:

$$\begin{aligned} \frac{2}{\pi}\mathcal{P}\int_0^\Lambda q^2 dq V_{\mathrm{low}\,k}(k,q)\left(\frac{\theta(q-k_\mathrm{F})-\theta(k_\mathrm{F}-q)}{k_0^2-q^2}\right)\Psi_\nu(q) &- ik_0 V_{\mathrm{low}\,k}(k,k_0)\Psi_\nu(k_0) \\ &= \eta_\nu(k_0^2)\Psi_\nu(k). \end{aligned} \tag{6.38}$$

Figure (6.3) shows the largest attractive eigenvalue at finite density ($k_\mathrm{F} = 1.0\,\mathrm{fm}^{-1}$) as a function of center of mass energy E_cm for the ${}^1S_0$ partial wave at $\Lambda = 2.0\,\mathrm{fm}^{-1}$. $V_{\mathrm{low}\,k}$ matrix elements are from the Argonne v_{18} potential using the sharp regulator. Though the eigenvalues are complex, we follow the principal value formalism, where the imaginary part in equation (6.38) is omitted. At this stage, the motivation for this prescription is not well understood and requires further investigation. At low-energies, the eigenvalues are small. As the energy approaches the Fermi energy ($2\varepsilon_\mathrm{F}$), the eigenvalues increase in magnitude, becoming arbitrarily large. This is reminiscent of the logarithmic singularity seen in equation (6.27) as $\kappa^2 \to k_\mathrm{F}^2$, where κ^2 is the anomalous eigenvalue of the Bethe-Goldstone equation. Large Weinberg eigenvalues are indicative of non-perturbative physics. Therefore this singular behavior of the eigenvalues close to the Fermi surface, signals the formation of Cooper pairs.

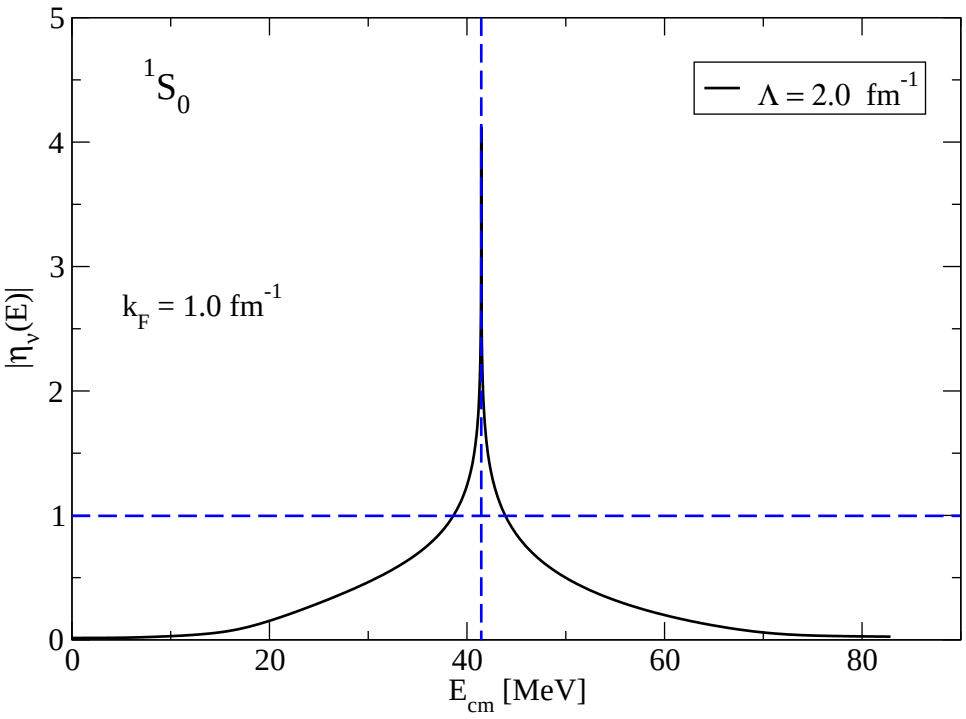

Figure 6.3: Largest attractive eigenvalue as a function of energy $E_{\rm cm}$. Notice that $E_{\rm cm}$ approaches $2\varepsilon_{\rm F} = k_{\rm F}^2$ (denoted by the vertical dotted line), the eigenvalue increases in magnitude and eventually shoots above 1, indicating the pairing instability.

6.3 Pairing Gap

We are now in a position to calculate the pairing gap from the Weinberg eigenvalues. The Weinberg eigenvalue equation (6.38) for the particle-particle, hole-hole propagator is given by:

$$\frac{2}{\pi}\mathcal{P}\int_0^\Lambda q^2 dq V_{\text{low }k}(k,q)\left(\frac{\theta(q-k_{\rm F})-\theta(k_{\rm F}-q)}{k_0^2-q^2}\right)\Psi_\nu(q) \;=\; \eta_\nu(k_0^2)\Psi_\nu(k). \quad (6.39)$$

Comparing the above equation (6.39) to the eigenvalue equation (6.25), we can argue that the critical eigenvalue k_c is the momentum corresponding to $\eta_\nu(k_c^2) = 1$. Once we know k_c, we can determine the pairing gap at $k_{\rm F}$ using equation (6.28).

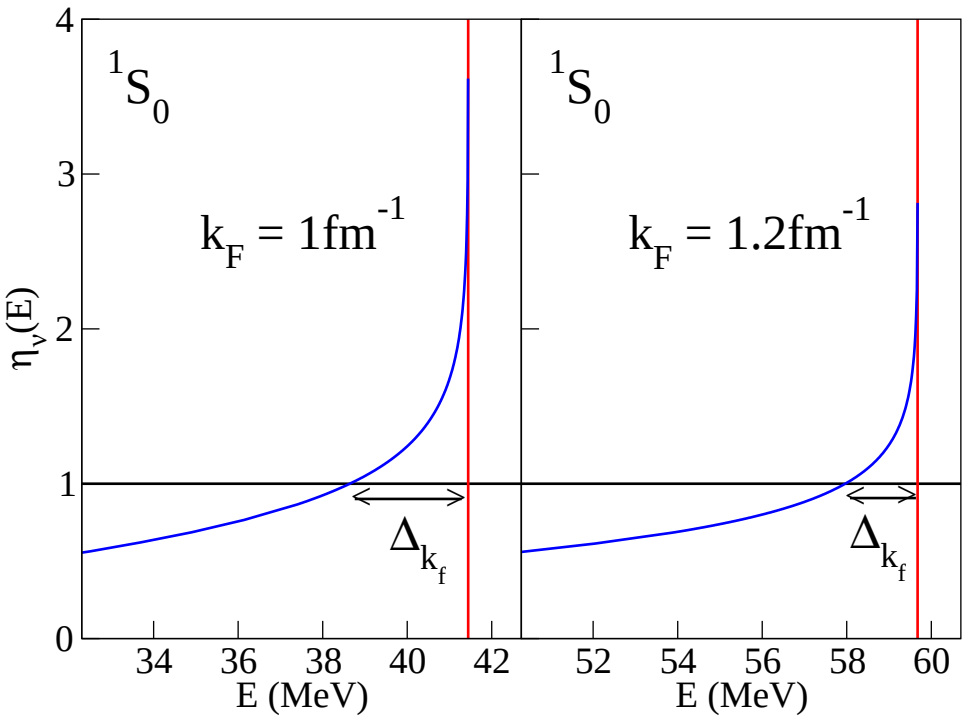

Figure 6.4: Paring gaps for Neutron Matter calculated from the largest attractive Weinberg eigenvalue in the principal value formalism. k_c corresponds to momentum value where $\eta_\nu = 1$ from which the gap can be calculated.

Figure (6.4) shows an estimation of the pairing gap for neutron matter at two different densities, $k_{\rm F} = 1.0\,{\rm fm}^{-1}$ and $k_{\rm F} = 1.2\,{\rm fm}^{-1}$, while figure (6.5) shows the corresponding density dependence of the paring gap for different values of Λ (the cut-off associated with $V_{{\rm low}\,k}$ potentials). Note that we are working in the weak-coupling limit, where the gap is independent of the momentum k and depends only the density $k_{\rm F}$. From figure (6.5) we also note that the Λ dependence of the gap is weak.

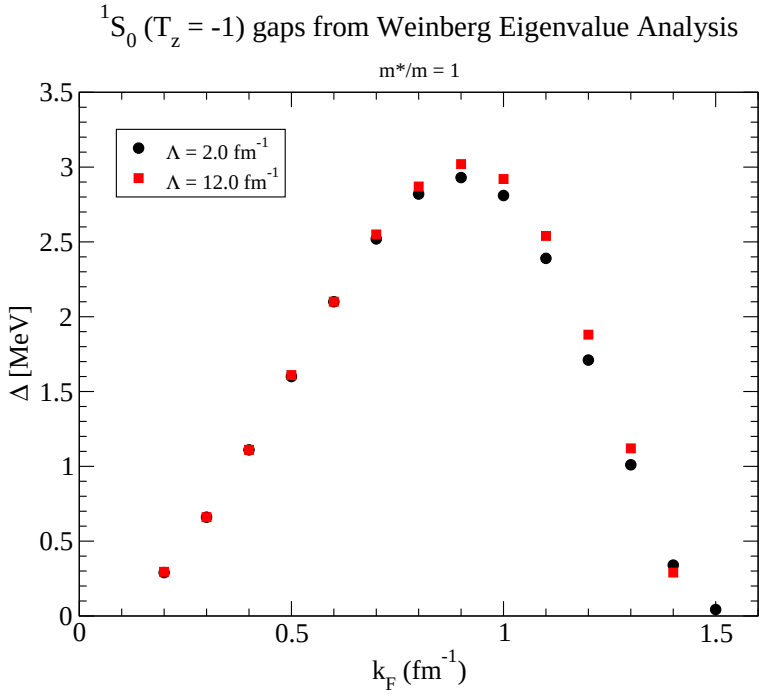

Figure 6.5: Density dependence of the gap for different Λ for Neutron Matter.

The in-medium Weinberg eigenvalues not only reflect the instability but also give a good estimate of the pairing gap. While the propagator used so far is the non-interacting propagator, we know that the Nambu-Gorkov propagator takes into account the new feature of the many-body system, namely pairing. We will set up the Nambu-Gorkov formalism in the next section and calculate what we expect for the corresponding Weinberg eigenvalues using a separable potential first. Then we extend these calculations to $V_{\mathrm{low}\,k}$.

6.4 Nambu-Gorkov Formalism

The Green's function which takes into account the pairing interaction turns out to be more complicated, so we will begin our study of the Nambu-Gorkov propagator by defining a two-component field operator [56, 70],

$$\widehat{\Psi}_K(\mathbf{x},t) = \begin{bmatrix} \widehat{\psi}_{K,\uparrow}(\mathbf{x},t) \\ \widehat{\psi}^\dagger_{K,\downarrow}(\mathbf{x},t) \end{bmatrix}. \tag{6.40}$$

where $\widehat{\psi}_{K,\uparrow}(\mathbf{x},t)$ and $\widehat{\psi}^\dagger_{K,\downarrow}(\mathbf{x},t)$ are defined in the "Heisenberg picture", with $\widehat{K}$ is the grand canonical hamiltonian

$$\widehat{K} = \widehat{H} - \mu\widehat{N}. \tag{6.41}$$

We define a 2×2 matrix Green's function,

$$\mathbf{G}(\mathbf{x}t,\mathbf{x}',t') \equiv -\langle T[\widehat{\Psi}_K(\mathbf{x},t)\widehat{\Psi}^\dagger_K(\mathbf{x}',t')]\rangle, \tag{6.42}$$

$$= \begin{bmatrix} -\langle T[\widehat{\psi}_{K,\uparrow}(\mathbf{x},t)\widehat{\psi}^\dagger_{K,\uparrow}(\mathbf{x}',t')]\rangle & -\langle T[\widehat{\psi}_{K,\uparrow}(\mathbf{x},t)\widehat{\psi}_{K,\downarrow}(\mathbf{x}',t')]\rangle \\ -\langle T[\widehat{\psi}^\dagger_{K,\downarrow}(\mathbf{x},t)\widehat{\psi}^\dagger_{K,\uparrow}(\mathbf{x}',t')]\rangle & -\langle T[\widehat{\psi}^\dagger_{K,\downarrow}(\mathbf{x},t)\widehat{\psi}_{K,\downarrow}(\mathbf{x}',t')]\rangle \end{bmatrix} \tag{6.43}$$

$$= \begin{bmatrix} \mathcal{G}(\mathbf{x}t,\mathbf{x}'t') & \mathcal{F}(\mathbf{x}t,\mathbf{x}'t') \\ \mathcal{F}^\dagger(\mathbf{x}t,\mathbf{x}'t') & -\widetilde{\mathcal{G}}(\mathbf{x}'t',\mathbf{x}t) \end{bmatrix} \tag{6.44}$$

where $\mathcal{G}$ and $\widetilde{\mathcal{G}}$ are the normal propagators, while $\mathcal{F}$ and $\mathcal{F}^\dagger$ are the anomalous propagators. $\mathcal{F}^\dagger$ creates two fermions with opposite spins (Cooper pair), while $\mathcal{F}$ destroys a Cooper pair. Note that the 2×2 matrix propagator, $\mathbf{G}(\mathbf{x}t,\mathbf{x}',t)$ is a fully interacting propagator satisfying the following Schwinger-Dyson equation:

$$\mathbf{G}_{\alpha,\beta}(x,x') = \mathbf{G}^0_{\alpha,\beta}(x,x') + \sum_{\gamma,\delta}\int d^4x_1 \int d^4x_2 \mathbf{G}^0_{\alpha,\gamma}(x,x_1)\Omega_{\gamma,\delta}(x_1,x_2)\mathbf{G}_{\delta,\beta}(x_2,x') \tag{6.45}$$

where $\alpha,\beta,\gamma,\delta$ refer to spin indices, $\mathbf{G}^0_{\alpha,\beta}$ is the free-propagator, which is diagonal in Nambu-Gorkov space, $\Omega_{\gamma,\delta}$ is the 2×2 matrix self energy, whose diagonal elements are $\Sigma(\mathbf{k},\omega)$ and $\Sigma(\mathbf{k},-\omega)$, the normal self energy, and the off-diagonal elements are

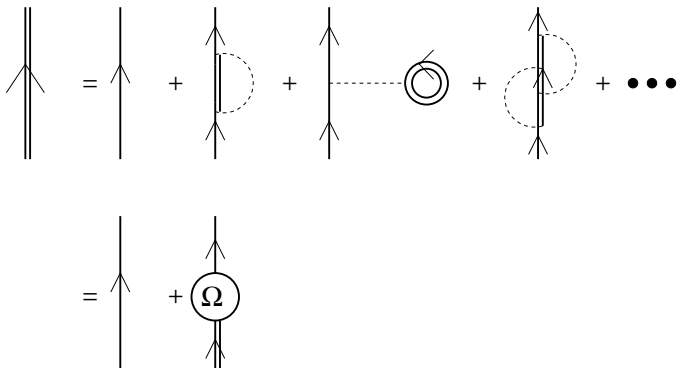

Figure 6.6: Dyson-Schwinger equation for the matrix propagator $\mathbf{G}$.

$\Delta(\mathbf{k})$ and $\Delta^\dagger(\mathbf{k})$, the anomalous self energy (gap functions) [70]. In momentum space these matrices are given as:

$$\mathbf{G}_{\alpha,\beta}(\mathbf{k},\omega) = \begin{pmatrix} \mathcal{G}_{\alpha,\beta}(\mathbf{k},\omega) & \mathcal{F}_{\alpha,\beta}(\mathbf{k},\omega) \\ \mathcal{F}^\dagger_{\alpha,\beta}(\mathbf{k},\omega) & -\widetilde{\mathcal{G}}_{\alpha,\beta}(\mathbf{k},-\omega) \end{pmatrix} \tag{6.46}$$

The free-propagator is given by:

$$\mathbf{G}^0_{\alpha,\beta}(\mathbf{k},\omega) = \begin{pmatrix} \mathcal{G}_{\alpha,\beta}(\mathbf{k},\omega) & 0 \\ 0 & -\widetilde{\mathcal{G}}_{\alpha,\beta}(\mathbf{k},-\omega) \end{pmatrix} \tag{6.47}$$

and finally the self-energy is

$$\Omega_{\alpha,\beta}(\mathbf{k},\omega) = \begin{pmatrix} \Sigma_{\alpha,\beta}(\mathbf{k},\omega) & \Delta_{\alpha,\beta}(\mathbf{k},\omega) \\ \Delta^\dagger_{\alpha,\beta}(\mathbf{k},\omega) & \Sigma_{\alpha,\beta}(\mathbf{k},-\omega) \end{pmatrix} \tag{6.48}$$

The figures (6.6) and (6.7) show the Dyson equation for $\mathbf{G}_{\alpha,\beta}$ and $\Omega_{\alpha,\beta}$. The self-energy in figure (6.7) is in the Hartree-Fock approximation. The two-particle propagator is built using these dressed one-particle propagator. Notice that the pairing is built in to the dressed propagator, while the non-interacting propagator is diagonal in the Nambu basis.

We are interested in forming a two-particle Green's function in the singlet channel using the normal and anomalous propagators. For a homogeneous system, we can

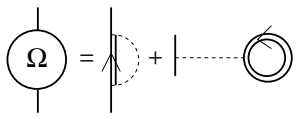

Figure 6.7: The figure shows the mean-field dressing for the self-energy.

write the two-body Green's function as:

$$G^{(2)}(\mathbf{x}_1, \mathbf{x}_2, \mathbf{x}_3, \mathbf{x}_4, t) = \tag{6.49}$$

$$\mathcal{G}(\mathbf{x}_1 - \mathbf{x}_3, t)\tilde{\mathcal{G}}(\mathbf{x}_2 - \mathbf{x}_4, t) + \mathcal{F}_s(\mathbf{x}_1 - \mathbf{x}_2, t)\mathcal{F}_s^\dagger(\mathbf{x}_3 - \mathbf{x}_4, t). \tag{6.50}$$

where $\mathcal{F}_s$ and $\mathcal{F}_s^\dagger$ stand for singlet projections of $\mathcal{F}$ and $\mathcal{F}^\dagger$ respectively. The singlet projection is defined as follows:

$$\mathcal{F}_s(\mathbf{x}_1 - \mathbf{x}_2, t) = \frac{1}{2}[\mathcal{F}(\mathbf{x}_1 - \mathbf{x}_2, t) + \mathcal{F}(\mathbf{x}_2 - \mathbf{x}_1, t)]. \tag{6.51}$$

This definition follows from the fact that any function $f(x_1, x_2)$ can be written as a sum of an even and an odd part so that $\mathcal{F}$ can be written as,

$$\mathcal{F}(\mathbf{x}_1 - \mathbf{x}_2, t) = \frac{1}{2}[\mathcal{F}(\mathbf{x}_1 - \mathbf{x}_2, t) + \mathcal{F}(\mathbf{x}_2 - \mathbf{x}_1, t] + \frac{1}{2}[\mathcal{F}(\mathbf{x}_1 - \mathbf{x}_2, t) - \mathcal{F}(\mathbf{x}_2 - \mathbf{x}_1, t)] \tag{6.52}$$

The even part corresponds to the singlet as,

$$\begin{aligned}
\mathcal{F}_s(\mathbf{x}_1 - \mathbf{x}_2, t) &= \frac{1}{2}[\mathcal{F}(\mathbf{x}_1 - \mathbf{x}_2, t) + \mathcal{F}(\mathbf{x}_2 - \mathbf{x}_1, t)] \\
&= -\frac{1}{2}\left[\langle T[\widehat{\psi}_{K,\uparrow}(\mathbf{x}_1, t)\widehat{\psi}_{K,\downarrow}(\mathbf{x}_2, 0)]\rangle + \langle T[\widehat{\psi}_{K,\uparrow}(\mathbf{x}_2, t)\widehat{\psi}_{K,\downarrow}(\mathbf{x}_1, 0)]\rangle\right] \qquad (6.53) \\
&= -\frac{1}{2}\left[\langle T[\widehat{\psi}_{K,\uparrow}(\mathbf{x}_1, t)\widehat{\psi}_{K,\downarrow}(\mathbf{x}_2, 0)]\rangle - \langle T[\widehat{\psi}_{K,\downarrow}(\mathbf{x}_1, t)\widehat{\psi}_{K,\uparrow}(\mathbf{x}_2, 0)]\rangle\right] \qquad (6.54)
\end{aligned}$$

where the last equation (6.54) shows the expected antisymmetry in the singlet channel. Now we will proceed to evaluate the two-body Nambu-Gorkov Green's function.

Working in relative coordinates as defined in equations (6.9 - 6.12) and setting $P = 0$, and fourier transforming equation (6.50) from $\mathbf{x}$ and t to $\mathbf{k}$ and ω,

$$\begin{aligned} G^{(2)}(\mathbf{k}, -\mathbf{k}, \omega) = & \int \frac{d\omega'}{2\pi i} \mathcal{G}(\mathbf{k}, (\omega)) \widetilde{\mathcal{G}}(-\mathbf{k}, (\omega - \omega')) \\ & + \frac{1}{4} \left(\mathcal{F}(\mathbf{k}, \omega) \mathcal{F}^{\dagger}(-\mathbf{k}, (\omega - \omega')) + \mathcal{F}(\mathbf{k}, \omega) \mathcal{F}^{\dagger}(\mathbf{k}, (\omega - \omega')) \right) \\ & + \frac{1}{4} \left(\mathcal{F}(-\mathbf{k}, \omega) \mathcal{F}^{\dagger}(-\mathbf{k}, (\omega - \omega')) + \mathcal{F}(-\mathbf{k}, \omega) \mathcal{F}^{\dagger}(\mathbf{k}, (\omega - \omega')) \right). \end{aligned} \tag{6.55}$$

In momentum space the normal and anomalous propagators is given by [71]:

$$\mathcal{G}(\mathbf{k}, \omega) = \frac{u_k^2}{\omega - E(k) + i\epsilon} + \frac{v_k^2}{\omega + E(k) - i\epsilon}, \tag{6.56}$$

$$\widetilde{\mathcal{G}}(\mathbf{k}, \omega) = -\frac{u_k^2}{\omega + E(k) - i\epsilon} - \frac{v_k^2}{\omega - E(k) + i\epsilon}, \tag{6.57}$$

$$\mathcal{F}(\mathbf{k}, \omega) = \mathcal{F}^{\dagger}(\mathbf{k}, \omega) = -u_k v_k \left(\frac{1}{\omega - E(k) + i\epsilon} - \frac{1}{\omega + E(k) - i\epsilon} \right). \tag{6.58}$$

where the spectral functions u_k and v_k are defined as:

$$u_k^2 = \frac{1}{2} \left(1 + \frac{\xi(k)}{E_k} \right) \tag{6.59}$$

$$v_k^2 = \frac{1}{2} \left(1 - \frac{\xi(k)}{E_k} \right) \tag{6.60}$$

$$E_k = \sqrt{\xi(k)^2 - \Delta(k)^2}. \tag{6.61}$$

Here $\xi(k) = \varepsilon_{\mathrm{k}} - \mu$, which is the single-particle energy measured from the chemical potential μ. At zero temperature, $\mu = \dfrac{k_{\mathrm{F}}^2}{2}$. In the equation (6.61), $\Delta(k)$ is the gap function. From the equations (6.56 - 6.58), it is clear that $\mathcal{G}(\mathbf{k}, \omega) = \mathcal{G}(-\mathbf{k}, \omega)$ and similar relations hold for anomalous propagators $\mathcal{F}$, $\mathcal{F}^{\dagger}$. As a result, equation (6.55) becomes

$$G^{(2)}(\mathbf{k}, \omega) = \int \frac{d\omega'}{2\pi i} \left(\mathcal{G}(\mathbf{k}, (\omega)) \widetilde{\mathcal{G}}(\mathbf{k}, (\omega - \omega')) + \mathcal{F}(\mathbf{k}, \omega) \mathcal{F}^{\dagger}(\mathbf{k}, (\omega - \omega')) \right). \tag{6.62}$$

Evaluating the contour integral in equation (6.62) we get the following expression for the two-particle Nambu-Gorkov propagator,

$$G^{(2)}(\mathbf{k},\omega) = \frac{u_k^2}{\omega - 2E_k + i\epsilon} - \frac{v_k^2}{\omega + 2E_k - i\epsilon}. \tag{6.63}$$

The final form of the above equation is valid for $P = 0$. At this point, setting the gap $\Delta(k) = 0$, reproduces the non-interacting two-particle G^0_{pphh} propagator. Now that we have the required two-particle Green's function, we can continue our analysis of Weinberg eigenvalues.

6.5 Weinberg Eigenvalues for Nambu-Gorkov Green's Function

We will first calculate the Weinberg eigenvalues of the Nambu-Gorkov propagator using a separable potential. The generic form we will use is as given below:

$$V = \lambda |f\rangle\langle f|, \tag{6.64}$$

where λ is a coupling that controls the strength of the potential. If $\lambda < 0$ then the potential is attractive and if $\lambda > 0$, then the potential is repulsive. The Weinberg eigenvalue equation (5.18) as seen in the chapter (5), section (5.2), can now be written in momentum space in the partial wave basis as:

$$\begin{aligned} G_0(k,E)V|\Psi_\nu(E)\rangle &= \eta_\nu(E)|\Psi_\nu(E)\rangle, \\ \frac{2}{\pi}\lambda\langle f|\Psi_\nu(E)\rangle \int_0^\Lambda k^2 dk G_0(k,E)\langle k|f\rangle|k\rangle &= \eta_\nu(E)|\Psi_\nu(E)\rangle. \end{aligned} \tag{6.65}$$

Therefore, from equation (6.65), we see that there is only one Weinberg eigenvalue for any rank-one separable potential, given by:

$$\eta_\nu(E) = \lambda\langle f|\Psi_\nu(E)\rangle, \tag{6.66}$$

and the corresponding eigenvector is given by:

$$|\Psi_\nu(E)\rangle = \frac{2}{\pi}\int_0^\Lambda k^2 dk G_0(k,E) f(k)|k\rangle. \tag{6.67}$$

Finally, substituting equation (6.67) into equation (6.66), we get the following closed expression for the Weinberg eigenvalue:

$$\eta_\nu(E) = \lambda\frac{2}{\pi}\int_0^\Lambda k^2 dk G_0(k,E)|f(k)|^2. \tag{6.68}$$

Notice that we have not yet chosen a form for the two-particle Green's function and equation (6.68) is a general expression for the Weinberg eigenvalue for a separable potential of the form given in equation (6.64). Using either the two-particle G^0_{pphh} propagator given by equation (6.38) or the two-particle Nambu-Gorkov propagator as given by equation (6.63), we can calculate the corresponding eigenvalue η_ν for the separable case. We choose the functions $f(k)$ to be a gaussian, i.e.,

$$f(k) = \exp\left[-\left(\frac{k}{\alpha}\right)^2\right], \tag{6.69}$$

so that the separable potential is now

$$V(k_i,k_j) = \lambda\exp\left[-\left(\frac{k_i}{\alpha}\right)^2\right]\exp\left[-\left(\frac{k_j}{\alpha}\right)^2\right], \tag{6.70}$$

where α is a constant with the same dimension as $k(\,\mathrm{fm}^{-1})$. Here for simplicity we set $\alpha = \sqrt{2}\,\mathrm{fm}^{-1}$ so that the diagonal matrix elements now become $|f(k)|^2 = \exp\left[-(k)^2\right]$. We also set $\lambda = -1$, so that the separable potential is attractive (as we are interested in studying the relation between pairing and Weinberg eigenvalues).

Figure (6.8) shows the Weinberg eigenvalue for the separable gaussian potential as a function of center of mass energy, E_{cm} for $\Delta_{k_\mathrm{F}} = 0\,\mathrm{MeV}$ and finite Δ_{k_F}. For $\Delta_{k_\mathrm{F}} = 0\,\mathrm{MeV}$ the eigenvalue shoots up close to $E_{\mathrm{cm}} = 2\varepsilon_\mathrm{F}$, as seen in figure (6.3). We

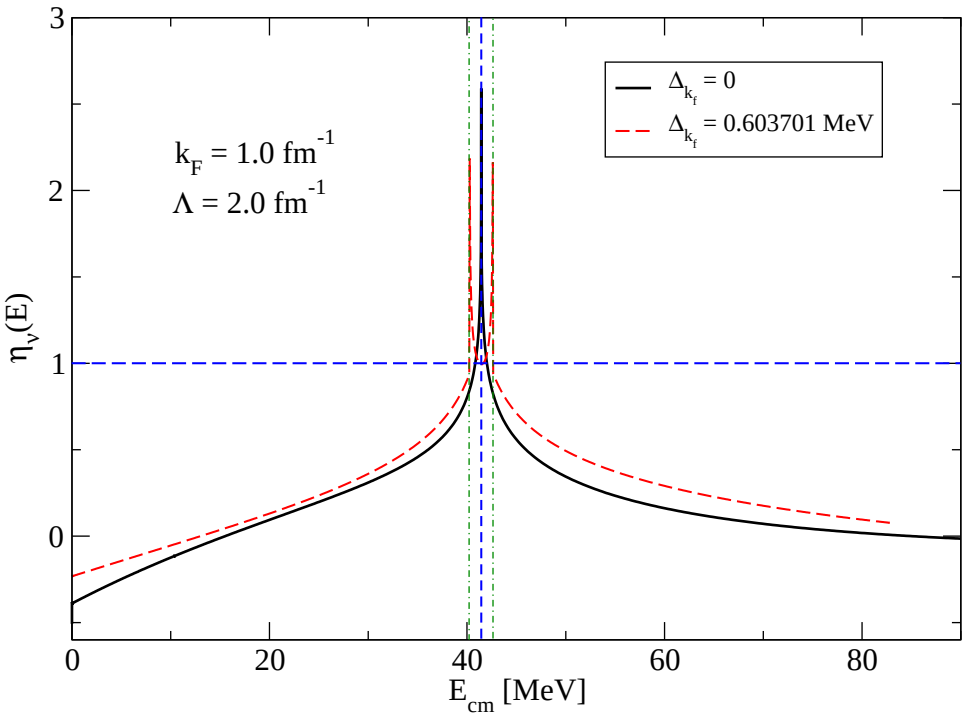

Figure 6.8: Plot of the Weinberg eigenvalue as a function of $E_{\rm cm}$ for both $\Delta_{k_{\rm F}} = 0\,{\rm MeV}$ and $\Delta_{k_{\rm F}} = 0.603701\,{\rm MeV}$. The solid line represents the eigenvalue for the non-interacting G^0_{pphh} propagator, while the dashed lines is for the Nambu-Gorkov propagator. Nambu-Gorkov eigenvalue $\eta_{\nu,{\rm NG}} \to 1$ close to $2\varepsilon_{\rm F}$, indicating formation of a new bound state (Cooper Pairs). The large singular values for η_ν observed at $2\varepsilon_{\rm F} \pm 2\Delta_{k_{\rm F}}$ represents the energy at which the pairs are broken and we now have excited states.

can determine the pairing gap from the energy eigenvalue for which $\eta_\nu(E_c) = 1$ using equation (6.28). The pairing gap for the separable form given by equation (6.68) turs out to be $\Delta_{k_{\rm F}} = 0.603701\,{\rm MeV}$. This value of the gap parameter, is then used in the two-particle Nambu-Gorkov propagator and the corresponding eigenvalue is evaluated using the following expression:

$$\eta_\nu(E) = \lambda \frac{2}{\pi} \mathcal{P} \int_0^\Lambda k^2 dk |f(k)|^2 \left(\frac{u_k^2}{\omega - 2E_k} - \frac{v_k^2}{\omega + 2E_k} \right). \tag{6.71}$$

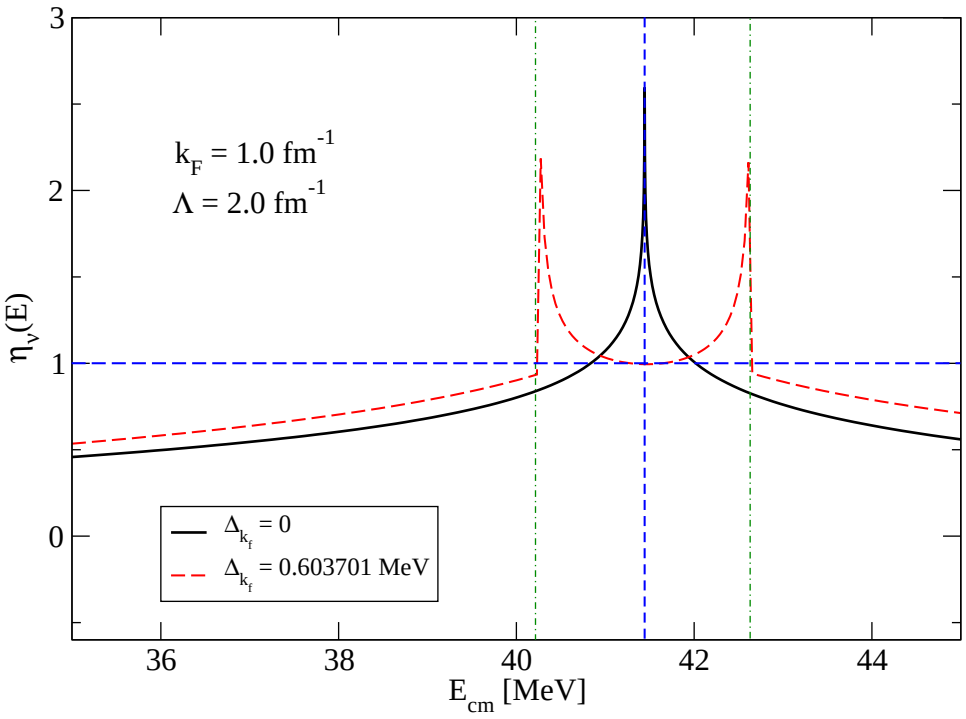

Figure 6.9: Zooming in on the behavior at $E_{\rm cm} = 2\varepsilon_{\rm F}$ and at $E_{\rm cm} = 2\varepsilon_{\rm F} \pm 2\Delta_{k_{\rm F}}$.

where $E_k = \sqrt{\xi(k)^2 - \Delta^2_{k_{\rm F}}}$. Note the we have used the value of the gap at $k_{\rm F}$ as a first approximation to $\Delta(k)$. We see that the eigenvalue $\eta_\nu(E)$ tends to 1 close to $E_{\rm cm} = 2\varepsilon_{\rm F}$. This indicates the presence of bound pairs close to the Fermi surface (Cooper Pairs). At $E_{\rm cm} = 2\varepsilon_{\rm F}$, the eigenvalue equation (6.65) reduces to the BCS gap equation. To prove this, we will first write equation (6.65) in momentum space as follows:

$$\frac{2}{\pi}\lambda \int_0^\Lambda k^2 dk G_0(k', E) V(k', k) \Psi_\nu(k, E) = \eta_\nu(E) \Psi_\nu(k', E). \tag{6.72}$$

As noted earlier, we can solve the above equation by converting it to a left-eigenvalue problem, or alternatively solve the right-eigenvalue problem,

$$VG_0(z)[V|\Psi_\nu(z)\rangle] = \eta_\nu(z)[V|\Psi_\nu(z)\rangle], \tag{6.73}$$

which has the same spectrum as $G_0(z)V$, and integrate over the singularity directly. We choose to solve for eigenvalues of $VG_0(z)$. Using the two-particle Nambu-Gorkov propagator, the right-eigenvalue problem equation (6.73) can be now written as:

$$\frac{2}{\pi}\mathcal{P}\int_0^\Lambda k^2 dk V(k',k)\left(\frac{u_k^2}{\omega - 2E_k} - \frac{v_k^2}{\omega + 2E_k}\right)\Psi_\nu(k,E) = (\eta_\nu(E))\Psi_\nu(k',E). \tag{6.74}$$

For $\omega = 0$, equation (6.74) reduces to:

$$-\frac{1}{\pi}\int_0^\Lambda k^2 dk V(k',k)\left(\frac{1}{\sqrt{\xi(k)^2 + \Delta(k)^2}}\right)\Psi_\nu(k,E) = \Psi_\nu(k',E). \tag{6.75}$$

where we have the fact that $\eta_\nu(E) \sim 1$ and $E_k = \sqrt{\xi(k)^2 + \Delta(k)^2}$. Equation (6.75) is the gap equation. Therefore the corresponding eigenvector $\Psi_\nu(k, E \to 2\varepsilon_{\rm F})$ is the gap function $\Delta(k)$. At energies of $2\varepsilon_{\rm F} \pm 2\Delta_{k_{\rm F}}$ we see that the eigenvalue is singular (figure (6.9)). This behavior is related to the breaking of Cooper pairs.

Before presenting results for $V_{{\rm low}\,k}$, we will prove a general result for the bound states of the T matrix equation. The T matrix equation in momentum space, in the partial wave basis, is given by:

$$T(k',k;E) = V(k',k) + \frac{2}{\pi}\int_0^\infty q^2 dq V(k',q)G(q,E)T(q,k;E). \tag{6.76}$$

Let us use the two-particle Nambu-Gorkov propagator, so that the T matrix equation (6.76) becomes:

$$\begin{aligned} T(k',k;E) &= V(k',k) \\ &+ \frac{2}{\pi}\mathcal{P}\int_0^\infty q^2 dq V(k',q)\left(\frac{u_k^2}{\omega - 2E_k} - \frac{v_k^2}{\omega + 2E_k}\right)T(q,k;E) \end{aligned} \tag{6.77}$$

As $\omega \to 0 \Rightarrow E \to 2\mu$, equation (6.77) has a pole (bound state), and the corresponding Weinberg eigenvalue $\to 1$. Close to a bound state the T matrix equation becomes separable [47] so that T matrix elements can be written as

$$T(k', k; E_b) \sim \frac{f(k')f(k)}{E - E_b}, \tag{6.78}$$

where E_b is the bound state energy. In this case $E_b = 2\mu$. Also the first term in equation (6.77) becomes negligible. Therefore we can write equation (6.77) as

$$f(k')f(k) = -\frac{1}{\pi}\int_0^\infty q^2 dq V(k', q)\left(\frac{1}{\sqrt{\xi(q)^2 + \Delta(q)^2}}\right) f(k)f(q), \tag{6.79}$$

$$\Rightarrow f(k') = -\frac{1}{\pi}\int_0^\infty q^2 dq V(k', q)\left(\frac{1}{\sqrt{\xi(q)^2 + \Delta(q)^2}}\right) f(q). \tag{6.80}$$

Comparing equation (6.80) to the gap equation

$$\Delta(k) = -\frac{1}{\pi}\int q^2 dq \frac{V(k, q)\Delta(q)}{\sqrt{\xi(q)^2 + \Delta(q)^2}}, \tag{6.81}$$

so we can identify $f(k) = \Delta(k)$. Thefore the separable form for the $T(k', k; 2\mu)$ can be written as

$$T(k', k; 2\mu) \sim \frac{\Delta(k')\Delta(k)}{E - 2\mu}, \tag{6.82}$$

which shows that the homogeneous gap equation can be understood as an equation for the residue of the pole of the T matrix [76].

Figure (6.10) shows the largest attractive Weinberg eigenvalue as a function of $E_{\rm cm}$ for $V_{{\rm low}\,k}$ in the ${}^1S_0$ partial wave at $k_{\rm F} = 1.0\,{\rm fm}^{-1}$. Apart from numerical instabilities outside the $\pm 2\Delta_{k_{\rm F}}$ region, the largest eigenvalue behaves similar to the eigenvalue in the separable case (firgure (6.8)) as $E_{\rm cm} \to 2\varepsilon_{\rm F}$. As seen in equation (6.75) and the discussion following it, the eigenvector corresponding to $\eta_\nu(E) = 1$, as $E \to 2\mu$, is the gap function. Figure (6.11) shows the eigenvector corresponding to the largest

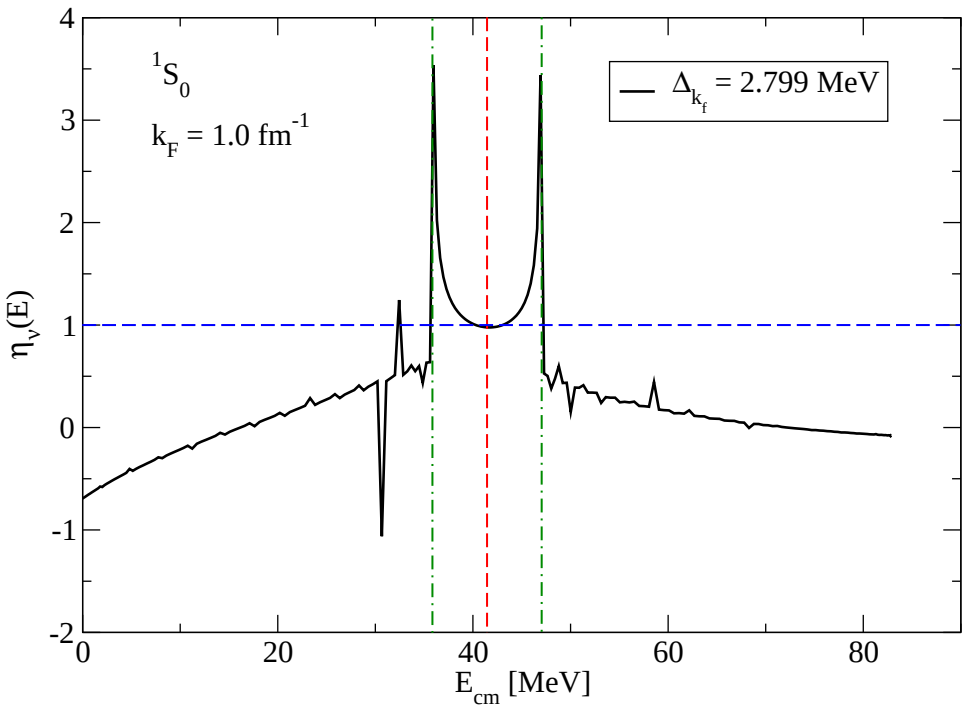

Figure 6.10: Largest attractive Weinberg eigenvalue as a function of energy $E_{\rm cm}$. Notice that as $E_{\rm cm} \to 2\varepsilon_{\rm F}$, $\eta_\nu(E)$ tend to 1.

eigenvalue at $E_{\rm cm} = 2\varepsilon_{\rm F}$. Using this as the first guess to the gap function $\Delta(k)$ and iterating the gap equation (6.81), yields the self-consistent BCS gap function shown in figure (6.12). As $k_{\rm F}$ increases, the gap closes for smaller momentum values, as observed in reference [72]. These results are consistent with the density dependence of the $^1S_0$ gap $\Delta_{k_{\rm F}}$. Notice that as $k_{\rm F}$ increases, the gap function initially increases, reaching a maximum value around $k_{\rm F} \approx 1\,{\rm MeV}$, after which the gap function rapidly decreases to zero for all k.

The gaps shown so far are the BCS results and do not include polarization effects. These effects are known to significantly reduce the gap in neutron matter [68, 73, 74,

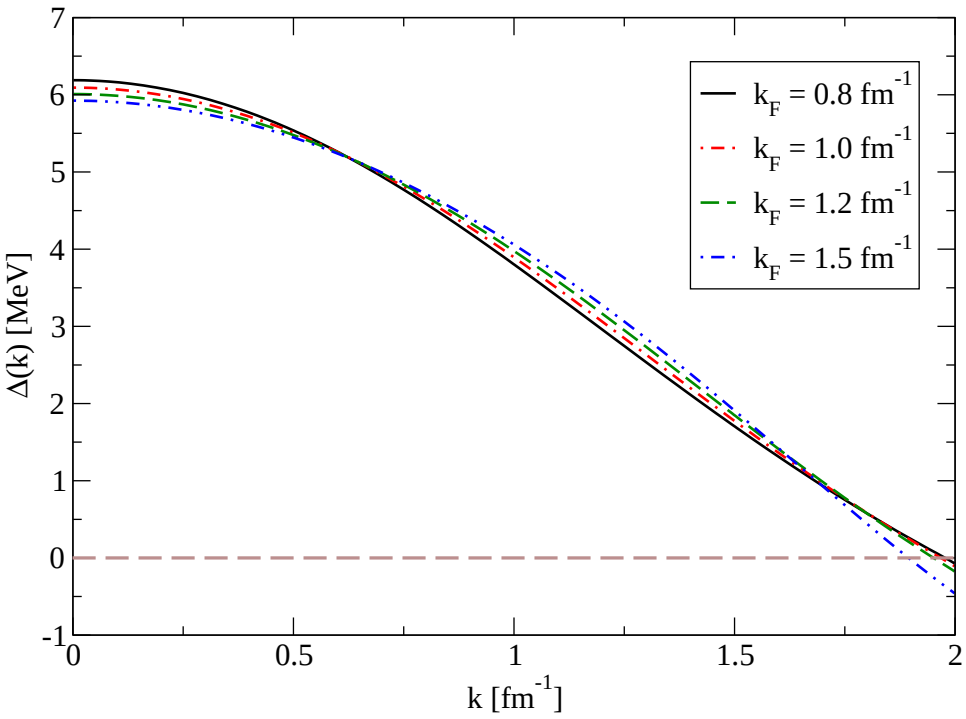

Figure 6.11: Momentum dependence of the gap function $\Delta(k)$: At this stage the gap function $\Delta(k)$ is the eigenvector corresponding to the largest eigenvalue at $\omega = 0$.

75]. These interactions can be taken into account by defining the potential as,

$$V(k', k) = V_0(k', k) + V_{\text{ind}}(k', k), \tag{6.83}$$

where $V_0(k', k)$ is the two-body interaction and $V_{\text{ind}}(k', k)$ is the induced interaction given in detail in references [73, 77]. Once again we can use the two-particle Green's function, G^0_{pphh} to calculate the eigenvalues close to the Fermi-surface and determine the pairing gap at k_{F} in a similar fashion. This method therefore offers an easy extension to include medium effects.

We have so far presented results for the $^1S_0$ channel for neutron matter. Pairing also occurs in the $^3P_2$-$^3F_2$ triplet channel at higher densities $k_{\text{F}} \geq 1.5\,\text{fm}^{-1}$, where

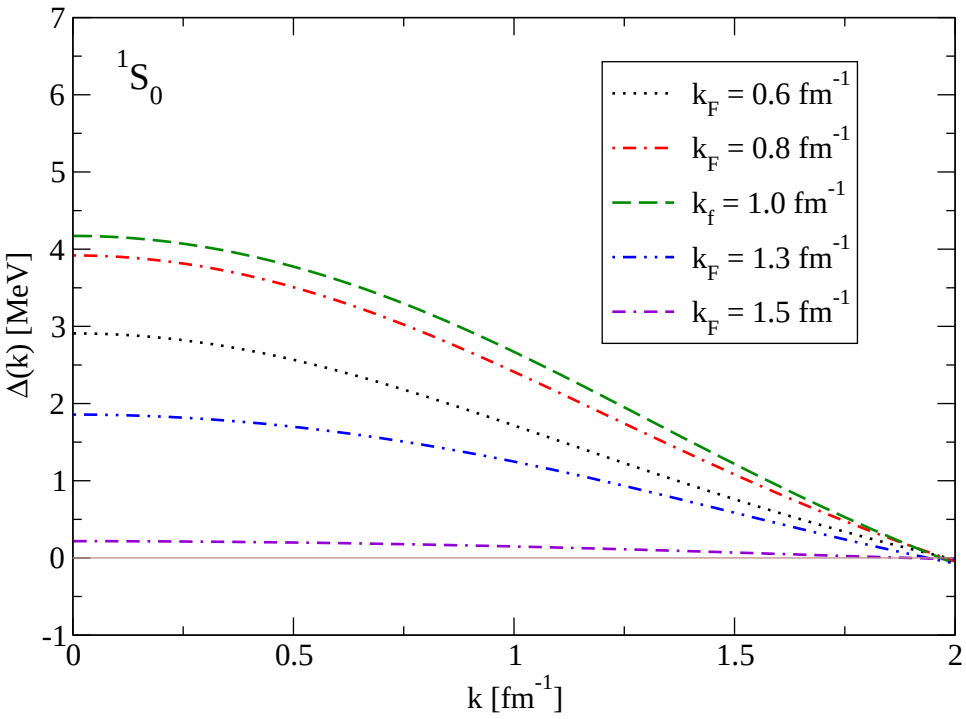

Figure 6.12: Momentum dependence of the self-consistent gap function $\Delta(k)$, obtained from the Weinberg eigenvectors corresponding to the largest eigenvalue at $\omega = 0$.

the interaction in this channel becomes attractive. It has been observed that the triplet pairing gaps are sensitive to the two-nucleon interaction beyond $k_{\rm F} = 2.0\,{\rm fm}^{-1}$, where the interactions themselves start to differ. It would be interesting to explore the interaction dependence for the Chiral N^{3}LO potentials [26, 27] as the cut-off is lowered. Using the Weinberg eigenvalue analysis has a two-fold advantage. It can be used as a tool to understand the underlying scale dependent physics as the interaction is evolved; secondly the influence of this physics on the pairing gap can be estimated by determining the critical energy E_c where the eigenvalues cross one. One can usually introduce Weinberg quasi-particles [41] to subtract out the non-perturbative physics

close to $2\varepsilon_{\mathrm{F}}$ so that the "Born-series" using the two-particle propagator becomes perturbative. It would be interesting to explore this quasi-particle method for the Gorkov propagator. Work in this direction is in progress [66]

CHAPTER 7

CONCLUDING REMARKS

Microscopic calculations of finite nuclei and nuclear matter require a good understanding of the two-body interaction. This has been one of the main focus of theoretical nuclear physics since the time of Yukawa when he first introduced a field theoretic model of the nuclear forces through meson exchange. Recent work has churned out several high-precision phase equivalent potentials (Argonne v_{18}, CD Bonn, Nijmegen I, II etc) which accurately fit the available two-body data ($\frac{\chi^2}{d.o.f.} \approx 1$) such as low-energy phase shifts and deuteron binding energy. These potentials use pion exchange for the long-distance part, while the intermediate and short range pieces are model dependent. Explicitly modeling the short-distance ("hard-core") leads to non-zero matrix elements for the interaction potential in momentum space at such large values of momentum ($\approx$ GeV) where a potential formulation is not even valid.

From an Effective Field Theory point of view, these potentials do not improve our understanding of short-distance physics, but only complicate low-momentum calculations by including model-dependent high-momentum states. The whole machinery of many-body techniques is based on the non-perturbativeness of the input interactions resulting in partial resummations such as the G matrix used in nuclear matter calculations, which sums ladder diagrams to all orders. The short-range repulsion

modeled in to the interaction potential render many-body calculations hard and numerically expensive. Therefore, for a low-energy process, it would be advantageous to integrate out the model-dependent high-momentum states and include the effect of these states in an EFT style, which is by simpler renormalized contact interactions. This led to the entire field of chiral effective theory which has been very successful in the few-body sector. The breakdown scale of nuclear EFT is usually around $\Lambda_\chi \approx 700\,\mathrm{MeV} - 1\,\mathrm{GeV}$.

The Renormalization Group approach to low-momentum potentials starts with any of the bare interactions, which usually have a large momentum cut-off (which we refer to as the bare cut-off Λ_0). The intermediate states are systematically integrated out by successively lowering the bare cut-off until a final $\Lambda \approx 2.0\,\mathrm{fm}^{-1}$ is reached. As noted earlier this cut-off value of $\Lambda = 2.0\,\mathrm{fm}^{-1}$ corresponds to lab energies of $E_{\mathrm{lab}} \approx 350\,\mathrm{MeV}$, which also marks the energy up to which we have elastic scattering data (which constrain the bare interactions). The potential usually referred to as $V_{\mathrm{low}\,k}$ has non-zero matrix elements only for $k \leq \Lambda$ and as a result has smaller model spaces. Successively integrating out the high-momentum states results in smearing out the short-range repulsion, yielding a soft low-momentum potential. These features make many-body calculations more tractable.

This work explores the regulator dependence of the $V_{\mathrm{low}\,k}$. As noted earlier, this investigation is important in order to better understand the two-body running in free-space so that we can separate numerics from physics. Though the sharp regulators give the most simplistic idea of cutting out high-momentum intermediate states, it is seen that it is advantageous to use smooth regulators instead. Using $V_{\mathrm{low}\,k}$ as

an input in many-body calculation leads to dramatic simplifications as the particle-particle channel now becomes perturbative [37]. Regulator artifacts are apparent in the work of Bogner *et. al* [38, 39] where smooth cut-offs leads to better convergence in deuteron and triton variational calculations, where they use simple ansätze for the wave functions. The reason for a simple ansatz to work lies in the fact that $V_{\mathrm{low}\,k}$ potentials are soft and the running decreases the correlations in the wave function which was needed conventionally for the expensive cancellations due to the presence of the "hard-core". These correlations are usually seen as the "wound" in the two-body wave function, while this is removed for the $V_{\mathrm{low}\,k}$ wave functions as seen in figure (4.16) in section 4.3 of chapter 4.

These ideas of "perturbativeness" of the two-body interaction can be made quantitative using the Weinberg eigenvalue analysis, which examines the eigenvalue spectrum of the kernel G_0V where V is a generic two-body interaction potential and G_0 is the two-body Green's function (propagator). The main result of this analysis was that as the cut-off is lowered in the RG running, the non-perturbative sources (short-range repulsion and the iterated tensor interactions) are softened, resulting in major decreases in the magnitude of the Weinberg eigenvalues in free-space. Therefore it is beneficial to lower the cut-off or the resolution scale for the conventional NN interactions. In fact, it is seen that lowering the cut-off even for the chiral potential softens the effect of new sources of non-perturbative physics, namely the singular part of the two-pion exchange which enters at fourth order ($\mathrm{N^3LO}$) in the chiral expansion. The same trends are observed at finite density, where Pauli-Blocking eliminates another source of non-perturbative physics which is independent of the cut-off Λ in free-space, namely the shallow bound states. But close to the fermi surface there is a pairing

instability as the two-body interaction is attractive in certain partial wave channels. This is reflected in the Weinberg eigenvalues by the arbitrary increase in its magnitude close to the fermi surface ($E_{\rm cm} \to 2\varepsilon_{\rm F}$). Further we can get a good estimate of the pairing gap from the real part of the largest eigenvalue. When pairing is included by using the two-particle Nambu-Gorkov Green's function, we observe that eigenvalues $\eta_{\rm NG} \to 1$ close to the fermi surface indicating the formation of a "bound" state, while at $\pm 2\Delta$ from the fermi surface, where Δ is the pairing gap, the eigenvalues become singular indicating the breaking of Cooper pairs. The eigenvectors corresponding to the largest eigenvalue at $E_{\rm cm} = 2\varepsilon_{\rm F}$ gives a first approximation to the gap function $\Delta(k)$ which can be further iterated to get the self-consistent gap function. Therefore the eigenvalue spectrum not only shows the behavior expected in free-space and in-medium, but also serves as a diagnostic to understand the physics at various cut-off scales. In addition this analysis gives a neat method to estimate the pairing gap which is a non-perturbative effect.

With all the progress made in understanding two-body interactions at low-momenta, it is but appropriate to discuss the possible future direction of this research. Traditional many-body techniques involve selective summations in order to account for the short-range repulsion of nuclear interactions [58, 59, 60]. Given the simplifications in nuclear matter and few-body (deuteron and triton) calculations, it is tempting to review the standard many-body approaches using these low-momentum two-body interaction as input (work in this direction is already in progress! [90]). But we need to fill in one more step before that, namely the three-body running giving the corresponding "$V_{\rm low\,k}$" for 3N interactions. The RG approach we discuss in this work is just one way to achieve decoupling of the low and high-momentum states of the interaction

potential. Other approaches exist such as Lee-Suzuki transformation [80, 81] and the recent Similarity RG transformation (SRG) [46], both of which are discussed in the appendices. Lee-Suzuki transformation decouples low- and high-momentum states using projection operators P and Q defined such that $PQ = 0$ and $P + Q = 1$. Here P and Q project on to the low and high momentum states respectively. The resulting low-momentum potential has non-zero matrix matrix elements only in the low-momentum sub-space P and is equivalent to a sharp cut-off RG evolution. It would be interesting to study the generalization of Lee-Suzuki transformation to smooth regulators, analogous to the smooth regulator form of RG.

On the other hand, SRG achieves decoupling by driving the matrix elements of the interaction potential to a band diagonal form. SRG has a further advantage of being automatically energy-independent and preserving the high-energy model dependent phase shifts. Most importantly, the same transformations renormalize all operators, including many-body operators. Using SRG, three-body running is straightforward, where the bare potential is now a three-body chiral potential and it leads to a set of coupled differential equations.

An alternative non-RG unitary transformation to reduce the correlations in the many-body wave functions is given by Unitary Correlation Operator Method [89] and references therein. As all these techniques such as $V_{\mathrm{low}\,k}$ evolution, SRG and Lee-Suzuki transformations, represent different ways to decouple low and high momentum states, it should be possible to connect them, which would further our formal understanding of the low-momentum interactions.

The low-momentum potentials for different starting potentials ($V_{\rm bare}$) are *nearly similar but not identical*. From the perspective of formally understanding these low-momentum potentials, it would be worth-while to explore the universality of the low-momentum potentials so that we can trace the source of "model dependence" which still exists at low momenta. Finally it would be interesting to extend these approaches to many-body problems in other areas of physics, in particular condensed matter systems. Low-momentum potentials and effective field theory approach have opened up an interesting channel which presents the hope of finally being able to have a microscopic calculation for finite nuclei and nuclear matter.

APPENDIX A

SCATTERING THEORY IN FREE SPACE

The sections in this appendix A briefly survey some elements of scattering theory, following the discussions in Taylor and Sakurai [43, 44], to supplement earlier sections (chapter 2, section 2.1)

A.1 Stationary Scattering States

In this section we will develop some more details on stationary scattering states. The in- and out-asymptotes $|\psi_{in}\rangle$ and $|\psi_{out}\rangle$ are related to the actual state $|\Psi\rangle$ at t by the following asymptotic condition:

$$\lim_{t\to-\infty} \widehat{U}(t)|\Psi\rangle = \widehat{U}_0(t)|\psi_{in}\rangle \tag{A.1}$$

and

$$\lim_{t\to+\infty} \widehat{U}(t)|\Psi\rangle = \widehat{U}_0(t)|\psi_{out}\rangle \tag{A.2}$$

which can be expressed in terms of Moller scattering operators as:

$$|\Psi\rangle = \lim_{t\to-\infty} \widehat{U}(t)^\dagger \widehat{U}_0(t)|\psi_{in}\rangle \equiv \Omega_+|\psi_{in}\rangle, \tag{A.3}$$

or equivalently

$$|\Psi\rangle = \lim_{t\to+\infty} \widehat{U}(t)^\dagger \widehat{U}_0(t)|\psi_{out}\rangle \equiv \Omega_-|\psi_{out}\rangle. \tag{A.4}$$

Therefore,

$$|\psi_{out}\rangle = \widehat{\Omega}_{-}^{\dagger}\,\widehat{\Omega}_{+}|\psi_{in}\rangle. \tag{A.5}$$

Defining a unitary operator $\widehat{S} = \widehat{\Omega}_{-}^{\dagger}\,\widehat{\Omega}_{+}$, we can write

$$|\psi_{out}\rangle = \widehat{S}|\psi_{in}\rangle. \tag{A.6}$$

where S is the scattering operator we had seen in chapter 2, section 2.1. Now we define stationary states $|\mathbf{p}_{\pm}\rangle$ at time t as follows:

$$|\mathbf{p}_{\pm}\rangle \equiv \widehat{\Omega}_{\pm}|\mathbf{p}\rangle \tag{A.7}$$

where $|\mathbf{p}\rangle$ represent the asymptotic stationary states. The in- and out-asymptote can be expanded in the $\{|\mathbf{p}\rangle\}$ basis as

$$|\psi_{in}\rangle = \int d^3p\, \psi_{in}(p)|\mathbf{p}\rangle. \tag{A.8}$$

Therefore the state at time t is given in terms of these stationary states as

$$\begin{aligned} |\Psi\rangle &= \Omega_{+}|\psi_{in}\rangle, && \text{(A.9)}\\ &= \int d^3p\, \psi_{in}(p)\Omega_{+}|\mathbf{p}\rangle, && \text{(A.10)}\\ &= \int d^3p\, \psi_{in}(p)|\mathbf{p}_{+}\rangle && \text{(A.11)} \end{aligned}$$

where the last equation (A.11), is obtained using equation (A.7). Similar relations hold for the out-asymptote. Therefore the state at $t = 0$ can be expanded using the stationary states $|\mathbf{p}_{\pm}\rangle$ analogous to the asymptotes being expanded in a basis of plane wave states $|\mathbf{p}\rangle$. We know that $\Omega_{\pm} = 1 + G_0(E \pm i\epsilon)V$, therefore equation (A.7) can be written as

$$|\mathbf{p}_{\pm}\rangle = \left[1 + G(E \pm i\epsilon)V\right]|\mathbf{p}\rangle \tag{A.12}$$

But $GV = G_0T$, so that

$$|\mathbf{p}_\pm\rangle = [1 + G_0(E \pm i\epsilon)T]\,|\mathbf{p}\rangle \tag{A.13}$$

which can also be written as

$$|\mathbf{p}_\pm\rangle = [1 + G_0(E \pm i\epsilon)V]\,|\mathbf{p}_\pm\rangle \tag{A.14}$$

where we used the definition for the $T = V + VGV$ operator and equation (A.12) to establish the relation $T|\mathbf{p}\rangle = [V + VGV]\,|\mathbf{p}\rangle = V|\mathbf{p}_\pm\rangle$. Equation (A.13) is the Lippmann-Schwinger equation for $|\mathbf{p}_\pm\rangle$. There the stationary state scattering wave functions satisfy

$$\langle\mathbf{x}|\mathbf{p}_\pm\rangle = \langle\mathbf{x}|\mathbf{p}\rangle + \int d^3x' \langle\mathbf{x}|\,G_0(E \pm i\epsilon)\,|\mathbf{x}'\rangle V(\mathbf{x}')\langle\mathbf{x}'|\mathbf{p}_\pm\rangle \tag{A.15}$$

We now establish the result that the scattered wave function for large r is a plane wave plus a spherical out-going part. We also choose the $+i\epsilon$ piece as this corresponds to the out-going spherical wave (as will be seen). As a next step we calculate $\langle\mathbf{x}|G_0(E + i\epsilon)|\mathbf{x}'\rangle$. G_0 is the free Green's function having the following form

$$G_0(z)|\mathbf{p}\rangle = \frac{1}{z - E_p}|\mathbf{p}\rangle \tag{A.16}$$

in momentum space and z represents complex energies. Therefore:

$$\langle\mathbf{x}|G_0(E + i\epsilon)|\mathbf{x}'\rangle = \int d^3p\,\langle\mathbf{x}|\,G_0(E + i\epsilon)|\mathbf{p}\rangle\langle\mathbf{p}|\mathbf{x}'\rangle \tag{A.17}$$

$$= \int \frac{d^3p}{(2\pi)^3}\frac{e^{i\mathbf{p}\cdot(\mathbf{x}-\mathbf{x}')}}{E - E_p + i\epsilon} \tag{A.18}$$

where there is a pole in the lower half plane. Evaluating the contour integral, we get,

$$\langle\mathbf{x}|G_0(E + i\epsilon)|\mathbf{x}'\rangle = -\frac{1}{2\pi}\frac{\exp\left(ip|\mathbf{x} - \mathbf{x}'|\right)}{|\mathbf{x} - \mathbf{x}'|} \tag{A.19}$$

which when subsituted into the LS equation (A.15) gives

$$\langle \mathbf{x}|\mathbf{p}_+\rangle = \langle \mathbf{x}|\mathbf{p}\rangle - \frac{1}{2\pi}\int d^3x' \frac{\exp\left(ip|\mathbf{x}-\mathbf{x}'|\right)}{|\mathbf{x}-\mathbf{x}'|} V(\mathbf{x}')\langle \mathbf{x}'|\mathbf{p}_+\rangle \tag{A.20}$$

Usually the potentials have finite range (with the exception of coulomb potential, but it is usually screened), therefore the integral is non-zero for $r' < R$, where R is the range of the potential. Therefore, $|\mathbf{x}-\mathbf{x}'|$ can be expanded in powers of (r'/r) as

$$|\mathbf{x}-\mathbf{x}'| = \sqrt{(\mathbf{x}^2 - 2\mathbf{x}\cdot\mathbf{x}' + (\mathbf{x}')^2)} = r\left[1 - \frac{\mathbf{x}\cdot\mathbf{x}'}{r^2} + \mathcal{O}\left(\frac{r'}{r}\right)^2\right] \tag{A.21}$$

so that in the limit $r \to \infty$, we get

$$\langle \mathbf{x}|\mathbf{p}_+\rangle \overset{r\to\infty}{\longrightarrow} C\left[e^{i\mathbf{p}\cdot\mathbf{x}} - \langle \mathbf{p}'|V|\mathbf{p}_+\rangle \frac{e^{ipr}}{r}\right]. \tag{A.22}$$

Using $f(\mathbf{p},\mathbf{p}') = -\langle \mathbf{p}'|V|\mathbf{p}_+\rangle$, we have

$$\langle \mathbf{x}|\mathbf{p}_+\rangle \overset{r\to\infty}{\longrightarrow} C\left[e^{i\mathbf{p}\cdot\mathbf{x}} + f(\mathbf{p},\mathbf{p}')\frac{e^{ipr}}{r}\right]. \tag{A.23}$$

This establishes the traditional interpretation of the scattering states as an incident plane wave plus a spherically spreading scattered wave. The out-going spherical wave stems from retaining $+i\epsilon$ is the definition for the Green's function. The other choice of $-i\epsilon$ leads to in-coming waves, which is acausal.

A.2 Scattering of Two Particles with Spin

We now briefly discuss scattering of two-particles with spin. The situation is complicated by the fact that the Hilbert space must also account for spin degrees of freedom and also the hamiltonian can be spin-dependent, such as the two-nucleon interactions. Despite these hassles, we will see that the scattering formalism for two-particles with spin can be set up analogous to spinless particles, as only asymptotes

are observed. The main difference is that now we have different scattering amplitudes and cross-sections for every possible choice of the initial and final spin states.

The Hilbert space for two particles with spin s_1 and s_2 is the direct product

$$\mathcal{H} = \mathcal{H}_1 \otimes \mathcal{H}_2 \tag{A.24}$$

where $\mathcal{H}_1$ and $\mathcal{H}_2 = \mathcal{H}_{space} \otimes \mathcal{H}_{spin}$. It is convenient to work in the center of mass (CM) frame so that

$$\mathcal{H} = \mathcal{H}_{cm} \otimes \mathcal{H}_{rel} \tag{A.25}$$

where $\mathcal{H}_{cm}$ describes the motion of the center of mass and $\mathcal{H}_{rel}$ describes relative motion, including both spins i.e, $\mathcal{H}_{rel}$ can itself be regarded as a product of space and spin (of the two particles). We can use either $|m_1, m_2\rangle$ or $|s, m\rangle$ as the basis for the spin space of the two particles. These are related as follows:

$$|s,\, m\rangle = \sum_{m_1,m_2} |m_1,\, m_2\rangle\langle m_1,\, m_2|s,\, m\rangle, \tag{A.26}$$

where $|m_1,\, m_2\rangle\langle m_1,\, m_2|$ are the Clebsch-Gordon (CG) coefficients. The general spin state of the two particles can be expanded as:

$$|\chi\rangle = \sum_{\xi} \chi_\xi |\xi\rangle \tag{A.27}$$

where $|\xi\rangle$ stands for either $|s, m\rangle$ or $|m_1, m_2\rangle$. The decomponsition of the two-particle motion into center of mass and relative coordinates simplifies the two-particle Moller operator as the center of mass piece factors out as follows:

$$\mathbf{\Omega}_\pm = \lim_{t\to\mp\infty} \widehat{U}^\dagger(t)\widehat{U}_0(t) = 1_{cm} \otimes \Omega_\pm. \tag{A.28}$$

This follows from the evolution operator $\widehat{U}(t)$ and $\widehat{U}_0(t)$ factorizing into a center of mass piece and relative motion piece. Therefore the unitary scattering operator for

the two particles can now be written as

$$\mathbf{S} = \mathbf{\Omega}_-^\dagger \mathbf{\Omega}_+ = 1_{cm} \otimes S. \tag{A.29}$$

Using the basis $\{|\mathbf{p}_1, \mathbf{p}_2, \xi\rangle\}$, the scattering operator is defined as:

$$\begin{aligned} \langle \mathbf{p}_1', \mathbf{p}_2', \xi' | \mathbf{S} | \mathbf{p}_1, \mathbf{p}_2, \xi \rangle &= \delta^3(\mathbf{p}_1' - \mathbf{p}_1)\delta^3(\mathbf{p}_2' - \mathbf{p}_2)\delta_{\xi,\xi'} - 2\pi i \delta(\sum_i E_i' - \sum_i E_i) \\ &\times \delta^3(\sum_i \mathbf{p}_i' - \sum_i \mathbf{p}_i) t(\mathbf{p}', \xi' \leftarrow \mathbf{p}, \xi). \end{aligned} \tag{A.30}$$

Here we have explicity displayed the energy and total momentum conservation property of the scattering operator $\mathbf{S}$. The first term is the amplitude in the absence of scattering, while the second term shows the effect of the scatterer. While the total enegy and momentum is conserved, the scattering operator generally connects states of different relative momenta and spins. Once we factor out the center of mass piece we have

$$\begin{aligned} \langle \mathbf{p}', \xi' | S | \mathbf{p}, \xi \rangle &= \delta^3(\mathbf{p}' - \mathbf{p})\delta_{\xi,\xi'} - 2\pi i \delta(\sum_i E_i' - \sum_i E_i) \\ &\times t(\mathbf{p}', \xi' \leftarrow \mathbf{p}, \xi). \end{aligned} \tag{A.31}$$

and once again the on-shell T matrix is proportional to the scattering amplitude as

$$f(\mathbf{p}', \xi' \leftarrow \mathbf{p}, \xi) = -(2\pi)^2 t(\mathbf{p}', \xi' \leftarrow \mathbf{p}, \xi). \tag{A.32}$$

But this is just for a single choice of spin states ξ and ξ'. In general we can represent the scattering amplitude as a matrix $F(\mathbf{p}' \leftarrow \mathbf{p})$ whose elements are $f(\mathbf{p}', \xi' \leftarrow \mathbf{p}, \xi)$. For the simple case of a spin-0 spin-half scattering (for example, pion-nucleon scattering) the matrix amplitude F can be defined as

$$F(\mathbf{p}', \mathbf{p}) = \begin{pmatrix} f_{++}(\mathbf{p}' \leftarrow \mathbf{p}) & f_{+-}(\mathbf{p}' \leftarrow \mathbf{p}) \\ f_{-+}(\mathbf{p}' \leftarrow \mathbf{p}) & f_{--}(\mathbf{p}' \leftarrow \mathbf{p}) \end{pmatrix} \tag{A.33}$$

where we have used $|+\rangle$ and $|-\rangle$ for the basis states corresponding to $m = \pm 1/2$ and $f_{m\,m'}(\mathbf{p}' \leftarrow \mathbf{p})$ is the amplitude for an initial particle with momentum $\mathbf{p}$ and z component of spin m to scatter into the state $\mathbf{p}', m'$. Then the cross-section is now defined as

$$\frac{d\sigma}{d\Omega}(\mathbf{p}', \chi' \leftarrow \mathbf{p}, \chi) = |\chi'^{\dagger} F(\mathbf{p}', \mathbf{p})\chi|^2 \tag{A.34}$$

where χ and χ' are the initial and final spinors. Equation (A.34) can be interpreted as follows. $F(\mathbf{p}', \mathbf{p})\chi$ is tbe actual spin state of the out-going particles and χ represents the incoming state. Then the cross section is just the probability that these emerging particles are in the state χ'.

A.3 Angular Momentum Basis

Consider a simple case of spinless two-particle scattering. In this case the matrix for the scattering amplitude, equation (A.33) reduces to a function $f(\mathbf{p} \leftarrow \mathbf{p}')$. If the system is rotationally invariant, then this amplitude, usually determined by five independent quantities, is now determined by two independent quantities. This is easily understood as rotational invariance requires that $\mathbf{p}$ and $\mathbf{p}'$ be combined to form scalars, which are $|\mathbf{p}|^2 = |\mathbf{p}'|^2$ (energy conservation) and $\mathbf{p} \cdot \mathbf{p}'$. Rotational invariance implies that the S matrix now commutes with H_0 and L^2 and it turns out that the angular momentum basis $|E, l, m\rangle$ is a convenient choice as the scattering operator is diagonal

$$\langle E', l', m_l'|S|E, l, m_l\rangle = \delta(E' - E)\delta_{l',l}\delta_{m_l',m_l} s_l(p) \tag{A.35}$$

where $s_l(p)$ are the corresponding eigenvalues and $p = \sqrt{2mE}$. In fact it is possible to relate the momentum and the angular momentum basis as follows:

$$\langle E, l, m_l | \mathbf{p} \rangle = \left(\frac{1}{p}\right)^{1/2} \delta(E - E_p) Y^*_{l,m_l}(\widehat{\mathbf{p}}). \tag{A.36}$$

As a result, the function $f(\mathbf{p} \leftarrow \mathbf{p}')$ can now be expanded in the angular momentum basis as

$$f(\mathbf{p} \leftarrow \mathbf{p}') = \sum_l (2l+1) f_l(p) P_l(\widehat{\mathbf{p}'} \cdot \widehat{\mathbf{p}}), \tag{A.37}$$

where

$$f_l(p) = \frac{s_l(p) - 1}{2ip} = \frac{e^{i\delta_l(p)} \sin(\delta_l(p))}{p} \tag{A.38}$$

For particles with spin, the angular momentum basis is no longer just $|E, l, m\rangle$, but

$$|E, l, s, j, m\rangle = \sum_{m_l, m_s} |E, l, s, m_l, m_s\rangle \langle l, s, m_l, m_s | j, m\rangle, \tag{A.39}$$

where $\langle l, s, m_l, m_s | j, m\rangle$ are the Clebsch-Gordon coefficient and

$$|E, l, s, m_l, m_s\rangle = |E, l, m_l\rangle \otimes |s m_s\rangle. \tag{A.40}$$

Equation (A.39) makes use of the fact that j is a good quantum number as $[S, J] = 0$ where J is the total angular momentum. In the basis of $|E, l, s, j, m\rangle$, the S operator is given by

$$\langle E', l', s', j', m' | S | E, l, s, j, m\rangle = \delta(E' - E) \delta_{j',j} \delta_{m',m} s^j_{l',s';l,s}(E). \tag{A.41}$$

where the pair (l', s') determine the rows and (l, s) determine the columns of the eigenvalue matrix $S^j(E)$. If the system is also invariant under parity, the S can only connect states with the same parity eigenvalue. For the simple example of spin-0 spin-1/2 scattering, S has the following form for $S^j(E)$

$$S^j(E) = \begin{pmatrix} e^{2i\delta^j_+} & 0 \\ 0 & e^{2i\delta^j_-} \end{pmatrix} \tag{A.42}$$

where + and − denote the two spin states $\pm 1/2$. We can define partial wave scattering amplitude as

$$f_l^j(E) = \frac{e^{2i\delta_l^j(E)} - 1}{2ip}. \tag{A.43}$$

The usefulness of the partial wave basis becomes apparant at low-energies, where the phase shifts of low l contribute. Then the scattering amplitude is determined by only few parameters.

A.4 Partial Wave Scattering States

The vectors $|E, l, m\rangle$ are simulataneous eigenvectors of the angular momentum and the free hamiltonian H_0. We can define analogous eigenvectors of the angular momentum and the full hamiltonian H denoted by $|E, l, m+\rangle$ and these are related to $|E, l, m\rangle$ as

$$|E, l, m+\rangle = \widehat{\Omega}_+ |E, l, m\rangle \tag{A.44}$$

analogous to the relationship of $|p+\rangle$ to $|p\rangle$. $|E, l, m+\rangle$ is the actual state at time t arising from the in-asymptote $|E, l, m\rangle$. Consider

$$H_0|E, l, m\rangle = E|E, l, m\rangle \tag{A.45}$$

$$\widehat{\Omega}_+ H_0 |E, l, m\rangle = E\,\widehat{\Omega}_+ |E, l, m\rangle. \tag{A.46}$$

Using $H_0 = \widehat{\Omega}_+^\dagger H \widehat{\Omega}_+$ equation (A.46) now becomes

$$H|E, l, m+\rangle = E|E, l, m+\rangle. \tag{A.47}$$

Therefore $|E, l, m+\rangle$ is the eigenvector of H with the same energy eigenvalue E.

The wave function in position space $\langle \mathbf{x}|E, l, m+\rangle$ can be written as:

$$\langle \mathbf{x}|E, l, m+\rangle = i^l \sqrt{\frac{2}{\pi p}} \frac{1}{r} \psi_{l,p}(r) Y_{l,m}(\widehat{\mathbf{x}}) \tag{A.48}$$

similar to the momentum space projection of $|E,l,m\rangle$ given in equation (A.36). $\psi_{l,p}(r)$ are solutions of the radial Schrödinger equation

$$\left[\frac{d^2}{dr^2} - \frac{l(l+1)}{r^2} - V(r) + p^2\right]\psi_{l,p}(r) = 0. \tag{A.49}$$

If $V(r) = 0$, then we get the free-space radial equation whose solutions are linear combination of the spherical bessel functions $j_l(pr)$ and $n_l(pr)$. Since $j_l(pr)$ has the desired behavior at $r = 0$, the eigenstates $|E,l,m\rangle$ has the following position space wave function

$$\langle \mathbf{x}|E,l,m\rangle = i^l\sqrt{\frac{2}{\pi p}}\frac{1}{r}j_l(pr)Y_{l,m}(\widehat{\mathbf{x}}). \tag{A.50}$$

The scattering states $|E,l,m+\rangle$ are normalized similar to $|E,l,m\rangle$, i.e.,

$$\langle E',l',m'+|E,l,m+\rangle = \delta(E'-E)\delta_{l',l}\delta_{m',m}. \tag{A.51}$$

Therefore, $\psi_{l,p}(r)$ are normalized as

$$\int_0^\infty \psi_{l',p'}(r)^*\psi_{l,p}(r) = \frac{\pi}{2}\delta(p'-p). \tag{A.52}$$

In the limit $r \to \infty$, the radial wave functions $\psi_{l,p}(r)$ are directly related to the partial wave amplitude $f_l(p)$ or the phase shifts $\delta_l(p)$. This relationship can be established as follows. We start by expanding $\langle \mathbf{x}|\mathbf{p}+\rangle$ in the basis of $|E,l,m+\rangle$

$$\langle \mathbf{x}|\mathbf{p}+\rangle = \sum_{l.m}\int dE\langle \mathbf{x}|E,l,m+\rangle\langle E,l,m+|\mathbf{p}+\rangle. \tag{A.53}$$

We need to evaluate $\langle E,l,m+|\mathbf{p}+\rangle$. But $\langle E,l,m+|\mathbf{p}+\rangle = \langle E,l,m|\widehat{\Omega}_+^\dagger\widehat{\Omega}_+|\mathbf{p}\rangle = \langle E,l,m|\mathbf{p}\rangle$. From equation (A.36), $\langle E,l,m_l|\mathbf{p}\rangle = \left(\frac{1}{p}\right)^{1/2}\delta(E-E_p)Y^*_{l,m_l}(\widehat{\mathbf{p}})$. Therefore

$$\langle \mathbf{x}|\mathbf{p}+\rangle = (2\pi)^{-3/2}\frac{1}{pr}\sum_l(2l+1)i^l\psi_{l,p}(r)P_l(\widehat{\mathbf{x}}\cdot\widehat{\mathbf{p}}) \tag{A.54}$$

where we have used equation (A.48) and the addition theorem of Legendre polynomials to arrive at equation (A.54). But at large r, i.e., $r \to \infty$ we already know that

$$\langle \mathbf{x}|\mathbf{p}+\rangle \overset{r\to\infty}{\longrightarrow} (2\pi)^{-3/2}\left[e^{i\mathbf{p}\cdot\mathbf{x}} + f(p\widehat{\mathbf{x}} \leftarrow \mathbf{p})\frac{e^{ipr}}{r}\right]. \tag{A.55}$$

Therefore inserting the expansion for $f(p\widehat{\mathbf{x}} \leftarrow \mathbf{p})$ as given in equation (A.37) and using the following expansion for the plane wave states

$$e^{i\mathbf{p}\cdot\mathbf{x}} = \langle \mathbf{x}|\mathbf{p}\rangle = (2\pi)^{-3/2}\frac{1}{pr}\sum_l (2l+1) i^l j_l(pr) P_l(\widehat{\mathbf{x}}\cdot\widehat{\mathbf{p}}) \tag{A.56}$$

we get

$$\langle \mathbf{x}|\mathbf{p}+\rangle \overset{r\to\infty}{\longrightarrow} (2\pi)^{-3/2}\frac{1}{pr}\sum_l (2l+1)\left[i^l j_l(pr) + p f_l(p) e^{ipr}\right] P_l(\widehat{\mathbf{x}}\cdot\widehat{\mathbf{p}}). \tag{A.57}$$

Comparing with equation (A.54), we get

$$\psi_{l,p}(r) \overset{r\to\infty}{\longrightarrow} j_l(pr) + p f_l(p) e^{i(pr - i\pi/2)}. \tag{A.58}$$

Now using the asymptotic form for $j_l(pr)$ and the definition for the partial wave amplitude $p\, f_l(p) = e^{i\delta_l(p)} \sin(\delta_l(p))$, we get

$$\psi_{l,p}(r) \overset{r\to\infty}{\longrightarrow} e^{i\delta_l(p)} \sin\left[pr - l\pi/2 + \delta_l(p)\right]. \tag{A.59}$$

Therefore we see that the scattered radial wave functions are shifted by an amount $\delta_l(p)$ compared to the free radial functions

$$j_l(pr) \overset{r\to\infty}{\longrightarrow} \sin\left[pr - l\pi/2\right] \tag{A.60}$$

An attractive potential "pulls" the wave inside and the corresponding phase shift is positive, while a repulsive potential "pushes" the scattered wave out, and the phase shift is negative. For example, the nucleon-nucleon scattering in the $l = 0$ partial

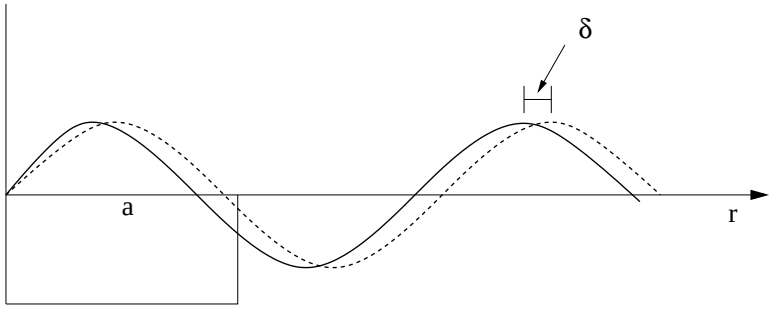

Figure A.1: Schematic of free- and scattered-radial wave functions in the s-channel for an attractive square well. The scattered wave (solid line) has a phase shift δ compared to the free-radial (dotted line) wave function and is positive for an attractive potential.

wave has both positive and negative phase shifts, corresponding to attractive and repulsive parts of the potential.

We conclude this section by surveying few general properties of partial-wave amplitude and phase shift. These properties can be obtained by studying the radial Schrödinger equation (A.49). Let us define the potential $V(R) = \lambda U(r)$ where λ is a strength parameter. Then equation (A.49) now becomes

$$\left[\frac{d^2}{dr^2} - \frac{l(l+1)}{r^2} - \lambda U(r) + p^2\right] \psi_{l,p}(r) = 0. \tag{A.61}$$

1. If the potential is such that $\left[\frac{l(l+1)}{r^2} - p^2\right]$ term dominates, then the equation (A.61) reduces to the free-space equation, and the solution $\psi_{l,p}(r) \to j_l(pr)$, the free-space solution. Then the partial wave amplitude $f_l(p)$ goes to zero and the phase shift $\delta_l(p)$ becomes an integral multiple of π.

2. At high energies, $p \to \infty$, for a given potential and partial wave, the partial wave amplitude goes to zero and once again the phase shifts $\delta_l(p) \to n\pi$.

3. For high partial-waves, i.e, in the limit where $l \to \infty$, the centrifugal barrier term dominates $\approx \frac{l^2}{r^2}$, driving $f_l(p) \to 0$.

From the high-partial wave result it is possible to get a rough estimate of the maximum value of l for which the phase shift $\delta_l(p)$ is appreciable. If the potential has a range R, then the height of the centrifugal barrier at $r \sim R$ is $\frac{l^2}{R^2}$. If the energy of the particle p^2 is less than this height, then the particle is unlikely to penetrate this barrier and feel the potential. Therefore we can define l_{max} as the maximum value of l for which the phase shifts are appreciable and is given by

$$l_{max} \approx R\,p \tag{A.62}$$

Immediately we can see that for low-momentum processes involving potentials of finite range, l_{max} is small. Therefore few partial waves will be sufficient to account for the scattering (such as contribution to the cross-section).

The partial wave amplitude $f(\mathbf{p}' \leftarrow \mathbf{p}) = -(2\pi)^2\langle \mathbf{p}'|V|\mathbf{p}+\rangle$ can be decomposed into partial wave amplitudes as follows

$$f_l(p) = -\frac{1}{p^2}\int_o^\infty dr\, j_l(pr)V(r)\psi_{l,p}(r). \tag{A.63}$$

In the limit $p \to 0$, it turns out that $\psi_{l,p}(r)$ has the same p dependence as $j_l(pr)$ i.e., p^{l+1}. Therefore at small p,

$$f_l(p) \xrightarrow{p\to 0} -a_l p^{2l} + \mathcal{O}(p^{2l+1}) \tag{A.64}$$

where a_l is a constant known as scattering length.

Therefore from the above discussions, it is clear that as p approaches the threshold $p = 0$, all partial wave amplitudes vanish except the s waves and for very low-energies

only the s wave amplitude is appreciable. Since $f_l(p) \to -a_l p^{2l}$ as $p \to 0$, the phase shift tends to a multiple of π as

$$\delta_l(p) \stackrel{p\to 0}{\longrightarrow} n\pi - a_l p^{2l+1}. \tag{A.65}$$

and

$$\delta_l(0) = n_l \pi. \tag{A.66}$$

where n_l denotes the number of bound states and equation (A.66) is the statement of Levinson's Theorem. The only exception is when the s wave scattering length is infinite, then the result of equation (A.66) is replaced by $\delta_0(0) = (n_0 + 1/2)\pi$.

Since S is a unitary operator, we can always write S as a function of Hermitian operator as follows:

$$S = (1 + iK)(i - iK)^{-1} \tag{A.67}$$

where K is hermitian. Both S and K commute with H_0 and L. Therefore K is diagonal in the partial wave basis i.e.,

$$\langle E', l', m'|K|E, l, m\rangle = \delta(E' - E)\delta_{l',l}\delta_{m',m}k_l(E) \tag{A.68}$$

Decomposing equation (A.67) in the partial wave basis we have the following eigenvalue equation

$$s_l(p) = \frac{1 + ik_l(p)}{1 - ik_l(p)}. \tag{A.69}$$

Using $s = \exp(2i\delta_l)$, we can write

$$k_l(p) = i\frac{1 - s_l(p)}{1 + s_l(p)} = \tan(\delta_l(p)). \tag{A.70}$$

In fact it can be shown that the K matrix is just the T matrix satisfying standing wave boundary conditions. From the threshold behavior of $\delta_l(p)$, we can deduce the

following

$$k_l(p) \xrightarrow{p\to 0} -a_l p^{2l+1} + \mathcal{O}(p^{2l+2}). \tag{A.71}$$

Therefore consider the following expansion

$$\frac{p^{2l+1}}{k_l(p)} = p^{2l+1}\cot(\delta_l(p)) = \frac{-1}{a_l} + \frac{r_l}{2}p^2 + \mathcal{O}(p^4). \tag{A.72}$$

This is known as the *effective range expansion*. Just retaining the first two terms, we get the *effective range approximation*. For $l = 0$, a_0 is the scattering length, r_0 is the effective range. We know that low-energy scattering processes can be well described by just the s waves. From the effective range approximation, we see that two parameters a_0 and r_0 parametrize low-energy scattering independent of the interaction potential.

A.5 NN scattering and phase shift conventions

While considering NN interaction, the two particles are either in the singlet state $S = 0$ or the triplet state, $S = 1$. As seen in the earlier discussions, the scattering states can be analyzed in the angular momentum basis, where they could be classified into various channels based on the values of L, S and J. We use the usual spectroscopic symbol to denote the different partial wave channels i.e., ${}^{(2S+1)}L_J$, where $(2S + 1)$ denotes the spin-multiplicity and $J = L + S$. The partial wave channels are also eigenstates of the partity operator whose eigenvalue is given by the quantum number $p = (-1)^L$. $L = J$ states correspond to singlet states (${}^1S_0$, ${}^1P_1$ etc) or uncoupled triplet states such as ${}^3P_1$, ${}^3F_3$ etc. The $l = J \pm 1$ correspond to the coupled states such as ${}^3S_1 - {}^3D_1$, ${}^3P_2 - {}^3D_2$ etc.

Let us consider the $L = J$ states first. From previous discussions the radial wave function has the following asymptote:

$$v_J(r) = Ae^{-i(kr-J\pi/2)} + Be^{i(kr-J\pi/2)} \tag{A.73}$$

Conservation of probability implies that

$$B = SA \tag{A.74}$$

where

$$S = e^{2i\delta_J(k)} \tag{A.75}$$

$$\Rightarrow v_J(r) \stackrel{r\to\infty}{\longrightarrow} C\sin(kr - J\pi/2 + \delta_J(k)). \tag{A.76}$$

Therefore for $L = J$ the S is just a number analogous to the case without spins.

The $L = J \pm 1$ are coupled by the NN interaction, so that the wavefunction can be written as

$$\Psi(\mathbf{r}) = \frac{u_J}{r}Y^M_{J,J-1,1}(\theta,\phi,\sigma) + \frac{w_J}{r}Y^M_{J,J+1,1}(\theta,\phi,\sigma) \tag{A.77}$$

where

$$Y^M_{J,L,S} + \sum_{M=m_l+m_s} \langle l, S, m_l, m_s|J, M\rangle Y_{l,m_l}(\theta,\phi)\chi_{s,m_s}(\sigma) \tag{A.78}$$

are the spin-sherical harmonics and $\chi_{s,m_s}(\sigma)$ are the spin eigenstates. The radial components $u_J(r)$ and $w_J(r)$ have the following asymptotes

$$u_J(r) = A_1e^{-i(kr-(J-1)\pi/2)} + B_1e^{i(kr-(J-1)\pi/2)} \tag{A.79}$$

$$w_J(r) = A_2e^{-i(kr-(J+1)\pi/2)} + B_2e^{i(kr-(J+1)\pi/2)} \tag{A.80}$$

Again probability conservation relates the amplitutes of the in-coming and out-going states i.e.,

$$\mathbf{B} = \mathbf{SA} \tag{A.81}$$

where

$$\mathbf{B} = \begin{pmatrix} B_1 \\ B_2 \end{pmatrix} \tag{A.82}$$

and

$$\mathbf{A} = \begin{pmatrix} A_1 \\ A_2 \end{pmatrix} \tag{A.83}$$

and the eigenstates satisfy $B_2/B_1 = A_2/A_1$.

In the case of coupled channels in NN scattering, there are two conventions for phase shifts, the Eigen phase and Bar conventions [92, 91, 47]. They differ in the way they parametrize the scattering matrix $\mathbf{S}$.

The eigen phases [92] uses the following parametrization for the $\mathbf{S}$ matrix

$$\mathbf{S} = U^{-1} e^{2i\Delta} U \tag{A.84}$$

where U is a unitary matrix defined as

$$U = \begin{pmatrix} \cos(\epsilon_J) & \sin(\epsilon_J) \\ -\sin(\epsilon_J) & \cos(\epsilon_J) \end{pmatrix} \tag{A.85}$$

and

$$\Delta = \begin{pmatrix} \delta_{J,\alpha} & 0 \\ 0 & \delta_{J,\beta} \end{pmatrix} \tag{A.86}$$

and α and β correspond to $J-1$ and $J+1$ states repectively.

The bar convention [91] parametrizes $\mathbf{S}$ as follows

$$\mathbf{S} = \exp(i\bar{\delta}) \exp(2i\bar{\epsilon}) \exp(i\bar{\delta}) \tag{A.87}$$

where $\bar{\delta}$ is a diagonal matrix with elements $\bar{\delta}_{J,l}$ and $\bar{\epsilon}$ is a symmetric matrix with zeros on the diagonal. $\mathbf{S}$ can be written as

$$\mathbf{S} = \begin{pmatrix} e^{\bar{\delta}_{J,J-1}} & 0 \\ 0 & e^{\bar{\delta}_{J,J+1}} \end{pmatrix} \begin{pmatrix} \cos(2\bar{\epsilon}_J) & i\sin(2\bar{\epsilon}_J) \\ i\sin(2\bar{\epsilon}_J) & \cos(2\bar{\epsilon}_J) \end{pmatrix} \begin{pmatrix} e^{\bar{\delta}_{J,J-1}} & 0 \\ 0 & e^{\bar{\delta}_{J,J+1}} \end{pmatrix}. \tag{A.88}$$

The eigen phases have the closest connection to the solution of the coupled channel Lippmann-Schwinger equation

$$\langle k'|T_{ll'}(k^2)|k\rangle = V_{ll'}(k',k) + \frac{2}{\pi}\sum_{l''}\mathcal{P}\int_0^\Lambda q^2 dq \frac{V_{ll''}T_{l''l'}}{k^2-q^2} \tag{A.89}$$

and are given by

$$\tan(\delta_l(p)) = -\frac{1}{2}\left[T_{ll}(p,p;p^2) + T_{l',l'}(p,p;p^2) + \left(\frac{T_{ll}(p,p;p^2) - T_{l'l'}(p,p;p^2)}{\cos(2\epsilon_J)}\right)\right], \tag{A.90}$$

$$\tan(\delta_{l'}(p)) = -\frac{1}{2}\left[T_{ll}(p,p;p^2) + T_{l',l'}(p,p;p^2) - \left(\frac{T_{ll}(p,p;p^2) - T_{l'l'}(p,p;p^2)}{\cos(2\epsilon_J)}\right)\right], \tag{A.91}$$

and

$$\tan(2\epsilon_J) = \frac{T_{ll'}(p,p;p^2) + T_{l'l}(p,p;p^2)}{T_{ll}(p,p;p^2) - T_{l'l'}(p,p;p^2)} \tag{A.92}$$

where $l = J-1$ and $l' = J+1$. Here we have dropped the subscript J on the phase shifts for notational convenience.

The nucleon bar convention is related to the eigen phases as follows:

$$\bar{\delta}_{l'} + \bar{\delta}_l = \delta_{l'} + \delta_l, \tag{A.93}$$

$$\sin(\bar{\delta}_l - \bar{\delta}_{l'}) = \frac{\tan(2\bar{\epsilon}_J)}{\tan(2\epsilon_J)} \tag{A.94}$$

and

$$\sin(\delta_l - \delta_{l'}) = \frac{\sin(2\bar{\epsilon}_J)}{\sin(2\epsilon_J)} \tag{A.95}$$

Using the above relations, we have the bar phase shifts and mixing angle defined in terms of the eigen phase conventions as

$$\bar{\epsilon}_J = \frac{1}{2}\sin^{-1}\left[\sin(2\epsilon_J)\sin(\delta_l - \delta_{l'})\right], \tag{A.96}$$

$$\bar{\delta}_l(p) = \frac{1}{2}\left[(\delta_l + \delta_{l'} + \sin^{-1}\left(\frac{\tan(2\bar{\epsilon}_J)}{\tan(2\epsilon_J)}\right)\right] \tag{A.97}$$

and

$$\bar{\delta}_{l'}(p) = \frac{1}{2}\left[(\delta_l + \delta_{l'}) - \sin^{-1}\left(\frac{\tan(2\bar{\epsilon}_J)}{\tan(2\epsilon_J)}\right)\right]. \tag{A.98}$$

A.6 Effective Range Expansion

In this section we present an entirely different approach to deriving the effective range expansion. Consider a particle of energy E_1 and wave number $\mathbf{k}_1$. If E_1 is in the lab system, then

$$E_1 = \frac{2\hbar^2 k_1^2}{M} \tag{A.99}$$

where $E_{\rm cm} = \dfrac{\hbar^2 k_1^2}{M}$ and M is mass of the particle and in the case of two-particle, it is the reduced mass. Let $u(r) = r\psi_1(r)$. Then the Schrödinger equation is

$$\frac{d^2u_1(r)}{dr^2} + k_1^2 u_1(r) - v(r)u_1(r) = 0. \tag{A.100}$$

where the potential $v(r) = MV(r)/\hbar^2$. For another energy E_2 and wave number $\mathbf{k}_2$ we have

$$\frac{d^2u_2(r)}{dr^2} + k_2^2 u_2(r) - v(r)u_2(r) = 0. \tag{A.101}$$

Next we multiply equation (A.100) by $u_2(r)$ and equation (A.101) by $u_1(r)$ and subtract one from the other so that,

$$u_2(r)\frac{d^2u_1(r)}{dr^2} - u_1(r)\frac{d^2u_2(r)}{dr^2} + (k_i^2 - k_2^2)u_1(r)u_2(r) = 0. \tag{A.102}$$

Integrating over r,

$$\left[u_2(r)u_1(r)' - u_1(r)u_2(r)'\right]\Big|_0^R = (k_2^2 - k_1^2)\int_0^R dr\, u_1(r)u_2(r) \tag{A.103}$$

where R is the upper limit (range of the potential). If $\psi_1(r)$ represents the asymptote of $u_1(r)$, then

$$\psi_1(r) = A_1 \sin(k_1 r + \delta) \tag{A.104}$$

where we choose $A_1 = \sin(\delta)$. Therefore the asymptote of $u_1(r)$ is

$$\psi_1(r) = \frac{\sin(k_1\, r + \delta)}{\sin(\delta)}. \tag{A.105}$$

Then analogous to equation (A.103), we can define

$$[\psi_2(r)\psi_1(r)' - \psi_1(r)\psi_2(r)'] \mid_0^R = (k_2^2 - k_1^2) \int_0^R dr\, \psi_1(r)\psi_2(r) \tag{A.106}$$

Subtracting equations (A.103) and (A.106) we get

$$\begin{aligned} &[\psi_2(r)\psi_1(r)' - \psi_1(r)\psi_2(r)'] \mid_0^R - [u_2(r)u_1(r)' - u_1(r)u_2(r)'] \mid_0^R \\ &\quad = (k_2^2 - k_1^2) \int_0^R dr\, \left[\psi_1(r)\psi_2(r) - u_1(r)u_2(r)\right]. \end{aligned} \tag{A.107}$$

In the limit $r = R \to \infty$, the LHS goes to zero and for $r = 0$, $u_1(0) = u_2(0) = 0$. Therefore equation (A.107) now becomes

$$[\psi_2(r)\psi_1(r)' - \psi_1(r)\psi_2(r)'] \mid_{r=0} = (k_2^2 - k_1^2) \int_0^\infty dr\, \left[\psi_1(r)\psi_2(r) - u_1(r)u_2(r)\right]. \tag{A.108}$$

Using the definition of the asymptote $\psi_1(r)$ as given in equation (A.105 and analogous definition for $\psi_2(r)$, equation (A.108) now becomes

$$(k_2 \cot(\delta_2) - k_1 \cot(\delta_1)) = (k_2^2 - k_1^2) \int_0^\infty dr\, \left[\psi_1(r)\psi_2(r) - u_1(r)u_2(r)\right]. \tag{A.109}$$

For small values of k_1, $k_1 \cot(\delta_1) = -\alpha = -\dfrac{1}{a}$, where a is the scattering length. Then

$$k \cot(\delta) = -\alpha + k^2 \frac{1}{2} \rho(0, E) \tag{A.110}$$

where we have taken $k_1 \to 0$ and

$$\rho(0, E) = \int_0^\infty dr\, \left[\psi_0(r)\psi(r) - u_0(r)u(r)\right]. \tag{A.111}$$

Since kr is small, the dependence on energy is weak and

$$k\cot(\delta) = -\alpha + k^2\frac{1}{2}\rho(0,0) = -\alpha + \frac{1}{2}kr_0^2 \tag{A.112}$$

where r_0 is called the effective range. Once again we note that at low energies, the scattering is determined by two parameters, the scattering length a and the effective range r_0.

APPENDIX B

SHARP RG AND FOLDED DIAGRAMS

This section proves the equivalence between sharp RG and the folded diagram techniques in effective interaction theory [32, 33]. We start by defining an energy independent vertex function $\widehat{Q}(E)$ box, which resums the effects of the high-momentum modes as follows:

$$\widehat{Q}(k',k;E) = V_{\rm NN}(k',k) + \mathcal{P}\frac{2}{\pi}\int_{\Lambda}^{\infty} p^2 dp \frac{V_{\rm NN}(k',p)\widehat{Q}(p,k;E)}{E-p^2} \tag{B.1}$$

which is the Bloch-Horowitz equation for the sharp regulator. The above equation (B.1) can be set up very easily as follows. For simplicity, we work with the corresponding operators and finally choose the momentum space basis. The T matrix equation is defined as [43]:

$$T_{\rm NN} = V_{\rm NN} + V_{\rm NN}\, G_0\, T_{\rm NN} \tag{B.2}$$

and

$$T_{\rm eff} = \widehat{Q} + \widehat{Q}\, G_0^{\Lambda}\, T_{\rm eff}. \tag{B.3}$$

where $T_{\rm NN}$ and $T_{\rm eff}$ are the bare and effective T matrices and G_0^{Λ} is the Green's function multiplied by a regulator function so that the intermediate states are cut-off at Λ. In this case it is a sharp regulator (theta function).

When high-momentum modes are intergrated out to get an effective potential, we need $T_{\rm NN} = T_{\rm eff} = T$, i.e., the bare and the effective interactions should give the same diagonal T matrix elements, which are related to phyical observables. In this case this invariance is extended to the off-shell T matrix elements as well, which is just a choice, analogous to the invariance of half-off shell T elements seen earlier with the energy-independent RG. As we shall see, this choice leads to an energy-dependent effective interaction (also encountered earlier with the three-step RG). Therefore,

$$T = V_{\rm NN} + V_{\rm NN}\, G_0\, T \tag{B.4}$$

$$= \widehat{Q} + \widehat{Q}\, G_0^{\Lambda}\, T. \tag{B.5}$$

From equation (B.4) we get $V_{\rm NN} = (1 - V_{\rm NN}\, G_0)\, T$. Therefore using equation (B.5),

$$V_{\rm NN} = (1 - V_{\rm NN}\, G_0) \left(\widehat{Q} + \widehat{Q}\, G_0^{\Lambda}\, T \right) \tag{B.6}$$

$$\Rightarrow V_{\rm NN} = \widehat{Q} - V_{\rm NN}\, G_0\, \widehat{Q} + (1 - V_{\rm NN}\, G_0\,)\, \widehat{Q} G_0^{\Lambda} T. \tag{B.7}$$

Using $\widehat{Q}\, G_0^{\Lambda}\, T = T\, G_0^{\Lambda}\, \widehat{Q}$ and $(1 - V_{\rm NN} G_0)\, T = V_{\rm NN}$ from equation (B.4). Therefore, equation (B.7) becomes

$$V_{\rm NN} = \widehat{Q} - V_{\rm NN}\, G_0\, \widehat{Q} + V_{\rm NN}\, G_0^{\Lambda}\, \widehat{Q}. \tag{B.8}$$

Therefore,

$$\widehat{Q} = V_{\rm NN} + V_{\rm NN} \left(G_0 - G_0^{\Lambda} \right)\, \widehat{Q}. \tag{B.9}$$

In momentum space basis, for a given partial wave, equation (B.9) now becomes

$$\begin{aligned} &\widehat{Q}(k', k; E) = V_{\rm NN}(k', k) \\ &+ \mathcal{P} \frac{2}{\pi} \int_0^{\infty} q^2 dq \frac{V_{\rm NN}(k', q) \widehat{Q}(q, k; E)}{E - q^2} - \mathcal{P} \frac{2}{\pi} \int_0^{\Lambda} q^2 dq \frac{V_{\rm NN}(k', q) \widehat{Q}(q, k; E)}{E - q^2} \end{aligned} \tag{B.10}$$

$$\tag{B.11}$$

Finally for an energy dependent effective interaction the Bloch-Horowitz equation is now given by

$$\widehat{Q}(k',k;E) = V_{\rm NN}(k',k) + \mathcal{P}\frac{2}{\pi}\int_{\Lambda}^{\infty} q^2 dq \frac{V_{\rm NN}(k',q)\widehat{Q}(q,k;E)}{E-q^2} \tag{B.12}$$

which proves equation (B.1).

In terms of the energy-dependent effective interaction $\widehat{Q}(k',k;E)$, the T matrix equation can be written as

$$T(k',k;k^2) = \widehat{Q}(k',k;k^2) + \mathcal{P}\frac{2}{\pi}\int_{0}^{\Lambda} p^2 dp \frac{\widehat{Q}(k',p;k^2)T(p,k;k^2)}{k^2-p^2}. \tag{B.13}$$

Next we define folded diagrams used in traditional effective interaction theory as the correction terms that must be added if all the $\widehat{Q}$ boxes are evaluated right side on-shell in the Lippmann-Schwinger equation (B.13). For example, expanding the T matrix equation (B.13) to second order we get:

$$T(k',k;k^2) = \widehat{Q}(k',k;k^2) + \mathcal{P}\frac{2}{\pi}\int_{0}^{\Lambda} p^2 dp \frac{\widehat{Q}(k',p;k^2)\widehat{Q}(p,k;k^2)}{k^2-p^2} + \mathcal{O}(\widehat{Q}^3), \tag{B.14}$$

where

$$T^{(2)}(k',k;k^2) = \mathcal{P}\frac{2}{\pi}\int_{0}^{\Lambda} p^2 dp \frac{\widehat{Q}(k',p;k^2)\widehat{Q}(p,k;k^2)}{k^2-p^2}. \tag{B.15}$$

Equation (B.15) can be written as

$$T^{(2)}(k',k;k^2) = \mathcal{P}\frac{2}{\pi}\int_{0}^{\Lambda} p^2 dp \frac{\widehat{Q}(k',p;p^2)\widehat{Q}(p,k;k^2)}{k^2-p^2} + \vartheta^{(1-fold)}(k',k), \tag{B.16}$$

where we have set all the effective interaction terms right-side on-shell and $\vartheta^{(1-fold)}(k',k)$ is defined

$$\vartheta^{(1-fold)}(k',k) = \mathcal{P}\frac{2}{\pi}\int_{0}^{\Lambda} p^2 dp \frac{\left[\widehat{Q}(k',p;k^2) - \widehat{Q}(k',p;p^2)\right]}{k^2-p^2}\widehat{Q}(p,k;k^2). \tag{B.17}$$

Similarly we can work out high-order correction terms. For example

$$\vartheta^{(2-fold)}(k',k) = \int_p \int_{p'} \frac{\left[\widehat{Q}(k',p';k^2) - \widehat{Q}(k',p';(p')^2)\right]}{(k^2-(p')^2)(k^2-p^2)} \widehat{Q}(p',p;k^2)\widehat{Q}(p,k;k^2)$$
$$- \int_p \int_{p'} \frac{\left[\widehat{Q}(k',p';p^2) - \widehat{Q}(k',p';(p')^2)\right]}{(p^2-(p')^2)(k^2-p^2)} \widehat{Q}(p',p;p^2)\widehat{Q}(p,k;k^2) \tag{B.18}$$

where $\int_p = \int_0^\Lambda p^2 dp$. Therefore we can replace the energy dependent effective interaction by an energy independent one by defining

$$V_{\mathrm{low}\,k}(k',k) = \widehat{Q}(k',k;k^2) + \vartheta^{(1-fold)}(k',k) + \vartheta^{(2-fold)}(k',k) + \cdots \tag{B.19}$$

Equation (B.19) expresses $V_{\mathrm{low}\,k}$ matrix elements as a folded-diagram series, which removes the energy-dependence of the effective interaction $\widehat{Q}(k',k;k^2)$. In fact it is possible to get the sharp RG equation starting with the energy dependent $\widehat{Q}$ box [32, 33].

Next we will prove that formal integration of the sharp RG equation,

$$\frac{dV_{\mathrm{low}\,k}(k',k)}{d\Lambda} = \frac{2}{\pi} \frac{V_{\mathrm{low}\,k}(k',\Lambda) T_{\mathrm{low}\,k}(\Lambda,k;\Lambda^2)}{1-(k/\Lambda)^2} \tag{B.20}$$

yields the series in equation (B.19), as claimed earlier in chapter 4. We demonstrate this result for a simple case. Expanding the left-on shell $T_{\mathrm{low}\,k}$ matrix to first order, we get

$$\frac{dV^{(1)}_{\mathrm{low}\,k}(k',k)}{d\Lambda} = \frac{2}{\pi} \frac{V_{\mathrm{low}\,k}(k',\Lambda) V_{\mathrm{low}\,k}(\Lambda,k)}{1-(k/\Lambda)^2} \tag{B.21}$$

where the superscript on the RHS refers to the order of expansion of $T_{\text{low}\,k}$. Now differentiating the expression for $\vartheta^{(1-fold)}$ (equation (B.17)),

$$\frac{d}{d\Lambda}\vartheta^{(1-fold)} = \frac{d}{d\Lambda}\left[\mathcal{P}\frac{2}{\pi}\int_0^\Lambda p^2 dp \frac{\left[\widehat{Q}(k',p;k^2)-\widehat{Q}(k',p;p^2)\right]}{k^2-p^2}\widehat{Q}(p,k;k^2)\right] \quad \text{(B.22)}$$

$$= \Lambda^2\frac{\left[\widehat{Q}(k',\Lambda;k^2)-\widehat{Q}(k',\Lambda;\Lambda^2)\right]}{k^2-\Lambda^2}\widehat{Q}(\Lambda,k;k^2) \quad \text{(B.23)}$$

$$= \Lambda^2\frac{\left[\widehat{Q}(k',\Lambda;k^2)\widehat{Q}(\Lambda,k;k^2)\right]}{k^2-\Lambda^2} - \Lambda^2\frac{\left[\widehat{Q}(k',\Lambda;\Lambda^2)\widehat{Q}(\Lambda,k;k^2)\right]}{k^2-\Lambda^2} \quad \text{(B.24)}$$

The first term in equation (B.21) is $-\dfrac{d\widehat{Q}(k',k;k^2)}{d\Lambda}$. This result can be seen easily by differentiating equation (B.1)

$$\frac{d\widehat{Q}(k',k;k^2)}{d\Lambda} = -\Lambda^2\frac{V_{\text{NN}}(k',\Lambda)\widehat{Q}(\Lambda,k;k^2)}{k^2-\Lambda^2} \quad \text{(B.25)}$$

where $E=k^2$ and the initial condition is $\widehat{Q}(k',\Lambda;k^2)=V_{\text{NN}}(k',\Lambda)$, which gives

$$\frac{d\widehat{Q}(k',k;k^2)}{d\Lambda} = -\Lambda^2\frac{\widehat{Q}(k',\Lambda;k^2)\widehat{Q}(\Lambda,k;k^2)}{k^2-\Lambda^2}. \quad \text{(B.26)}$$

The second term has on-shell $\widehat{Q}$ and is the first term in the folded-diagram expansion for $V_{\text{low}\,k}(k',k)$ as seen in equation (B.19), Therefore

$$\Lambda^2\frac{\left[\widehat{Q}(k',\Lambda;\Lambda^2)\widehat{Q}(\Lambda,k;k^2)\right]}{k^2-\Lambda^2} = -\frac{2}{\pi}\frac{V_{\text{low}\,k}(k',\Lambda)V_{\text{low}\,k}(\Lambda,k)}{1-(k/\Lambda)^2} \quad \text{(B.27)}$$

Substituting the results of equation (B.26) and (B.27) into equation (B.24), we get

$$\frac{d}{d\Lambda}\vartheta^{(1-fold)} = -\frac{d}{d\Lambda}\widehat{Q}(k',k;k^2) + \frac{2}{\pi}\frac{V_{\text{low}\,k}(k',\Lambda)V_{\text{low}\,k}(\Lambda,k)}{1-(k/\Lambda)^2}. \quad \text{(B.28)}$$

Finally we have the result

$$\frac{dV^{(1)}_{\text{low}\,k}(k',k)}{d\Lambda} = \frac{d}{d\Lambda}\left[\widehat{Q}(k',k;k^2)+\vartheta^{(1-fold)}(k',k)\right]. \quad \text{(B.29)}$$

Extending the above arguments term by term in the $T_{\mathrm{low}\,k}$ matrix expansion, we can generalize equation (B.29) as follows:

$$\frac{dV_{\mathrm{low}\,k}(k',k)}{d\Lambda} = \frac{d}{d\Lambda}\left[\widehat{Q}(k',k;k^2) + \vartheta^{(1-fold)}(k',k) + \vartheta^{(2-fold)}(k',k) + \cdots\right] \qquad \text{(B.30)}$$

Therefore, we get the result that formally integrating the sharp cut-off energy-independent RG equation results in generating the folded-diagram series for $V_{\mathrm{low}\,k}(k',k)$.

APPENDIX C

DECOUPLING SCHEMES

Solving the set of first-order coupled differential equations using any of the regulators, hermitization schemes etc., present one way of decoupling low- and high-momentum modes (chapter 2 and chapter 4). In this section, we will see other equivalent ways of getting a low-momentum effective potential.

C.1 Projection Operator Methods

Consider the following two projection operators:

$$P = \sum_{i=1}^{d} |i\rangle\langle i| \tag{C.1}$$

and

$$Q = \sum_{i=d+1}^{\infty} |i\rangle\langle i|, \tag{C.2}$$

satisfying the usual relations, $P^2 = P$, $Q^2 = Q$, $P + Q = 1$ and $PQ = QP = 0$. Let H be the hamiltonian acting on the full Hilbert space. Then

$$H|\psi\rangle = E|\psi\rangle \tag{C.3}$$

is the solution we are seeking. Using the projection operators, we write equation (C.3) as

$$H(P + Q)|\psi\rangle = E|\psi\rangle \tag{C.4}$$

Acting on equation (C.4) from the left by P, we get

$$PH(P+Q)|\psi\rangle = EP|\psi\rangle \tag{C.5}$$

$$\Rightarrow (PHP + PHQ)\,|\psi\rangle = EP|\psi\rangle. \tag{C.6}$$

Similarly by acting on equation (C.4) from the left by Q, we get

$$(QHP + QHQ)\,|\psi\rangle = EQ|\psi\rangle. \tag{C.7}$$

Equations (C.6) and (C.7) can be written in a matrix form as

$$\begin{pmatrix} PHP & PHQ \\ QHP & QHQ \end{pmatrix} \begin{pmatrix} P|\psi\rangle \\ Q|\psi\rangle \end{pmatrix} = E \begin{pmatrix} P|\psi\rangle \\ Q|\psi\rangle \end{pmatrix} \tag{C.8}$$

where PHP and QHQ represent projections on to the low and high-momentum states, while the off-diagonal blocks QHP and PHQ mixes these states. Using equation (C.7) we can eliminate $Q|\psi\rangle$ from equation (C.6) as follows

$$Q|\psi\rangle = -\frac{1}{QHQ - E}\, QHP(P|\psi\rangle) \tag{C.9}$$

Substituting equation (C.9) into equation (C.6) we get,

$$\left[PHP + PHQ\frac{1}{E - QHQ}\, QHP\right](P|\psi\rangle) = E(P|\psi\rangle). \tag{C.10}$$

Now we can define $\mathcal{H}_{\text{low}\,k}(E)$ as

$$\mathcal{H}_{\text{low}\,k}(E) = H + HQ\frac{1}{E - QHQ}QH \tag{C.11}$$

so that equation (C.10) becomes

$$H_{\text{low}\,k}(E) = P\mathcal{H}_{\text{low}\,k}(E)P \tag{C.12}$$

which we immediately recognize as the Bloch-Horowitz equation.

A refinement of the Bloch-Horowitz theory is the Lee-Suzuki transformation that eliminates this energy dependence. This is defined as

$$\theta^{-1} H \theta = \mathcal{H}_{\text{low}\,k} = \begin{pmatrix} P\mathcal{H}P & P\mathcal{H}Q \\ 0 & Q\mathcal{H}Q \end{pmatrix} \tag{C.13}$$

where the decoupling condition is $Q\mathcal{H}P = 0$. We parametrize θ as a non-orthogonal transformation in terms of the wave operator ω as

$$\theta = 1 + \omega \tag{C.14}$$

and

$$\theta^{-1} = 1 - \omega \tag{C.15}$$

and $Q\omega P = \omega$. Once again $H_{\text{low}\,k} = P\mathcal{H}_{\text{low}\,k}P$. It can be easily shown that

$$H_{\text{low}\,k} = PHP + PHQ\omega = PHP + PHQ\omega P \tag{C.16}$$

But $H = T_0 + V$, where T_0 is the kinetic energy or the unperturbed hamiltonian and V is the interaction. P and Q commute with T_0. Therefore,

$$V^{LS}_{\text{low}\,k} = H^{LS}_{\text{low}\,k} - PT_0P \tag{C.17}$$

$$= PVP + PVQ\omega P \tag{C.18}$$

Now we can write equation (C.18) in momentum space for a given partial wave using the following definition for projection operators

$$P = \frac{2}{\pi} \int_0^{\Lambda} p^2 dp |p\rangle\langle p| \tag{C.19}$$

and

$$Q = \frac{2}{\pi} \int_{\Lambda}^{\infty} p^2 dp |p\rangle\langle p| \tag{C.20}$$

so that

$$V^{LS}_{\text{low}\,k}(k',k) = V_{\text{NN}}(k',k) + \frac{2}{\pi}\int_{\Lambda}^{\infty} p^2 dp V_{\text{NN}}(k',p)\omega(p,k). \tag{C.21}$$

Comparing equation (C.21) with the Bloch-Horowitz equation for the energy dependent effective interaction $V_{\text{eff}}(E)$

$$V_{\text{eff}}(k',k;E) = V_{\text{NN}}(k',k) + \frac{2}{\pi}\int_{\Lambda}^{\infty} p^2 dp V_{\text{NN}}(k',p)G_0(p,E)V_{\text{eff}}(p,k;E) \tag{C.22}$$

we can see that the wave operator ω transforms the energy-dependence for momentum dependence. Once again it is possible to derive the sharp RG equation using Lee-Suzuki equarions as the starting point [33]. It would be interesting to explore the possibility of a similar equivalence relationship between smooth RG and a smooth generalization for the Lee-Suzuki transformation.

C.2 Similarity Renormalization Group

Similarity Renormalization Group [46] achieves the decoupling of low- and high-momentum modes using unitary transformations of the Hamiltonian. This has the unique feature of driving the high-momentum states towards the diagonal, which makes it different from the RG methods so far seen. To elaborate further, we saw earlier that $V_{\text{low}\,k}$ potentials, obtained from the half-off shell T matrix invariance for instance, preserves phase shifts up to the cut-off Λ. Above the cut-off the phase shifts are zero. The low-momentum potential obtained using Similarity Renormalization Group (SRG) denoted as V_{SRG}, preserves all the phase shifts with respect to the bare potential. As shown clearly in [93], this requirement of reproducing high-energy phase shifts is *not needed* for preserving low-energy observables. In this section we discuss the SRG approach.

Consider the following transformation on the hamiltonian

$$H_s = U(s)HU^\dagger(s) \equiv T_{\rm rel} + V_s \tag{C.23}$$

where $U(s)$ and $U^\dagger(s)$ are unitary operators. Now

$$\frac{dH_s}{ds} = \frac{dU_s}{ds}HU^\dagger(s) + U(s)H\frac{dU^\dagger}{ds} \tag{C.24}$$

$$= \frac{dU_s}{ds}U^\dagger(s)U(s)HU^\dagger(s) + U(s)HU^\dagger(s)U(s)\frac{dU^\dagger}{ds}. \tag{C.25}$$

Consider $\eta(s) = \dfrac{dU(s)}{ds}U^\dagger(s) \Rightarrow \eta^\dagger(s) = U(s)\dfrac{dU^\dagger(s)}{ds}$. Therefore,

$$\frac{dH_s}{ds} = \eta(s)H_s + H_s\eta^\dagger(s). \tag{C.26}$$

Using $U^\dagger(s)U(s) = 1$, we can establish the following

$$\frac{d}{ds}(U^\dagger(s)\,U(s)) = 0 \Rightarrow \left(\frac{d}{ds}\,U^\dagger\right)\,U(s) + U^\dagger(s)\,\left(\frac{d}{ds}U(s)\right) = 0 \tag{C.27}$$

$$\Rightarrow \eta^\dagger(s) + \eta(s) = 0. \tag{C.28}$$

Therefore using the above result, equation (C.26) can be written as

$$\frac{dH_s}{ds} = \eta(s)\,H_s - H_s\,\eta(s) = [\eta(s), H_s]\,. \tag{C.29}$$

We have the freedom to choose $\eta(s)$. Consider the following choice

$$\eta(s) = [T_{\rm rel}, H_s] = \frac{dU(s)}{ds}\,U^\dagger(s). \tag{C.30}$$

The flow equations (C.29) now becomes

$$\frac{dH_s}{ds} = [[T_{\rm rel}, H_s]\,, H_s]\,. \tag{C.31}$$

After some algebra we can show that equation (C.31) reduces to

$$\frac{dV_s(k',k)}{ds} = -(k^2 - (k')^2)^2\,V_s(k',k) + \frac{2}{\pi}\int_0^\Lambda q^2dq\,(k^2 + (k')^2 - 2q^2)\,V_s(k',q)\,V_s(q,k) \tag{C.32}$$

Far away from the diagonal (i.e., $k \neq k'$), the first term in equation (C.32) dominates, so that

$$\frac{dV_s(k',k)}{ds} = -(k^2-(k')^2)^2\, V_s(k',k) \tag{C.33}$$

$$\Rightarrow V_s(k',k) = V_0(k',k)e^{-(k^2-(k')^2)^2 s}. \tag{C.34}$$

Therefore it is clear that the off-diagonal elements are exponentially supressed. We can define $\lambda = s^{-1/4}$, where λ measures the spread of the off-diagonal strength. Now we can decrease λ analogous to the cut-off Λ in the $V_{\mathrm{low}\,k}$ approach.

The simplicity of the flow equations (C.31) help specify the running of any operator $\widehat{\mathcal{O}}$ i.e.,

$$\frac{d\widehat{\mathcal{O}}_s}{ds} = \left[\left[T_{\mathrm{rel}}, V_s\right], \widehat{\mathcal{O}}_s\right]. \tag{C.35}$$

A good check for the convergence property of V_{SRG} are the Weinberg eigenvalues. Figure (C.1) shows the repulsive Weinberg eigenvalues for Av_{18} potential (bare) and the corresponding V_{SRG} potentials ($\lambda = 2.0\,\mathrm{fm}^{-1}$) while figure (C.2) shows the attractive eigenvalues. The figures also show the corresponding $V_{\mathrm{low}\,k}$ eigenvalues (sqaures). We see that lowering the cut-off from bare value of $\lambda = 30\,\mathrm{fm}^{-1}$ to $\lambda = 2.0\,\mathrm{fm}^{-1}$ results in the major decreases in the repulsive eigenvalues (analogous to $V_{\mathrm{low}\,k}$ - refer chapter 5). Note that there are differences in the eigenvalues for $V_{\mathrm{low}\,k}$ and V_{SRG}, but the trends remain the same. This is important for the convergence of the in-medium Born-series. The attractive eigenvalues for V_{SRG} in the S channel do not change much in free-space, due to the presence of shallow bound states.

SRG approach provides a neat way to explore the three-body running and work in this direction is already in progress [94].

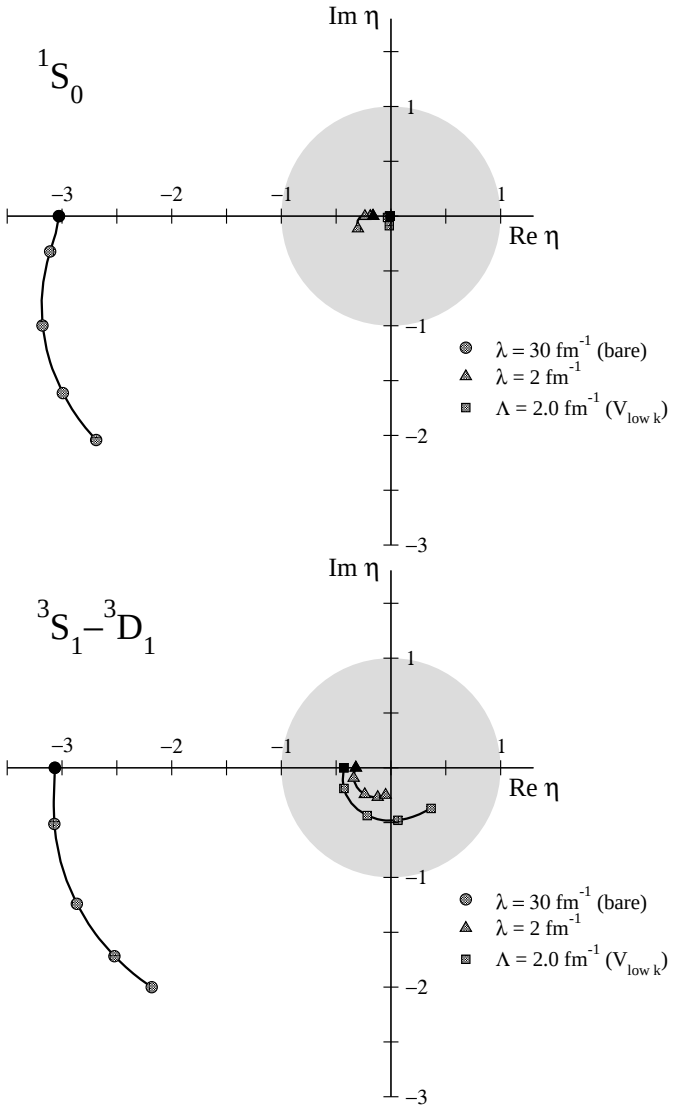

Figure C.1: Largest Repulsive Weinberg eigenvalues for $V_{\mathrm{low}\,k}$ and V_{SRG} for Av_{18} potential. The filled squares denote Weinberg eigenvalues corresponding to $V_{\mathrm{low}\,k}$ for $\Lambda = 2.0\,\mathrm{fm}^{-1}$. Notice similar trends as λ is decreased analogous to decreasing Λ.

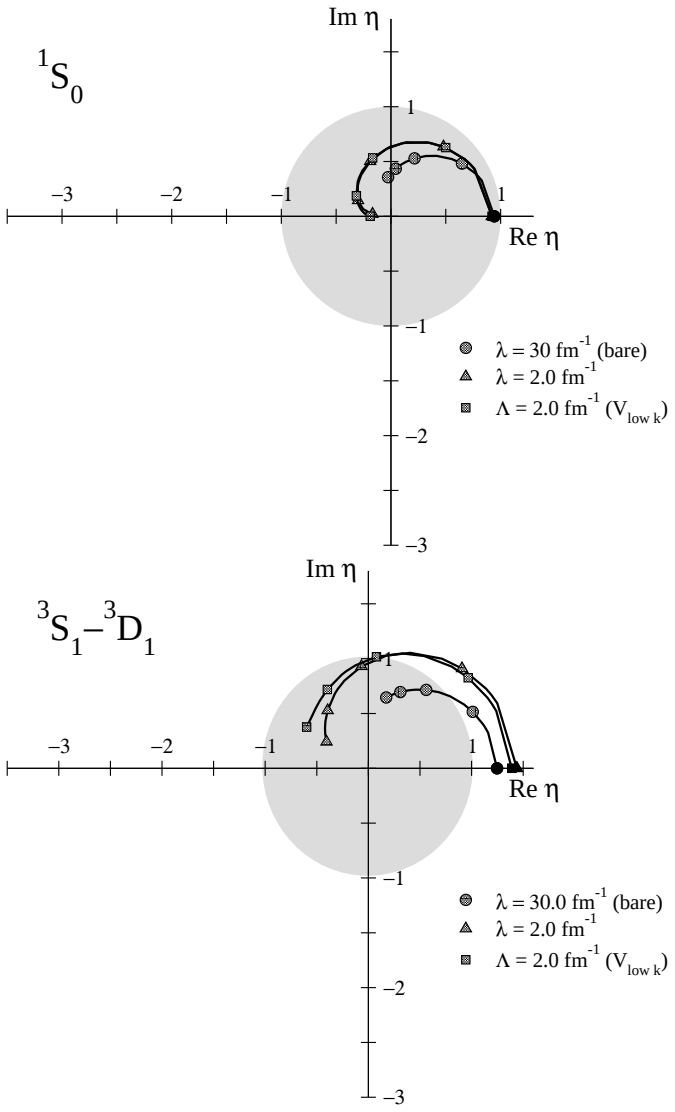

Figure C.2: Largest Attractive Weinberg eigenvalues for $V_{\mathrm{low}\,k}$ and V_{SRG} for Av_{18} potential. Notice similar trends as λ is decreased analogous to decreasing Λ.

BIBLIOGRAPHY

[1] R. J. Furnstahl arXiv:nucl-th/0109007.

[2] B. K. Jennings and A. Schwenk arXiv:nucl-th/0512013.

[3] R. Machleidt and D. R. Entem, arXiv: nucl-th/0309026

[4] David. B. Kaplan, *"Effective Field Theories"*, Lectures at the Seventh Summer School of Nuclear Physics, June 1995. arXiv: nucl-th/9506035

[5] Aneesh V. Manohar, *"Effective Field Theories"*, Lectures at the Schladming Winter School, March 1996.

[6] Daniel Phillips, arXiv: nucl-th/0203040.

[7] G. P. Lepage, *"How to Renormalize the Schrödinger Equation"*, Lectures given at the 9th George Andre Swieca Summer School,Brazil, Feb. 1997, arXiv:nucl-th/9706029

[8] S. R. Beane, P. F. Bedaque, W. C. Haxton, D. R. Phillips and M. J. Savage, *At the Frontier of Particle Physics* Ed. M. Shifman, Vol. 1, p. 133, World Scientific, arXiv:nucl-th/0008064

[9] H. Georgi, Ann. Rev. Nucl. Part. Sci.**43** (1993).

[10] Martin J. Savage arXiv:nucl-th/0301058.

[11] Martin J. Savage arXiv:nucl-th/0601001.

[12] A M. Green *'Hadronic Physics from Lattice QCD'*, 249-367, arXiv:nucl-th/0409021.

[13] N. Kaiser, Phys. Rev. **C64** (2001) 057001.

[14] R. J. Furnstahl arXiv:nucl-th/0307111

[15] S. Weinberg Phys. Lett. **B251** (1990), 228; Nucl. Phys **B363** (1991) 3.

[16] S. Weinberg, Phys. Lett. **B251** (1990).

[17] S. Weinberg, Nucl. Phys. **B363** (1991).

[18] V. Bernard, N. Kaiser and U.-G. Meißner, Int. J. Mod. Phys. E4, 193 (1995)

[19] D. B. Kaplan, M. J. Savage and M. B. Wise, Phys.Lett, **B424**, 30 (1998); Nucl. Phys. **B534**, 329 (1998), arXiv:nucl-th/9802075

[20] E. Epelbaum, W. Glöckle, A. Krüger and U.-G. Meißner, Nucl. Phys. **A645**, 413 (1999)

[21] P. Bedaque et al., (eds.) *Nuclear Physics with Effective Field Theory II*, (1999), World Scientific Press.

[22] P. Bedaque and U. van Kolck, Ann. Rev. Nucl. Part. Sci. **52** 329 (2002), arXiv: nucl-th/0203055.

[23] D. R. Phillips, Czech. J. Phys. **52** B49 (2002), arXiv: nucl-th/0203040

[24] U. van Kolck, Prog. Part. Nucl. Phys. **43** 409 (1999).

[25] W. Haxton and C. L. Song, Phys. Rev. Lett. **84**, 5484 (2000), arXiv: nucl-th/9907097

[26] D. R. Entem and R. Machleidt, Phys. Rev. **C68** (2003) 041001(R).

[27] E. Epelbaum, W. Glöckle and U.G. Meißner, Nucl. Phys. **A747** (2005) 362.

[28] S. K. Bogner, T. T. S. Kuo, A. Schwenk, D. R. Entem and R. Machleidt, Phys. Lett. **B576** (2003) 265;
S. K. Bogner, T. T. S. Kuo and A. Schwenk, Phys. Rept. **386** (2003) 1.

[29] S. K. Bogner, A. Schwenk, T. T. S. Kuo and G E. Brown, nucl-th/0111042.

[30] A. Nogga, S. K. Bogner and A. Schwenk, Phys. Rev. **C70** (2004) 061002(R).

[31] R. B. Wiringa, V. G. J. Stoks and R. Schiavilla, Phys. Rev. **C51** (1995) 38.

[32] A. Schwenk, Ph.D Thesis, State University of New York, Stony Brook, 2002.

[33] S. K. Bogner, A. Schwenk, T. T. S. Kuo and G. E. Brown, arXiv:nucl-th/0111042.

[34] A. Schwenk, B. Friman, S. K. Bogner, G. E. Brown and T. T. S. Kuo, arXiv:nucl-th/0207005 2 Jul 2002.

[35] S. K. Bogner, T. T. S. Kuo, A. Schwenk, D. R. Entem and R. Machleidt, arXiv:nucl-th/108041, 25 Jan 2002.

[36] A. Nogga, S. K. Bogner, and A. Schwenk, Phys. Rev. **C70**(2004) 061002(R).

[37] S. K. Bogner, A. Schwenk, R. J. Furnstahl and A. Nogga, arXiv:nucl-th/0504043.

[38] S. K. Bogner, and R. J. Furnstahl, Phys.Lett.**B632** (2006) 501-506, arXiv:nucl-th/0508022.

[39] S. K. Bogner and R. J. Furnstahl, Phys.Lett. **B639** (2006) 237-241, arXiv:nucl-th/0602017.

[40] S. K. Bogner, R. J. Furnstahl, S. Ramanan, and A. Schwenk, Nucl.Phys.A **784**, 79-103,2006, arXiv:nucl-th/0609003.

[41] S. Weinberg Phys. Rev. **131** (1963), 440.

[42] S. K. Bogner, R. J. Furnstahl, S. Ramanan, and A. Schwenk, Nucl.Phys.A **773**, 203-220,2006 arXiv:nucl-th/0602060.

[43] John R. Taylor, *Scattering Theory*, John Wiley and Sons, New York.

[44] J. J. Sakurai, *Modern Quantum Mechanics*, Addison Wesley, New York.

[45] A. Schwenk, B. Friman, and G. E. Brown, arXiv:nucl-th/0302081.

[46] S. K. Bogner, R. J. Furnstahl, R. J. Perry arXiv: nucl-th/0611045.

[47] G. E. Brown and A. D. Jackson, *The Nucleon Nucleon Interaction*, American Elsevier Publishing Company INC.

[48] Michael C. Birse, Judith A. McGovern and Keith G. Richardson, arXiv:hep-ph/9008398 24 Aug 1998.

[49] Thomas Bradford and Michael C. Birse, arXiv:hep-ph/0206146, 17 June 2002.

[50] Philip J. Siemens and Askel S. Jensen, *"Elements of Nuclei - Many-body Physics with the Strong Interaction"* Addison-Wesley, New York.

[51] Kenneth G. Wilson, Rev. of Mod. Phys, **Vol 55**, (583), July 1983.

[52] W. Gloeckle, *The Quantum Mechanical Few-Body Problem* (Springer-Verlag, New York, 1983).

[53] A. Nogga, R. G. E. Timmermans, U. van Kolck Phys. Rev. C **72:054006** (2005) arXiv:nucl-th/0506005

[54] Jason D. Holt, T. T. S. Kuo, G. E. Brown and Scott K. Bogner Nucl.Phys.**A733** (2004) arXiv: nucl-th/0308036.

[55] E. Epelbaum, W. Glöckle and U. G. Meißner, Eur. Phys. J. **A19** (2004) 401.

[56] A. L. Fetter and J. D. Walecka, *Quantum Theory of Many-Particle Systems* (Dover Publications, New York, 2002).

[57] N. H. March, W. H. Young and S. Sampanthar, *The Many-Body Problem in Quantum Mechanics*, Cambridge University Press, (1967).

[58] B. D. Day, Rev. Mod. Phys. **39** (1967) 719.

[59] R. Rajaraman and H. A. Bethe, Rev. Mod. Phys. **39** (1967) 745.

[60] B. D. Day, Rev. Mod. Phys. **50** (1967) 495.

[61] B. D. Day and R. B. Wiringa, Phy. Rev. C **32** (1985) 1057.

[62] R. Lazauskas, J. Carbonell, A.C. Fonseca, M. Viviani, A. Kievsky and S. Rosati, Phys. Rev. **C71** (2005) 034004.

[63] A. Nogga *et al.*, nucl-th/0602003.

[64] G. H. Rawitscher and L. Canton, Phys. Rev. **C44** (1991) 60.

[65] L. Canton and G. H. Rawitscher, J. Phys. **G17** (1991) 429.

[66] S. K. Bogner, R. J. Furnstahl and S. Ramanan, *in preparation*

[67] H. A. Bethe and J. Goldstone, Proc. Roy. Soc. (London), **A238**:551 (1957)

[68] A. Schwenk, B. Friman and G. E. Brown, arXiv:nucl-th/0207004

[69] A. Sedrakian, T. T. S. Kuo, H. Muther and P. Schuck, Phys. Lett. B **576**, 68 (2003) [arXiv:nucl-th/0308068].

[70] A. Sedrakian, and J. W. Clark, arXiv:nucl-th/0607028.

[71] A. A. Abrikosov. L. P. Gorkov and I. E. Dzyaloshinski, "*Methods of Quantum Field Theory in Statistical Physics*", Dover Publications, New York.

[72] V. A. Khodel, V. V. Khodel and J. W. Clark, Nucl. Phys. A., **598**, 390-417, (1996).

[73] H. Heiselberg, C. J. Pethick, H. Smith, and L. Viverit, Phys. Rev. Lett., **85**, 12, 2418, (2000).

[74] A. Schwenk, Int. J. Mod. Phys. **B20**, 2724-2729,(2006), arXiv:nucl-th/0411070.

[75] A. Schwenk, arXiv:nucl-th/0611046.

[76] K. Hebeler, A. Schwenk, B. Friman, arXiv:nucl-th/0611046.

[77] H. -J. Schulze, J. Cugnon, A. Lejeune, M. Baldo and U. Lombardo, Phys. Lett. B., **375** (1996).

[78] W. H. Press, S. A. Teukolsky, W. T. Vetterling and B. P. Flannery, Numerical Recipes in C, Cambridge University Press, 1992.

[79] J. D. Holt, T. T. S. Kuo, G. E. Brown, Phys. Rev. **C69** (2004) 034329.

[80] S. Y. Lee and K. Suzuki, Phys. Lett. **B91** (1980) 173.

[81] K. Suzuki and S. Y. Lee, Prog. Theor. Phys. **64** (1980) 2091.

[82] S. Okubo, Prog. Theor. Phys. **12** (1954) 603.

[83] K. Suzuki and R. Okamoto, Prog. Theor. Phys. **70** (183) 439.

[84] F. Andreozzi, Phys. Rev. **C54** (2004) 684.

[85] L. Giraud, J. Langou and M. Rozloznik, Computer and Mathematics with Applications **50** (2005) 1069.

[86] S.-B. Liao, J. Polonyi and M. Strickland, Nucl. Phys. **B567** (2000) 493, and references therein.

[87] M. Garcon and J. W. Van Orden, arXiv:nucl-th/0102049.

[88] E. Epelbaum, W. Glöckle and U.G. Meißner, Nucl. Phys. **A671** (2000) 295.

[89] R. Roth, H. Hergert, N. Paar, P. Papakonstantinou, arXiv:nucl-th/0608018.

[90] S. K. Bogner, R. J. Furnstahl, R. J. Perry, A. Schwenk, *in preparation.*

[91] H. P. Stapp, T. J. Ypsilantis and N. Metropolis, Phys. Rev. **105**, 302 (1957).

[92] J. M. Blatt and L. C. Biedenharn, Phys. Rev. **86** (1952), 399.

[93] S. K. Bogner, R. J. Furnstahl, R. J. Perry and A. Schwenk arXiv:nucl-th/0701013.

[94] S. K. Bogner, R. J. Furnstahl and R. J. Perry *in preparation.*